



Journal of

METALS

Published to provide a continuing, authoritative, and up-to-date record of technologic, engineering, and economic progress in all branches of the metals industry by the

Metals Branch
American Institute of Mining and Metallurgical Engineers, Inc.
29 West 39th Street, New York 18

○ ○ ○

THOMAS E. LLOYD
Manager of Publications
Editor, Journal of Metals

○ ○ ○

JAMES A. STANGARONE
Advertising Manager

○ ○ ○

HAROLD N. UNDERHILL, ALVIN S. COHAN, DOROTHY G. GARRETT, MARGARET BAGG, Assistant Editors; GRACE PUGSLEY, Production Manager; WALTER J. SEWING, Assistant.

○ ○ ○

OFFICERS, AIME

D. H. McLaughlin	President
A. B. Kinzel	Vice President
Philip Kraft	Vice President
R. W. Thomas	Vice President
C. H. Benedict	Vice President
C. V. Millikan	Vice President
Andrew Fletcher	VP & Treasurer

○ ○ ○

AIME STAFF

E. H. Robie	Secretary
H. A. Maloney	Asst. Treasurer
E. J. Kennedy, Jr.	Asst. Secretary
Ernest Kirkendall	Asst. Secretary
H. Newell Appleton	Asst. to Secretary

○ ○ ○

Technical Publications Committee

F. B. Foley	Chairman
E. J. Kennedy, Jr.	Secretary

○ ○ ○

Auxiliary Publications Committee

O. B. J. Fraser	Chairman, IMD
Michael Tenenbaum	Chairman, ISD
Philip T. Stroup	Chairman, EMD

○ ○ ○

The AIME Publishes:

Mining Engineering
Journal of Metals

Journal of Petroleum Technology

VOL. 188, NO. 9

SEPTEMBER, 1950

COVER

Moving internal parts of an infrared spectrograph while in a high vacuum is a new use of synchros at the Beacon, N. Y. laboratory of the Texas Co. These devices are used to indicate angular motion at a distance from the object to be moved, and this is believed their first application to initiate controlled motion in a vacuum. Operating at a vacuum of the order of 0.02 mm. Hg, the synchros enable the operator to adjust prisms and mirrors in infrared radiation studies.

FEATURES

Journal of Metals REPORTER	1083	Metal Congress Program (AIME)	1177
"Drift of Things"	1084	AIME Annual Meeting Committees	1179
Engineering Employment Service	1079	U. S. Steel Expansion Program	1085
Authors in This Issue	1074	Kaiser to Increase Aluminum Capacity	1085
New Products and Literature	1080	Ohio Minerals Industry Conference	1085
Personals and Obituaries	1180	Riverside Increases Strip Capacity	1086
Coming Meetings	1086	Optimist at 83	1182

TECHNICAL ARTICLES

Taconite Are Ready	J. V. Beall	1087
Charging Practice: Its Effect on Open Hearth Output	W. Schwinn	1089
Metal Fractures Modelled by Other Materials	A. M. Sullivan, J. A. Kies	1090
AC—A New Corrosion Test	T. E. Lloyd	1092
Nitriding—Effect on Fatigue Strength of Stainless Steel	V. T. Malcolm, S. Low	1094
Flameproof Clothing Guards Against Burns From Hot Metal Splash		1096

TRANSACTIONS

Metallurgy Behind the Decimal Point	E. E. Schumacher	1097
Mechanism of Sulphur Transfer Between Carbon-Saturated Iron and CaO-SiO ₂ -Al ₂ O ₃ Slags	G. Derge, W. O. Philbrook, K. M. Goldman	1111
Young's Modulus and Its Temperature Dependence in 36 to 52 Pct Ni-Fe Alloys	M. E. Fine, W. C. Ellis	1120
A Study of Strain Markings in Aluminum	B. R. Banerjee	1126
Quantitative Stress-Strain Studies on Zinc Single Crystals in Tension	D. C. Jillson	1129
Vapor Pressure of Silver	H. M. Schadel, Jr., C. E. Birchenall	1134
On the Martensite Transformation at Temperatures Approaching Absolute Zero	S. A. Kulin, Morris Cohen	1139
Supercooling of Aggregates of Small Metal Particles	David Turnbull	1144
Ductility of Cast Molybdenum	R. B. Fischer, J. H. Jackson	1149
Textures of Cold-Rolled and Annealed Titanium	H. T. Clark, Jr.	1154
Migration of Carbon in Steel Under the Influence of Direct Current	P. Dayal, L. S. Darken	1156
A Study of the Plastic Behavior of High-Purity Aluminum Single Crystals at Various Temperatures	F. D. Rosi, C. H. Mathewson	1159
Equilibrium in the Reaction of CO ₂ with Liquid Copper from 1090° to 1300°C	D. J. Girardi, C. A. Siebert	1168
The Effect of Sodium Contamination on Mg-Li Base Alloys	P. D. Frost, J. H. Jackson, A. C. Loonam, C. H. Lorig	1171
Structure of Intermediate Phases in Alloys of Ti with Fe, Co and Ni	Pol Duwez, J. L. Taylor	1173

Published the first day of each month by the American Institute of Mining and Metallurgical Engineers, Inc., 29 West 39th Street, New York 18, N. Y. Telephone: PEnnsylvania 6-9220. Subscription \$8 per year for non-AIME members in United States and North, South and Central America; \$9, foreign; \$6 for AIME members, or \$4 in combination with a subscription to *Mining Engineering* or the *Journal of Petroleum Technology*. Single copies, 75 cents; special issues, \$1.50 . . . The AIME is not responsible for any statement made or opinion expressed in its publications. . . . Copyright 1950 by the American Institute of Mining and Metallurgical Engineers, Inc. . . . Registered cable address, AIME New York . . . Indexed in Engineering Index, Industrial Arts Index and Chemical Abstracts . . . Reentered as second-class matter Sept. 21, 1949, at the post office at New York, N. Y., under the Act of March 3, 1879.



P. Dayal



C. H. Lorig



E. E. Schumacher

S. A. Kulin (p. 1139) is Research Assistant at the Dept. of Metallurgy, Massachusetts Institute of Technology, where he received his B.S. degree. He was previously Chief Metallurgist for the Power Tube Div. of Raytheon Mfg. Co., Waltham, Mass. A student associate of AIME, he enjoys sailing, music, and contract bridge.

P. Dayal (p. 1156) is Asst. Director of Supplies for the Directorate General of Industries & Supplies, Government of India. He was formerly Asst. Professor of Metallurgy at Benares Hindu University. Born in India, he attended Benares Hindu University and Polytechnic Institute of Brooklyn, earning B. Sc. of M. E. degrees.

G. Derge (p. 1111). See JOURNAL OF METALS, September, 1949.

W. O. Philbrook (p. 1111). See JOURNAL OF METALS, February, 1950.

Kenneth M. Goldman (p. 1111). See JOURNAL OF METALS, February, 1950.

M. E. Fine (p. 1120). See JOURNAL OF METALS, July, 1950.

W. C. Ellis (p. 1120). See JOURNAL OF METALS, June, 1950.

D. C. Jillson (p. 1129). See JOURNAL OF METALS, August, 1950.

C. E. Birchenall (p. 1134). See JOURNAL OF METALS, January, 1950.

Morris Cohen (p. 1139). See JOURNAL OF METALS, September, 1949.

David Turnbull (p. 1144). See JOURNAL OF METALS, September, 1949.

Howard T. Clark, Jr. (p. 1154). See JOURNAL OF METALS, October, 1949.

C. H. Mathewson (p. 1159). See JOURNAL OF METALS, September, 1949.

C. A. Siebert (p. 1168). See JOURNAL OF METALS, February, 1950.

Pol Duwez (p. 1173). See JOURNAL OF METALS, July, 1950.



B. R. Banerjee



J. L. Taylor



P. D. Frost

Earle E. Schumacher (p. 1097) joined the Western Electric Co., the manufacturing unit of the Bell Telephone System, during World War I, interrupting his advanced studies as Research Assistant at the University of Michigan. He was instrumental in the organization and expansion of the metallurgical dept in 1925; and for many years as Chief Metallurgist, he has directed the activities of this division. During 1949 he served on the metallurgy panel of the Government's Research and Development Board. A Director of AIME, in February, 1950, he delivered the annual Institute of Metals Div. Lecture. In September he will be the guest lecturer at the meeting of the British Iron and Steel Institute in England.

Bani R. Banerjee (p. 1126) hails from the land that Kipling loved, but now is associated with Standard Oil Co. (Indiana), Chicago, as Research Engineer. He taught at Illinois Institute of Technology, was a Graduate Fellow at the Institute for the Study of Metals at the University of Chicago, and worked as Metallurgist for Universal-Cyclops Steel Corp. Born in Calcutta, he received his B. Met. from University of Calcutta, and his M. Eng. and D. Eng. degrees from Yale. A Junior Member of AIME, he likes photography and fishing.

L. S. Darken (p. 1156) has been Physical Chemist for the Research Lab of U.S. Steel Corp., Kearny, N.J., since 1935. He has made several contributions to AIME Transactions, and is an AIME member. Born in Brooklyn, he obtained his A.B. from Hamilton College, and a Ph.D. from Yale. For relaxation he likes writing, bowling, and gardening.

F. D. Rosi (p. 1159) is Senior Engineer for Sylvania Electric Products, Inc., Bayside, L. I. Born in Meriden, Conn., he studied at Yale and received B.E., M.E., and Ph.D.

degrees. He is a Junior Member of AIME.

C. H. Lorig (p. 1171), Assistant Director of the Battelle Memorial Institute, Columbus, Ohio, started there in 1930 as Research Metallurgist. He received B.S., M.S., and Ph.D. degrees from the University of Wisconsin.

P. D. Frost (p. 1171) is Research Engineer for Battelle Memorial Institute. He has also worked at the Cornell Aeronautical Lab, Republic Steel Corp., and taught an extension course at Cornell University. He has a B. Met. E. degree from Rensselaer Polytechnic Institute, and is studying for his M.S. at Ohio State. A member of AIME, he enjoys golf and swimming.

Jack L. Taylor (p. 1173) is Research Engineer at California Institute of Technology's Jet Propulsion Lab, Pasadena, Cal. His previous position with J. H. Pomeroy & Co., as Chief of Party on Guam Island, led to his spending 44 months as a prisoner of war in Japan. He is a member of AIME, and likes photography, outboard boating, fishing, and dogs.

Miss A. M. Sullivan (p. 1090), Metallurgist at the Mechanics Div., Naval Research Lab, at Washington, D.C., studied at George Washington University for her A.B. degree. Previous associations were with the National Bureau of Standards and the Carnegie Institute of Washington. Her hobbies are reading, travel, and obedience work with dogs.

J. A. Kies (p. 1090) was with the National Bureau of Standards, Western Regional Research Lab, Oak Ridge National Lab, and is presently Metallurgist for the Naval Research Lab, Mechanics Div., Washington, D.C. He attended the University of Illinois, and received his B.S., and an M.S. in Physics. An AIME member, he is interested in fishing, gardening, and camping.

New Products, Services and Information....

Products and services recently announced are described here. Also, new publications offered free by producers servicing the metalworking industry are listed.

For further information on any product or for your copies of the free publications, fill in the coupon below and send it to the Journal of Metals.

1) FORCE INDICATORS: For determining forces necessary for such operations as precise adjustments of springs, the *Hunter Spring Co.* makes 12 models of Force Indicators. They come in the following capacities: 1, 2, 5, 10 and 20 lb; 16, 32, 80 and 160 oz; and 500, 1000, and 5000 gr. The Hunter Force Indicator is designed for one-hand operation and is supplied with six stainless steel force-transmission rod fittings.

2) STORAGE JAR: The *Bethlehem Apparatus Co.* presents the Bethlehem Dri-Jar for drying, storing, and filing samples and specimens in industrial and scientific laboratories. It is a wide-mouthed glass jar 3 in. diam x 7 in. high, with screw lid. Rigidly suspended from the lid is a series of four metal storage shelves. Material can be placed on the shelves uncovered, boxed or otherwise separated.

3) GRAPHITE FLUXING TUBES: The National Graphite Fluxing tubes, used for the injection of gases such as nitrogen, chlorine, argon, and helium into molten nonferrous metals to reduce hydrogen, oxides and inclusions, do not dissolve in aluminum, magnesium, brasses and most other nonferrous baths. They will not contaminate the metal; and metal and dross will not adhere tightly to them. The tubes, manufactured by the *Union Carbide and Carbon Corp.*, are made in three general types: A, B and C, the selection of which is determined by the requirements of the particular job. They come in 1½ and 2 in. diam sizes and in lengths of 24 to 108 in.

4) SIMPLYTROL PYROMETERS: *Assembly Products, Inc.* offer a temperature controller with automatic protection from thermocouple burnout. It has control action and no vacuum tubes or meters. Eight standard ranges cover temperatures from 75° to 3000° F. Standard calibrations are for use with iron-constantan, chromel-alumel and platinum type thermocouples.

5) MOLTEN METAL THERMOCOUPLE: To withstand melting temperatures up to 3200° F and all casting temperatures normally encountered in producing precision steel castings, a new Molten Metal Thermocouple for ferrous metals has been developed by the

Wheelco Instruments Co. Accurate temperature readings can be made in less than 30 sec. It is a well balanced immersion-type sensing unit for use with any pyrometer, it has an adjustable extension, and uses a 27 gage platinum-platinum 10 pct rhodium element.

6) ALUMINUM ETCHING: *Pennsalt AE-18*, a new, highly concentrated alkaline compound for etching aluminum without forming hard sludge deposits on the bottom of the etching tanks has been announced by *Pennsylvania Salt Mfg. Co.* It is packaged in 300-lb non-returnable drums, and can be used in concentrations of 5 to 7 oz per gal of water at temperatures of 140° to 150° F.

7) GLASSWARE MARKER: A new tungsten carbide pencil for permanently marking glassware is available from the *Fischer Scientific Co.* It is useful in the laboratory for identifying sealed vials of standard colorimetric samples; sheets of glass can be accurately scored for breaking; and tubes and rods can be scored more rapidly than with a file. Price: \$1.25.

8) NEW DEMAGNETIZER: For eliminating undesirable magnetic flux from tools, drills, punches, small arms, and machined parts that may have become magnetized, a coil has been developed by the *General Electric Co.* The demagnetizer is also useful in equalizing and stabilizing magnetic flux in permanent magnet assemblies used in electrical instruments and control devices. It is rated at 115 volts, 60 cycles, and is equipped with switch, pilot lamp, and a flexible lead fitted with a standard plug.

9) CUSTOM MADE ALLOYS: Extensive research facilities for the development of custom tailored alloys for industry have been established by *Specialloy, Inc.* Alloy addition agents will be engineered for specific industrial problems and allow wider application of existing metals.

10) SPRING MOTORS: Characterized by constant torque and long running time is the new spring motor designed around the Neg'ator. Neg'ator is the new elastic member made from prestressed flat spring stock by the *Hunter Spring Co.* The spring motor is adaptable for use on cameras, time recorders, mechanical recording instruments, automatic reels, anti-backlash mechanisms and balancing devices. Power takeoff from the Neg'ator motor is from the large bushing, which may be attached directly to the driven shaft or operated through a gear train.

11) SOLENOID-HYDRAULIC VALVE: A new double solenoid operated four-way hydraulic valve is announced by *Rivett Lathe & Grinder, Inc.* Principal feature in the design of the Series 5500 is the hydraulically balanced piston with an integral spool and stem. The entire piston surface is hardened, ground and lapped with special grooving to minimize possibility of binding under high pressure conditions. Designed for pressures up to 1500 psi, the Series 500 is available in five sizes: ¼, ⅜, ½, ¾ and 1 in., for standard 110, 220, and 440 volt, 50 or 60 cycles.

12) BRAZING STAINLESS STEELS: A new product called Colmonoy Nicrobraz is a heat and corrosion resistant alloy for brazing stainless steels, and at 2000° F the joint possesses equal strength with the parent metal.

Journal of Metals
29 West 39th St.
New York 18, N. Y.

September

Please send me More Information
Free Literature
Price Data

on items indicated.

1	2	3	4	5	6	7	8	9	10
11	12	13	14	15	16	17	18	19	20
21	22	23	24	25	26	27	28	29	30
31	32	33	34	35	36	37	38	39	40

Name Title.....
Company
Street
City and Zone State.....

Nicrobraz can be used to braze 300 and 400 series stainless steel, Inconel, S-590, Monel, alloy steels, tool steels, carbon steels, and special stainless steels. The physical properties of this alloy make it suitable for use in jet engines, as well as in other commercial applications, including those in the food, chemical, mercury, nuclear energy, automotive, and oil industries. It is available as a powder in 1 lb containers. Nicrobraz cement comes in pint containers.

13) LIQUID SOLDERING FLUX: A time-saver for metal joining is the new Divco #229 Liquid Soldering Flux, which eliminates practically all of the cleaning and burnishing of metal parts usually necessary before soldering. No brush is necessary. "Just Squirt!" say the directions. Cost of 4 oz can is 50¢, less trade discount. They are packed in cartons of 12 cans by the manufacturers, *Division Lead Co.*

14) BOILER ALARM: An alarm for boilers, to sound when the water reaches a low level, has been devised by the *J. A. Campbell Co.* The Campbell Micro-Thermal Low-Level Boiler Alarm consists of a $\frac{3}{8}$ in. expansion tube with its inner end connected to the lower end of the water column on the boiler. The switch will throw on and off on a temperature change of only 5° . It can be attached to any boiler water column regardless of boiler size or of length of column.

15) CRANE CAB CONDITIONERS: *Dravo Corp.* has de-

veloped two new types of cab conditioners. One type, Model VHDF, is designed to provide continuous ventilation, heating, dust filtering, and fume protection for crane cabs and small confined spaces in industrial plants. The other unit, Model VHD, performs the same functions except for fume removal. This model is for use where noxious fumes are not a problem, but where dust filtering, ventilation or heating may be required. Either unit will operate on ac or dc power. Model VHDF is 16 in. deep, 26 in. wide and 42 in. high. Model VHD is the same depth and width but is 26 in. high.

16) SOLDERING KIT: Joining metals, including aluminum, stainless steel, copper, steel, brass, zinc base die castings and plated metals, is facilitated by the use of a compact soldering kit prepared by *Fusion Engineering*. Nine types of joining alloys in compact jars, together with a new methamine type dry fuel torch, are included in the selection. The K-9 Fusion Master Soldering Kit sells for \$11.

17) NEW DISSOLVER: *The Cowles Co., Inc.*, announces a new dissolver, Model 7VT, which works batches of 5 to 100 gal of material ranging in viscosity from 1 to 30,000 centipoises. The entire motor, bridge, and dissolver unit may be adjusted in height through a range of 11 in. by means of an elevating screw. It is designed for a wide range of production operations, but may be used for laboratory and pilot plant work. The price of the unit is \$795.

- * An Army Air Corps contract has been let for further investigation of electronic heating for hot machining. The contract was placed with an aircraft company, and involves, curiously, electronic heating of aluminum -- and possibly other metals -- for band sawing.
- * Aluminum has been extensively used in chassis parts for a heavy duty, special six-wheeled tractor for drawing a full trailer. Cross members of the chassis, the rear axle banjo type housing, and spring mountings were constructed with aluminum. The same truck also had aluminum disk wheels, not new, but to reduce weight.
- * A magnesium-alloy aircraft skin seven times as thick as the normal thin aluminum-alloy skin is being studied. The plane would require fewer fittings and fastenings, and dispense with internal formers and supports that take up precious fuel space in wings. Range of the F-80 jet Shooting Star has been increased 30 pct by these means.
- * British interest in pre-stressed concrete has extended to the construction of a multi-floor building in Edinburgh, Scotland. Pre-stressed concrete sleepers are being produced in three factories of Richard Costain, Ltd., and the Edinburgh project has aroused nationwide technical interest.
- * A national roster of scientific personnel similar to the one used in the last war will be established by the Office of Education, by agreement with the National Security Resources Board. The new unit, the National Scientific Register Project, will make studies of the nation's scientific manpower supply and recommend steps to increase the numbers of skilled personnel where needed.
- * A magnesium-cuprous chloride battery activated by tap water, which has long storage life, good low-temperature operation, and high service qualities at low cost, has been developed for high altitude meteorological research. It weighs 400 gm, operates at 65°F, has a capacity of 12 watt-hr, a unit size of 16 cu in., and is cheaper than the magnesium-silver chloride type.
- * American companies are placing large orders for steel in West Germany, and Germany is seeking for permission from Western Allies to boost steel production, now limited to 11,100,000 tons a year, and steel capacity, now at 14,500,000 tons a year. Twenty-five pct of current orders are coming from American firms.
- * Rocket-propelled anchors may solve landing problems in confined or rough terrain. Consisting of a 28 in. steel tube 1 3/8 in. diam, filled with rocket propellant, the anchor may be fired 18 in. into the ground at a 45° angle by a glider or small plane. Shock is absorbed by 200 ft of stainless-steel tape wound on a hydraulic brake.
- * An adjustable fork lift boom unit for handling sheet aluminum has been devised by an employee of the Naval Supply Center, Oakland, Calif. Built to fit the face plate of any automatic fork truck, the boom has a 180° swing, is 26 in. long, and has a set of clamps with an opening of 5 ft. The clamps, adjustable to fit any box, are suspended from the boom and are tightened by lever action.

The

Drift of Things as followed by Edward H. Robie

Start of a War

"My first intimation of trouble came early on Sunday afternoon, June 25, when I was called to the Embassy and told that the North Korean Army had crossed the border in force, 30 miles away. While this was the largest scale operation yet reported on the border, we were told that the South Korean forces would undoubtedly shoo them back to the north, as they had done repeatedly before.

"The evening news was encouraging and our military observers at the front reported that the enemy reconnaissance forces had been stopped. During the night, however, enemy infiltrations succeeded in cutting communications between Korean Army units,

A first-hand account, from an AIME member, of the first few days of the Korean War as experienced by a resident of Seoul was received late in July. The writer, Don L. Carroll, was for a time associate editor of Oil Weekly, and recently has been with the Oil and Gas Div., of the Dept. of the Interior. He was a member of the ECA mission to Korea. His wife, Catharine, and children were with him in Seoul when the war started.

and confusion began to develop. By 2:30 a.m. on Monday, the enemy forces had penetrated to within 17 miles of Seoul, and the Ambassador issued the order to evacuate wives and children to Ascom, about halfway to the port at Inchon. This assured easier evacuation from Seoul itself in case of eventual full evacuation of all Americans in Korea. By 6 p.m. of the same day, all dependents had been placed aboard the Norwegian freighter Reinhold in Inchon harbor. C rations, blankets, water, etc., were loaded aboard and the ship sailed for Japan an hour later. Fighter planes had been sent over from Japan to cover the whole operation and to escort the ship at sea.

"This protection was necessary because Communist planes had been strafing Seoul, Inchon, and the airports at Kimpo and Yongdongpo most of the day. One Red plane crossed Seoul after I had seen my brood safely aboard the ship and had returned home to do some hasty packing for myself. The plane had just shot up the Yongdongpo airfield about 3 miles from our house and had then come in over town at a low level with guns blazing away. I had run out into the backyard to watch for a moment, but when I noted that our house was in the line of fire and observed tiles flying off the roof, I immediately returned to my packing, and with some enthusiasm. I finished with my two bags (no more allowed) and prepared for a potential night's rest. I had a good start towards that objective when I was called back to the Embassy for around-the-clock duty. I could hear the battle noise north of town as I drove downtown.

"By 6:30 p.m. on Tuesday this operation was essentially completed and I had destroyed my files except for the contents of my briefcases, which represented all that I know, and which I therefore felt I must salvage. Who wants to be uninformed when he is supposed to be an expert? At 7 a.m. it was decided to evacuate nonessential mission personnel, including all women employees who had been kept on the job. Transport planes and fighter escort had been ordered from Japan to evacuate this group from Kimpo airport. In spite of air attacks at Kimpo during this operation, all of this group were safely evacuated to Japan by noontime. Three of Uncle Joe's angels

descended from the heavens to interrupt this operation, and continued right on down into the ground as a result of the interest of our own F-80 fighters.

"As the above group were being assembled at the Embassy, I was told that because of my family status I was eligible to be included, and that I could leave with the group 'if I insisted.' So, I stayed on the job. By 9 a.m. Tuesday, the Reds had moved up to the outskirts of Seoul, and with tanks. Since the South Koreans had run short of ammunition, had no anti-tank guns, and no effective staff control, we knew that we must now take it on the lam, as it were. More transport planes were requested from Japan, and at 10:15 we took to the busses to rendezvous with the planes at Kimpo. During our last hour at Seoul, I joined a team swinging sledgehammers at the Embassy. We wrecked the radio station, telephone exchange and message center, and completed destruction of files with incendiary bombs which we set off in the piles of papers in the parking lot.

"I remember thinking at that point that I would feel much more like being evacuated if I could only have a shower. I was practically out on my feet, since as my children insist, I am an old man now. Even so, I had the situation right in the hollow of my head, to the level of the hole that penetrates it.

"I did get the shower, a few minutes later—after our motor convoy got underway headed for Kimpo. It was a shower of bullets from a Yak fighter that buzzed us right on the main drag in town. No one was hit in our convoy, but Koreans on the other side of the street were mowed down like grass. We had expected to be attacked as we were making the slow crossing of the long Ham River bridge at the south edge of town since it had been jammed with refugees for hours, all heading south. It required 20 min to negotiate the crossing, after which we began to breathe abnormally again.

"By 1:30 p.m. our own fighters appeared over Kimpo and set to work shooting down or chasing away all enemy aircraft within ten miles of the spot. Lots of planes, lots of action, and lots of noise, but poor visibility because of clouds. The transport planes came in promptly after the way had been cleared and by 4 p.m. we were all on our way to Japan, which is very beautiful at the end of June.

"I have been told that Tiff distinguished himself on the ship, getting women and their luggage aboard and carrying small children up the ladder. He spent the night organizing and serving with the young men in white—a night bucket brigade, which was necessary because of the fact that there were only two single latrines on the ship, for some 700 women and children. Tiff and three of his strong-stomached pals carried the buckets from the live cargo hold to the rail and return, ad nauseum and ad infinitum. I was very proud of him. He wasn't spoiled after all—he just smelled that way.

"Maxie naturally spent his waking hours in the radio room, and enjoyed the whole voyage. Julie helped entertain the 'little' children. Catharine just held back on her respiration and kept her mouth closed—a difficult feat for her, and one that distinguished her from the run of women aboard, many of whom pulled out all the stops, pulled the rank of their husbands, and complained to the Captain about their accommodations. The gamut was just as long as regards the actions and reactions of the menfolk. I was amazed at some of them, and increased my respect for others, although few of the shots could have been called in advance.

U. S. Steel to Add 1,660,000 Tons Capacity

The United States Steel Corp. will increase its annual steel capacity by 1,660,000 ingot tons through improvements at Pittsburgh and Chicago plants of Carnegie-Illinois Steel Corp.

The new program will be completed as rapidly as possible, and should result in an increase of 1,215,000 tons in the annual steel capacity within a year. The remainder of the program, now in the engineering stage, will make an additional 445,000 tons capacity available by the fall of 1951. The major part of the program will get under way immediately, and the construction will not interfere with existing production.

This program for additional steel capacity can be installed in about half the time required for the construction of entirely new facilities. The additional capacity will result from the addition of improved facilities, as well as from certain alterations and rearrangement of existing equipment, and technological improvements, in steel and iron making.

The plants where steel capacity will be so increased are Gary and South Works in the Chicago district; Homestead, Edgar Thomson, Clairton, Duquesne, and Ohio Works (Youngstown) in the Pittsburgh district.

In addition, United States Steel plans to commence construction in 1951 of the first parts of its proposed new mill on the Delaware River south of Trenton, N. J., with a minimum ingot capacity of around 700,000 tons annually.

Pittsburgh Steamship Co. and Bradley Transporta-

tion Co., U.S. Steel Corp.'s iron ore and limestone carrying subsidiaries on the Great Lakes will order the construction of four vessels similar in type to the largest vessels now in use. Construction of the ships will be completed in time for the opening of the 1952 iron ore shipping season, which normally begins early in April.

Western U. S. Steel subsidiaries are planning expansion of finishing capacity. Geneva Steel Co., Geneva, Utah, will install facilities for producing 100,000 tons a year of hot rolled sheets, to be in operation by mid-Summer 1951. Columbia Steel Co. at Pittsburg, Calif., will add cold reduced sheet and tinplate facilities to the extent of about 215,000 net tons a year. These facilities also are expected to be in operation by mid-1951. Geneva currently supplies hot rolled coils for Columbia's cold rolling and tinplate mills, and after the expansion of facilities at both plants, sheet and tinplate capacity of the combination will be about 640,000 tons a year.

Columbia's new installations will include a continuous pickler, a four-stand 54-in. cold mill, an electrolytic cleaning line, an electrolytic tinning line, four coil annealing furnaces, a side trim and recoil line, and a continuous sheet galvanizer. The latter will be the first of its kind installed in the west. Plans are also underway for expansion of facilities of Columbia Steel Co. near Los Angeles, but details will be announced later.

British Tinplate Production Hampered by Acute Labor Shortages

British tinplate production is far below capacity because of severe shortages of labor, a handicap common to all pack mills in the British trade. British steel experts feel that annual demand for British tinplate will hold at about 800,000 long tons for many years to come, and may increase to as much as 1,000,000 long tons a year if export trade is fostered, as it has been since the war.

Tinplate production in 1937 in the United Kingdom was 957,800 tons, all of which was hot dipped. During the war production fell off sharply to a low of 258,700 tons in 1943; but the end of the war saw a steady rise in output to 571,700 tons of hot dipped and 37,752 tons of electrolytic tinplate in 1948. While 1949 figures are not available, indications are that output was well over 600,000 tons.

Present plans provide for the expansion of electrolytic tinplate capacity to about 500,000 tons a year. This will leave about 300,000 tons a year to be produced by hot dipping, or about what the present pack mill output is running. Thus, it is felt that all pack mills now in operation are likely to be needed for some years longer than was contemplated just after the war, when a general conversion to electrolytic production was anticipated.

Kaiser to Increase Aluminum Capacity

Kaiser Aluminum & Chemical Corp., Oakland, Calif., announced plans for increasing its aluminum pig production by 80,000,000 lb to a total of 340,000,000 lb a year. Immediately available is an increase of 40,000,000 lb of pig in the annual capacity of the reduction plants at Tacoma and Spokane. A complete seventh line of 140 electrolytic cells, reduction pots, will be installed at Spokane. The equipment was purchased from the Government aluminum plant at Riverbank, Calif., which has been idle since 1945, principally because of lack of low cost electric power.

Plans also call for an increase in capacity at the

Trentwood rolling mill at Spokane, which will enable the plant to produce 25 pct more sheet products; and a step-up in production at the company's bauxite refining plant at Baton Rouge, La. In addition, the Newark, Ohio, plant is completing expansions and diversifications for additional products, and has brought out an entire line of rod, bar, and wire products.

Kaiser Aluminum has also submitted to Government defense agencies a number of alternate plans to increase aluminum production at least 400,000,000 lb annually, as may be required by national defense emergency.

D. H. McLaughlin to Speak At Ohio Mineral Industries Conference

Ohio will take stock of its assets and evaluate its future at an Ohio Mineral Industries Conference, Sept. 25 and 26, in Columbus, sponsored by Ohio State University in conjunction with industry and the Ohio Department of Natural Resources. Horton H. Hampton, vice-president, Industrial Development, Nickel Plate Railroad, who will handle registration and program details, cited the mounting international crisis as a factor in the need for the conference. The meeting will enable top management in the various branches of the mineral industry to discuss problems of mutual interest, and acquaint industry with the research facilities available in the state.

Donald H. McLaughlin, president of AIME, and president of Homestake Mining Co., will be the principal speaker on the opening day program. Papers will be given by S. J. Bowers, assistant director of the State Department of Taxation, on the tax situation as it affects the mineral industries; Dr. Richard J. Lund of Battelle on the mineral marketing situation; C. V. Youngquist, chief of the Division of Water in Ohio, and Donald Gillis of Republic Steel Corp. on the future iron ore sources. Congressman John M. Vorys, member of the House Foreign Affairs Committee, will review the Korean situation, as dinner speaker at the Faculty Club.

Riverside Installs Two High Speed Strip Mills

Two of the most modern strip mills have been placed in operation at the Riverside, N.J., plant of the Riverside Metal Co. One is a United Engineering and Foundry Co., mill a fully automatic, four-high strip mill. Installation of this and a smaller mill represents the first step in the complete modernization of the company's strip mill capacity. Other new heat treating, rolling, and material handling equipment was placed in operation during July.

The larger mill, a $6\frac{3}{4} \times 23 \times 18$ in. four-high mill, embodies the latest automatic design from the standpoints of both manipulation and material handling. It will take coils weighing 700 lb and roll them at a speed of 200 to 600 fpm. It is capable of reducing 0.050 in. thick sheet down to 0.005 in., the number of passes depending on the work hardening properties of the metal and the finish temper specified.

A roller conveyor system surrounds the mill, so that as a coil is drawn through the mill, it may be sent back to the payoff reel over the conveyors or to the Drever furnace for process annealing.

Continued productivity of the mill is protected by three selectively timed howlers. One goes into action in the event of a rise in temperature at the motor generator bearings; the second is actuated by a drop in pressure in the mill lubricant; and the third sounds if there is any interruption in the flow of coolant. In addition, strip thickness may be controlled instantly and without stoppage of the mill with a flying micrometer.

The smallest unit is a $2\frac{1}{2} \times 9 \times 9$ in. four-high mill, with a top speed of 700 fpm. It rolls stock of a maxi-

mum thickness of 0.030 in. down to 0.003 in. This range, significantly, covers a large volume of Riverside production of copper alloys in thinner gages.

Both mills are capable of producing to finished tolerances much closer than those allowed under industry standards.

Eutectic Sponsors Prize Competition

Eutectic Welding Alloys Corp., New York, announced it would sponsor a \$1000 prize competition for technical papers on research and development in non-fusion welding. The contest opens Sept. 1, 1950 and closes May 31, 1951. The competition is open to welding engineers, researchers, metallurgists, instructors, university students and all others qualified to present basic principles of the art and science of non-fusion welding. Three prizes will be awarded: \$500 as first prize, \$300 as second prize, and \$200 as third prize.

Bush to Receive Fritz Medal

The John Fritz Medal Board of Award, consisting of four representatives each from the Founder Societies, ASCE, AIME, ASME, and AIEE, have unanimously voted to present the John Fritz Medal for 1951 to Vannevar Bush, for "outstanding scientific contributions to his Country and to his fellow men".

The medal was established in 1902, and is awarded "for notable scientific or industrial achievement". Walter Hull Aldridge, president of the Texas Gulf Sulphur Co., was the recipient of the 1950 medal.

Taconites Are Ready

by John V. Beall
Editor, MINING ENGINEERING



Mining ore by jet-piercing for the first experimental taconite concentration plant of the Erie Mining Co., at Aurora, Minn.

POLITICAL developments, the impact of Korean warfare necessitating immediate rearmament plans, and recent developments in mining taconites, a low-grade iron ore, have focused attention on their immediate exploitation to fill the gap of diminishing high grade reserves. The question of rich foreign ores vs. low grade development is past. Both sources are needed, and emphasis is on the immediate large scale utilization of taconites.

In the past three months several things have occurred that add to the taconite picture: (1) Pellets have been used successfully in the blast furnace by steel producers. (2) In Congress, HR 8512 was introduced by Congressman Blatnik of Minnesota to amend the lending powers of RFC to permit long term loans on basic mining developments, particularly the taconites, which may be needed for the strengthening of the national economy. (3) Walter S. Tower, president of the American Iron and Steel Institute, announced that American steel companies are planning expansion of 6,000,000 tons of steel-making capacities in the next few years. (4) The outbreak of war in Korea has obliged the United States to rearm and make plans for a semi-permanent defense establishment to which 10 to 12 pct of the national income will be budgeted. (5) Startling new advances have been made in The Linde Air Products Co.'s jet-piercing drilling.

The United States is now confronted with the problem of increasing steel capacity and at the same time of insuring enough iron ore to supply this increase as well as make provision for the rapidly decreasing supply of rich iron ore on the

Mesabi Range. Taconites, the low grade iron ore at the east end of the Mesabi Range, of which there are literally billions and billions of tons, are the immediate answer.

According to the *Wall Street Journal* on July 24: "The Reserve Mining Co., backed by such steelmakers as the Armco Steel Corp., Wheeling Steel Co., and Republic Steel Corp., is reported ready—as soon as the pending bill clears (HR 8512)—

For a comprehensive review of current and future conditions in relation to iron ore supplies for the American steel industry, see **Journal of Metals**, February, 1950—"CERRO BOLIVAR—Saga of an Iron Ore Crisis Averted." Domestic reserves of low grade ores and concentration investigations are described.

to seek a \$100 million federal loan to build a taconite processing plant at Beaver Bay, Minn., to produce about 5 million tons annually of 60 pct to 65 pct in iron ore . . ."

Experimental work indicates that pellets may be the final form, rather than nodules, agglomerates, or sinter. At Ashland, Ky., the Reserve Mining Co., which has obtained a lease from Mesabi Iron Co. on its holdings, built a pelletizing plant that has been in operation since last spring. Sufficient pellets have been accumulated to start test runs in the blast furnace, starting with low percentages of pellets. Recent charges up to 70 pct of pellets have been handled satis-

factorily in the blast furnace.

The Oliver Iron Mining Co. is going ahead with the construction of its experimental plant at Virginia City to determine whether agglomerates, nodules, pellets, or sinter is the best product for its fine ores and possibly concentrates from its future taconite developments.

The Pickands Mather & Co., in which Bethlehem Steel and Youngstown Sheet & Tube have an interest, formed the Erie Mining Co., to mine the taconites at the west end of the Mesabi Iron Co. holdings at the east end of the Mesabi Range. Here, an experimental mill of 2000 tons daily capacity has been operating for more than a year to study the various production problems of crushing, concentrating, and pelletizing. The results of these studies will be used for the design and location of a large scale taconite processing plant.

Shipments of pellets have been made to the Zenith furnaces of the Interlake Iron Co., but smelting results are not available yet. At Lebanon, Pa., studies on pelletizing are being conducted by Bethlehem Steel Co.

Improved Jet-Piercing

One of the factors that makes the mining of taconites economic and feasible has been the development of the Linde Air Products Co.'s jet-piercing drill. The magnetic taconites are extremely hard. Formerly, no more than 10 to 15 ft a day could be drilled with a churn drill. Jet-piercing literally can burn holes in the taconites at an average speed of 17 fph, but improvements in burner heads will probably increase this figure. Present nominal 6-in. diam jet-pierced holes are a large percentage +8-in. diam. Jet pierced reaming of these holes, presently under study, will make possible the use of an 8-in. explosive charge instead of the present 6-in. The increased powder charge improves breakage of these larger holes; far better than breakage in the early 6-in. holes, which gave around 30 tons per ft of hole. A complete test unit of the Linde Air Products Co. jet-piercing drill has been in operation at the Erie Mining Co.'s taconite operation for the past year or so. This remarkable innovation in drilling hard ground, still being improved for more effective performance (deeper and larger holes), is no less revolutionary in the taconites than was flotation in the case of the porphyry coppers. The impact of jet-piercing will in time make itself felt.

No costs of jet-piercing have been published, but it is reasonable to expect something less than \$3.00 per ft. Due to the speed of drilling, however, the Linde device can perform the equivalent work of ten churn drills in a single shift. This means some large indirect economies in operation, such as being obliged to provide housing for one-tenth of a normal drilling force, a large capital saving in a region like northeast Minnesota where there is no existing housing for the new personnel. Jet-piercing is revolutionary in its impact on lowering mining costs of taconites. With negligible stripping and reduced oxygen cost for piercing by building a liquid oxygen plant on the range (or the use of lower purity oxygen than the present 98 pct being used), tac-

onites of Reserve Mining Co. and Erie Mining Co. should be mined at no greater cost per ton than the open pit porphyries; namely, 25¢ per ton.

It is possible only to speculate as far as costs of producing taconite concentrates are concerned. Presumably they will not exceed production cost per unit of iron content of product of present underground ores. For an estimate of costs and profits, reference is made to the Congressional Record on May 23 wherein a letter from Arnold Hoffman is entered by the Honorable John A. Blatnik.

The following is a quotation from a portion of the letter: "The following estimate is based on an assumed concentrating ratio of 2.75 tons crude ore to 1 ton of pellets or sinter and costs determined from presently available data and figures of comparative open pit operations:

Mining and milling per ton concentrate,	
2.75 x 65¢	\$1.79
Pelletizing, per ton concentrate	1.00
Local and State taxes, per ton concentrate	.15
Royalties, 8¢ per ton crude ore, 2.75 x 8¢	.22
Haulage, Babbitt to Beaver Bay, 2 tons at 1¢ per ton mile, 55 miles	1.10
(Up to 35 pct gangue eliminated at mine)	
Amortization, 18¢ per ton crude ore,	
2.75 x 18¢	.50
Haulage, Beaver Bay to Ohio port	1.16
Total cost per ton pellets	
Value ton 51 pct Fe ore at Ohio port	\$7.70
Value ton 65 pct Fe ore at Ohio port at 15.1¢ per unit above 51 pct	9.81
Operating profit, per ton pellets	
Operating profit, per ton crude ore	\$3.89
	\$1.40

"This \$1.40 profit figure makes no provision for a possible premium on pellets. A substantial premium is possible, however, since pellets are preferable to direct shipping ores in the furnaces. Not only is the blast furnace provided with a selected feed, hard and higher grade, resulting in greater unit production per ton of charge with consequent lower cost, but the introduction of pellets in the open hearth can reduce scrap requirements to a level where 'home' scrap from fabricating plants should meet such needs. Pellets make an excellent substitute for scarce lump ore, and with other advantages can easily command a premium from the hard pressed steel industry. In this event, profit estimate submitted might be revised upwards.

"It must be remembered, also, that there is an important saving in the transportation of pellets containing 65 pct Fe as compared to the lower grade direct shipping ores."

The capital investment for development of taconite is admittedly large, \$15 to \$20 per ton of pellets, but this compares with the cost of building a fleet of ore vessels and other development work in isolated or uninhabited areas to supply the needs of our steel industry from abroad. Especially with the uncertain international picture and the threat of war, it is of prime importance to the security of the United States that an adequate supply of iron ore be developed within our own borders.

Charging Practice:

Its Effect on Open Hearth Output

by William Schwinn

TO obtain a more uniform charge and faster charging time at Keystone Steel & Wire Co., the time of the scrap preparation crew and the stockers is scheduled to make the best use of the scrap available.

Previously, the use of the scrap preparation crew in loading No. 2 heavy melting scrap in charging boxes lying on the ground was described. This is believed the most satisfactory way to obtain the highest weight per buggy.

During May and June, 1949, two furnace operation was in effect the greater part of the time and one buggy of coke (3900 lb) was charged with 80,000 lb of iron. The average charging time was 5 hr, 55 min, averaging 57 buggies of scrap and iron per charge. The average production of ingot for this time was 12.42 tons per hr. The No. 2 heavy melting loaded in boxes on the ground averaged 760 lb heavier per buggy than those loaded on the buggy.

During July, 1949, on three-furnace operation, 142 heats were charged, of which 31 pct used one buggy of coke (3800 lb) with 80,000 lb of iron with an average charging time of 6 hr, 14 min, averaging 55 buggies of scrap and iron. No coke was used on 69 pct of the charges but 33 pct iron was charged, with an average charging time of 5 hr, 34 min; averaging 37 buggies of scrap and iron per charge. The No. 2 heavy melting loaded in boxes on the ground was 900 lb heavier than when loaded on the buggies (5253 to 4351 lb, respectively). The average production in July was 12.39 net tons of ingot per hr.

In September, 1949, the scrap loading personnel was changed by decreasing the size of the scrap preparation crew and using the men to add to the stockers. A scrap foreman was assigned to each turn to supervise loading all material used to charge the furnaces spotted by the stock foreman. During that month, no coke was used and 36 pct iron was used, of which 20 pct was mold scrap, 10 pct cast iron carwheels, 3.5 pct pig iron, and 2.5 pct miscellaneous cast. No. 2 heavy-melting loaded on the buggies accounted for 10 pct of the steel charge, averaging 4290 lb per buggy; 14 pct was No. 1 heavy-melting averaging 5880 lb per buggy. The remainder was 7 pct turnings, 2 pct No. 2 bundled sheets and miscellaneous (mill scrap, No. 2 bushelings, etc.). Average charging time was 5 hr, 34 min, averaging 46 buggies of scrap and iron per charge. Ingots produced totalled 12.66 net tons per hr.

William Schwinn is associated with the Keystone Steel & Wire Co., Peoria, Ill.

The use of oxygen would be impractical unless it is possible to keep the average charging time below 5 hr, 30 min. The average charging time, fast and slow, of five heats was taken to show that by decreasing the charging time through the use of heavier scrap and good iron, ingot production is greatly affected when using oxygen. On five heats charging in less than 4 hr, the average charging time was 3 hr, 42 min, using 36 buggies of scrap and iron, consisting of 41.6 pct iron, 40.7 pct No. 1 scrap, and 17.7 pct miscellaneous (mill scrap and bundled sheets). The average tap to tap time was 10 hr, 11 min, and ingots produced was 15.91 net tons per hr using 13,000 cu ft of oxygen per heat. Five heats averaged 6 hr, 32 min, using 53 buggies of scrap and iron consisting of 30.3 pct iron, 8.2 pct No. 1 scrap and 35.1 pct No. 2 scrap and 26.4 pct miscellaneous. The average tap to tap time was 13 hr, 25 min, and ingot production was 12.25 tons per hr using 16,000 cu ft of oxygen per heat.

October, 1949, was an all-time record month. A total of 192 heats of all grades were charged and tapped using a 31 pct iron charge, consisting of 15 pct mold scrap, 5 pct cast iron carwheels, 2 pct pig iron, and 7 pct miscellaneous cast. The steel charge consisted of 20 pct No. 2 heavy-melting, averaging 4290 lb per buggy, 14 pct No. 1 heavy melting averaging 6080 lb per buggy, 6 pct No. 2 bundled sheets, 6 pct turnings, 14 pct blooming-mill crops, and the rest miscellaneous. The average charging time was 5 hr, 30 min, using 44 buggies of scrap and iron per charge. Ingot production for this month was 14.49 net tons per hr.

Realizing that ample switching facilities are important in obtaining a low average charging time, a 65-ton diesel electric locomotive was purchased to serve the open hearth along with a 70-ton steam locomotive. These two engines were put on a 24-hr schedule to service the open hearth floor and deliver ingots to the soaking pits. They are under the direct supervision of the stock foreman. A further reduction in charging time was realized by the addition of a scrap loading foreman, thus allowing the stock foreman to give more attention to the switching needs. Not enough time has been available to make a thorough check of what has been accomplished but it is felt that charging time and production have been improved. During the last 17 days of March, 1950, 90 heats of all grades were tapped with an average charging time of 5 hr, 5 min. A new higher average of 14.84 net tons per hr of ingots produced was obtained during this period, with an average consumption of oxygen of 17,900 cu ft per heat.



Fig. 1A (left) Bakelite ($\times 15$)
B (right) Molybdenum ($\times 100$)

Metal Fractures Modeled By Other Materials

by A. M. Sullivan
and
J. A. Kies

IN interpreting the features observed visually on fractured surfaces, it is important to distinguish between markings characteristic of the material under observation and those characteristic of fracture itself.

Examination of surfaces of plastics fractured by various methods has indicated that these materials may serve as convenient models to study the morphology of fracture^{1, 2, 3}. However, a basic understanding of fracture mechanisms can be evolved only from those features which are common to all materials which break. For this reason, it seems pertinent to illustrate the similarities observed to date. Fig. 1 to 7 are provided for this purpose, although some have appeared separately as indicated.

In Fig. 1A the fan-shaped pattern results from the impact of a nail punch, which initiated fracture at this point in the Bakelite specimen. The same type of pattern is seen on the molybdenum surface of Fig. 1B, indicating fracture initiation here also. This feature has been remarked by De Leiris⁴. Within polycrystalline material, it must be noted that regardless of the position of the outside force with respect to the specimen, alterations in the stress distributions will cause initiations of fracture in variously oriented grains at variance to the direction of overall fracture.

Fig. 2 contrasts Lucite (A), and a high manganese steel, (B). The parabola shaped elements indicating separately nucleating fracture are identical even to the circular area at the focus showing the position of the operative flaw^{1, 2}.

Fig. 3 shows how changes in velocity are translated into surface features. Fig. 3A shows a face spall from heavy armor. The smooth and rough bands, indicating changes in fracture velocity², find their counterpart in similar regions of Fig. 3B, which shows the back of a sheet of film from which the emulsion has been stripped at varying speeds¹.

Fig. 4 illustrates this same feature in another way. In Fig. 4A a 0.25 in. piece of cellulose acetate was loaded in a tensile machine and unloaded at regular increments of crack extension. These unloadings correspond to the spaced curved lines in the photomacrograph. By analogy, Fig. 4B, a strip tensile specimen of silicon

ferrite, which was broken in tension without unloading, was subject to velocity changes during fracture since these same curved markings appear in the surface of a cleavage type fracture.

Similarly, one may recognize such regions in Fig. 5, where fractures of Lucite, glass, coal and molybdenum are available for comparison.

Finally, in Fig. 6 are examples of so-called explosive type of fracture. This occurs when separately initiating discrete elements of fracture, occurring ahead of a main fracture path, join to separate the material. Here can be seen wheels rather than parabolas, since the speed of fracture of these separately nucleating elements is the same in all directions and greater than that of any main fracture which might overtake them^{1, 2}. In Fig. 6 such a wheel is seen in Lucite (A); in tool steel (overheated and slowly cooled before fracture) (B); in Lucite (C) a series of separate wheels formed under shock conditions, which have not joined one another on the same level as yet; and the shattered surface of a hardened steel bearing (D) shows the same type of configuration.

The similarities displayed are emphasized so that it may be recognized that many fractures in various materials occur by the same basic mechanism, the observed differences being the result of the scale of the operations. This mechanism consists in the opening and joining up of initially independent elements of fracture which start ahead of and finally determine the main fracture path. The individual starts and groupings of these elements are influenced by flaws, velocity changes, and unloading stiffness and are reflected on a larger scale in the overall appearance of the fracture whose grosser elements have been produced in the same general way.

References

¹ J. A. Kies and A. M. Sullivan: "Fracture Markings in Plastics". Presented at American Physical Society Meeting, New York, February, 1950.

² J. A. Kies, A. M. Sullivan, and G. R. Irwin: "Interpretation of Fracture Markings," *Journal of Applied Physics*, 21, July, 1950.

³ J. A. Kies: "The Origin and Interpretation of Fracture Markings in Plastic Materials". Presented at Massachusetts Institute of Technology, Conference on the *Mechanical Properties of Plastics*, June, 1950.

⁴ H. de Leiris: "l'Analyse Morphologique des Cas-sures," *Association Technique Maritime et Aeronau-tique Memoire*, 801, 1945.

Fig. 2A (left) Lucite ($\times 500$)

B (right) Manganese Steel ($\times 40$)

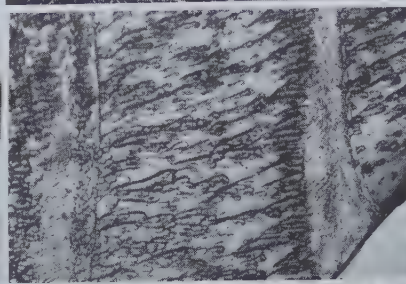


Fig. 4A (left) Cellulose Acetate ($\times 51$)

B (right) Silicon Ferrite ($\times 1000$)

Fig. 3A (left) Armor Spall ($\times 0.5$)

B (right) Stripped Film Back ($\times 100$)

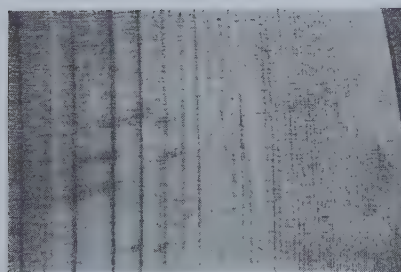
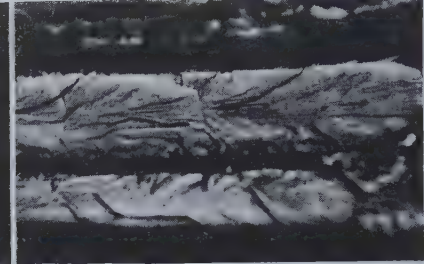
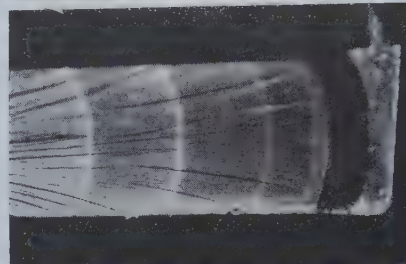


Fig. 5C (left) Coal ($\times 500$)

D (right) Molybdenum ($\times 500$)

Fig. 5A (left) Lucite ($\times 100$)

B (right) Glass ($\times 100$)

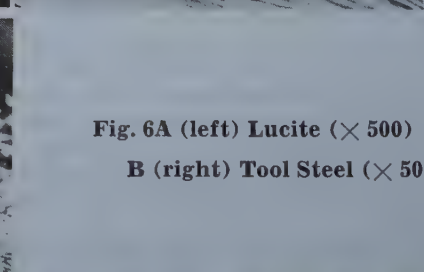


Fig. 6C (left) Lucite ($\times 20$)

D (right) Steel

Bearing ($\times 20$)



A New Corrosion Test

by Thomas E. Lloyd
Editor, JOURNAL OF METALS

THE Alternate Condensation method for testing corrosion resistance of a metal or the corrosion protection provided by a coating on a metal appears to offer a technique more comparable to normal weather corrosion action than any yet devised. Unlike any of the generally used corrosion resistance testing methods, it uses a condensate rather than a dip or a spray to effect the corrosive action on the metal.

Salt spray tests, universally used, have been accepted as a standard method of measuring continuity of surface coatings rather than corrosion protection. Such tests are subject to certain limitations. They are applicable directly only where sea or salt air is a factor. Other types of tests are in use in various procedures for corrosion testing, such as artificial rain. The latter, however, will frequently bridge over pinholes so that no particular effect is shown, even though the surface may have imperfections. Spray washes as used in some weathering machines frequently serve to clean the surface of the test sample, washing away the corrosion products and decreasing the corrosion rate.

The Alternate Condensation method has none of these particular limitations. Dew is water condensed from the atmosphere. Water in the form

of a thin layer of dew or condensate is water of maximum corrosivity in most intimate contact with the surface of a sample. It actually searches out pinholes, and never bridges them.

Sam Tour & Co., New York, worked out this Alternate Condensation corrosion testing method, which appears to fulfill the need for a corrosion testing technique that closely approximates actual weathering conditions in areas not affected by salt spray or salt air. It accelerates to about a 4 min time cycle the weathering action of a full day in any area where the day to night temperature gradient is sufficient to cause dewing.

One of the main features of the testing method is its adaptability to a variety of atmospheric conditions. Specimens can be exposed to varying temperature and varying humidity conditions, as well as to air carrying desired contaminants in controlled quantities. Furthermore, the equipment is inexpensive and quite easily assembled.

The apparatus consists of a turntable, upon which samples to be tested are mounted, and chambers or tunnels through which the turntable revolves so that samples are exposed to the atmospheric conditions of each chamber. In one chamber, there is directed against the samples a

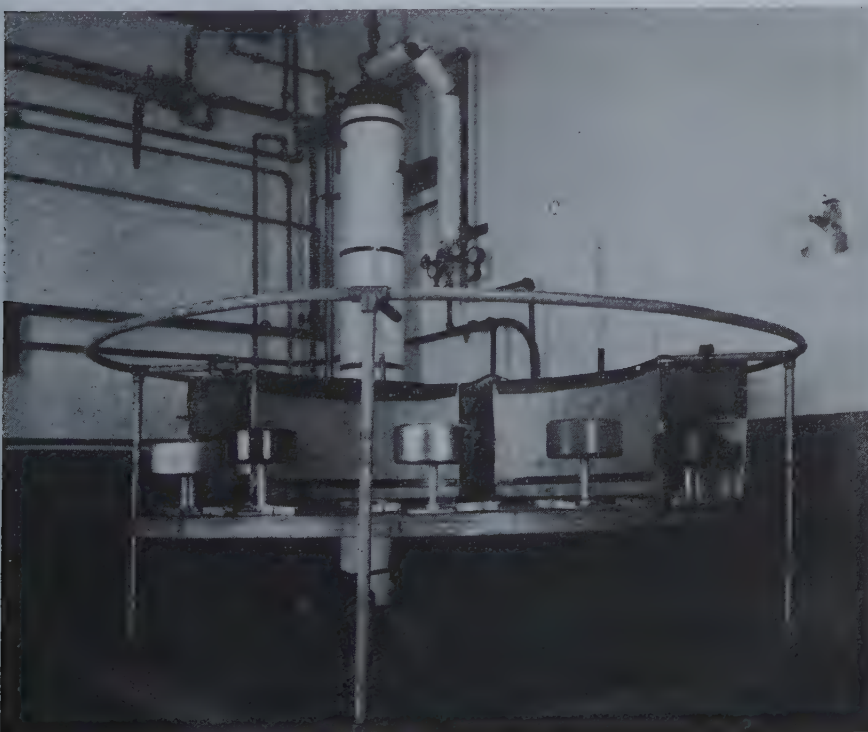


Fig. 1—The Alternate Condensation corrosion testing machine is inexpensive to construct, and duplicates atmospheric conditions. The dewing or condensing chamber is to the left and the drying chamber is to the right. Similar chambers can be added for the use of atmosphere contaminants such as SO_2 and H_2S . The drum-type specimens have various finishes, which are being tested.

stream of air that has been saturated with water vapor at a thermostatically controlled temperature of 160° to 170°F. As the sample is dry and relatively cool upon entering this chamber, contact with the warm, humid air causes it to be covered rapidly with a film of condensed moisture. This condensate remains on it as it passes through the chamber.

In the second chamber, air at an approximate temperature of 70°F and a relative humidity of 25 pct is directed against the sample. This air condition is obtained by compressing air to 75 to 100 psi and then passing it through an after-cooler and separator to bring it back to room temperature and remove the condensed moisture. The cooled and dried air upon expanding against the face of the test panel, rapidly absorbs heat and moisture from it.

The turntable used for mounting the specimens is driven at a predetermined speed by a geared motor. A controlled hot water tower is used to produce the warm saturated air at any desired temperature, and a water-cooled condenser is used to cool the dry air for chilling the samples. If warm air drying is desirable, an electric heating element can be provided for a drying fan, and chilling can be subsequently handled. If sulphur dioxide or hydrogen sulphide, or other contaminants are desired, they can be introduced in a chamber arranged to follow the condensing chamber.

After drying and cooling, the sample again passes into the first chamber where it again condenses a film of moisture on its surface, and the cycle is repeated. The complete cycle can be carried out every 4 min or 15 times an hr. These alternate exposures to cool dry and warm humid conditions cause rather rapid corrosion of the test specimens, and are more clearly an accelerated reproduction of the actual corrosion conditions most commonly met than most other accelerated corrosion tests.

Samples of various sizes and shapes can be handled equally well. Fig. 1 shows a series of drum type specimens mounted in the testing equipment. In another test, a sample of steel was tested that was triangular in shape and measured about $\frac{1}{8} \times \frac{1}{4} \times \frac{1}{4}$ in. It was first mounted in Lucite so as to expose one surface, which surface was ground to remove hardness impressions that had been made previously. It was then polished with No. O paper. After four control samples had been prepared, all specimens were cleaned with carbon tetrachloride and methyl alcohol, and then exposed to the test.

The specimens were exposed on the basis of a 4 min cycle, with the warm air at 120° to 130°F and 100 pct humidity. They were fan dried at room temperature and chilled with dry air at 60°F. This cycle of exposure was continued for 4 hr or 60 complete cycles. Fig. 2 shows the five samples after the exposure test, the control samples being those of rectangular shape and the test sample being the small triangular piece.

This method of corrosion resistance testing permits many specimens to be placed on the turntable. As in all corrosion testing, however, specimens must be properly prepared and thoroughly cleaned. In one particular exposure test made at the laboratories of Sam Tour & Co., the following specimen preparation and testing tech-

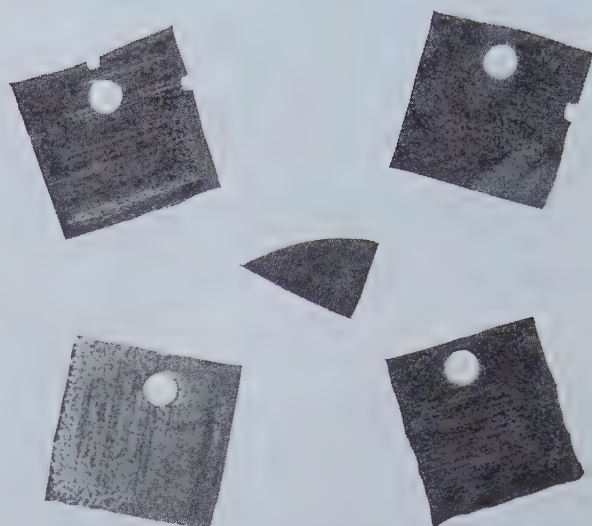


Fig. 2—The enlarged triangular sample shown in the center was actually about $\frac{1}{8} \times \frac{1}{4} \times \frac{1}{4}$ in. in size, and for corrosion testing was mounted in Lucite. The four other specimens were control samples.

niques were used.

Plates, 3x4 in. and 3x6 in. were cut from 0.030 in. thick steel sheet. Each plate was surface ground on one face to remove all surface film and oxides, carefully weighed, and then coated with a rust preventive solution until all specimens were ready for exposure. When ready for exposure, specimens were degreased in carbon tetrachloride solution and mounted on the turntable.

The specimens were visually examined every 24 hr for the first ten days, and weekly thereafter. After 35 days of continuous exposure, the samples were cleaned to remove the corrosion products. This cleaning consisted of scrubbing with a bristle brush; washing in warm water; and cleaning with a steel wire brush in a 5 pct sulphuric acid solution containing 2 ml of Rodine per liter of solution. The samples were then reweighed and the loss in weight, in milligrams per square decimeter per day (mg per dm² per day), and inch penetration per year, was calculated.

In addition to these Alternate Condensation tests, salt spray examinations and many months of outdoor exposure tests were made on this same series of steels. These steels ranged from ordinary carbon steels to 17 pct chromium stainless steel, and included certain special analysis steels that were being tested for their alleged high resistance to surface attack.

The results of these examinations showed that the special analysis steels were not superior to other carbon grades as far as resistance to corrosion attack on the surface was concerned, and it was quite evident that the Alternate Condensation method of testing bore out these findings as clearly and as conclusively as any of the other methods of testing.

While not a cure-all for difficulties encountered in procedures of corrosion resistance examination, the Alternate Condensation technique offers the laboratory technician a new tool and one that will approximate actual conditions caused by weather exposure. Furthermore, the technique permits acceleration of these conditions sufficiently to make the method adaptable where time is short and concrete evidence is required.

NITRIDING—

Effect on Fatigue Strength of Stainless Steel

by V. T. Malcolm

and

S. Low

The Malcomizing process is a surface hardening process developed and patented by the Chapman Valve Mfg. Co., Indian Orchard, Mass. This process is an exclusive nitriding process primarily developed to permit surface hardening of both the austenitic and ferritic stainless steels. The stainless steels cannot be successfully nitrided by the conventional nitriding process because of the chemically inactive film of chromium oxide on the surface of the work. It is necessary to reduce this film by means of nascent hydrogen before the surface of the material will combine with nitrogen.

There are many applications of stainless steel that subject the part to repeated full, or partial, reversals of stress. The choice of stainless steel for these service conditions is usually based on the materials resistance to other of the service conditions such as corrosion, oxidation, etc. Unfortunately, neither the austenitic nor straight chrome stainless steels have particularly high fatigue strengths, especially in the notched condition.

Nitriding the stainless steels is the most satisfactory means of increasing the fatigue life without materially sacrificing the other desirable properties of the base material. This increase in fatigue life is attributed to the compressively stressed case on the surface of the piece. X-ray diffraction measurements of this stress indicate it to be in the order of 38,000 psi. Fig. 1 illustrates the stress distribution in the case of a nitrided material.

The case depth of Malcomized stainless steels is 0.007 to 0.010 in. for the austenitic stainless steels and 0.014 to 0.020 in. for the ferritic stainless steels. The case hardness is approximately 1050 Knoop hardness number. Fig. 2 is typical of case hardness surveys for AISI Types 304 and 410 Malcomized stainless steels. The compositions of the steels tested are given in Table I, and heat treatments and room temperature physical properties are given in Table II.

The effect of nitriding on the fatigue strength

of stainless steel has been investigated by means of three types of tests, the rotating beam fatigue test, the *Eden-Foster* repeated impact test, and the *Rayflex* vibratory fatigue test. The rotating

Table I—Chemical Compositions of Steels Tested, Pct

Designation	Type 410	Type 304
C	0.09	0.05
Mn	0.40	0.58
Si	0.32	0.52
P	0.02	0.03
S	0.01	0.01
Cr	12.31	18.70
Ni	—	9.29

Table II—Heat Treatment¹: Type 304-1950° F Anneal; Type 410-1580° F, Oil Quench

Designation	Room Temperature Physical Properties			
	Type 304	Type 410		
Designation	Annealed	Malcomized		
Tensile Strength, Psi	89,850	87,500	130,150	118,750
Yield Strength, Psi	51,900	47,600	109,300	95,360
Proportional Limit	14,000	14,600	47,500	46,000
Elongation in 2 in., Pct	56.0	56.0	20.0	18.0
Reduction of Area, Pct	70.0	66.0	60.0	52.0
Bhn, Kg per Sq mm	170 ²	170 ²	321 ²	280 ²
Keyhole Charpy Impact, Ft-Lb	68.0	50.0	25.7	29.5

¹ U. S. Patent Nos. 2,262,690 and 2,218,973

² Core

³ Case

beam fatigue tests were run on both notched and unnotched bars in a R.R. Moore high speed fatigue testing machine. Typical "S-N" curves for Types 304 and 410 steels are illustrated in

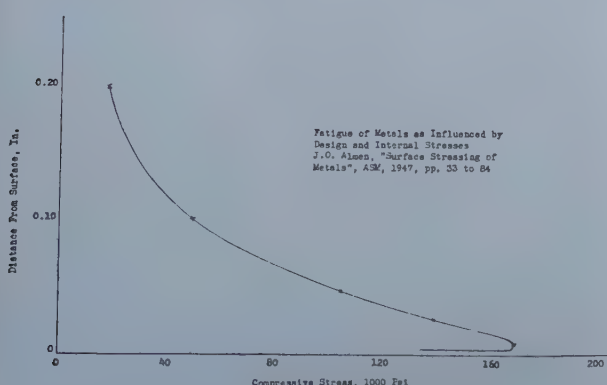


Fig. 1—Surface Stress Imposed by Nitriding.

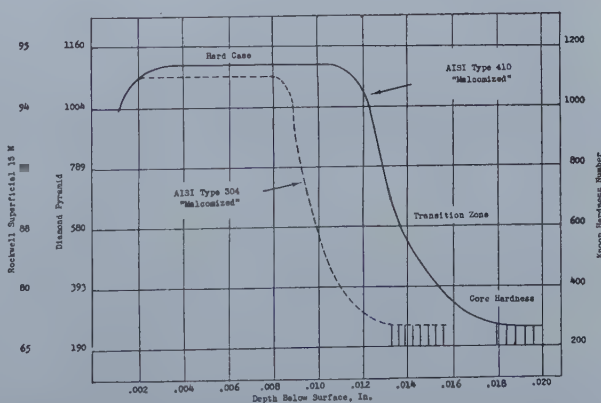


Fig. 2—Transverse Case Hardness of Stainless Types 304 and 410, Malcomized.

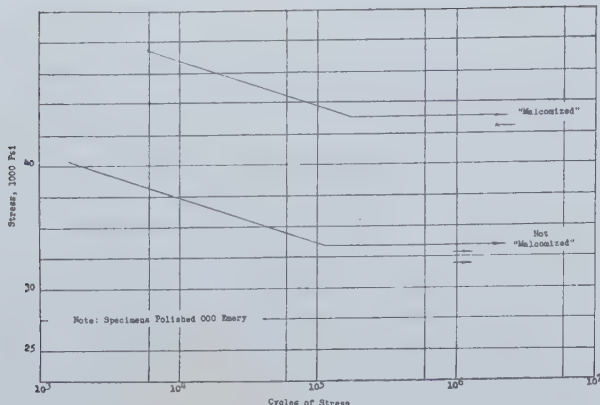


Fig. 3—Fatigue Test AISI Type 304, Annealed.

Figs. 3 to 5. The effect of the compressively stressed case may be readily noted.

The effect of the case on Type 304 is revealed in Table III, which contains data obtained from two vibratory fatigue tests. The effect on the core of aging at the time and temperature of the surface hardening treatment, with respect to energy absorbed in the repeated impact test is clearly shown in Table IV, which with Fig. 6 illustrate the effect of the core on repeated impact type tests. The effect of surface hardening

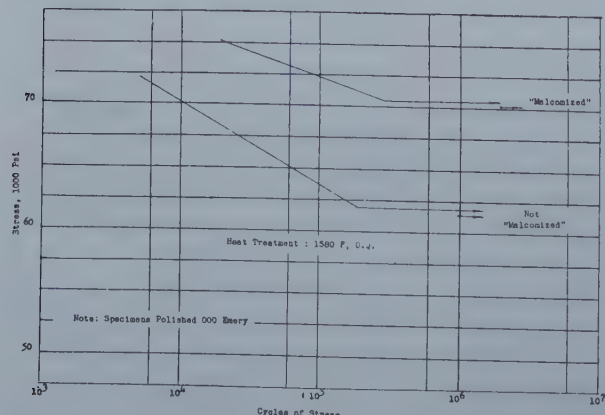
Table III—Rayflex Fatigue Test: Type 304 Cold Rolled Sheet, 0.031 in. thick

	Not Malcomized	Malcomized
Extreme Fiber Stress, Psi	40,000	40,000
Frequency of Vibration, Cps	58	58
Specimen Dimensions, In.	0.031 x 1/2 x 2.88	0.031 x 1/2 x 2.88
Cycles to Failure	1,300,000	10,000,000 (No Failure)

on this type of test is more complex. In general, the case effect is overshadowed by the core effect. From the hardness data plotted in Fig. 6 for Type 410, it is apparent that the effect of the surface hardening treatment is approximately equivalent to a 1580°F oil quench followed by a two hour draw at 1150°F with respect to the total energy absorbed in the repeated impact test.

Although there is some carbide precipitation during surface hardening of Type 304, there is

Fig. 4—Fatigue Test AISI Type 410, Heat Treatment: 1580°F, O. Q.



V. T. Malcolm is Director of Research and S. Low is Research Engineer for the Chapman Valve Mfg. Co., Indian Orchard, Mass.

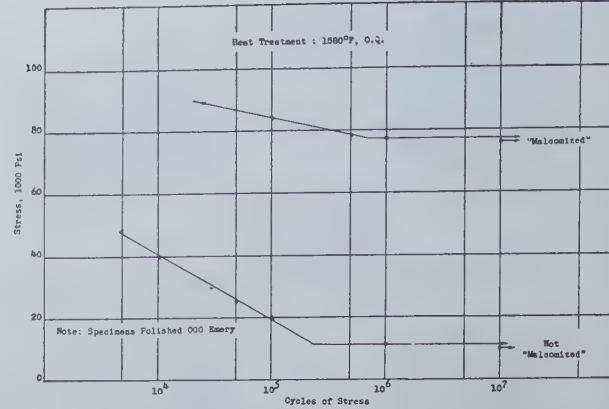


Fig. 5—Fatigue Test AISI Type 410, Heat Treatment: 1580°F, O. Q. Notched Bar.

no conclusive evidence of sigma formation. The deleterious effects of this carbide precipitation may be overcome by the use of columbium stabilized 18-8.

Generally speaking, the fatigue strength of unnotched Type 410 material may be increased 15 pct by means of surface hardening. A corresponding increase of fatigue life of 30 pct may be obtained for Type 304 material by surface hardening. The fatigue strength of notched Type 410 material may be increased 750 pct by means of

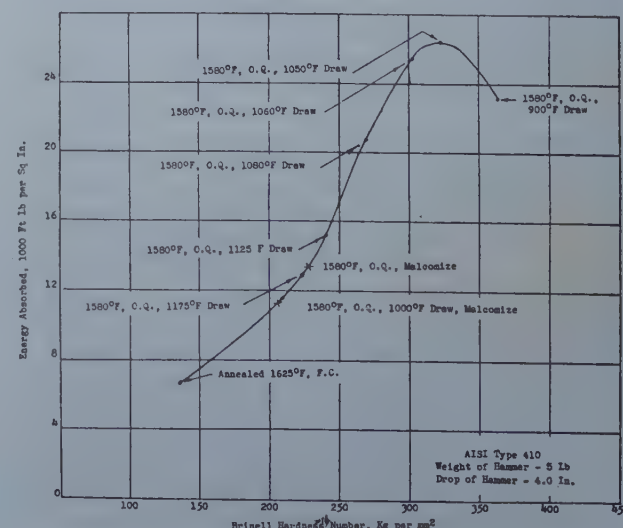
Table IV—Eden-Foster Repeated Impact Test Results: Type 304 Material

Thermal History	Energy Absorbed, Ft-Lb per Sq In.
Annealed	6740
Surface Hardened	4890
Aged at the Time and Temperature of the Surface Hardening Treatment	6460

surface hardening.

There have been many applications of the surface hardening process to stainless steel parts to improve their fatigue life. Notable among these are collector rings for aircraft engines, expansion joints for the exhaust of internal combustion aircraft and locomotive engines, flexible exhaust ducts for jet aircraft engines, sucker rods for oil pumps, steam turbine blading and many others.

Fig. 6—Eden Foster Repeated Impact, AISI Type 410.



Flameproof Clothing Guards Against

Burns From Hot Metal Splash

A NEW flameproofing chemical for cotton textiles was accidentally discovered by the Treendale Laboratories, Inc., Mars, Pa. Called "Permaproof 300," the compound is unaffected by repeated washings and has undergone stringent tests by Jones & Laughlin Steel Corp., Pittsburgh.

The compound originally under investigation for the prevention of mildew in textiles, accidentally spilled over on a fragment of cotton cloth. Some time later, an inquisitive technician happened to hold the piece of saturated cloth over an open flame and discovered that it would not burn.

Chemists of the B. F. Goodrich Chemical Co., developed one of the basic ingredients of the compound and "Permaproof 300," after 10 years of research, is ready for commercial use. Not only can cloth treated with the compound be subjected to repeated commercial washing without any effect on its flameproof quality, but the cloth retains much of its softness and porosity, does not become tacky, color is not affected, and the chemical contains no skin poisons or irritants. The treated cloth is shrink resistant, and will

not mildew. Processing adds to the cloth durability and although cloth will char when exposed to intense flame, it does not burn or glow after the source of heat is removed.

Always searching for new safety ideas, Jones & Laughlin Steel Corp., one of the country's largest steel makers, had cotton work clothing treated with the compound. For years cotton cloth treated with a soluble flameproofing has been available, but the flameproofing is effective only as long as the material is not washed or exposed to moisture. For a year the J&L safety department subjected clothing treated with the new compound to extremes of operation hazards. After hanging up treated work trousers and pouring molten metal over them, welding within inches of the jackets, and putting the torch to the cloth, safety men were convinced that the cloth was flameproof.

The haunting fear, facing many industrial safety men, that a spark or splash of molten metal might set fire to the clothing of exposed workmen, should gradually disappear with the expanding use of flameproofed clothing.



Fig. 1—These flameproofed trousers were subjected to several severe washings with the most caustic materials and then completely dried before the test was made. After the ladle containing liquid metal at 2800°F from the open hearth was emptied there was no flame or glow (Left).

Fig. 2—The trousers are slightly charred but intact after one of the toughest tests that could have been conceived (Above).

Metallurgy Behind the Decimal Point

by Earle E. Schumacher

Institute of Metals Division Lecture

IN a laboratory devoted to the furtherance of the science of communication, the breadth and variety of the problems encountered are challenging to a metallurgist. In my own long association with the Bell Telephone Laboratories, our metallurgical group has dealt with a vast number of alloys, both ferrous and nonferrous, and with many materials in the border range of metallic properties. The objectives of our design engineers embrace every phase of telephony, and the properties they desire in metals are generally unusual, frequently unique, and often conflicting. Commercial alloys have not always been available with properties to meet a special requirement in the telephone plant, and many alloys have had, therefore, to be custom-made.

Anyone who has had the opportunity to observe the results of tests of all types on numerous such alloys, both commercially and specially produced, or who has taken part in the development of an alloy of some necessary, but new or unusual combination of properties, could not fail to be impressed by the frequency with which a desired goal has been reached or adequately approached through the presence of decimal quantities of alloying elements. Nor could one fail to be struck by the occasions when, conversely, removal of a minute amount of impurity element has rendered an alloy useful.

It is no exaggeration to state that the content be-

EARLE E. SCHUMACHER, Member AIME, is Chief Metallurgist, Bell Telephone Laboratories, New York, N. Y.

AIME New York Meeting, February 1950.
TP 2882 E. Manuscript received April 5, 1950.

hind the decimal point often spells success or failure, and the critical content is sometimes far to the right of the decimal point as I shall later illustrate.

The great effects of small additions have long been recognized and have, in fact, been described by many investigators. The importance of the minute, however, cannot be overemphasized. Therefore, in this discussion, I propose to illustrate for you some of the startling instances, drawn primarily from our own experiences, wherein small, even vanishingly small, proportions of stranger elements in otherwise common aggregates have completely changed the customary pattern of behavior.

No one property has a monopoly as to being disproportionately affected by minor elements. Nearly all properties are affected, but there is time here to include only a selected few. I have chosen, therefore, three of general interest: strength, magnetic, and electrical properties. I shall inquire into both the mechanisms and consequences of these disproportionate effects and try to share with you the fascination and challenge of this field.

Strength Properties of Lead and Lead Alloys

To illustrate the effect of the minute on strength properties I have selected lead and its alloys, with which we have worked extensively for many years. Lead has the advantages of being available in quantity in a state of high purity and of being fairly easy to melt and fabricate without contamination to any extent detectable by the spectrograph. It has the interesting disadvantages of recovery and recrystallization at room temperature. Whether I

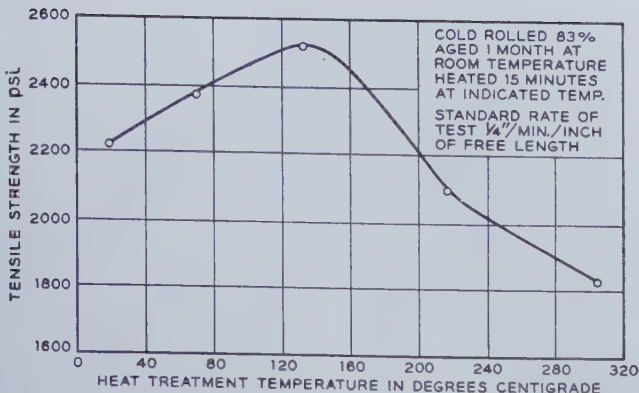


Fig. 1—Effect of heat-treatment temperature on the tensile strength of severely cold-rolled high-purity lead.

should use the term "recovery" at all is perhaps questionable, considering that for lead, working at room temperature is the equivalent of hot working for most industrial metals. It is, for example, uncertain that we can produce in lead any substantial residual stresses that persist for an appreciable time. In any event, what we normally consider recovery effects are masked by the predominance of recrystallization at room temperature, and I shall use the term recrystallization in what follows to denote both nucleation and grain growth, and, as well, any "recovery" which may have had opportunity to occur. The recrystallization variable requires that one apply meticulous attention to all details in fabrication and testing to avert unpleasant surprises in the form of seemingly unorthodox behavior. On the other hand, there is presented an excellent opportunity to observe some fascinating phenomena.

High-purity Lead: Before proceeding to a consideration of the effects of small additions it is desirable to examine the strength characteristics of the commercial high-purity lead that was used in these studies. This lead has a purity of 99.998 pct, no other metallic element being present in amount

exceeding five ten-thousandths of one percent. When an attempt is made to anneal cold-rolled pure lead at moderate temperatures, its tensile strength is increased and not, as might have been expected, decreased. This is shown in fig. 1, where tensile strength, after 83 pct reduction, is given as a function of temperature of heat treatment. The strength rises to a maximum for a 130°C treatment, then falls off. The peak suggests an optimum aging temperature such as is usual under conditions of precipitation hardening. However, the response to other heat treatments attempted in pursuit of such a mechanism fails to indicate that any such occurs here.

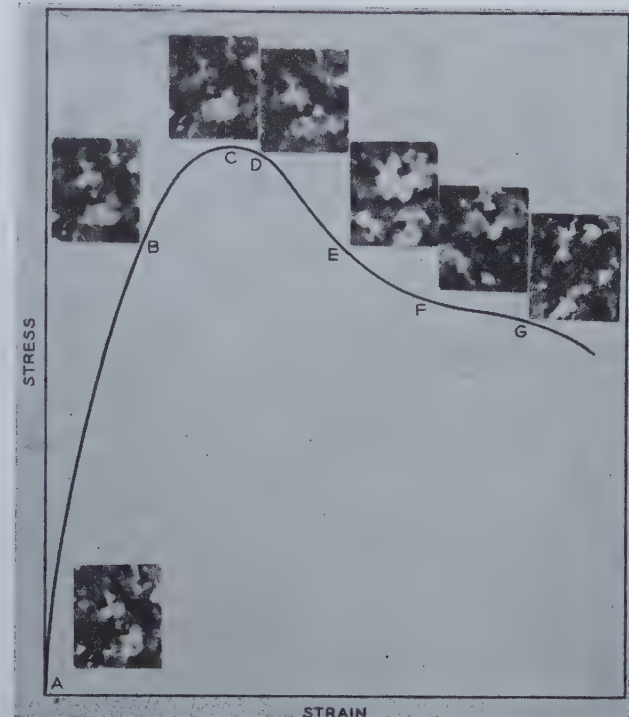


Fig. 3—Grain structure of the identical area of a severely cold-rolled pure lead sample photographed during the progress of a tensile test.

X8. Area reduced approximately three quarters in reproduction.

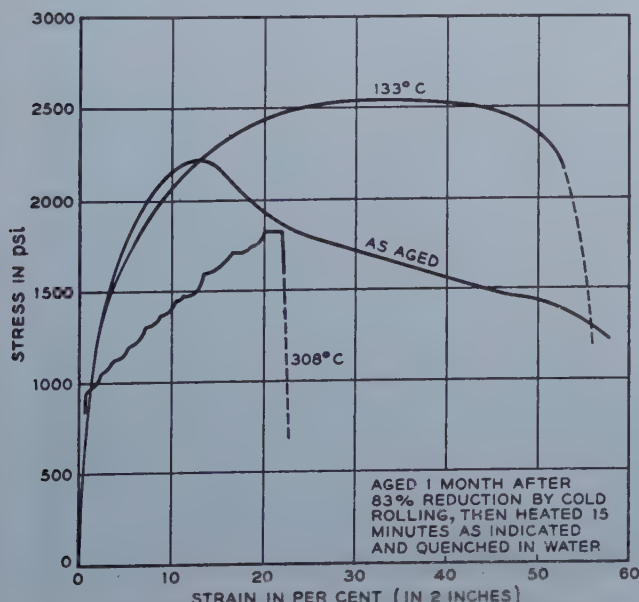


Fig. 2—Stress-strain characteristics of high-purity lead.

Clues as to the reason for this unusual strengthening on annealing a pure material were found only when a detailed study was made of the tensile properties of lead both as rolled and as heat treated after rolling. The information is presented as conventional stress-strain curves, that is, not converted to true stress and true strain, for on making the conversion for all these curves no differences significant to those conclusions which I have time to give at the present were obtained. However, one does detect by the conversion further phenomena which I hope we may bring to you in the near future.

In the first set of these, fig. 2, the middle curve, for cold-rolled lead, shows that it strain hardens continuously up to 13 pct extension, after which it softens as shown by the dip in the curve. No such softening is indicated in the other two curves which represent the behavior of the rolled lead after heat treatment at a moderate and at a higher temperature. The jagged nature and low maximum stress shown by the lowest curve result from the large grain size produced by the high-temperature treatment. The grains grew so large that a few individual

crystals occupied a dominant portion of the sample cross-section.

The drop in stress, or softening, on extending the rolled lead (the middle curve again) might reasonably suggest recrystallization. This time, lead does the reasonable. An analogous sample was etched continuously and periodically photographed on the same area in the course of the tensile test. The successive grain structures revealed in this area are shown in fig. 3 and correspond to the adjacent locations on the stress-strain curve. Definite recrystallization begins at point C, the start of the dip, and continues with further extension.

This dip, resulting from decrease of stress with further strain, requires that the rate of softening with recrystallization be greater than the rate of strain hardening produced by the forcible extension of the test sample. The rate of strain hardening can be controlled through the rate of extension. In doing so the time available for recrystallization is altered. The balance between these simultaneous and opposing processes is illustrated nicely in fig. 4 by stress-strain curves at various extension rates. The greatest rate of softening with strain occurs at the lowest rate of extension; the maximum negative slope of the curves becomes less pronounced as the speed of straining is increased. Furthermore, the strain at which the maximum stress occurs, located by the open circles, increases with the extension rate, and the maximum stress itself is raised from 1600 to 2500 psi. More extensive analysis will show that increased rate of strain hardening prior to recrystallization also is associated with increasing extension rate.

Let us now re-examine the upper two curves of fig. 2 and recall the fact that the softening dip is associated with recrystallization and is completely eliminated by a moderate temperature heat treatment. It should follow that the heat treatment necessarily accomplishes some structural alteration which either prevents recrystallization, or which has some effect equivalent to this on the stress-strain curve. The upper curve shows that in this case

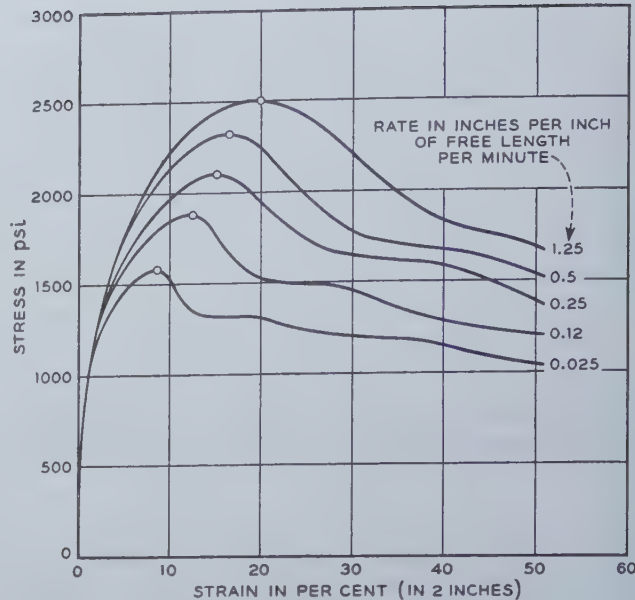


Fig. 4—Effect of rate of extension on the stress-strain characteristics of severely cold-rolled pure lead.

strain hardening continues throughout the test, past the previous critical point of strain at which softening and recrystallization otherwise took place. The grain structures corresponding to each of the two curves, photographed on one area before and after the 133°C heat treatment, are shown in fig. 5. The structures are almost identical. Other samples, however, rolled somewhat differently, may undergo major grain growth during heat treatment while maintaining the difference in tensile behavior. Exhaustive examination leads to the conclusion that the changes responsible for the difference between the stress-strain curves must be submicroscopic.

The strain-hardening behavior of severely rolled pure lead is thus seen to be as if—and at this stage I can claim only "as if"—very severe working pro-



Fig. 5—Grain structure of an identical area of a cold-rolled high-purity lead sample, before and after the heat treatment shown in fig. 2.

X8. a. As aged one month. b. Plus 15 min. at 133°C.

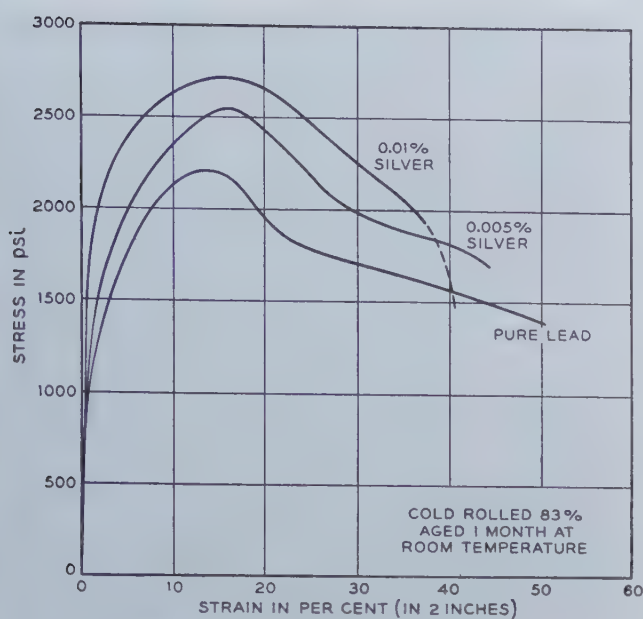


Fig. 6—Effect of silver on the stress-strain characteristics of lead.

duced a system of ill-comprehended "microfaults," which might possibly be residual microstrains or possibly minute structural discontinuities. These persist after the recrystallization incident to rolling, or actually are produced by the incompleteness of such recrystallization at room temperature. The addition of sufficient strain energy to this system by the tensile test might then, after a certain amount of further hardening, initiate the recrystallization observed during test.

The recrystallization is attended by softening, that is, decreasing stress as extension is continued. The softening is due, at least in part, to recrystallization itself. In addition, it may be aided by the energy released with the relaxation or removal of the microfaults. On the other hand a moderate prior heat

treatment may be postulated to remove the faults initially, as by more complete recrystallization, and so allow strain hardening to continue uninterrupted throughout the tensile test. The fundamental question then seems to be: what structural inhomogeneities, residual stresses, or other effects, are produced in pure lead by severe cold working, cause a relaxation of strain hardening at a critical degree of strain, and are removed or negated by a moderate heat treatment? We hope some day to have the answer.

The data presented thus far lend added meaning to my previous statement regarding the need for extreme attention to details in making and testing lead samples. The danger of unsuspected variables is so great that the effects of impurities can best be investigated with limited batches of a number of materials similarly prepared and carried through identical rolling, aging, and testing schedules as a group. Great care must be taken in comparing the results of one experiment with those of another because of the probability that differences in processing do exist and affect the data.

Lead Alloys: With this somewhat lengthy background I can proceed to the discussion of small alloying additions. The effects of the added elements on the strength properties of lead are, as would be expected, related to their influence on recrystallization. Fig. 6 presents stress-strain curves for pure lead and for lead containing 0.005 and 0.010 pct silver, respectively. The curves for the two alloys have steeper initial slopes; the silver has stiffened the lattice. Further, it has retarded recrystallization; the softening dip is increasingly de-emphasized with greater silver content. And it has obviously raised the tensile strength.

Fig. 7 shows that silver has a marked effect on the grain size of rolled lead. We have found from optical and electron microscopy that lead-silver is a precipitation hardening system. The solid solubility of silver is about 0.10 pct at eutectic temperature (304°C) and is less than 0.005 pct at room temperature. Therefore the observed hardening and

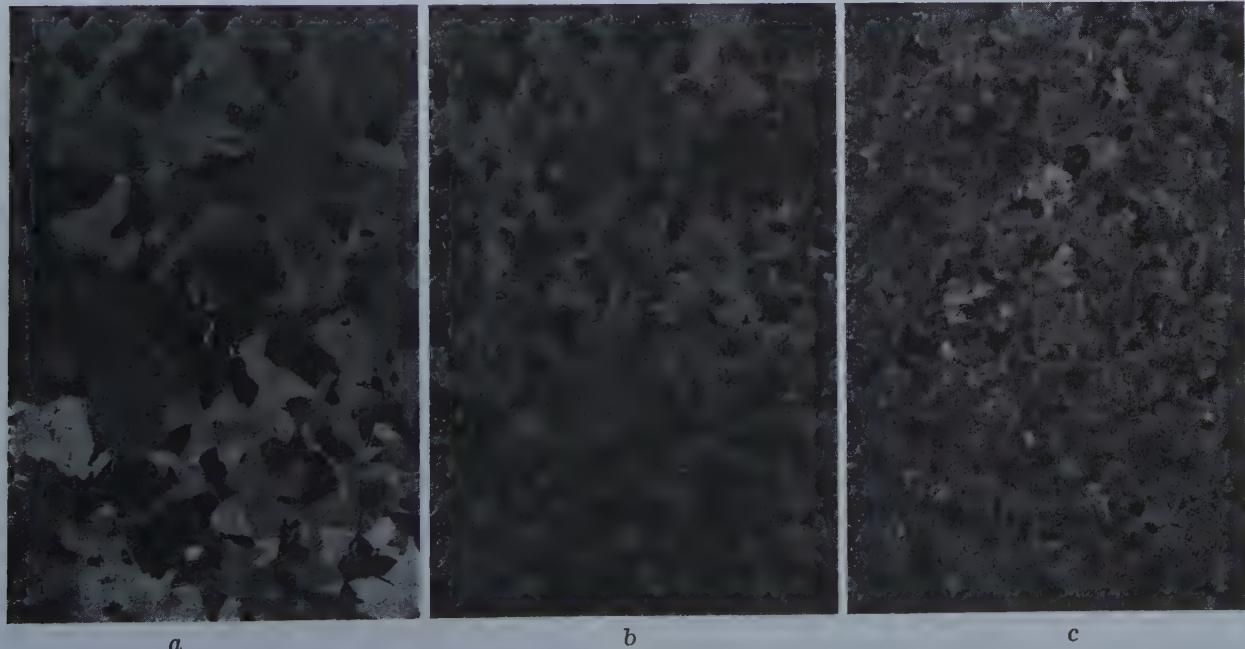


Fig. 7—Effect of silver on grain size. One month after severe cold rolling.

X8. a. Pure lead. b. 0.005 pct silver. c. 0.010 pct silver.

the retarding of recrystallization are associated with a solid solution plus a finely dispersed precipitate.

Another precipitation hardening system, involving minute quantities of a minor element, and one for which the solid solubility has been determined accurately, offers a fine opportunity to examine how hardening and recrystallization are affected when the small quantity of added element is, first, entirely in solid solution and then present partially as precipitate. The solid solubility of calcium in lead decreases from 0.10 pct at 328°C, the peritectic temperature, to 0.010 pct at room temperature. The stress-strain curves for pure lead and for three lead-calcium alloys are illustrated in fig. 8. Comparing the curves for the 0.005 and 0.010 pct calcium materials, the solid solution alloys, with the curve for pure lead, it can be seen that as the amount of calcium in solid solution is increased the lattice is stiffened, and the tensile strength is increased. Yet

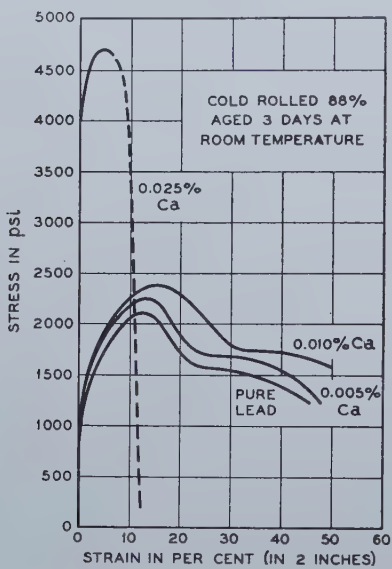


Fig. 8—Effect of calcium on the stress-strain characteristics of lead.

these are small changes compared with the very large change occurring when the calcium content is sufficiently high to yield both the solid solution and a precipitate phase (0.025 pct curve). This shows quite clearly that with lead-calcium alloys the presence of the precipitate has far the greater effect on hardening. Evidence of the pronounced influence exerted by the Pb₂Ca precipitate on recrystallization can be seen in fig. 9 at X500 instead of X8, the magnification of the previous photographs. Although the 0.03 pct calcium alloy was extruded 20 years ago, in foresighted preparation for this occasion, it still retains the elongated grain structure characteristic of extrusion.

To add to the variety of the phenomena obtainable there are instances also where small quantities of elements exert relatively little effect on the properties of pure lead when acting alone but disproportionately large consequences in combination. Consider the striking illustration furnished by the stress-strain curves in fig. 10. When 0.005 pct nickel is added to high-purity lead A, some changes in strength and recrystallization properties are obtained. However, when high-purity lead B, containing only slightly greater amounts of impurities,



Fig. 9—Grain structure of lead-0.03 pct calcium tape extruded at 205°C and aged 20 years at room temperature. X500.

is used, the addition of the same amount of nickel results in a very significant change in the properties. The difference in impurity content of the two leads is shown in the upper right hand corner of the figure. The exact combination of minor elements and nickel that is responsible for this behavior is not known.

From the engineering standpoint our main concern with minor elements in lead has been in relation to the effects, good or bad, that they may have on cable-sheathing materials. One example will here have to suffice to illustrate the need for a vigilant watch over the impurity content of the cable-

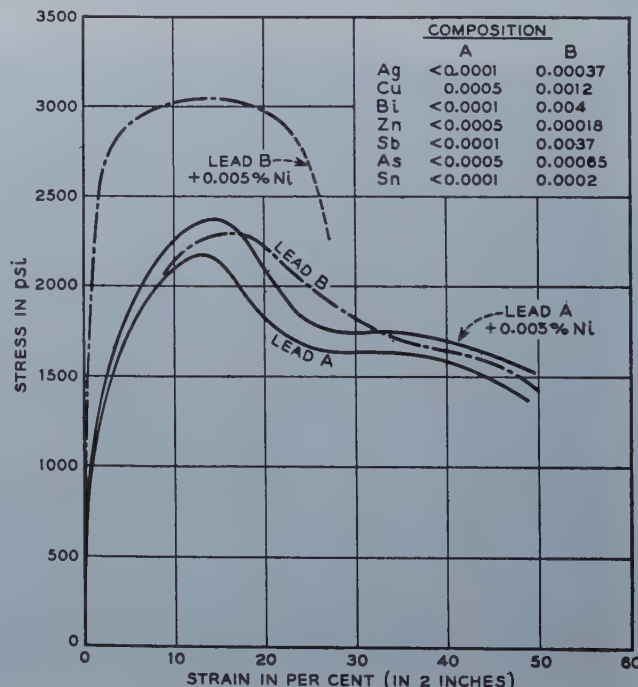


Fig. 10—Effect of slight change in purity of base lead on the stress-strain characteristics of cold-rolled lead plus nickel.

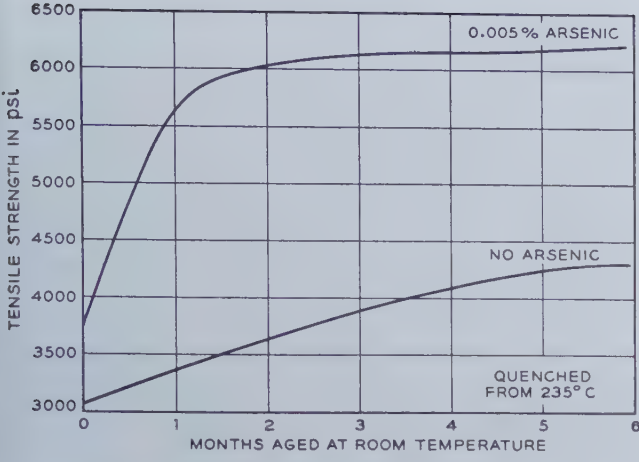


Fig. 11—Effect of arsenic on the age hardening of high-purity lead-1 pct antimony alloy.

sheathing alloy. It was noted that when one commercial composition of antimony was used for making our lead-1 pct antimony cable sheath a variety of distressing troubles was encountered in the extrusion of the material. Moreover, the sheath produced aged so fast and became so hard that it was difficult to unreel and install the cable. We found that the difficulty was due to small quantities of arsenic present in the antimony. The unhappy efficiency of arsenic in promoting rapid age hardening in this system is shown in fig. 11. Here two alloys, both water quenched, one containing no arsenic and the other 0.005 pct, were tested for tensile strength after various aging periods. The more rapid hardening and the higher strengths for the arsenical alloy are evident. The extrusion difficulties, too, were contributed by the arsenic. When arsenic-bearing lead-1 pct antimony alloys were extruded in the laboratory under normal conditions, invariably Christmas tree shapes were produced instead of sound rectangular strip. The hot shortness is illustrated in fig. 12. The product is decorative but not useful. Only by lowering the extrusion temperature and



Fig. 12—Hot shortness in extruded 1½-in. wide lead-1 pct antimony tape caused by 0.008 pct arsenic contamination.

slowing down the rate of extrusion was it possible to produce sound material. This behavior is due to the intergranular presence of a low melting lead-antimony-arsenic phase which is liquid at normal extrusion temperatures.

Before proceeding to the next section you may be interested in a photograph, fig. 13, showing a portion of our field laboratory at Chester, N. J. Here is shown an experimental installation of 36,000 ft of full size aerial cable used to check and supplement the laboratory data on the lead-calcium alloy that I mentioned previously.

Properties of Magnetic Alloys

Turning now to a consideration of the effect of minor elements on magnetic properties, I shall show how sensitive the ferromagnetic materials are to the presence or absence of small amounts of various elements.

It is convenient as well as desirable for clarity to differentiate sharply, yet without too much detail, between the two subdivisions of magnetic materials. The first includes all the mechanically soft, easily



Fig. 13—Field laboratory for testing aerial cable sheath alloys.

magnetized, and, we might say, "temporary" magnetic materials as they are also easily demagnetized. The second includes all the mechanically hard, not easily magnetized materials, the "permanent" magnets. Although there are exceptions to the classification "soft" and "hard," the use of these terms is quite apt. In a given soft magnetic material increasing softness parallels increasing freedom from minor constituents and, indeed, is conditioned by this freedom. The use of the term magnetic hardness conveys both the ideas of permanency of magnetization and of mechanical hardness. Hence in the permanent magnetic materials we seek a highly strained lattice through proper choice of alloying elements which, either by compound formation or by the formation of intermediate phases, will give possibilities of controllable precipitation. These precipitates under the correct physical metallurgical treatment may attain an optimum dispersion, resulting in a corresponding optimum of properties characteristic of the particu-

lar alloy concerned. Presence of quantities of other elements which may interfere with the efficiency of the strain-producing process is thus highly undesirable. A few examples from each of the two classes of magnetic materials will be discussed in turn.

High Permeability Materials: The work of Cioffi and of Yensen and Zeigler in the field of soft magnetic materials has shown the remarkable improvements in quality obtainable in iron by the successive reduction to vanishingly small amounts of a group of elements commonly present in iron. A typical illustration from Cioffi is given in table I.

It will be noted that carbon, sulphur, oxygen, and nitrogen have undergone significant relative percentage reductions by just 3 hr of treatment at 1475°C in dry H₂, and that the value for maximum permeability has increased by more than four-fold. A further 15-hr treatment resulted in further decreases of sulphur and nitrogen with a thirty-fold improvement in maximum permeability over the original. The elements reduced in quantity by this treatment are the ones which in solid solution in α-iron would be expected to strain the structure to a considerable degree because of their difference in valence from iron and probable interstitial location. Thus their reduction in quantity by purification has a relatively large effect on magnetic softness as measured by permeability.

An example of the effect on a specific magnetic property of a single element is that of carbon on the maximum permeability of iron crystals containing almost negligible amounts of sulphur, oxygen, and nitrogen. Yensen's data, as indicated by the curve

Table I. Effect of Impurities on the Permeability of Iron

Material	Percent							Maximum Permeability
	C	S	P	O	N	Mn	Si	
Armco Iron	0.012	0.018	0.004	0.030	0.0018	0.030	0.002	7,000
After 3 hr at 1475°C in dry H ₂	0.005	0.006	0.004	0.003	0.0003	0.028		30,000
After 18 hr at 1475°C in dry H ₂	0.005	0.003	0.004	0.003	0.0001	0.028		227,000

in fig. 14, show that the maximum permeability increases rapidly as the carbon content decreases below 0.005 pct.

An example of the effect of a precipitated phase on magnetic properties is that of nitrides in ingot iron. Nitrogen has a markedly deleterious effect on the permeability of iron, an effect which increases with time. That, for years, this effect was not generally recognized is not surprising because of the slowness of the aging at room temperature, and also perhaps because physical changes or the action of other minor constituents may have obscured the normally observable effects. Two typical cases from a series of carefully controlled experiments are illustrated in fig. 15. The aging process was accelerated by heating for 700 hr at 100°C. The extent of the loss of quality in the aged low-nitrogen alloy is dependent upon the nitrogen content up to the solid solubility limit at room temperature of, probably, about 0.001 pct of interstitially dissolved nitrogen. Hence in the samples of the 0.001 pct N alloy the course of the curve, permeability vs. flux

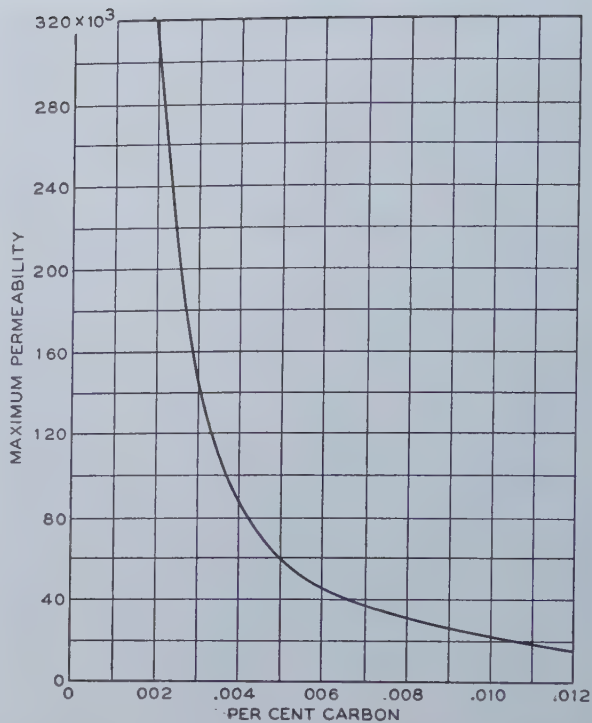


Fig. 14—Effect of carbon on maximum permeability of iron.

density, is not affected significantly by aging at 100°C. With the alloy of higher nitrogen content, 0.005 pct N, there is superimposed upon the solution hardening an effect due to the formation and precipitation in critical dispersion from supersaturated solid solution of a nitride. Illustration of this is given by the two lower curves. The difference in the position of the curves represents the loss in permeability due to the "hardening effect" of the nitride precipitate. This effect is substantially eliminated by heating to 200°C which dissolves the precipitated nitride. That this represents a return to a state of supersaturated solid solution is indicated by the reversibility of the process. The effect of nitrogen on magnetic properties is further illustrated by fig. 16 which shows how the maximum permeability for aged low-carbon iron varies with nitrogen content.

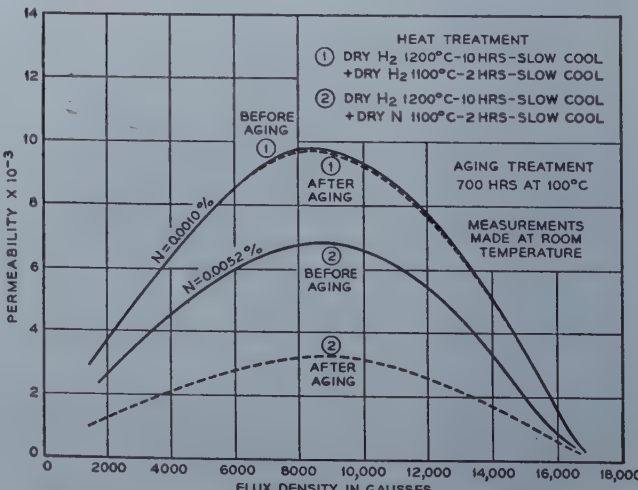


Fig. 15—Effect of nitrogen on permeability of Armco iron.

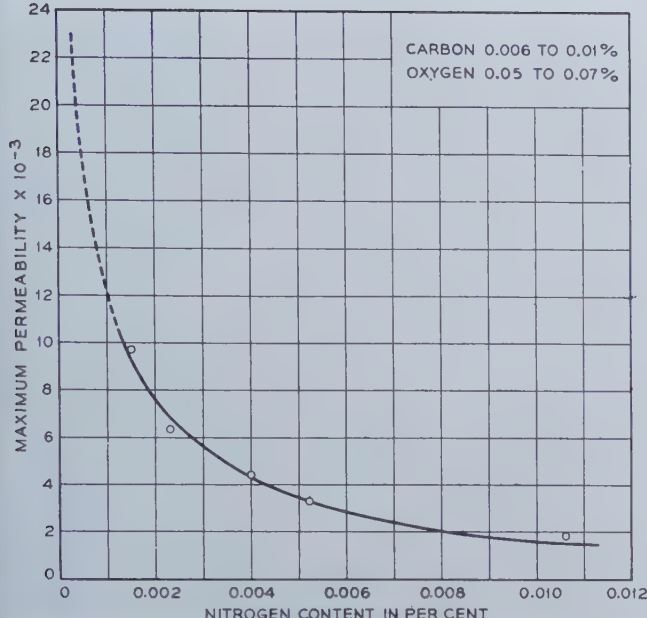


Fig. 16—Maximum permeability vs. nitrogen content for aged low-carbon iron.

Before leaving the soft magnetic materials, an instance will be given to show the profound effect on magnetic quality of a small concentration of a refractory oxide, an incidental component of an alloy resulting from the process of deoxidation. The example is the effect of MgO, generated by deoxidizing a melt with magnesium, on the properties of an iron-nickel-molybdenum alloy. This ternary alloy when treated properly may be endowed with the highest initial and maximum magnetic permeabilities yet attained in polycrystalline material. For example, alloy No. 1, shown in table II, has an initial permeability of 105,000 and a maximum permeability of 1,300,000. This alloy was prepared without the addition of magnesium as indicated. The properties of the alloy of the same composition, with magnesium

added under conditions permitting the formation of MgO, are shown for comparison in the line below. Comment is hardly necessary on the very great increase in the initial permeability and the ten-fold increase in maximum permeability attainable by the absence of the 0.1 pct of magnesium. Microstructurally alloy No. 2 contains finely dispersed MgO which has been trapped during solidification and which prevents the attainment of optimum permeabilities by restricting the growth and orientation of magnetic domains.

In sharp contrast to these instances where extraordinary procedures are utilized to remove small quantities of impurities in order to achieve the special properties such as the high permeabilities we have just been discussing, there are instances where these ordinarily harmful ingredients are purposely added for other beneficial effects. Additions of sulphur may be used for illustrative purposes. An obvious instance that suggests itself is its use in free machining steels. A less well-known but equally important use is its incorporation in 80 pct nickel-20 pct iron alloy where under certain conditions it makes the material so friable that fine powders, for use in low-loss loading coil cores, may be produced readily. When sulphur is present in amounts of the order of a few thousandths of 1 pct, the wrought alloy is extremely cold short. The amount of sulphur added is critical. Essentially it is that quantity

Table II. Effect of MgO on Magnetic Permeability

Alloy, No.	Fe, Pct	Ni, Pct	Mo, Pct	Mn, Pct	Additions Mg, Pct	Initial Permeability	Maximum Permeability
1	15.4	79	5	0.6	0	105,000	1,300,000
2	15.4	79	5	0.6	0.1	38,000	130,000

which produces just enough thin sulphide film to envelop the grains and produce cold brittleness but is not sufficient to interfere seriously with the hot-rolling properties. Such a sulphide film at a grain boundary is shown in the micrograph, fig. 17.

Permanent Magnets: Although carbon has an adverse effect on the quality of soft, or high permeability, magnetic materials, it is an essential element in a class of quench-hardening permanent magnet alloys like the chromium magnet steels and 36 pct cobalt magnet steel. Like tool steels, these permanent magnet alloys depend upon the hardening action of carbon for their useful properties.

There are other types of permanent magnet alloys that are carbon free, however, and depend for their hardness upon the formation of intermediate phases of the major constituents. Carbon then, as with the high permeability materials, plays no beneficial role and, in fact, even small amounts of it are found to be objectionable. One set of illustrative data is given in fig. 18 where the curve is a plot of coercive force against carbon content for Alnico V, a dispersion-hardening, permanent magnet alloy, composed of Fe 51 pct, Ni 14 pct, Co 24 pct, Al 8 pct, Cu 3 pct.

The exceptionally high, permanent magnet qualities of this material are obtained normally by first heating to a high temperature to insure complete homogeneity of the constituents to solid solution form, followed by cooling at a critical rate in a magnetic field, and subsequent aging at a temperature of approximately 600°C. The coercive force



Fig. 17—Sulphide film at grain boundary in 80 pct nickel-20 pct iron alloy. X2000.

referred to in fig. 18 is the magnetic field strength required to reduce the residual magnetism of the specimen to zero after magnetizing to saturation. The curve shows most clearly that the desired high coercive force values of Alnico V are obtained only when the carbon content is not greater than a few hundredths of one percent.

A metallographic study of the structure of fully heat-treated Alnico V samples containing graded amounts of carbon has shown some of the microstructural changes resulting from the presence of this element. In the next three figures, 19, 20, 21, these manifestations are revealed. With almost negligible carbon (the specimen was analyzed at 0.005 pct), the alloy looks clean except for a few oxide particles. With a very little increase in carbon, a feathery constituent makes its first appearance at a grain boundary. This specimen analyzed 0.006 pct carbon although the actual carbon content in the grain boundary area examined may have been somewhat in excess of this due to segregation. With increasingly greater carbon content, the feathery phase appears more and more until, at about 0.08 pct carbon, the second phase appears additionally within the grains exhibiting a Widmanstätten pattern. With a relatively large amount of carbon, 0.50 pct, the structure shows a conglomeration of phases which fill the whole field.

The mechanism of the adverse effect of carbon on the magnetic quality in these nominally carbon-free alloys has not yet been developed satisfactorily. The microstructure is so greatly affected by carbon that it may be used to estimate magnet quality. Where the carbon concentration is low, close estimates of its amount sometimes may be made from the magnetic characteristics. Practice and technology are satisfied by this limited understanding and correlation. The fundamental relationships of the effect of a sixth element, carbon, on a five-component system, which is itself only incompletely understood, awaits the enthusiasms and energies of another generation. Several theories have been proposed to account for the mechanism, but they appear to be different aspects of a yet more fundamental phe-

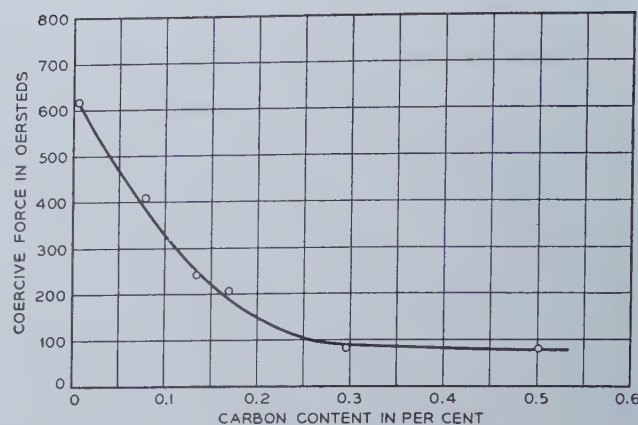


Fig. 18—Effect of carbon on the coercive force of Alnico V.

nomenon. One of these, for example, is the suggestion that carbon lowers the Curie temperature, the temperature above which the material loses its ferromagnetism. This temperature should be high enough in Alnico V to remain appreciably above the minimum temperature necessary to permit unfettered the desired alignment effects during cooling in the applied field.

Electrical Properties of Silicon and Germanium Alloys

The effect of small additions on both strength and magnetic properties has been illustrated. Let us now consider the effect on electrical properties. The electrical properties of metals are sharply dependent on small alloying additions in solution; in the semimetals, silicon and germanium, used in such electronic devices as the point-contact rectifier and transistor, the dependence is even more striking. These materials afford outstanding examples of very large effects from minute component additions. If I seem to be departing from the usual roster of metallurgical materials, I may perhaps be forgiven on showing that, in their processing at least, these



a



b

Fig. 19—Alnico V.

a. Carbon, 0.005 pct. Magnetite quality, excellent. X250. b. Carbon, 0.006 pct. Magnetite quality, still excellent. X250.

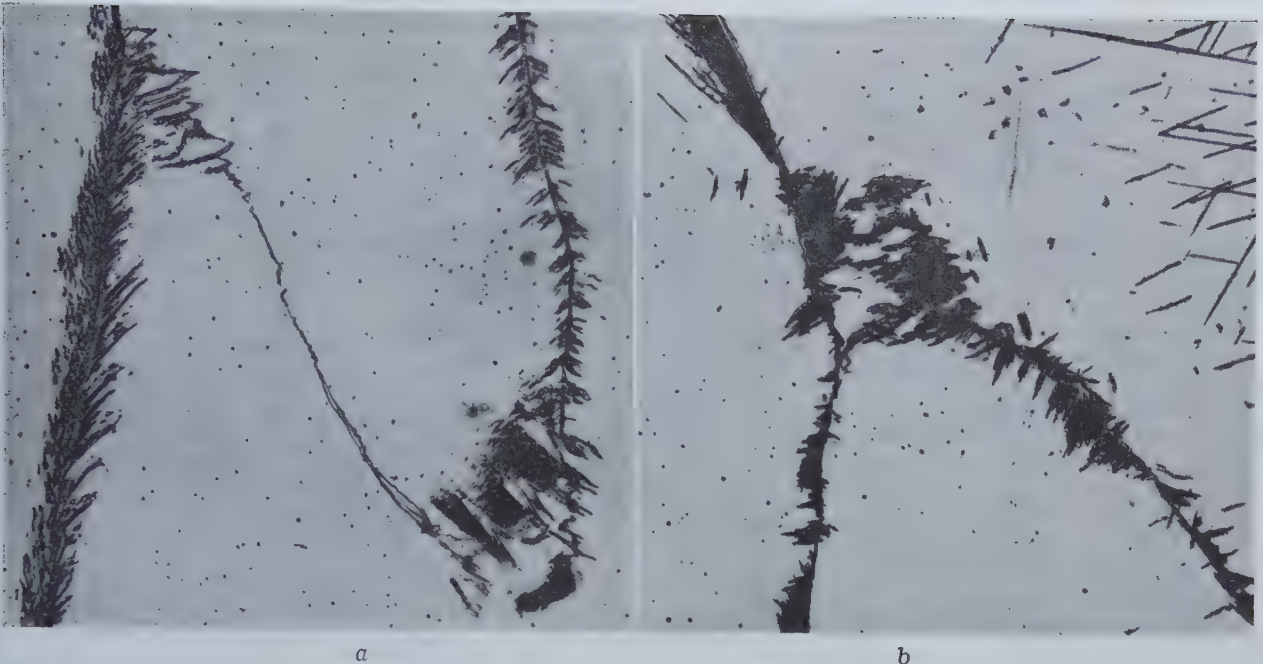


Fig. 20—Alnico V.

a. Carbon, 0.038 pet. Magnetic quality, fair. X250.

b. Carbon, 0.084 pet. Magnetic quality, poor. X250.

elements are not only amenable to, but require careful metallurgical techniques.

I shall therefore conclude my discussion with the electrical property, conductivity, or its reciprocal, resistivity, of silicon and germanium. The term semiconductor was coined, somewhat loosely, for materials like silicon and germanium because their electrical conductivity lies between that of metals and insulators. As is well known, conduction in metals is by electrons, which carry a negative charge. The concentration of conduction electrons is very high, of the order of one per atom. The solution of foreign elements in a metal such as copper reduces the conductivity by disturbing the periodicity of the lattice field and thereby interfering with the flow of electrons. On the other hand, in silicon and germanium

electrical conductivity is several orders of magnitude below that of metals. Conductivity is limited principally by the number of carriers, which is small; lattice scattering plays a lesser part. Certain elements, when present in solid solution in either of these semiconductors, increase the electrical conductivity by furnishing carriers of charge. The picture is complicated here by the fact that two mechanisms of electrical conduction are possible, each corresponding to a separate class of addition element.

Although the details of how certain elements affect the conductivity of silicon and germanium properly lie in the realm of quantum physics, I shall attempt to describe certain basic concepts by means of a somewhat oversimplified picture. Fig. 22 is a schematic representation of valence bonding in silicon. Silicon (and also germanium) is in group IV of the periodic system and crystallizes in the diamond-cubic structure. Each atom of silicon has four valence electrons which it shares with four neighboring atoms. The valence electrons are held tightly and cannot easily participate in electrical conduction.

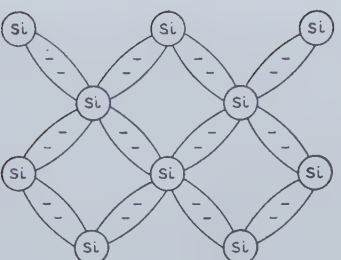
If an atom with five valence electrons, such as phosphorus, is placed substitutionally in the silicon lattice, as shown schematically in fig. 23, an extra electron will be present. Only four of the five phosphorus valence electrons enter covalent bonds; the remaining electron is relatively free. It is easily moved by an electric field, leaving behind a positively charged phosphorus ion, and is a carrier of electrical current. An element of group V, such as phosphorus, is called a donor for silicon or germanium, because it donates a conduction electron to the parent substance. Such conductivity is called n-type ("n" for negative), because the mobile carriers are negatively charged.

Now let us consider a substitutional element with three valence electrons such as boron. One electron is missing from the lattice at the location of the boron atom as suggested by fig. 24. The vacancy is filled by an electron from elsewhere in the lattice, producing thereby a negatively charged boron ion



Fig. 21—Alnico V.

Carbon 0.50 pet. Magnetically worthless. X250.



NEUTRAL SILICON ATOM

Fig. 22—Pure silicon.

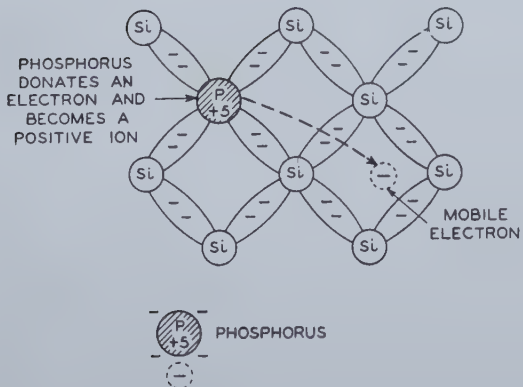


Fig. 23—N-type silicon.

and a mobile hole having a positive charge. If an electric field is applied, the hole will move through the lattice, just as an electron does, except that the direction of motion of the hole is opposite to that of the electron. An element of group III is called an acceptor for silicon or germanium because it accepts an electron from a covalent bond in the lattice, leaving there a mobile positive hole which enters the process of conduction. The conductivity is called p-type, because the mobile carriers behave as though positively charged.

Thus we have two mechanisms of conduction: the carriers may be regarded as electrons in n-type semiconductors, as holes in p-type semiconductors.

Electrical conduction in silicon and germanium has another significant feature. When both donors and acceptors are present in the lattice, the observed conductivity is not proportional to their sum but corresponds more nearly to their difference. The reason for this is that donors and acceptors neutralize or compensate each other. One may think of compensation as a conduction electron falling into a hole, with resultant neutralization of both charges and removal of both carriers from the process of conduction.

The Resistivity of Silicon Ingots: Before considering the effects of minor elements on the resistivity of silicon, a few words about the preparation of ingots of this material seem in order. It is our practice to solidify silicon melts into cylindrical ingots by slow-cooling from the top downward. Silicon, and

germanium as well, expand on freezing. Hence if melts of either of these elements are cooled from all sides simultaneously the outer shell of the ingot, which solidifies first, is under severe expansive forces. Since silicon is very brittle, these forces usually are sufficient to crack the ingot. Fig. 25 a shows a longitudinal section of a desirable sound ingot, prepared by end cooling, while fig. 25 b shows an ingot with a sound upper half resulting from end

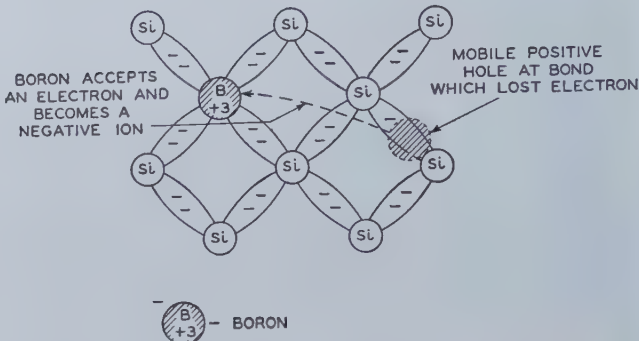


Fig. 24—P-type silicon.

cooling, but with a cracked lower half due to cooling from all sides simultaneously. Another result of end cooling is the concentrating of minor elements in the end of the ingot last to freeze.

Now let us consider the effect of an acceptor element, boron, on resistivity. For two silicon-boron alloys, and for silicon of exceptional purity, this effect is shown in fig. 26 where resistivity is

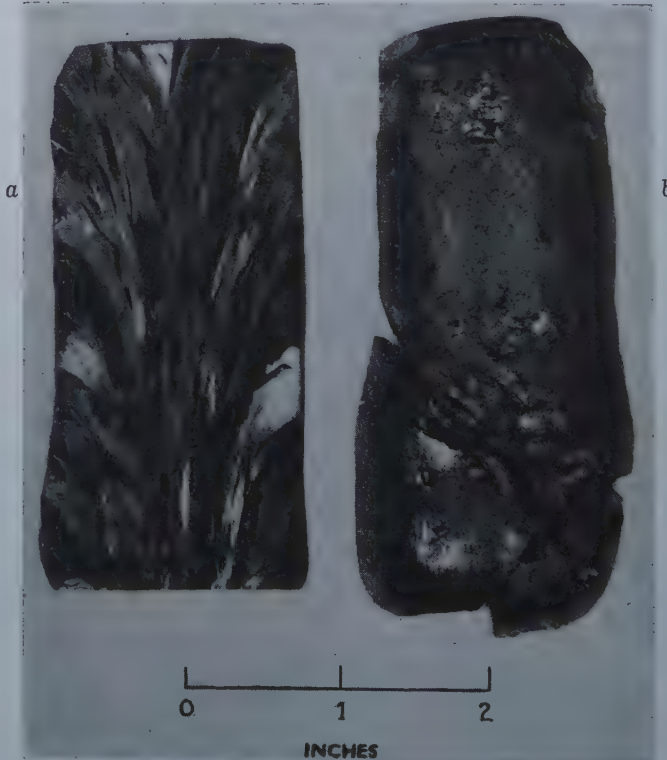


Fig. 25—Silicon ingots.

- a. Longitudinal section through sound ingot prepared by cooling from top downward.
- b. Upper half end-cooled; lower half cooled from all sides with resultant cracking.

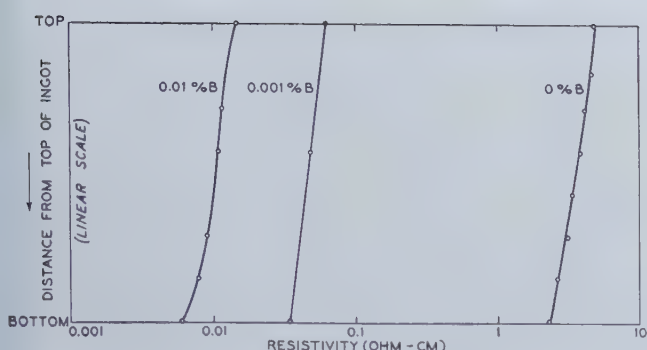


Fig. 26—Effect of added boron on the resistivity of silicon.

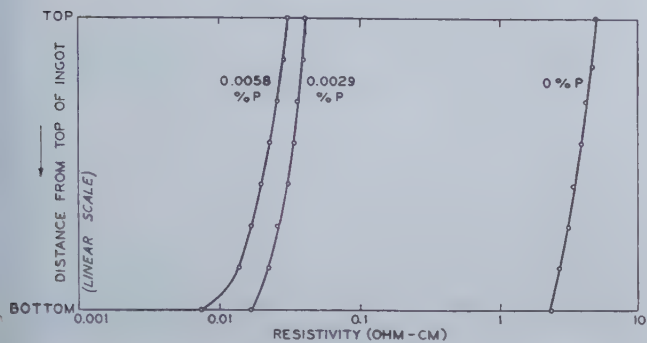


Fig. 27—Effect of added phosphorus on the resistivity of silicon.

plotted as a function of sample location in the ingot. Very small concentrations of boron markedly reduce the resistivity as indicated by the displacement of the curves. Even though the unalloyed silicon is of exceptional purity, its resistivity is far below the theoretical value of about 10^6 ohm-cm at room temperature for the element silicon.

The second important effect is that resistivity is a function of depth in the ingot, being greatest at the top, which is first to freeze. This variation is a result of normal segregation of boron during solidification. Such nonuniformity of resistivity is undesirable and, as we shall see later, can largely be obviated.

Fig. 27 shows the effect of a donor, phosphorus, on the electrical resistivity of silicon. Again, the extreme sensitivity of resistivity to solute concentration is apparent and again segregation is normal.

Let us now examine the properties of an ingot containing both boron and phosphorus. Fig. 28 shows resistivity as a function of location and reveals some interesting effects of the combined action of segregation and compensation. The first material to freeze, at the top of the ingot, contains a higher atomic concentration of boron than phosphorus in solution and hence is p-type. However, the rate of segregation is greater for phosphorus than for boron. Hence the excess of acceptors decreases with depth and at first the resistivity rises, reaching a maximum at the point at which the atomic concentrations of boron and phosphorus are equal. Below this posi-

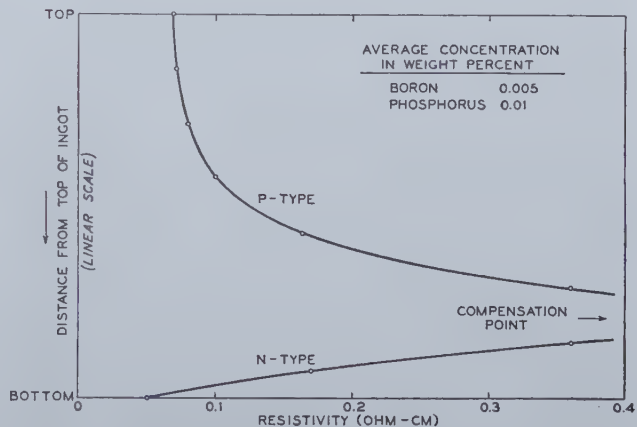


Fig. 28—Resistivity as a function of location for an ingot of silicon containing both boron and phosphorus.

tion continued segregation causes donors to be in excess by an amount which increases with depth. Hence below the compensation point the silicon is n-type and its resistivity decreases with depth.

The region of compensation in such an ingot is known as the p-n barrier. Associated with it are



Fig. 29—P-N barrier in slowly cooled ingot of silicon containing both boron and phosphorus. X22.

Area reduced approximately one half in reproduction.

photovoltaic properties and an unusual microstructure, an example of which is given in fig. 29. Here we see a longitudinal section through a slowly cooled ingot containing both boron and phosphorus. Grain growth has been columnar and segregation has been reasonably uniform from grain to grain, with the result that the p-type and n-type regions in each grain are well aligned. The microstructural discontinuity at the p-n boundary is believed to be an etching effect associated with electrochemical differences between p-type and n-type silicones.

Such microstructures show graphically the inhomogeneity which can be caused by segregation. An extreme case is revealed in fig. 30. Cooling was rapid and grain growth was noncolumnar, proceeding from nuclei throughout the ingot. As a result the p-type regions in individual grains appear as islands surrounded by regions of n-type silicon.

I should mention that most applications of these semiconductors place a premium on uniformity of resistivity. We have seen how segregation of a single element defeats this aim and how compensation effects between two segregating elements add further complications. One solution to the problem might seem to be rapid cooling of an ingot followed by a homogenizing heat treatment. We have not found this technique to be particularly useful for silicon because of the low rates of diffusion of the elements concerned. However, the information already presented contains a key to the solution of this problem. Fig. 26 shows that additions of boron to relatively pure p-type silicon result in ingots in which resistivity decreases with depth. In fig. 28, we see that in an ingot containing both boron and phosphorus, resistivity in the p-type region increases with depth. These data suggest that at some intermediate boron-to-phosphorus ratio it should be possible to produce an ingot in which resistivity is substantially constant with depth. As the curves of fig. 31 demonstrate, this can be done. Resistivity, now on an arithmetic scale, is plotted against location in the ingot for three silicones containing different proportions of boron and phosphorus. When the

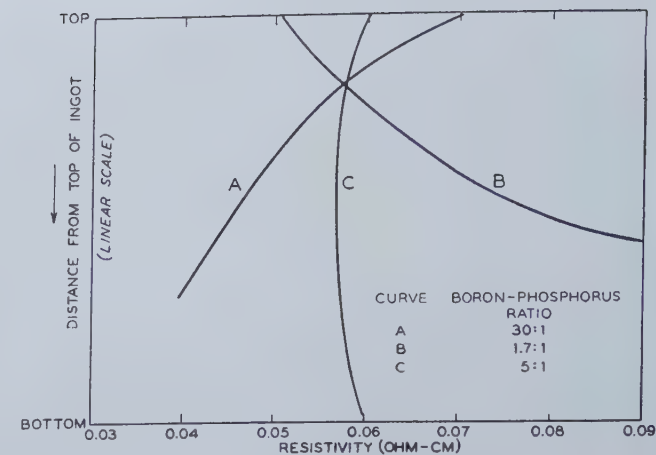


Fig. 31—Effect of boron-phosphorus ratio on uniformity of resistivity in ingots of p-type silicon.

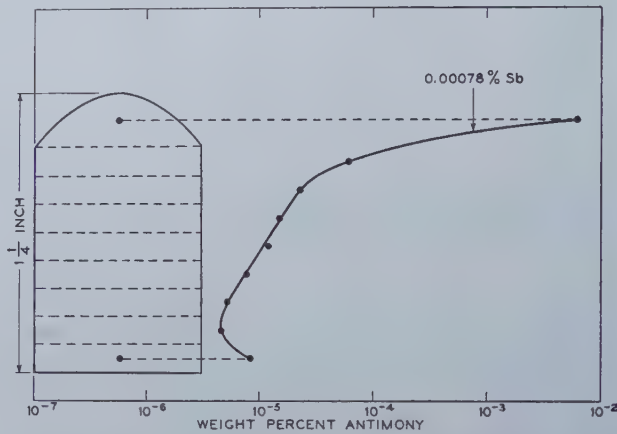


Fig. 32—Distribution of antimony in ingot of germanium containing 0.00078 pct antimony.

ratio of the atomic concentrations of these elements is about 5 to 1 the resistivity is quite uniform throughout the ingot as shown by curve C. Provided this ratio of boron-to-phosphorus is maintained, uniformity can be produced at other values of resistivity also.

Thus we produce a useful semiconductor by controlling the difference in concentrations of two significant elements, each of which is present in minute amounts and each of which segregates severely during solidification of the ingot.

The Resistivity of Germanium Ingots: The story for germanium is much the same as that for silicon. Elements of group III are acceptors, of group V donors, and when both are present compensation occurs. Ingots are prepared by end-cooling, in this case from the bottom upward, and normal segregation concentrates the solutes in the upper regions of the ingot.

Great extremes of solute concentration can be produced by segregation of minor elements and this fact has at times been overlooked in quantitative interpretations of the electrical properties of semiconductors as a function of nominal composition. An ingot of relatively pure n-type germanium containing 0.00078 pct by weight of antimony may be used as an illustration. Data on the distribution of antimony in the ingot according to Pearson, Stru-



Fig. 30—P-N barriers in rapidly cooled ingot of silicon containing both boron and phosphorus. X50.

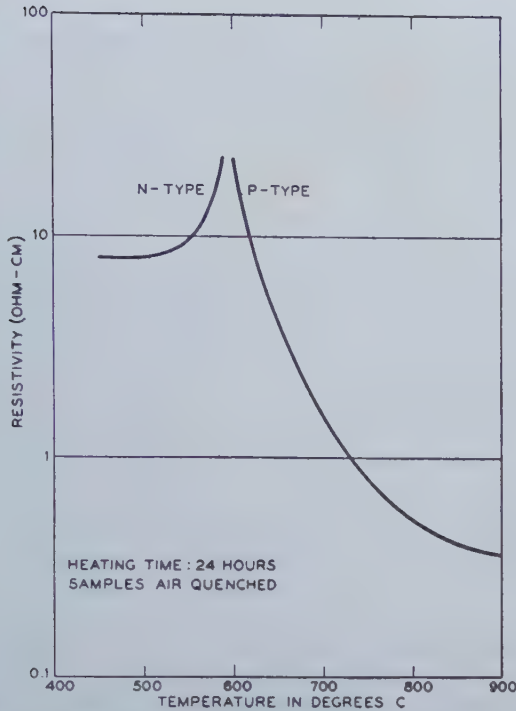


Fig. 33—Effect of temperature of heat treatment on resistivity of germanium at room temperature.

thers, and Theuerer are shown in fig. 32. In the lower half of the ingot the concentration of antimony is about 1 pct of the average value; almost all of the antimony appears in the top section. Although segregation does cause undesired variations in resistivity, these data show that it can reduce the impurity concentration of a large portion of an ingot to a value much below the average for the ingot as a whole. By taking advantage of such segregation and rejecting the portion of the ingot in which the impurities are concentrated, germanium of high purity is readily prepared.

We have seen in silicon that the balance between donors and acceptors is affected by segregation and have indicated that, once established, the balance can not be changed easily. In germanium, however, we have found that the effective concentration of one kind of acceptor can be altered by heat treatment. The effect is illustrated in fig. 33 where resistivity at room temperature is plotted against temperature of heat treatment for a specimen of relatively pure germanium. After heating at 500°C the germanium is n-type, donors being in excess of acceptors. As the temperature of treatment is raised the relative concentration of acceptors increases. Hence the resistivity of the n-germanium increases, reaching a maximum at a heat-treating temperature of 600°C, which is the n-p conversion temperature. After higher temperatures of treatment acceptors are in excess, the germanium is p-type, and its resistivity decreases with increasing temperature of treatment. The heat-treating effect is completely reversible; points on the curve in this figure are independent of the prior thermal history of the germanium.

One hypothesis for the variation of acceptor concentration with temperature of treatment is that the solid solubility of an acceptor impurity increases with temperature, much as does the minor element in an age-hardening alloy. (Theory indicates that acceptors must be in solid solution to be effective.)

A second hypothesis is that the acceptor is not an impurity at all but simply a lattice defect, the concentration of such lattice defects at room temperature increasing with temperature of treatment. In any event it is clear that we are concerned here not only with "concentration" but with "effective concentration" which depends on the thermal treatment of the germanium.

I should like to give a numerical example of the concentrations with which we are concerned here. The 500°C point in fig. 33 corresponds to n-germanium having a resistivity of about 8 ohm-cm, or a conductivity of 0.12 reciprocal ohm-cm. The number of excess donors required to produce this conductivity is extremely small, about one donor per 100,000,000 atoms of germanium. Furthermore, the conductivity can be doubled by adding one additional donor atom, such as antimony, to these 100,000,000 atoms of germanium. The quantities are calculated readily from the expression $\sigma = ne\mu$, in which σ is the electrical conductivity, n is the concentration of donors, e is the charge of the electron, and μ (a constant that has been determined) is the mobility of electrons in germanium.

It is not suggested that the development of these semiconductors is completed although much progress has been made. Many problems remain and are being investigated actively by physicists, chemists, and metallurgists. The fact that the solute concentrations involved are beyond the reach of conventional analytical methods has added to the difficulty of investigation and indirect methods have had to be used. For example, the data of fig. 32 on antimony distribution were obtained by radioactive tracer analysis. Also measurements of the Hall effect, which is a transverse voltage in a current-carrying conductor produced by a magnetic field, have provided information on the sign and number of extremely small concentrations of carriers.

Thus we have now seen that in these semimetals we are concerned with things which most unmistakably are not pure and do not behave as pure materials, even though the effective solute content may be no more than a few parts in a hundred million. These infrequent atoms none the less contribute directly to the useful electrical properties.

What constitutes a "minor" amount of added element we now see to be a matter of degree: 5 parts of silver in 100,000 of lead change the strength of the latter; the removal of 30 parts of sulphur and 2 parts of nitrogen from 1,000,000 parts of iron produces a seven-fold increase in permeability; 1 part of antimony in 100,000,000 of germanium doubles the conductivity.

Perhaps some day we shall be privileged to study the properties of really pure metals. The first problem is to secure them.

Acknowledgment

And now I close with the most pleasant task of the acknowledgment of my indebtedness to several of my colleagues in the Metallurgical Department of the Bell Telephone Laboratories. They have been thoughtful in their counsel, unsparing in their criticism, and unstinting with their help in the preparation of this paper. These words do not, however, express my full feelings. I can do no better than paraphrase Montaigne's words of many years ago: "I have gathered me a posy of other men's flowers, only the thread that binds them is my own."

The Mechanism of Sulphur Transfer between Carbon-Saturated Iron and CaO-SiO₂-Al₂O₃ Slags

by G. Derge, W. O. Philbrook, and Kenneth M. Goldman

The area of the slag-metal interface is a rate-determining factor in the transfer of sulphur from iron to CaO-Al₂O₃-SiO₂ slags in a carbon-saturated system. Concentration gradients are removed by convection rather than diffusion. The sulphur crosses the interface in chemical combination with iron which is later reduced to pellets, accompanied by evolution of CO gas and formation of a stable calcium-sulphur compound in the slag.

EQUILIBRIUM conditions for steelmaking reactions have been studied extensively over the past two decades by a number of investigators, with gratifying results. Equilibrium data are essential to the understanding of any process, and such knowledge has the practical utility of placing a limit beyond which control measures cannot succeed. When, however, the driving rate of an industrial process is so fast that there is not time for reactions to reach equilibrium, it then becomes necessary that the factors which control the rates of reaction be known in order to establish full control of the process.

The desulphurization of molten pig iron by slags within the iron blast furnace is one such process in which the actual degree of sulphur absorption by the slag does not approach the equilibrium distribution obtained for similar slag-metal systems in the laboratory.¹ A study of the rate-controlling factors governing the desulphurization of iron by slags is becoming increasingly important as the sulphur content of raw materials increases with depletion of higher grade ores and coal. Following up an initial

study on kinetics,² this paper reports some results of a continuing laboratory investigation on the mechanism of sulphur transfer between molten iron saturated with carbon and slags of the CaO-SiO₂-Al₂O₃ system. Laboratory experiments cannot reproduce in detail the conditions which prevail in the hearth of a blast furnace, but they will contribute to an understanding of the smelting reactions and perhaps will explain some apparent inconsistencies in the factors controlling the equilibrium distribution of sulphur between iron and slags under reducing compared with oxidizing conditions.

The mechanism of a reaction—that is, the individual steps and the sequence in which they occur to produce the overall reaction which is ordinarily observed—must be elucidated to learn which steps are the slow ones, or “bottlenecks,” that fix the pace of the process as a whole. In the desulphurization reaction, for example, the overall rate might, in principle, depend upon the rate of diffusion of sulphur in the metal or in the slag, upon the speed of some homogeneous reaction taking place entirely within one of the phases, or upon some heterogeneous reaction taking place across the slag-metal interface. Even some side reaction or the back reaction might have some influence. Evidence on all of these points will be presented in this paper.

The rate of diffusion of sulphur in both iron and slag is so slow that it seems necessary to assume that convection provides the mechanism of carrying

G. DERGE, W. O. PHILBROOK, Members AIME, and KENNETH M. GOLDMAN, Junior Member AIME, are associated with the Metals Research Laboratory, Carnegie Institute of Technology, Pittsburgh, Pa.

AIME New York Meeting, February 1950.

TP 2885 C. Discussion (2 copies) may be sent to Transactions AIME before Dec. 15, 1950. Manuscript received Feb. 13, 1950; revision received July 3, 1950.

sulphur to and from the interface. Holbrook, Furnas, and Joseph³ found the diffusion constant for sulphur in carbon-saturated liquid iron to be of the order of 0.0001 cm² per sec.,* and data reported here provide

* The authors acknowledge the discussion of L. S. Darken in reporting this constant. The relation between the diffusion coefficient, D, in cm² per sec, and K, of reference 3, is D = 7K/100, where 7 is the density of liquid iron.

an upper limit for the diffusion constant for sulphur in molten slags.

It will be shown that the net rate of desulphurization of iron by slag is directly proportional to the area of slag-metal interface. Then, since the reaction is interface controlled, it was of interest to learn the nature of the reaction occurring there. The experiments indicated that iron and sulphur leave the metal and enter the slag together. Because the slags sometimes contained relatively large amounts of iron, it was necessary to prove that the iron in question was chemically combined and not entrapped metallic iron. This lead both to interesting observations concerning reactions involving iron and sulphur within the slag phase and to evidence on the origin of droplets of metallic iron in the slag which is contrary to the interpretation given by Holbrook and Joseph⁴ in their classic paper on the desulphurizing power of blast furnace slags.

These various experiments support the view that sulphur originally present in the iron is transferred across the interface into the slag in combination with iron, and the sulphur then is stabilized in the slag by combination with calcium. The iron oxide resulting from this slag phase reaction is in turn reduced to iron by carbon. The process may be described schematically as the following sequence:

1. $\text{FeS}_{(\text{Fe})} \rightleftharpoons \text{FeS}_{(\text{slag})}$
2. $\text{FeS}_{(\text{slag})} + \text{CaO}_{(\text{slag})} \rightleftharpoons \text{CaS}_{(\text{slag})} + \text{FeO}_{(\text{slag})}$
3. $\text{FeO}_{(\text{slag})} + \text{C}_{(\text{truecible or metal})} \rightarrow \text{Fe} + \text{CO}_{(\text{gas})}$

Steps 1 and 3 are heterogeneous and 2 is homogeneous.

The foregoing sequence of reactions has long been surmised, as will be noted in the following section, but detailed quantitative observations have heretofore been lacking.

Literature Survey

The general problem of desulphurization in iron and steelmaking has been the object of so many reviews and discussions that it does not seem appropriate to make an exhaustive literature survey here. Only the more recent papers dealing with those phases of the problem which are pertinent to this investigation of the mechanism and kinetics of sulphur transfer under reducing conditions will be cited.

Holbrook and Joseph⁴ measured the relative desulphurizing powers of blast furnace slags without reference to equilibrium conditions. They made many observations on the mechanism and noted that there was an evolution of gas, presumably CO, which accompanied sulphur transfer. They also found an accumulation of sulphur at the slag-metal interface and surrounding the gas bubbles in the slag. Iron beads or pellets were found in the slag when the system contained sulphur, but not when the system was sulphur-free. These iron pellets were almost completely desulphurized. The movement of metal beads into the slag by the action of the gas bubbles was explained by Holbrook and Joseph as follows:

A bubble of CO, formed at the slag-metal interface by the reaction $\text{FeO} + \text{C} = \text{Fe} + \text{CO}$, remains attached to the metal bath until it grows so large that its buoyancy in the slag causes it to leave the metal and rise into the slag. The CO bubble apparently carries small particles of molten iron with it into the slag, where they are desulphurized.

Herty and Gaines⁵ state that the key to the process of sulphur elimination is the relative oxidation of the slag, with low FeO and MnO, high CaO, and high temperature favoring desulphurization. Another necessary factor is the proper means of absorbing sulphides from the metal by the slag. Since it is assumed that desulphurization takes place at the interface between slag and metal and in the slag but not in the metal, it is necessary that sulphur be transferred from metal to slag in order for the desulphurizing reactions in the slag to take place.

It is concluded by Wüst⁶ that the major portion of sulphur removal in the blast furnace occurs while the metal is passing through the slag and a negligible part while slag and metal exist as contiguous layers in the hearth. This idea is substantiated in part by diffusion studies of sulphur in molten iron made by Holbrook and coworkers,³ who observed that the diffusion of sulphur in liquid iron is extremely slow.

Chang and Goldman⁷ measured the rate of sulphur transfer across a slag-metal interface and found that the rate from slag to metal was nearly independent of slag composition, while that in the reverse direction increased with increase in basicity. They also observed that there was a very definite color change in the quenched slag samples during the course of any one experiment. The color changed from colorless, through green, yellow, orange, brown to black as desulphurization proceeded. In the field of colored glasses, ferrous sulphide is known as a strong color producer, yielding yellow, orange, brown, blue, and black. Martin, Glockler, and Wood⁸ investigated the form of sulphur in blast furnace samples which had been quenched and which contained ferrous, manganese, and calcium sulphide.

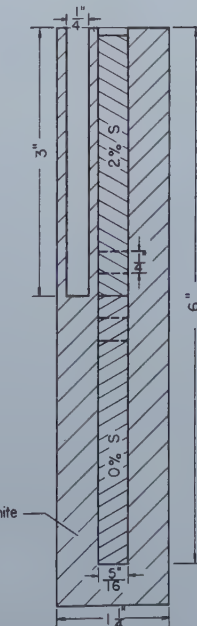


Fig. 1—Schematic diagram of crucible assembly for sulphur diffusion in slag.

Table I. Sulphur Diffusion at 1600°C

Nominal Slag Composition: SiO_2 37.1 pct, Al_2O_3 14.1 pct, CaO 45.3 pct, MgO 3.5 pct—based on weights of dried oxides. Sufficient CaS was added to give about 2 pct S in the high-sulphur slag.

Run 1, 5 min at temperature			Run 3, 6 hr at temperature		
Section No.	Sample Wt	S, Pct	Section No.	Sample Wt	S, Pct
2	0.0732	1.86	5	0.0659	1.80
3	0.0545	1.95	6	0.0468	1.84
4	0.0617	1.93	7	0.0477	1.86
5	0.0566	1.90	8	0.0609	1.88
6	0.0461	1.84	9	0.0510	1.78
7	0.0541	1.08	10	0.0723	1.10
8	0.0891	0.03	11	0.0643	0.26
9	0.0866	0.0	12	0.0506	0.0
10	0.1022	0.0	13	0.0429	0.0
11	0.0973	0.0	14	0.0614	0.0
			15	0.0491	0.0
			17	0.0532	0.0

They found that ferrous sulphide caused rapid color changes and that the amount of FeS required to form a colloid was about 0.03 pct. The color of slags containing more than 0.25 pct sulphur as calcium sulphide ranged from light yellow to deep orange. It appears that the slags used in this investigation contained FeS, and this points to the probable mechanism of sulphur transfer as being a direct transfer of ferrous sulphide. Philbrook, Goldman, and Helzel⁸ showed that the calcium content of iron under conditions similar to those in sulphur transfer experiments is so low that it is highly improbable that any effective combination of calcium and sulphur can be formed within the metal.

Diffusion

The first step in this investigation was the determination of a limiting value for the rate of diffusion of sulphur in slag. The experimental procedure was as follows: A graphite crucible, shown schematically in fig. 1, 5/16 in. ID, 1 1/4 in. OD, 6 in. deep, was used to melt a 3 in. column of low-sulphur slag, and, after all gas evolution ceased, the crucible was cooled to about 950°C in a small pot furnace. A high-sulphur slag was then poured over the low-sulphur slag, and the crucible containing the couple was placed in an induction furnace holding a graphite container near the temperature desired for the diffusion run. Temperature was measured by means of a tungsten-molybdenum thermocouple placed in a hole extending from the top of the crucible 3 in. down into the crucible wall. The furnace design gave a uniform temperature region over the entire length of slag column. After a definite time interval, the power was shut off, and the furnace was cooled more rapidly at the bottom than at the top to give progressive freezing and thus prevent stirring and piping. The graphite crucible and slag column were then sliced into sections about 1/4 in. long. Observations of the slag near the couple interface indicated that the joint was very clean, with no graphite present to interfere with diffusion. Each sample was analyzed for sulphur content. Table I gives data for two typical runs in which all experimental conditions were under satisfactory control. Diffusion curves are plotted in fig. 2.

Run 1, in which the slag was at temperature for only 5 min, was intended to serve as a blank. It indicates the amount of disturbance to be expected at the interface as a result of melting and freezing,

without allowing time for diffusion. Run 3 was comparable with run 1 in every way except that the couple was held at temperature for 6 hr, which approached the longest time during which conditions could be maintained sufficiently constant to be considered reliable. It is apparent from fig. 2 that the differences between runs 1 and 3 are so slight as to be insignificant and that diffusion of sulphur under these conditions is too slow to be measured by this type of experiment.

The principal limitations to the accuracy of the determination of the rate of diffusion of sulphur in slag by this method are the influence of melting and freezing on the shape of the interface and the size of the section which can be removed from the slag couple by the carborundum cutting wheel.

The particular solution of the general (Fick's law) diffusion equation which satisfies the initial and boundary conditions of this experiment is the following:

$$C = \frac{C_0}{2} \left\{ 1 - \psi \left(\frac{x}{2\sqrt{Dt}} \right) \right\}$$

where C is the concentration at some distance x from the interface after diffusion time t ; C_0 is the difference between initial concentrations of sulphur in high and low-sulphur slag; D is the diffusion coefficient, cm^2 per sec; and $\psi \left(\frac{x}{2\sqrt{Dt}} \right)$ is Gauss' error integral.¹⁵

The minimum rate of diffusion which could be measured by the present technique may be estimated in the following way. The limits of accuracy and of measurement are such that it is reasonable to assume that a change of sulphur concentration (due to diffusion) of 5 pct of the maximum spread in sulphur content between high and low-sulphur slags could be detected at a distance of 1/8 in. from the interface. By substituting these limits of detection into the diffusion equation for a time of 6 hr, the limiting value of D which could be measured is obtained:

$$C = 0.95 C_0$$

$$\text{at } x = -\frac{1}{8} \text{ in.} = -0.32 \text{ cm}$$

$$\text{and } t = 6 \text{ hr} = 21,600 \text{ sec}$$

$$0.95 C_0 = \frac{C_0}{2} \left\{ 1 - \psi \left(\frac{0.32}{2\sqrt{21,600 D}} \right) \right\}$$

$$D = 9 \times 10^{-7} \text{ cm}^2 \text{ per sec}$$

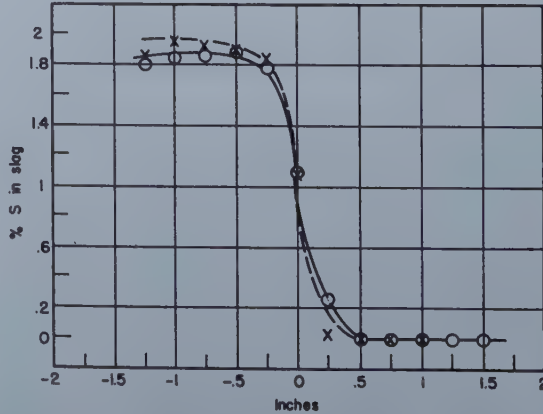


Fig. 2—Diffusion penetration curves.

— X — Blank run 1, 5 min, 1600°C.
— O — Diffusion run 3, 360 min, 1600°C.

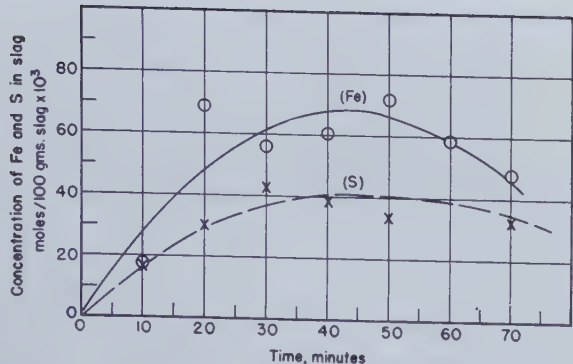


Fig. 3a—Rate curves for iron and sulphur in slags, experiment 63, table IV.

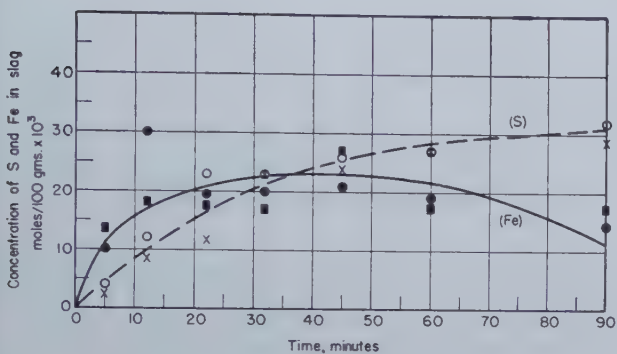


Fig. 3b—Rate curves for iron and sulphur in slags, experiments 1 and 2, table III.

The measured diffusion coefficient, calculated from the data of experiment 3, was $D = 6 \times 10^{-6} \text{ cm}^2$ per sec for $C = 2.02$ pct sulphur at $x = -\frac{1}{4}$ in. This was the largest value of D which was observed. In view of the fact that the slags were rather fluid at 1600°C , it is entirely possible that the small penetration of sulphur observed may have been caused, at least in part, by stirring rather than by diffusion. This would have the effect of giving an observed value of D higher than the true value. Thus it may be concluded that the diffusion constant for sulphur in slags of the composition studied is less than 10^{-5} cm^2 per sec. This is about ten times less than the diffusion coefficient of sulphur in carbon-saturated iron.³ In order to account for observed rates of desulphurization, it must be concluded that sulphur

concentration gradients in slag and metal are dissipated by convection rather than by diffusion.

Influence of Interface Area on Sulphur Transfer

Although most investigators have either inferred or postulated that sulphur transfer is an interface reaction, direct quantitative proof of this is incomplete. This evidence is augmented by the following experiments made under conditions similar to those already described by Chang and Goldman.² If the rate of sulphur transfer from metal to slag is proportional to the sulphur concentration in the metal and to the interfacial area, then it can be described by the following equation:

$$-\frac{dS}{dt} = KA \frac{S \times 100}{W_{Fe}}$$

where, S is total amount of sulphur in the metal phase at any time, g ; A is area of the slag-metal interface, cm^2 ; t is time in min; K is rate constant, $\text{g per (min)} (\text{cm})^2$ (unit concentration, wt pct, of sulphur in iron); and W_{Fe} is weight of iron, g .

Integration of this equation gives:

$$K = \frac{W_{Fe}}{100 A t} \ln \frac{S_0}{S_t}$$

where, S_0 is total amount of sulphur in the iron at $t = 0$, and S_t is total amount of sulphur in the iron at time t .

Assume that in the early stages of the process, the sulphur transfer in the reverse direction from slag to metal is relatively small and can be neglected. Table II shows the calculated values of K for several different runs with the same nominal slag composition (39 pct SiO_2 , 47 pct CaO , 14 pct Al_2O_3) but with initial sulphur contents of the iron covering a nominal range of 0.5 to 2 pct and the interfacial area showing a fourfold increase from 2.8 to 11.4 cm^2 . The excellent consistency of the rate constant K for this range of conditions confirms the belief that sulphur transfer is indeed an interface-controlled reaction. This same conclusion was indicated by the Chang and Goldman work² in which the same specific rate constants were found for runs in both stationary and rotating crucibles, although the net

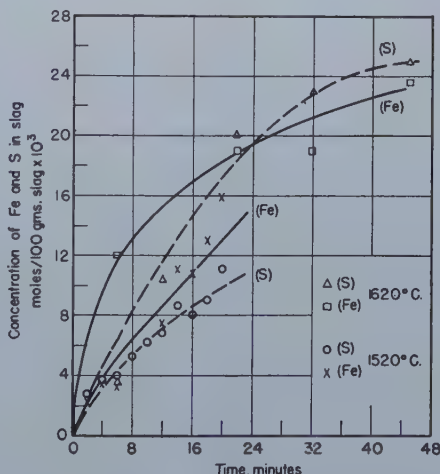


Fig. 4—Effect of temperature on rates of transfer of iron and sulphur. Experiments 1 and 2 at 1620°C , experiment 27 at 1520°C , 1530 slag.

Table II. Initial Rates of Sulphur Transfer Reaction (Graphite Crucible)

Experiment No.	Graphite Crucible ID, cm	Inter-face Area, cm^2	Temp, $^\circ\text{C}$	W_{Fe} , g	Initial S in Iron, g	Slag Wt, g	Time, Min	K
2	2.54	5.1	1,580	104.5	1.94	29.6	5	0.0070
8	2.54	5.1	1,580	101	0.99	30.0	7	0.0061
24	2.54	5.1	1,580	101	0.57	30.2	7.2	0.0057
6	1.90	2.8	1,580	64.7	0.72	19.7	6.8	0.0059
5	3.81	11.4	1,580	202	2.04	60.3	5.75	0.0057
							avg.	0.0060

rate of sulphur transfer was less with stationary crucibles because of the smaller slag-metal interface.

Iron Transfer

The preceding sections have established that the rate of desulphurization is controlled by a slag-metal interface reaction. The details of the mechanism of this reaction have been investigated by observing changes in iron content of the slag coincident with sulphur transfer.

Slag-Metal Reactions: Experimental Procedures and Equipment: The induction-heated graphite crucible and methods of sampling slag and metal were the same as those described by Chang and Goldman² except that the crucible was enlarged to provide more material for sampling. The crucible used for this work was 2 1/4 in. ID and 5 in. deep.

The experimental procedure consisted of melting 530 g of ingot iron in a graphite crucible and saturating with carbon, introducing approximately 1 pct sulphur as FeS, then adding 80 g of solid, prefused slag. Samples were taken at definite time intervals and analyzed for iron and sulphur. In some experiments, the slag was melted separately and then poured onto the molten iron to define the starting time more clearly.

Data and Discussion: The experiments and pertinent data are listed in table III. Some typical curves showing the time dependence of iron and sulphur transfer are shown in figs. 3 to 6. Two typical complete experiments are shown in figs. 3a and b. It is seen that there is a rapid initial increase of both iron and sulphur content of the slag, but that while the sulphur approaches a high steady value asymptotically, the iron passes through a maximum and approaches a low final value cor-

Table III. Iron Transfer Data

Experiment No.	Temp., °C	Total Time, Min	Max. Pct Fe in Slag	Time to Reach Max. Pct Fe in Slag, Min	Nominal Initial Pct S in Iron	Slag Designation*
1	1,620	150	1.50	45	1	1530
2	1,620	180	1.68	12	1	1530
3	1,620	121	1.15	45	1	1549
5	1,620	180	4.30	32	1	1549
6	1,610	180	3.40	120	1	1530
7	1,620	180	2.71	1	1	1549
8	1,620	150	1.2	12	0.03	1530
9	1,620	180	0.610	32	0.03	1530
10	1,620	180	0.511	90	0.03	1549
11	1,570	120	0.511	13	0.03	1549
12	1,580	120	0.587	12-33	1	1530
13	1,580	120	0.976	32	1	1530
14	1,560	120	0.941	60	1	1530
15	1,540	120	0.244	32-45	1	1530
16	1,520	120	0.689	60	1	1530
17	1,510	120	0.383	45	1	1530
18	1,560	80	0.355	8	0.03	1549
29	1,585	20	0.350	14	0.03	1549
30	1,580	20	0.344	4	0.03	1549
33	1,550	20	0.303	18	0.03	1530
34	1,540	20	0.340	2	0.03	1530
22	1,540	20	0.859	**	1	1530
23	1,560	20	0.569	**	1	1530
24	1,600	20	1.322	**	1	1549
25	1,575	20	1.59	**	1	1549
27	1,524	20	0.890	**	1	1530
28	1,600	20	1.546	**	1	1549

* In this code, the first two digits represent pct Al_2O_3 , the last two digits pct CaO; for example: Slag 1530 = 15 pct Al_2O_3 , 30 pct CaO, 55 pct SiO_2 (bal.).

** These experiments were terminated at the end of 20 min, during which time no maxima were observed.

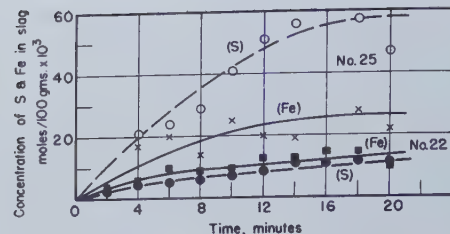


Fig. 5—Effect of slag composition on rates of transfer of iron and sulphur.

○ Mols S per 100 g slag { 49 pct CaO
 × Mols Fe per 100 g slag { 36 pct SiO_2
 ■ Mols S per 100 g slag { 30 pct CaO
 ▨ Mols Fe per 100 g slag { 55 pct SiO_2
 Temp = 1550°C

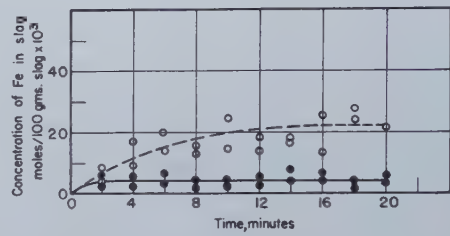


Fig. 6—Effect of sulphur in the iron on rates of iron transfer.

○ Initial pct S in iron = 0.85, experiments 24 and 25.
 ● Initial pct S in iron = 0.03, experiments 29 and 30.
 1549 slag Temp = 1580°C

responding to the equilibrium value observed by Hatch and Chipman.¹ Within the entire range of slag composition and temperature studied, the relative amounts of the iron and sulphur varied considerably during the initial stage, but the maximum in the iron curve always appeared. Figs. 4 to 6 show the influence of temperature, slag basicity, and initial sulphur content of the iron on the initial stages only. From these it may be observed that: (1) The amount of sulphur transferred increases with temperature, slag basicity, and sulphur in the iron, in agreement with most previously published work. (2) The initial rate of iron transfer varies in the same manner as the sulphur. (3) The iron content of the slag passes through a maximum and finally reaches some steady low value which appears to be independent of the sulphur content. (4) The magnitude of the maximum in iron content and the time at which it occurs are erratic.

The above relations between iron and sulphur in the slag indicate that the sulphur enters the slag from the metal as some iron-sulphur compound. The maximum in the iron curve indicates further that this compound disappears through reaction with other constituents in the slag. When the rates of such a series of consecutive reactions are comparable, it can be shown by classical chemical kinetics that a maximum will occur when the concentration of the intermediate product is plotted against time.⁹ The series of reactions 1, 2, 3 suggested in the introduction would provide a satisfactory model for the experimental observations if it is assumed that the

Table IV. Data on Reduction of Slag in Carbon and Non-Carbon Systems

A—Composition of Initial Slags

Experiment No.	Slag Composition, Pct				
	Al ₂ O ₃	CaO	SiO ₂	S	Fe
63	14.6	42.0	42.0	1.1	2.7
66	14.0	30.8	52.0	0.4	1.4

B—Data on Remelted Slags

Experiment No.	Initial Slag	Final Analysis, Wt Pct					Crucible Material	Temp, °C	Time, Min	Remarks
		S	Fe	Al ₂ O ₃	CaO	SiO ₂				
69	63	1.1	1.3	17.5	39.9	42.0	Graphite	1,500	15	Iron bead, 0.6 g
74	63	1.0	1.3	13.9	43.4	39.9	Graphite	1,580	105	Iron bead, 1.2 g
75	63	1.2	2.0	29.4	40.4	25.3	Graphite	1,600	390	Iron bead, 1.1 g
115	63	1.2	0.19	19.7	39.0	39.0	Graphite	1,600	90	Scattered beads
119	63	1.4	0.17	18.5	39.4	41.2	Graphite	1,600	90	Scattered beads
120	63	1.0	0.27	18.8	39.3	39.7	Graphite	1,600	90	Scattered beads
79	63	3.6	24.0	24.0	34.0	BeO	1,600	60	No beads	
95	63	0.5	0.87	6.9	59.0	33.0	CaO	1,600	60	No beads
96	63	0.41	1.1	7.8	58.0	30.0	CaO	1,600	60	No beads
72	63	0.46	1.4	17.3	38.9	40.4	Pt	1,300	15	No beads
90	66	0.4	1.4	19.0	30.2	49.0	Graphite	1,600	72	Iron bead, 0.11 g
110	66	0.4	0.4	14.5	25.1	59.0	SiO ₂	1,600	60	No beads
111	66	0.4	0.6	13.5	22.9	60.1	SiO ₂	1,600	60	No beads

rate of the homogeneous slag reaction 2 is very much greater than the rates of the heterogeneous reactions 1 and 3.

Slag Reactions

In order to learn more about the observed behavior of iron in slag, a detailed study of the behavior of iron and the form of occurrence of iron and sulphur in slags of two compositions was made by the following experiments: (1) Slag containing iron and sulphur was remelted over low-sulphur iron. (2) The same slag was remelted in the absence of iron under both neutral and reducing conditions.

had become saturated with carbon, 150 g of ferrous sulphide was introduced to give about 1 pct sulphur in the iron.

A metal sample was taken by means of a 12 in. length of $\frac{1}{8}$ in. ID fused silica tube to which was attached a rubber suction bulb. Then a charge of prefused, crushed slag was added and after it was molten, slag samples were removed at 10-min intervals by means of copper samplers described elsewhere.² At the end of the run, a final metal sample was taken, after which all of the slag was removed from the crucible by hot-dipping. The heat log showed that the iron content of the slag was near its maximum at this time. The slag samples and the entire quantity of final slag were crushed, screened through a 100-mesh sieve, and cleaned magnetically. They were analyzed for S, Fe, Al₂O₃, SiO₂, and CaO. The magnetic fraction of the slag was analyzed for C, S, and Fe. The iron samples were analyzed for S, Si, and C.

The magnetically cleaned, final slag from such a heat will be referred to as a "reacted slag." Two such slags, 63 and 66, were made to represent acid and basic compositions; their analyses appear in table IV. Portions of the reacted slag were subjected to the sequence of experiments portrayed by the flowsheet, fig. 7. Samples of this reacted slag were remelted over a bath of carbon-saturated, low-sulphur iron to study the transfer of sulphur from slag to metal. Similar samples were melted in graphite without iron and also in refractory cruci-

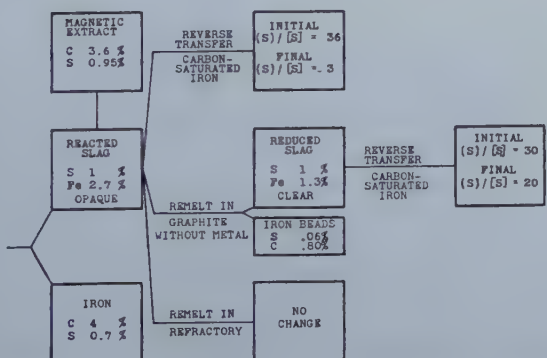


Fig. 7—Flowsheet of experimental procedures used in iron transfer experiments.

Starting material from experiment 63. See tables IV, V, and VI.

(3) Slags which had been treated by step 2 were remelted over low-sulphur iron.

The results indicate that the iron analyzed in the slag was chemically combined and not mechanically entrapped metallic iron.

Experimental Procedure: A charge of 3630 g of ingot iron was melted in a 6 in. OD, 4½ in. ID, 5½ in. deep graphite crucible with cover. After the iron

Table V. Data on Metal Samples from Slag Reduction Experiments

	C, Pct	S, Pct
Reduced Pellets	0.81	0.058
Magnetic Extract	3.59	0.95
Iron Bath	4.0	~ 1

Table VI-A. Sulphur Transfer from Reacted Slag No. 63
Temp, 1500°C

Experiment No.	Time, Min	Sulphur, Pct				(S)/[S]	
		Initial Metal	Final Metal	Initial Slag	Final Slag	Initial	Final
67	90	0.03	0.100	1.1	0.31	36	3.2
68	60	0.03	0.136	1.1	0.36	36	3.8
70	102	0.03	0.110	1.1	0.54	36	2.0

bles such as BeO, SiO₂, CaO, and Pt to study the reduction or coagulation of iron from the slag. Pertinent data from these experiments are listed in tables IV, V, and VI.

Discussion: Several significant factors have appeared as a result of these experiments: (1) When a reacted slag containing approximately 1 pct S was placed over a bath of carbon-saturated iron containing only 0.045 pct S, there was the expected transfer of sulphur from the slag to the iron, indicating that the preparation and remelting of the reacted slag did not alter it in any fundamental way. (2) When a reacted slag containing 1 pct S and 2.7 pct Fe was remelted in a graphite crucible without an iron bath, beads of iron were formed. (3) When the same reacted slag was remelted in BeO, SiO₂, CaO, or Pt crucibles, no beads of iron were formed.

These experiments were repeated several times with the same results. The iron beads from several such slags were combined to give the required weight for analysis. Analysis showed 0.8 pct C and 0.06 pct S. It is noteworthy that the sulphur content of the reduced slag remained at about 1 pct, whereas the iron content decreased to a value of 1.3 pct. These results indicate that the beads resulted from reduction of the combined iron in the slags rather than agglomeration of dispersed metallic iron, for no iron pellets were produced in the carbon-free systems. It should be noted also that the carbon and sulphur contents of the pellets reduced from the slag were much lower than the analysis of the magnetic extract from the reacted slag, table V. The magnetic extract was comparable to the iron bath. It was observed that when these high-sulphur slags were remelted in graphite under helium, they changed from a black, opaque material to an almost colorless glass after the iron was reduced, whereas there was no change in appearance after remelting under neutral conditions.

An additional and most interesting observation may be made by contrasting table VI-B with table VI-A. When a reacted slag was placed over a new bath of low-sulphur iron, the result was that expected of a sequence of reversible reactions, namely the net rate of sulphur transfer was greater from slag to metal under these circumstances, and a com-

Table VI-B. Sulphur Transfer from Reduced Slag
(Starting material, slag from No. 63)

Experiment No.	Time, Min	Sulphur, Pct				(S)/[S]	
		Initial Metal	Final Metal	Initial Slag	Final Slag	Initial	Final
116	60	0.04	0.062	1.15	1.15	29	18.6
117	60	0.04	0.060	1.15	1.55	29	25.8
118	60	0.04	0.046	1.15	1.21	29	26.3
121	60	0.04	0.082	1.15	0.838	29	10.2
122	60	0.04	0.088	1.15	0.765	29	8.7
123	60	0.04	0.083	1.15	1.088	29	13.1

paratively low ratio of (S)/[S] was reached after an hour's reaction time. On the other hand, when the reacted slag had been reduced first by remelting in graphite, it showed a greatly diminished tendency to transfer sulphur to a new bath of low-sulphur iron. The reduction of iron from the slag apparently stabilized the sulphur content of the slag.

A final interpretation of this phenomenon will not be offered at this time because more extensive investigation is being made. The observation does not seem to be inconsistent with the proposed mechanism. If reaction 3 has been driven nearly to

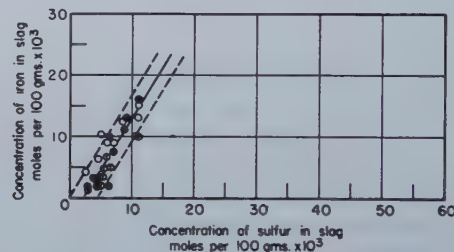


Fig. 8—Concentration of sulphur vs. concentration of iron in acid slags.

— Determined by least squares.
— — — 2 σ limits

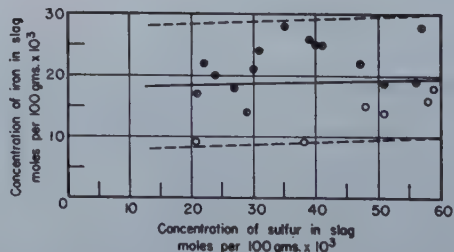


Fig. 9—Concentration of sulphur vs. concentration of iron in basic slags.

— Determined by least squares.
— — — 2 σ limits

completion by isolating part of the system, then reactions 2 and 1 can proceed in the reverse direction when the system has been reconstituted only in so far as oxygen (represented as FeO in the equations) may be available.

Kinetics of Reaction Mechanism

Information on the relative rates of the three reactions involved in the desulphurization mechanism

Table VII. Correlation Coefficients for Iron and Sulphur in Slag

Experiment No.	Slag Designation	Correlation Coefficient	Slope
22,23,27	1530 (acid)	0.98	1.7
24,25,28	1549 (basic)	0.05	0.02

can be obtained by consideration of the relation between iron and sulphur in the slag during the initial stages of the process. Data from the first 20 min of the various experiments in the previous sections are included in fig. 8 for acid slags and in fig. 9 for basic slags. Molar concentrations have been used. In these figures the lines were fitted by the method of least squares and the 2σ limits are also shown. It is apparent from figs. 8 and 9 that: (1) The slope of the line for acid slags is much greater than that

phase. This reduction could occur at either the slag-metal or slag-graphite interface. The majority of the pellets were found near the graphite crucible walls and this was also reported by Holbrook and Joseph,⁴ so the graphite interface is apparently the more important one. Contrary to the latter authors' interpretation, it does not seem likely that the pellets were pulled from the iron bath by the CO gas evolved, for the desulphurizing process is not rapid enough to produce the low sulphurs found in these pellets during their short transit through the slag. The pellets contained equilibrium sulphur because they are actually produced by reduction from the slag.

Gas Evolution

The discussion up to this point has indicated a reaction mechanism which finally requires the reduction of iron oxide in the slag with the evolution of CO gas, according to reaction 3. This gas evolution has been observed by most investigators, but again, a detailed study of the factors determining the rate of gas evolution is required.

Experimental Procedure: The equipment for these experiments consisted of a graphite crucible 1 in. ID and 4 in. deep, surrounded by a layer of graphite powder contained in an alundum thimble. The entire setup was enclosed in a fused silica tube with suitable outlets to a vacuum pump, two gas burettes, and a helium or nitrogen tank.

An ingot iron charge (106 g) was melted in the graphite crucible together with 3.2 g of FeS. After melting, the system was closed, evacuated to about 2 mm Hg pressure, and then flushed several times with nitrogen or helium. A charge of 16 g of pre-fused slag, contained in an iron cup and attached to the end of the thermocouple protection tube, was then lowered into the iron bath, thus determining the starting time of the experiment. The volume of gas evolved was measured by the gas burettes, and gas samples were analyzed for CO_2 and CO and found to be only CO. No sulphur could be detected in the gas. The iron was analyzed for Si and S, and the slag for S, Al_2O_3 , CaO, SiO_2 , and Fe. Temperatures were measured with a calibrated platinum-platinum-rhodium thermocouple, dipped into the slag.

Data Results: Effect of Temperature, Slag Composition, and Sulphur Content in the Metal During Sulphur Transfer: Typical data from these experiments are shown in table VIII and plotted in fig. 10. The curves show that CO evolution is favored by

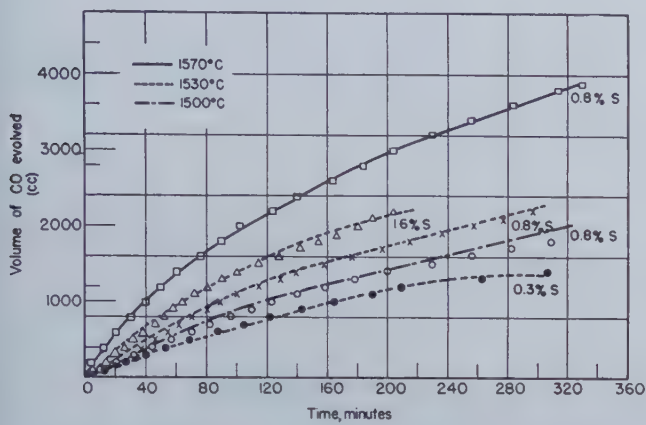


Fig. 10—Effect of temperature and sulphur concentration of the iron on the rate of evolution of carbon monoxide gas.

for basic slags (see table VII). (2) The absolute values of the concentration of iron and sulphur are higher in the basic than in the acid slags. (3) The correlation between iron and sulphur is high in acid slags, but apparently absent in basic slags (see table VII). These features will be discussed in terms of the desulphurization mechanism in which reactions 1 and 3 are heterogeneous while reaction 2 is homogeneous.

Since heterogeneous reactions are usually slower than homogeneous reactions, 1 and 3 may be thought of as the rate-controlling reactions for sulphur transfer. Reaction 1 represents the input of iron and sulphur to the slag and 3 represents the output of iron from the slag. The slope 1.7 for the acid slags as compared to 0.02 for the basic slags indicates that in the acid slags the initial rate of input of iron to the slag per unit of sulphur, reaction 1, is greater than the rate of output of iron from the slag, reaction 3, because the low activity of CaO prevents the formation of FeO by reaction 2. In the basic slags, however, there is little correlation between iron and sulphur because reactions 2 and 3, which determine the iron output, proceed so rapidly that the iron content of the slag actually is determined by its state of oxidation rather than its sulphur content. Since iron and sulphur transfer together initially, the absolute values for both iron and sulphur must be greater in the case of a slag containing large quantities of lime. The equilibrium of course requires that the final sulphur values shall be higher in the basic slag. No effect of temperature was observed on the slope of the lines in figs. 8 and 9.

The various observations described in the preceding sections indicate strongly that the iron pellets found in the slag after sulphur transfer result from chemical reduction of oxidized iron in the slag

Table VIII. Effect of Temperature, Slag Composition, and Sulphur Content in the Metal on Rate of Gas Evolution During Sulphur Transfer

Ex-periment No.	Initial Slag Designation	Temp, °C	Time, Min	Total Vol, cc*	Initial Pct S in Metal	Final Pct Si in Metal
53	1831	1,570	331	3,900	0.8	0.951
54	1831	1,570	329	2,275	0.03	0.884
56	1831	1,500	309	1,800	0.8	0.402
57	1831	1,500	309	1,350	0.03	0.439
58	1831	1,530	307	2,250	0.8	0.613
59	1831	1,530	307	1,400	0.03	0.519
60	1831	1,530	204	2,200	1.6	0.500
41	1951	1,520	136	600	0.8	0.02
42	1951	1,530	422	1,250	0.8	0.210
44	1951	1,560	168	850	0.8	0.042
45	1951	1,590	242	1,200	0.8	0.148

* Standard temperature and pressure.

high temperature and by high sulphur in the iron, the same factors which favor sulphur transfer. These facts establish that CO evolution is associated with the sulphur reaction. On the other hand, significant amounts of CO were evolved in blank runs when the iron contained only 0.03 pct S, and the sulphur reaction alone cannot account for this gas. Side reactions, such as the reduction of silica in the slag, must be responsible for this discrepancy, but a satisfactory material balance for CO on the basis of conventional slag and metal analyses has not yet been achieved. This and other phenomena connected with gas evolution are the subject of a current research program which will be reported separately.

Slag Constitution

The experiments of the previous sections provide a picture of sulphur transfer involving an iron-sulphur compound as an important intermediate in the process. Although no further direct evidence is available, it is pertinent to visualize the role of this intermediate in terms of the more recent pictures of slag constitution.¹⁰⁻¹² The slag may be regarded as a network of silicate tetrahedra with the small, highly charged silicon ions at the centers of tetrahedra and oxygen ions at the corners. Each corner is shared by two tetrahedra except where the linkage is broken by larger calcium and ferrous ions. Although not exhibiting the complete regularity of crystals, these slags approach an arrangement of the closest possible packing of the constituents in a statistical manner. From consideration of chemical similarity, it might be expected that sulphur would substitute for oxygen when it enters this network, but spatially it has a larger diameter than oxygen, which might require a high activation energy for the process. Similarly, iron should substitute for calcium, and it can do this readily because it has a smaller diameter. These compensating volume effects thus facilitate the entrance of sulphur into the silicate network when it is combined with iron instead of calcium. This can be followed by a rearrangement within the slag in which the sulphur will become bound statistically to calcium rather than iron, the latter becoming an oxide rather than a sulphide. This is the end state required for thermodynamic equilibrium.^{13, 14} The iron-sulphur combination thus plays the characteristic role of an intermediate compound in facilitating the process without remaining as a final product. The diameters of the various ions under discussion are as follows:¹⁵

Ion	Diam, Å	Ion	Diam, Å
Fe ⁺⁺	1.50	O=	2.80
Ca ⁺⁺	1.98	S=	3.68
Si ⁺⁺⁺⁺	0.82		

Summary

Based largely on experimental evidence, a detailed picture has been developed for the mechanism of sulphur transfer between iron and slag in equilibrium with a graphite crucible.

1. Diffusion of sulphur in an Al₂O₃-SiO₂-CaO slag is so slow at 1600°C that concentration gradients are eliminated by convection rather than diffusion.

2. The area of the slag-metal interface is a determining factor in the rate of the process.

3. Iron transfers across the interface with sulphur. The time curve for iron in the slag contains

a maximum which can be interpreted as showing that the iron-sulphur compound is an intermediate rather than an end product of the reaction.

4. The analyzed iron in the slags in these experiments was chemically combined iron, not mechanically entrapped, metallic iron.

5. The iron pellets resulting from desulphurization are produced by the reduction of combined iron in the slag rather than the entrainment of parts of the metal bath by CO evolution.

6. The rate of gas (CO) evolution accompanying the sulphur reaction increases with temperature and with the sulphur content of the iron.

7. The experiments provide quantitative proof and an elaboration in detail of the most widely accepted mechanism for desulphurization under reducing conditions:

1. $\text{FeS}_{(\text{Fe})} \rightleftharpoons \text{FeS}_{(\text{slag})}$
2. $\text{FeS}_{(\text{slag})} + \text{CaO}_{(\text{slag})} \rightleftharpoons \text{CaS}_{(\text{slag})} + \text{FeO}_{(\text{slag})}$
3. $\text{FeO}_{(\text{slag})} + \text{C}_{(\text{crucible or metal})} \rightarrow \text{Fe} + \text{CO}_{(\text{gas})}$

Acknowledgments

The research on diffusion and influence of interface area was conducted by the late Dr. Sheng-Nien Wang, and the authors wish to call special attention to his contribution.

The remainder of the paper was part of a research program sponsored by the Office of Naval Research in the Metals Research Laboratory at the Carnegie Institute of Technology, under Contract N6ori-47/IV, Project NR 031-014. The authors wish to acknowledge the assistance of other members of the project, particularly M. M. Helzel and E. E. Duncan for supervision of the analytical work and Siu Hwa Chang, Saul Gilbert, and J. P. Martin, Jr., for laboratory assistance.

References

- ¹ G. G. Hatch and J. Chipman: *Trans. AIME* (1949) **185**, 274; *Jnl. Met.* (April 1949) TP 2556C.
- ² L. C. Chang and K. M. Goldman: *Trans. AIME* (1948) **176**, 309; *Met. Tech.* (June 1948) TP 2376C.
- ³ W. F. Holbrook, C. C. Furnas, and T. L. Joseph: *Ind. and Eng. Chem.* (1932) **24**, 993.
- ⁴ W. F. Holbrook and T. L. Joseph: *Trans. AIME* (1936) **120**, 99.
- ⁵ C. H. Herty and J. M. Gaines: *Blast Furnace and Steel Plant.* (1928) **16**, 233.
- ⁶ J. Wüst: *Jnl. Iron and Steel Inst.* (1927) **116**, (No. II) 65.
- ⁷ A. E. Martin, G. Glockler, and C. E. Wood: U. S. Bur. Mines. R. I. No. 3552 (1941).
- ⁸ W. O. Philbrook, K. M. Goldman, and M. M. Helzel: *Trans. AIME* (1950) **188**, 361; *Jnl. Met.* (Feb. 1950) TP 2811C.
- ⁹ S. Glasstone: *Textbook of Physical Chemistry.* 2nd Ed. p. 1077. 1946. D. Van Nostrand Co.
- ¹⁰ A. E. Martin and G. Derge: *Trans. AIME* (1943) **154**, 104.
- ¹¹ G. Derge: *Yearbook. A.I.S.I.* (1949) 368.
- ¹² J. Chipman and L. C. Chang: *Trans. AIME* (1949) **185**, 191; *Jnl. Met.* (Feb. 1949) TP 2529C.
- ¹³ L. S. Darken and B. M. Larsen: *Trans. AIME* (1942) **150**, 87.
- ¹⁴ J. Chipman and Ta Li: *Trans. A.S.M.* (1937) **25**, 435.
- ¹⁵ R. F. Mehl: *Trans. AIME* (1936) **122**, 13.
- ¹⁶ L. Pauling: *The Nature of the Chemical Bond.* 1939. Ithaca, N. Y. Cornell Univ. Press.

Young's Modulus and Its Temperature Dependence in 36 to 52 Pct Nickel-Iron Alloys

by M. E. Fine and W. C. Ellis

Young's modulus and its temperature coefficient in 36 to 52 pct Ni-Fe alloys depend upon composition and also the straining-annealing history. Alloys near 42.5 pct Ni, when worked cold and then annealed at 400° or 600°C, have nearly zero mean thermoelastic coefficients between -50° and 100°C. A discussion of the theory is given.

YOUNG'S modulus of elasticity in metals ordinarily decreases with rising temperature. The range of the thermoelastic coefficient at room temperature (temperature coefficient of modulus, $\frac{1}{E} \frac{dE}{dT}$) is illustrated¹ by the values for tungsten and hard-drawn aluminum, -95 and -1220×10^{-6} deg C⁻¹. However, a nearly zero thermoelastic coefficient is observed in some ferromagnetic alloys over a limited temperature range. In these alloys, as the temperature is raised, an increase in modulus arising from loss of ferromagnetism compensates the normal decrease. Iron-nickel alloys containing 36 to 52 pct Ni behave in this manner. In the present investiga-

M. E. FINE and W. C. ELLIS, Members AIME, are on the Technical Staff, Bell Telephone Laboratories, New York, N. Y.

AIME Chicago Meeting, October 1950.

TP 2921 E. Discussion (2 copies) may be sent to Transactions AIME before Dec. 15, 1950. Manuscript received April 14, 1950; revision received July 7, 1950.

tion, the dependence of the modulus and thermoelastic coefficient on cold working and annealing were studied in iron-nickel alloys in this range of nickel. Although these alloys, when fully annealed, have a coefficient near zero over a very small temperature interval, the temperature range of low coefficient can be extended greatly by straining and then stress-relief annealing.

The modulus of face-centered cubic iron-nickel alloys annealed at 1000°C does not vary linearly with composition at room temperature but, as

shown by the solid line of fig. 1, from Köster,² is minimum at 40 pct Ni and maximum at 87 pct Ni. The modulus increases with applied magnetic field but retains the minimum near 40 pct Ni.

Schematic change of modulus with temperature for three compositions is shown in fig. 2.^{2, 3} With increasing temperature, the slope becomes less negative, goes through zero (temperature of minimum modulus for the alloy), becomes positive, and resumes its normal negative value above the Curie

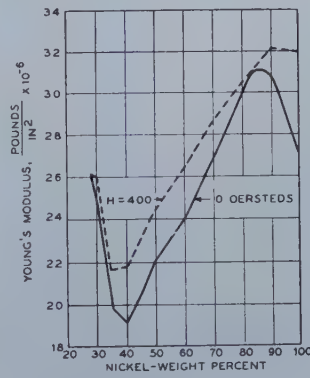


Fig. 1—Young's modulus (room temperature) of face-centered cubic Fe-Ni alloys annealed at 1000°C. From Köster.²

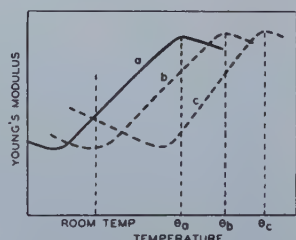


Fig. 2—Relation between Young's modulus and temperature in 36 to 52 pct Ni-Fe alloys.

Illustrating negative, near zero, and positive thermoelastic coefficients.

Ni Pct	Curie Temp
36	225°C (θ_a)
40	330°C (θ_b)
45	430°C (θ_c)

temperature. The temperature of the minimum modulus increases with Curie temperature and, hence, with nickel content. When the Curie temperature is just above the temperature of measurement, the thermoelastic coefficient is positive; when the Curie temperature is much higher, the coefficient is negative. A flat minimum at room temperature is the necessary condition for a nearly zero coefficient over a useful temperature range. Guillaume⁸ obtained a flat minimum by adding chromium. The present investigation shows that the flat minimum can be obtained in binary iron-nickel alloys by a straining and annealing treatment.

Experimental Procedure and Test Data

The major series of alloys (K-series, table I) was melted and cast in vacuum from electrolytic nickel and electrolytic iron. This series was supplemented by a number of alloys (table I) to which manganese was added. Most of these were prepared by melting in air under a slag, but two, designated CA, were melted in vacuum and cast in a helium atmosphere. All of the alloys contain 0.3 to 0.4 pct Co originating from the nickel. The samples were swaged cold to the desired diameters with intermediate anneals.

The method for measuring the modulus and the thermoelastic coefficient was devised by Wegel and Walther.⁴ In this method, the resonant frequency of a rod is determined in forced longitudinal vibration. The specimen, approximately 2 in. long and 0.200 in. in diam, was suspended by two pegs which fit into a small groove machined in the center of the sample (fig. 3). A variable frequency oscillator acting through a polarized bi-polar magnetic unit forced the ferromagnetic specimen to vibrate. The detector was an identical magnetic unit.

The frequency of the oscillator was varied until the maximum response was obtained on a vacuum tube voltmeter in the detecting circuit. This frequency, the resonant frequency of the rod (approximately 50 kc), was measured to within 1 to 5 cycles per sec, depending on the sharpness of the resonance. The maximum strain amplitude was approximately 1×10^{-7} . The data consist of the resonant frequencies of each of the samples at a series of temperatures controlled to within 1°C. Typical data are given in fig. 4.

For a rod vibrating in the first longitudinal mode, the resonant frequency, f , and Young's modulus, E , are related by eq 1, provided the length is sufficiently greater than the diameter, a condition⁵ fulfilled in the specimens used.

$$E = 4l^2 \rho f^2, \text{ where } \rho = \text{density and } l = \text{length. [1]}$$

The moduli at 25°C (figs. 5 to 7) were calculated using eq 1. The densities were determined by the method of weighing in air and reweighing in redistilled bromobenzene and are accurate to three significant figures. This limits the accuracy of the moduli to $\pm 0.005 \times 10^{12}$ dynes per cm².

The moduli at other temperatures (figs. 5, 6, 8, and 9) were calculated from those at 25°C using eq 2 which follows from eq 1, neglecting trivial terms.

$$\Delta E = E_T - E_{25} = E_{25} \left[\frac{2(f_T - f_{25})}{f_{25}} - \alpha(T - 25) \right] \quad [2]$$

In figs. 8 and 9, the origins of the curves were moved to -50°C. The coefficients of expansion (α) were

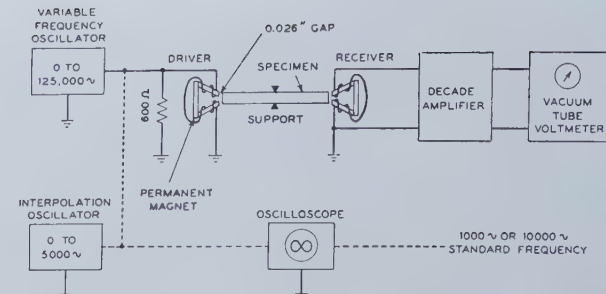


Fig. 3—Apparatus for measuring resonant frequency of a ferromagnetic rod vibrating longitudinally.

obtained from Lohr and Hopkins⁶ and unpublished data of the authors. The difference, ΔE , is accurate to $\pm 0.0005 \times 10^{12}$ dynes per cm².

The thermoelastic coefficients $\left(\frac{1}{E} \frac{dE}{dT} \right)$ (figs. 10

and 11) were calculated from the slopes of the frequency-temperature curves using eq 3, derived

Table I. Chemical Analyses of Iron-Nickel Alloys

Sample Design.	Wt Pct					
	Ni	Fe	Mn	Co	Si	C
Vacuum Melted Series						
K370	35.7	63.9		0.31		
K366	39.7	59.7		0.36		
K387	42.4	57.0	<0.01	0.36		
K368	45.5	53.8		0.41		
K369	49.0	50.4		0.40		
K371	51.9	47.5		0.38		
Manganese Containing Air Melted Series						
6584	33.7	65.7	0.47			
6583	35.6	63.8	0.38			
6566	39.5	59.8	0.38			
6567	40.8	58.5	0.47			
Manganese Containing Low Coefficient Air Melted Series						
6568	41.7	57.6	0.42			
6537	42.7	56.3	0.66			
6536	43.5	55.4	0.65			
Manganese Containing Controlled Atmosphere Series (Vacuum Melted, Cast in Helium)						
CA-294	48.8	50.7	0.31			
CA-293	52.4	47.0	0.32	0.42		

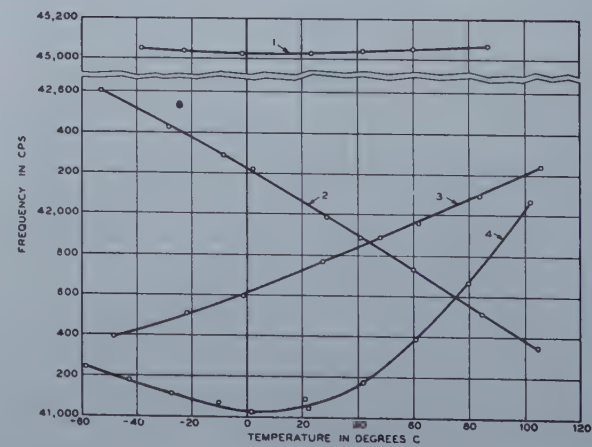


Fig. 4—Plots of resonant frequency as function of temperature.

Curve 1—Heat 6536, 43.5 pct Ni, 56.4 pct Fe, 0.65 pct Mn, cold reduced from 0.375 to 0.250 in. diam, annealed 1 hr at 400°C.

Curve 2—Heat K368, 45.5 pct Ni, 58.8 pct Fe, cold reduced from 0.390 to 0.200 in. diam, annealed 1 hr at 950°C.

Curve 3—Heat K366, 39.7 pct Ni, 59.7 pct Fe, cold reduced from 0.390 to 0.200 in. diam, annealed 1 hr at 400°C.

Curve 4—Heat K369, 39.7 pct Ni, 59.7 pct Fe, cold reduced from 0.390 to 0.200 in. diam, annealed 1 hr at 950°C.

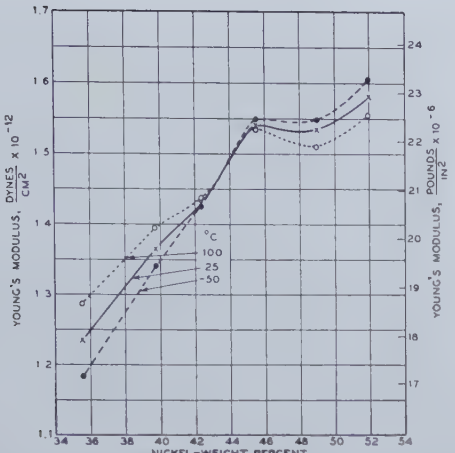


Fig. 5—Young's modulus (-50° , 25° , and 100°C) of iron-nickel alloys cold swaged 74 pct and annealed 1 hr at 400°C .

from eq 1. The values of coefficient determined in this way are reproducible to approximately $\pm 0.25 \times 10^{-6}$.

$$\frac{1}{E} \frac{dE}{dT} = \frac{2}{f} \frac{df}{dT} - \alpha. \quad [3]$$

The Modulus and Its Temperature Coefficient

Young's modulus and its temperature dependence in iron-nickel alloys, 36 to 52 pct Ni, are not only related to composition but also depend upon working and annealing history. In the K-series of alloys, the samples were prepared by first reducing the cross-sectional area 74 pct by cold swaging. Then one set of samples was stress-relieved for 1 hr at 400°C , and another set was recrystallized, 1 hr at 950°C . Certain of the alloys containing manganese were measured in a greater variety of conditions. Data are not included for unannealed cold-worked

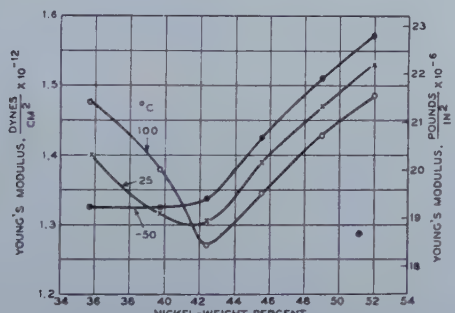


Fig. 6—Young's modulus (-50° , 25° , and 100°C) of iron-nickel alloys cold swaged 74 pct and annealed 1 hr at 950°C .

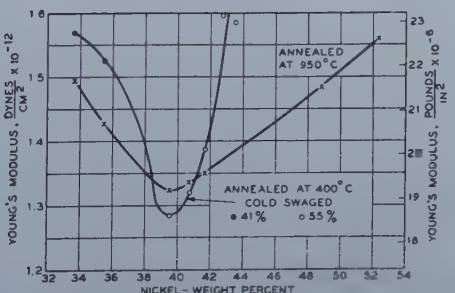


Fig. 7—Young's modulus (25°C) of iron-nickel alloys containing approximately 0.5 pct Mn.

alloys since the modulus of such specimens, probably due to strain relief, increased on heating.

Modulus: In the alloys annealed at 400°C , fig. 5, the modulus, in general, increases with nickel content. Between 43 and 44 pct Ni, the curves for the three temperatures intersect and are closely coincident, indicating a small mean thermoelastic coefficient in this composition range.

A recrystallizing anneal (950°C), fig. 6, results in a substantially different modulus-composition dependence. The modulus-composition curves for 25° and 100°C go through well-defined minima. These minima occur at lower nickel contents and are less sharp as the temperature of measurement is lowered.

In the K-series alloys having 39.7 pct and more nickel, the moduli, compared at the same temperature, are larger when the alloys are annealed at 400°C than at 950°C . However, the 35.7 pct Ni alloy has an opposite relation. In this alloy the

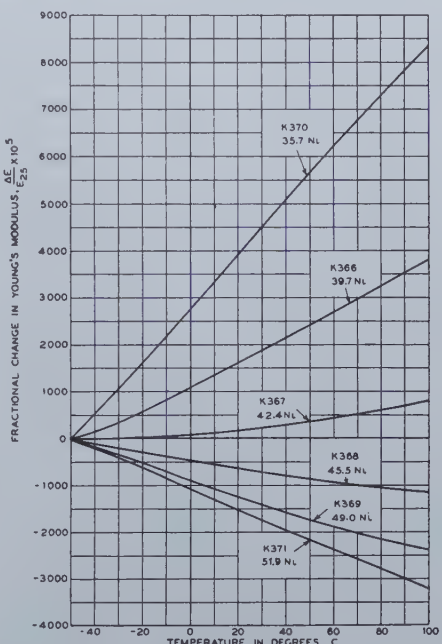


Fig. 8—Fractional change of Young's modulus with temperature in iron-nickel alloys cold swaged 74 pct, annealed 1 hr at 400°C .

moduli for the two annealing conditions approach each other as the temperature of measurement is lowered.

The shape of the modulus-composition curve for Fe-Ni alloys annealed at 400°C is modified greatly by sample purity. The moduli at 25°C in Fe-Ni alloys containing approximately 0.5 pct Mn (fig. 7) are minimum near 39 pct Ni for samples in both annealing conditions (400° and 950°C).

Temperature Dependence of the Modulus: The temperature dependence of the modulus in alloys annealed at 400°C and 950°C is given in figs. 8 and 9 which show the fractional change in modulus $\left(\frac{\Delta E}{E_{25}} \right)$ as the temperature is increased above -50°C . In figs. 10 and 11, the thermoelastic coefficients, $\frac{1}{E} \frac{dE}{dT}$ (slopes of the curves in figs. 8 and 9), are given for four temperatures, -20° , 20° , 50° , and 80°C . For a given alloy and treatment, the spread among the values of the coefficients indicates the departure from linearity of the modulus-temperature curves.

These observations are best correlated in conjunction with the schematic modulus-temperature curves (fig. 2). When cold worked 75 pct and then annealed at 950°C (figs. 9 and 11), alloys near 40 pct Ni have minimum moduli and zero thermoelastic coefficients near room temperature. In the compositions with less nickel, the modulus increases with temperature between -50° and 100°C. In compositions with more nickel, the modulus decreases with temperature. The minimum in the modulus-temperature curve for this annealing condition, 950°C, is sharp as shown by the curve for 39.7 pct Ni alloy (fig. 9).

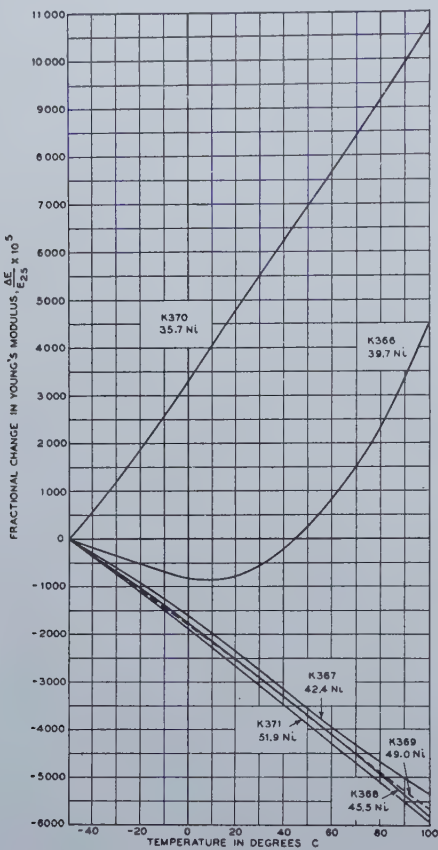


Fig. 9—Fractional change of Young's modulus with temperature in iron-nickel alloys cold swaged 74 pct, annealed 1 hr at 950°C.

When cold worked 75 pct and annealed at 400°C, alloys near 43 to 44 pct Ni have their minimum moduli and zero thermoelastic coefficients near room temperature. The temperature of the minimum generally decreases upon straining. Furthermore, straining broadens the trough in the modulus-temperature curve.

Addition of manganese, not shown, in general decreases the coefficient by a small amount.

Adjusting the Straining and Annealing to Produce Low Thermoelastic Coefficient: The alloys for this part of the investigation contained manganese and were melted in air under a slag. The compositions, 41.7, 42.7, and 43.5 pct Ni (table I), were chosen to have low thermoelastic coefficients when cold worked and stress-relief annealed. The fractional variation in modulus with temperature, $\frac{\Delta E}{E_0}$, is given in figs. 12 to 14.

Increasing the temperature of anneal displaces the minimum value of modulus and the region of low

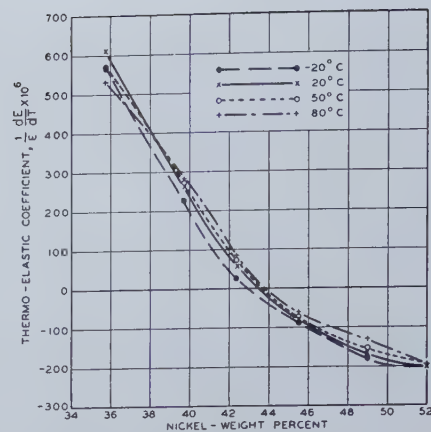


Fig. 10—Thermoelastic coefficients of iron-nickel alloys, cold swaged 74 pct, annealed 1 hr at 400°C.

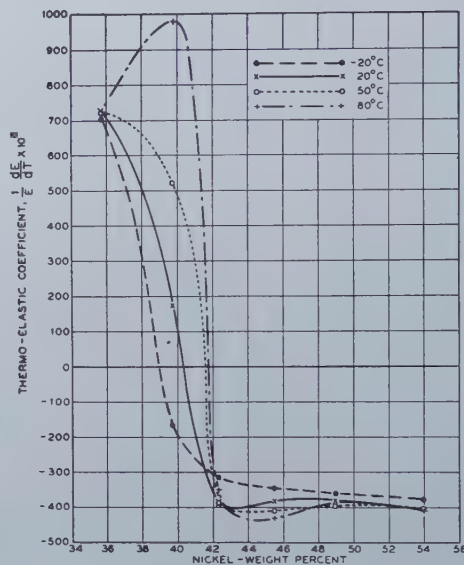


Fig. 11—Thermoelastic coefficients of iron-nickel alloys cold swaged 74 pct, annealed 1 hr at 950°C.

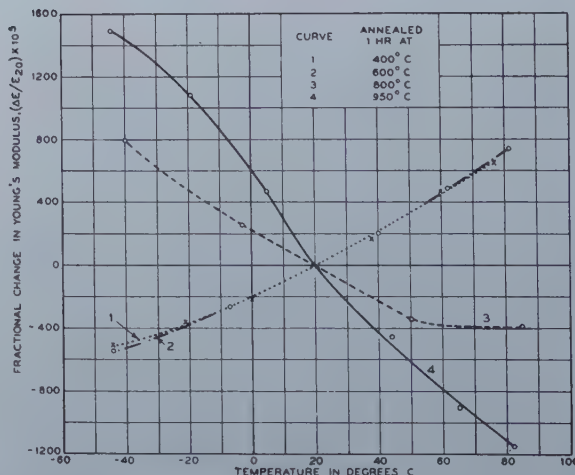


Fig. 12—Fractional change of Young's modulus with temperature in an iron-nickel alloy (6568) containing 41.7 pct Ni and 0.42 pct Mn, cold swaged 55 pct previous to annealing.

thermoelastic coefficient to a higher temperature. Conversely, starting with an annealed alloy, the temperature of minimum modulus at first decreases

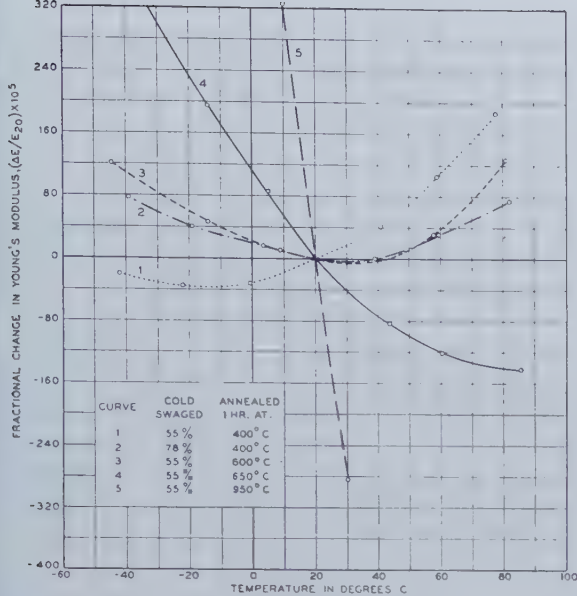


Fig. 13—Fractional change of Young's modulus with temperature in an iron-nickel alloy (6537) containing 42.7 pct Ni and 0.66 pct Mn.

with cold working. This is not true for all degrees of strain, for if the straining prior to a 400°C anneal is increased from 55 to 78 pct, the temperature of minimum modulus increases—perhaps due to preferred crystal or domain orientations depending on the degree of strain. In the 42.7 and 43.5 pct Ni alloys, the trough in the modulus-temperature curve is flatter, the greater the prior deformation and the lower the annealing temperature. The sample most nearly isoelastic (broadest trough) in the -40° to +80°C temperature range is the 42.7 Ni alloy (curve 2, fig. 13) when it has been cold swaged 78 pct and annealed for 1 hr at 400°C.

Theory of the Modulus in Nickel-Iron Alloys

The modulus-composition and modulus-temperature relations in these 36 to 52 pct iron-nickel alloys, figs. 1 and 2, for the most part, can be explained by present concepts of ferromagnetism. Ferromagnetism modifies the normal paramagnetic modulus in three ways: (A) The addition of the energy of magnetization to the potential energy of the crystal alters the modulus directly. (B) At temperatures just below the Curie point, stress induces a change in the intensity of magnetization in a single ferromagnetic domain. This involves a volume change and an additional strain.⁷ (C) Stress causes the domains to change their size and orientation producing an increase in strain (linear magnetostriction).^{7, 8}

Process A may increase or decrease the value of the modulus; B and C always lower the modulus; C will disappear if the material is saturated by an external magnetic field. Since they are processes within the domain and depend only slightly on domain orientation, A and B are independent of an ordinary external magnetic field.

The stress-produced linear magnetostriction^{7, 8} (C) and the stress-produced volume magnetostriction⁷ (B) have been fully described. Since the direct effect of the energy of magnetization (A) does not appear to have been explicitly recognized before, details of the mechanism are included here. The addition of the energy of magnetization, in general,

causes the equilibrium interatomic distance and the relation between potential energy and interatomic distance in the ferromagnetic state to be different from those in the paramagnetic state.⁹ Since the addition of the energy of magnetization changes the relation between the potential energy and the interatomic distance in a crystal, the second derivative of this relation, of which the modulus is a function, will be changed also. From a consideration of the energy-interatomic distance relations, a correlation between the signs of the modulus change and the volume change can be deduced. This is supported by some experimental data. For the condition $r_{\text{ferro}} > r_{\text{para}}$, the case for the iron-nickel alloys considered here, the modulus is decreased from its paramagnetic value.¹⁰ For the condition $r_{\text{para}} > r_{\text{ferro}}$, the modulus is increased over its paramagnetic value. This has been observed in nickel.²

Modification of the modulus-temperature curve by A, B, and C in 36 to 52 pct Ni-Fe alloys is shown in fig. 15a. The result is a curve resembling those in figs. 2 and 9 with a minimum at some temperature and a positive slope just below the Curie point. All three effects, in these alloys, lower the moduli from their paramagnetic values. Since the energy of magnetization decreases with loss of ferromagnetism, the direct effect of the energy of magnetization on the modulus (A) becomes smaller on heating as the temperature approaches the Curie point. This makes the slope more positive (curve A). In fact, Engler's¹⁰ measurements of the modulus of a 42 pct Ni-Fe alloy in a reasonably saturating magnetic field ($H=575$ oersteds) show that A in itself is large enough to cause a positive slope. The stress-produced volume magnetostriction (B) is in effect only just below the Curie point (curve A B). The stress-produced linear magnetostriction (C) lowers the modulus still further as shown by curve A B C and, in the region of loss of ferromagnetism, also causes the thermoelastic coefficient to be positive. Curve A B applies when the alloy is magnetically saturated. Curve A B C applies otherwise.

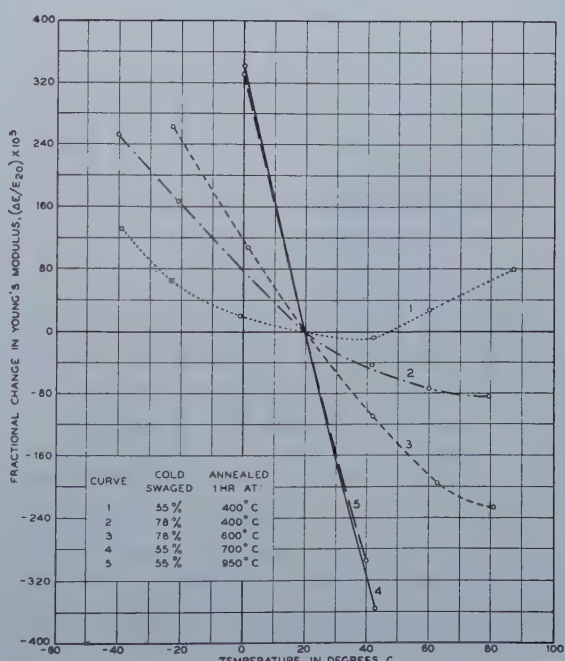


Fig. 14—Fractional change of Young's modulus with temperature in an iron-nickel alloy (6536) containing 43.5 pct Ni and 0.65 pct Mn.

Experiment confirms this theory. Near room temperature the ferromagnetic effects in the higher nickel alloys (the Curie points are far above room temperature) are insensitive to the temperature of measurement, and the modulus decreases with rise in temperature as shown in figs. 5 and 6. For the lower nickel contents, the Curie points are just above room temperature, and the modulus increases as the temperature is raised.

Strain hardening reduces the stress-produced linear magnetostrictive strain (for a given stress) by obstructing domain movement⁸ and by causing a preferred domain orientation.¹¹ The result is a flatter minimum in the modulus-temperature curve (compare figs. 8 and 9) the behavior being more nearly like curve A B.

The occurrence of a minimum in the modulus-composition curves (figs. 1, 6, and 7) may be attributed to the composition dependence of A, B, and C as represented in fig. 15b. If the temperature of measurement is far below the Curie point, as in the higher nickel alloys, the direct effect of the energy of magnetization (A) diminishes with increasing nickel since the difference between the potential energy curves for the paramagnetic and ferromagnetic states decreases.⁹ Furthermore, the linear magnetostriction (C) decreases as nickel is added.¹² The modulus thus increases with nickel content in the higher nickel alloys. As the nickel is lowered, the Curie point nears room temperature and is at room temperature for an alloy of approximately 28 pct Ni. The magnitudes of A and C diminish with increasing intensity as the temperature of measurement nears the Curie point. The increase in the modulus at room temperature (figs. 6 and 7) as the nickel is reduced below approximately 42 pct thus is caused by increasing loss of ferromagnetism. The increase in modulus due to loss of ferromag-

nism is greatest at the highest temperature of measurement shown in fig. 6. Decreasing the temperature of the measurement lowers the nickel content corresponding to the minimum as shown by the dotted curve A B C in fig. 15b.

Strain hardening, by largely eliminating the stress-produced linear magnetostriction, is expected to increase the modulus. Furthermore, the effect of strain hardening in increasing the modulus diminishes as the nickel is lowered, since the Curie point nears the temperatures of measurement. Comparison of figs. 5 and 6 shows this to be the case with but one exception, the alloy containing 35.7 pct Ni. The exception, the 35.7 pct Ni alloy in which the modulus decreases with strain hardening, may be due to partial transformation of the face-centered cubic phase.^{13, 14} The effect of manganese in changing the modulus-composition curve of the low-nickel alloys may also be associated with the phase transformation.

Summary

In 36 to 52 pct Ni-Fe alloys there is a temperature at which an increase in Young's modulus, arising from loss of ferromagnetism, exactly compensates the normal decrease, and a zero thermoelastic coefficient results. The temperature of zero coefficient depends upon composition and on straining and annealing history. The temperature range of low coefficient is greatly extended by cold work. For example, alloys near 42.5 pct Ni, when worked cold and then annealed at 400° or 600°C, have nearly zero mean thermoelastic coefficients between -50° and 100°C.

The general behavior of the modulus and its temperature dependence is explained on the basis of three ferromagnetic effects: (A) direct effect of the energy of ferromagnetism on the modulus, (B) the stress-produced volume magnetostriction within the domains, and (C) the stress-produced linear magnetostriction.

Acknowledgments

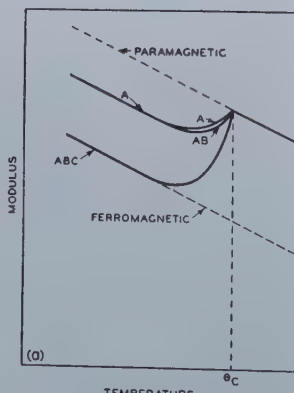
The authors are pleased to acknowledge the contributions made to this investigation by D. H. Wenny and H. E. Johnson for preparation and analyses of the alloys, and T. G. Kinsley and W. P. Mason for assistance in developing the method of measurement. E. E. Schumacher assisted greatly through his helpful counsel and guidance.

References

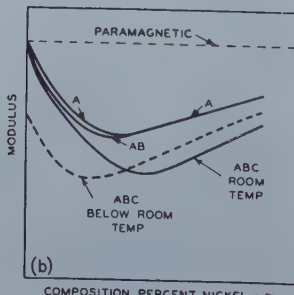
- ¹ W. Brombacher: *Rev. Sci. Inst.* (1933) **4**, 688.
- ² W. Köster: *Ztsch. Metallkunde*. (1943) **35**, 194.
- ³ C. Guillaume: *Comp. Rendu*. (1920) **171**, 83; *Proc. Phys. Soc. (London)* (1920) **32**, 374.
- ⁴ R. Wegel and H. Walther: *Physics*. (1935) **6**, 141.
- ⁵ R. Cabarat, L. Guillet, and R. Le Roux: *Jnl. Brit. Inst. of Met.* (1949) **74**, 391.
- ⁶ J. Lohr and C. Hopkins: *Trans. AIME* (1939) **135**, 535.
- ⁷ R. Becker and W. Döring: *Ferromagnetismus*. 337. (1939) Julius Springer.
- ⁸ M. Kersten: *Ztsch. Phys.* (1933) **85**, 708.
- ⁹ W. Shockley: *Bell System Tech. Jnl.* (1939) **18**, 721.
- ¹⁰ O. Engler: *Ann. Phys.* (1938) **31**, 145.
- ¹¹ H. Conradt, O. Dahl, and K. Sixtus: *Ztsch. Metallkunde*. (1940) **32**, 231.
- ¹² A. Schulze: *Ztsch. Phys.* (1928) **50**, 448.
- ¹³ E. Owen and A. Sully: *Phil. Mag.* (1941) **31**, 314.
- ¹⁴ J. Spretnak and G. Sachs: *Trans. AIME* (1941) **145**, 340.

Fig. 15—Effect of ferromagnetism on the modulus of iron-nickel alloys.

a. In curves marked A the paramagnetic modulus is modified by the energy of magnetization. In curves marked AB the stress-produced volume magnetostriction is included also. In the curves marked ABC the modulus is further modified by the stress-produced linear magnetostriction.



b. The Curie point of alloy on left hand side of b is at room temperature (approximately 28 pct Ni).



A Study of Strain Markings in Aluminum

by Bani R. Banerjee

This paper reports metallographic evidence of strain markings in high-purity aluminum (99.998 pct), hitherto unobserved, and a study of their crystallography. Some incidental observations tend to provide indirect evidence of a close relationship between strain markings and annealing twins, to clarify the peculiar behavior of aluminum in its reluctance to form banded annealing twins, and to indicate that the type of localized strain at the slip interfaces, which are responsible for the etching effects that render strain markings visible, consists of a twinning displacement.

MATERIAL used throughout this investigation was high-purity aluminum (99.998 pct). The $\frac{1}{2}$ -in. cubes were cut out of a cold-rolled slab and annealed at 550°C for 1 hr before deformation.

The single crystal specimen was 1 in. in diam \times 0.33 in. thick, cut from a cylindrical crystal produced by cooling at about 55°C per hr in a furnace which had a convenient gradient of about 10°C in every 4.5 in. vertical crucible length. Specific data on the ten specimens studied are summarized in table I.

Three types of deformation were employed: (1) compression in a hand-operated hydraulic press; (2) impact with a 7-lb sledge hammer; and (3) rolling, using a wedge-shaped specimen² to obtain

BANI R. BANERJEE, Junior Member AIME, formerly on the faculty of the Department of Metallurgical Engineering, Illinois Institute of Technology, Chicago, is now Research Engineer, Engineering Research Division, Standard Oil Co. (Ind.), Chicago, Ill.

AIME Chicago Meeting, October 1950.

TP 2919E. Discussion (2 copies) may be sent to Transactions AIME before Dec. 15, 1950. Manuscript received Dec. 16, 1949; revision received June 26, 1950.

a gradient of deformations varying from 0 to 50 pct along the length of the wedge.

Specimens were either deformed at room temperature, or first cooled in a freezing mixture of dry ice and ether at a temperature of -72°C and then deformed between steel blocks cooled with dry ice.

The specimens deformed at the low temperature were ground and polished through 000 emery paper and wheels impregnated with alundum and alumina No. 1. During this entire procedure the specimens were dipped frequently in the freezing mixture of dry ice and ether in order to maintain constantly a frosty surface as insurance against overheating.

All specimens were given a final electrolytic polish, using two different electrolytes* to insure that the surface effects observed were not char-

acteristic of the polishing technique. With both electrolytes, the annealed specimens gave even surfaces with good polish.

Several standard etchants were tried without success. The best results were obtained with an immersion etchant, developed in this connection, containing: hydrofluoric acid, 4 parts; nitric acid, 1 part; glycerine, 3 parts.

Discussion of Results

Typical strain markings have been observed within deformation bands, as shown in figs. 1, 2, and 4.

By stereographic plotting of metallographic measurements, the strain markings within a deformation band in a single crystal of aluminum deformed by compression were found to be traces of (111) planes within a maximum scatter of 6° . The edges of the deformation band were found to be traces of the (100) planes also within the maximum scatter of 6° (in agreement with previous workers). At 30 pct deformation, this scatter was considered quite normal because of the fragmentation and rotation of the crystal. This solution, based on the traces on one plane of observation is not unique, but as the planes were observed to be those normally and logically to be expected, further work in this regard was not felt to be necessary.

The study of strain markings in a wedge-shaped specimen, rolled to obtain a gradient of deformation from 0 to 50 pct, revealed prominent strain markings at 25 pct reduction in thickness (fig. 5). Faint and weak strain markings were visually observable up to a minimum reduction in thickness of about 12 pct.

Since strain markings have been observed in other face-centered cubic metals after much smaller deformations;^{1, 2} and since the rate of recovery in aluminum is high, it is believed that, at lower deformations, self-recovery removes the localized strains at the slip interfaces, thus removing the source of the etching effects that give rise to strain markings.

At high magnifications, strain markings sometimes seem to appear as very thin, light-banded regions bounded by a pair of dark edges. This so-

* First electrolyte: nitric acid (conc.), 12 parts; alcohol (methyl), 56 parts; chromic acid (sat. soln.), 3 parts; acetic acid, 8 parts; current density, 6.4 amp per sq. in. at 42 v. Second electrolyte: perchloric acid, 1 part; acetic acid, 6 parts; current density, very low at 45 v.

called "double nature of the bands" has been considered by some³ as evidence that the strain markings are thin mechanical twins. That the grooved nature of the etching effect along the planes of slip renders the strain markings visible and gives rise to the above-named banded nature of the strain markings was clearly evident upon slightly changing the focus of the eyepiece on the microscope, focusing first on the polished surface and then changing the focus to the bottom of the grooves.

Fig. 3, in which two sets of strain markings (fairly irregular and wavy at this stage of deformation) are shown crossing one another in the large grain, is certainly reminiscent of the typical cross-slip reported by Maddin, Mathewson and Hibbard⁴ in alpha brass single crystals and by G. J. Ogilvie and W. Boas⁵ in large-grained, high-purity aluminum.

In addition to the use of a proper etching reagent, the prime requisite for rendering strain markings visible in pure aluminum seems to be the maintenance of a low temperature throughout the process of deformation and subsequent mechanical polishing. Any heat generated during these stages is sufficient to cause the disappearance of the strain markings even though no signs of recrystallization are visible in these specimens at the highest optical microscopic magnifications (around X2500). Specimens, deformed and polished under low-temperature conditions (specimen Nos. 3, 8, and 9 in table I), in which these markings actually occurred, failed to reveal them when they were repolished and re-etched, after aging at room temperature from three to four weeks (no recrystallization). Thus, strain markings in aluminum are thermally unstable and disappear before any observable recrystallization occurs in the matrix. In all other face-centered cubic metals and alloys, strain mark-

Fig. 1—Specimen No. 10, strain markings within a deformation band in single crystal of aluminum.

X500
Area reduced approximately two thirds for reproduction.



ings seem to possess a considerable degree of thermal stability, and persist until the cold-worked matrix is entirely replaced by recrystallization.

Aluminum appears to be the only face-centered cubic metal in which: (1) strain markings are thermally unstable below the recrystallization temperature, and (2) banded annealing twins are not ordinarily found. This, in addition to the results of previous researches, suggests an association, first between the reorientation process that gives rise to the formation of the annealing twins in face-centered cubic metals and strain markings, and, second, between the twin or stacking faults and both strain markings and annealing twins. If it is accepted that annealing twins originate from a reorientation process nucleated either by the twin or stacking faults,^{7,8} or by an extended dislocation,⁹ it logically might be hypothesized that, in aluminum, the introduction of a stacking or twin fault sets up an unstable state of affairs by introducing a much higher energy condition than is found in other face-centered cubic metals. This assumption would result, in terms of the dislocation picture,⁹ in a ten-

Table I. Analyses of Ten Specimens of High-purity Aluminum

Specimen No.	Extent of Deformation, Pct	Nature of Deformation	Temp of Deformation	Electro Polishing Bath	Results
1	0	Specimen annealed 1 hr at 550°C		HNO ₃ , alcohol Cr ₂ O ₃ , acetic acid	Even surface, good polish.
2	60	Same; compressed in hand press	Room Temp	HNO ₃ , alcohol Cr ₂ O ₃ , acetic acid	No strain markings. Deformation bands visible. No signs of recrystallization.
3	40.2	Same; compressed between blocks cooled with dry ice and ether	-72°C	HNO ₃ , alcohol Cr ₂ O ₃ , acetic acid	Strain markings observed. See figs. 2 and 3.
4	0	Specimen annealed 1 hr at 550°C		HClO ₄ , acetic anhydride	Even surface, good polish.
5	36.6	Same; compressed in hand press	Room Temp	HClO ₄ , acetic anhydride	No strain markings. Deformation bands visible. No signs of recrystallization.
6	56.2	Same; further compressed	Room Temp	HClO ₄ , acetic anhydride	No strain markings. Deformation bands visible. No signs of recrystallization.
7	49.4	Same; impact hammered	Room Temp	HClO ₄ , acetic anhydride	No strain markings. Deformation bands visible. No signs of recrystallization.
8	48.0	Same; impact hammered	-72°C	HClO ₄ , acetic anhydride	Strain markings visible. See fig. 4.
9	0-50	Rolled, wedge-shaped specimen	-72°C	HClO ₄ , acetic anhydride	Strain markings prominent up to a minimum deformation of 25 pct (fig. 5). Faintly discernible up to 12 pct.
10	30	Compressed single crystal	-72°C	HClO ₄ , acetic anhydride	Strain markings visible within deformation bands. See fig. 1.
3, 8, 9		Repolished after 3 to 4 weeks			No strain markings visible. No signs of recrystallization.

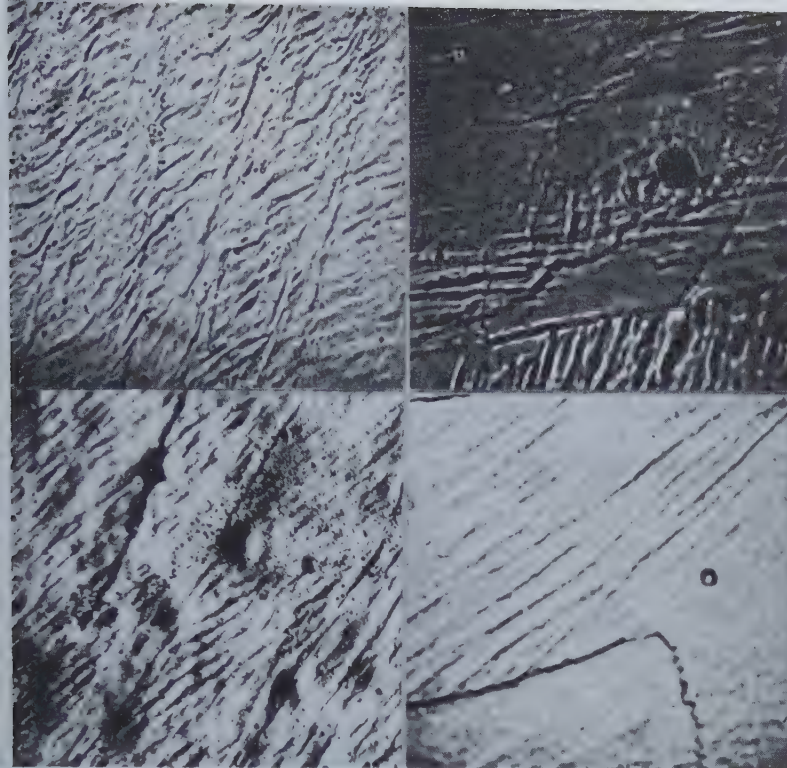


Fig. 2—Specimen No. 3, deformed 40.2 pct by compression (low temperature) showing strain markings within deformation bands. Deformation bands slightly inclined to vertical are roughly parallel to plane of compression. X1000. (Upper left.)

Fig. 3—Same specimen, showing strain markings reminiscent of cross slip. X1000. (Upper right.)

Fig. 4—Specimen No. 8, impact deformed 40 pct (reduction in thickness) at low temperature showing strain markings within deformation bands. X2000. (Lower left.)

Fig. 5—Specimen No. 9, wedge-shaped specimen rolled. Spot represents 25 pct deformation. Strain markings within a grain. X2000. (Lower right.)

Figs. 2-5—Area reduced approximately two thirds for reproduction.

dency for the two half dislocations to be pulled together, overcoming the repulsive forces. This, in turn, would set into motion a train of redistribution of stresses and strains or a reorientation of atoms corresponding to a rapid rate of recovery, as observed also by Heidenreich.⁹ This reorientation of atoms and consequent dissolution or diffusion of dislocations is in conformity with Buergers¹⁰ description of the recovery process. The redistribution of strains, pictured in the sense of recovery, would be expected to dissipate the highly localized strains at the slip interface, distributing them more evenly over the entire structure.

On the basis of the above discussion, it may be suggested now that the thermal instability of the twin faults causes the disappearance of the strain markings, and, in turn, is responsible for the lack of annealing twin bands in aluminum. In other face-centered cubic metals, the twin-faults and, in turn, the strain markings are stable and persist in the structure, setting into motion the reorientation process giving rise to the recrystallized twin bands.

Summary

1. Strain markings have been observed in high-purity aluminum deformed by compression, by hammer impact, or by rolling.

2. The minimum amount of deformation by rolling a wedge-shaped specimen required to produce visible strain markings was approximately 12 pct reduction in thickness.

3. From a study of a single crystal, strain markings were concluded to be traces of the (111) planes.

4. Strain markings were found to be thermally unstable since they disappeared with aging at room temperature and they were not visible in specimens deformed and polished at room temperature (because of overheating). This is believed to be the reason why strain markings have not previously been found in aluminum.

5. The combination of the thermal instability of the strain markings and the reluctance of alu-

minum to form banded annealing twins suggests a rationalization of the strain-anneal phenomena in the face-centered cubic metals, in general, and in aluminum, in particular.

6. Strain markings reminiscent of cross-slip have been noted.

7. The grooved nature of the etching effect giving rise to strain markings has been pointed out.

Acknowledgment

The author wishes to thank the Reynolds Metals Co. who supplied the high-purity aluminum used in this research. Thanks are due, in particular, to Carl H. Samans, of Standard Oil Co., who kindly read over the manuscript and helped materially to improve the text. The assistance of Robert J. Adamo, who prepared some of the specimens and micrographs, is also gratefully acknowledged.

References

- J. E. Burke and C. S. Barrett: *Trans. AIME* (1948) 175, 106; *Met. Tech.* (Feb. 1947) TP 2327.
- W. R. Hibbard, Jr. et al.: *Trans. AIME* (1948) 175, 74; *Met. Tech.* (Feb. 1948) TP 2336.
- C. F. Elam: Discussion to F. Adcock. *Jnl. Inst. Met.* (1922) 27, 73.
- R. Maddin, C. H. Mathewson, and W. R. Hibbard, Jr.: *Trans. AIME* (1948) 175, 86; *Met. Tech.* (Feb. 1948) TP 2331.
- G. J. Ogilvie and W. Boas: Discussion of reference 4. *Trans. AIME* (1948) 175, 102; *Met. Tech.* (Aug. 1948) TP 2449.
- R. D. Heidenreich and W. Shockley: Rept. on Conf. on the Strength of Solids. Physical Soc. London. (1948) 57.
- R. Maddin, C. H. Mathewson, and W. R. Hibbard, Jr.: *Trans. AIME*, 185, 655; *Jnl. Met.* (Sept. 1949) TP 2676.
- F. H. Wilson and M. L. Kronberg: *Trans. AIME*, 185, 501; *Jnl. Met.* (Aug. 1949) TP 2634.
- R. D. Heidenreich: *Trans. A.S.M.* (1945) 41A, 57.
- W. G. Buergers: *Proc. Roy. Acad. Sci. Amsterdam* (1947) 50, 452. *Nature*. (London) (1947) 160, 398. Rept. on Conf. on the Strength of Solids. Physical Soc. London. (1948) 134.

Quantitative Stress-Strain Studies on Zinc Single Crystals in Tension

by D. C. Jillson

Highly consistent data were obtained for the critical resolved shear stress for slip of zinc single crystals of high purity and quality under one particular set of conditions. The effects of many variables remain to be investigated. An effort to confirm the hypothesis of slip by alternating [210] unit movements was unsuccessful.

THE data on the critical resolved shear stress for zinc single crystals published by Rosbaud and Schmid¹ showed many irregularities, as seen in fig. 1. There have been subsequent investigations,^{2, 3} but no one has repeated this work with a wide range of orientations, with specimens of a higher degree of purity and perfection, and with improved experimental techniques in order to determine whether these variations were entirely experimental or whether they might have been due, at least in part, to some feature of the mode of deformation not known or understood.

Mathewson⁴ and others have long felt that the glide observed in a [100]* direction between two (001)* planes in the zinc lattice might be actually

the net effect of many consecutive unit glides or movements in two alternating [210] directions (fig.

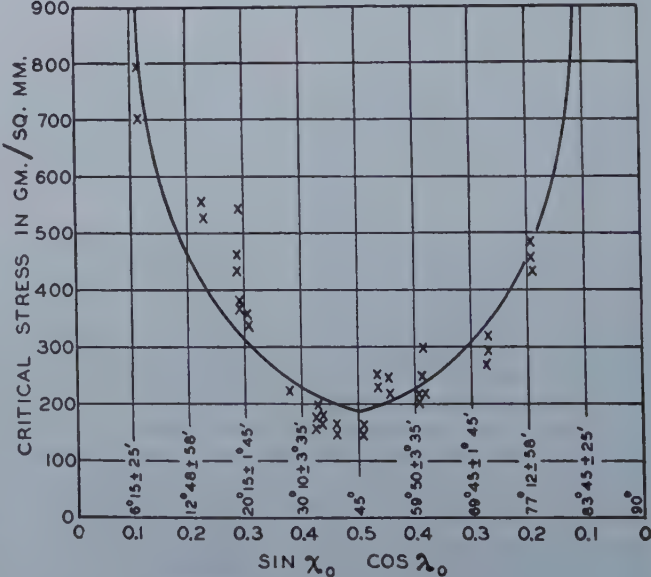


Fig. 1—Dependence of tensile yield stress on orientation of single crystals of zinc containing 0.03 pct cadmium as determined by Rosbaud and Schmid.

χ = angle between basal plane and specimen axis.
 λ = angle between slip direction and specimen axis.

* Three-coordinate Miller indexes are used throughout for planes and directions. Parentheses and brackets are used to indicate families as well as particular planes or directions.

Table I. Data for Tensile Stress-Strain Tests on Single Crystals of 99.999+ Pct Zinc

Specimen	γ	λ_o	$\sin \gamma$	$\cos \lambda_o$	$\sin \gamma / \cos \lambda_o$	A	RL	F	S λ_o	λ_a	$\cos \lambda_a$	$\sin \gamma / \cos \lambda_a$	S λ_a	λ_b	$\cos \lambda_b$	$\sin \gamma / \cos \lambda_b$	S λ_b
XL45C	6½	18	0.1132	0.9511	0.1076	122.46	113.5	20,730	18.23	15	0.9659	0.1093	18.51	47	0.6820	0.0772	13.07
XL47E	6½	10½	0.1132	0.9833	0.1113	122.01	115.7	20,406	18.62	22	0.9272	0.1051	17.58	39	0.7771	0.0880	14.72
XL47B	19½	29	0.3388	0.8746	0.2919	122.60	43.29	7,867	18.74	21	0.9336	0.3115	20.00	55	0.5736	0.1912	12.28
XL48F	20	22	0.3420	0.9265	0.3170	122.58	38.78	7,071	18.28	28	0.8829	0.3020	17.42	44	0.7026	0.2402	13.86
XL45F	30	30½	0.5000	0.8625	0.4313	122.79	28.44	5,276	18.54†	41	0.7547	0.3773	16.22	43	0.7325	0.3662	15.74
XL47F*	33	36	0.5446	0.8090	0.4406	122.72	27.80	{ 5,073 5,518	18.21 19.81	36	0.8090	0.4406	{ 18.21 19.81	53½	0.5948	0.3236	{ 13.88 14.55
XL44	38	38½	0.6157	0.7826	0.4820	123.21	25.50	4,683	18.32†	45	0.7071	0.4355	16.55	50	0.6428	0.3958	15.05
XL48G	40	40	0.6414	0.7660	0.4913	123.09	24.84	4,602	18.37	47	0.6820	0.4377	16.36	50	0.6441	0.4133	15.45
XL48B	46¾	49	0.7284	0.6547	0.4773	123.43	25.73	4,976	19.03	48	0.6691	0.4875	19.44	63	0.4555	0.3320	13.24
XL47D	53	53½	0.7986	0.5948	0.4755	123.36	26.02	4,780	18.44	56½	0.5591	0.4410	17.10	61½	0.4772	0.3813	14.78
XL47C	61	62½	0.8746	0.4617	0.4038	123.72	30.62	5,597	18.15	62	0.4695	0.4110	18.46	70½	0.3338	0.2921	13.13
XL45A	67½	69	0.9239	0.3584	0.3311	123.80	37.32	6,924	18.53†	68	0.3746	0.3460	19.36	76	0.2419	0.2234	12.51
XL48A	77	78	0.9744	0.2079	0.2054	124.60	60.79	11,126	18.34	78	0.2096	0.2042	18.23	82	0.1392	0.1357	12.12
XL45B	85	85½	0.9962	0.0785	0.0758	124.39	163.2	28,533	17.40†	85	0.0872	0.0869	19.93	87	0.0523	0.0521	11.96
XL47G	86	86	0.9974	0.0698	0.0696	124.22	178.7	32,505	18.22†	86	0.0698	0.0696	18.22	87	0.0523	0.0522	13.65
								Avg	18.4								

χ = angle between (001) and specimen axis.

λ_o = angle between [100] and specimen axis.

λ_a = angle between nearest [210] and specimen axis.

λ_b = angle between next nearest [210] and specimen axis.

A = cross-sectional area in mm².

* The two sets of values for XL47F represent alternative interpretations of the same test data.

† Values obtained by extrapolation of straight-line portion of stress-shear curve.

RL = rate of loading in g per min.

F = critical load in g.

S λ_o = critical stress resolved in (001) in [100] in g per mm².

S λ_a = critical stress resolved in (001) in nearest [210] in g per mm².

S λ_b = critical stress resolved in (001) in next nearest [210] in g per mm².

2). Mathewson has reasoned that, if this is true, the intermediate position of the atoms, after the first [210] movement, is one of lower stability or higher energy than the normal position and that, to attain this position, an atom must be raised from its normal, low-energy valley up over an energy hill and down into the higher energy valley of the intermediate position. This is represented in fig. 3 by the first half of the lower curve, and the increase in energy required is represented by ac. The second part of the movement requires only that the atom be raised from this intermediate valley to the top of a similar hill so that it can drop into a normal valley. In this case, the increase in energy required is only bc. The upper curve represents hypothetical conditions for a [100] movement. It occurred to Mathewson that there might be different critical resolved shear stresses for the two parts of the lower curve and that in order for a complete glide to take place both

of them would have to be reached. In some orientations the critical stress for the first movement would be reached before that for the second, and the latter would be the limiting stress for glide. In other orientations the reverse would be true. A re-analysis of the data of Rosbaud and Schmid on this basis was inconclusive because of the magnitude of the experimental variations. A new investigation with improved specimens and techniques was indicated.

Experimental Procedure

Specimens 16 in. long were grown of 99.999+ pct zinc in ½ in. ID, precision-ground pyrex glass tubes, as described in another paper,⁵ and were etched for 5 sec with 50-50 HCl, rinsed in distilled water and then alcohol, and allowed to dry. Their orientations, determined by X-ray methods, are listed in table I. The analysis of zinc used, in percent, was: lead, 0.00013; iron, 0.0006; cadmium, 0.00003; and copper,

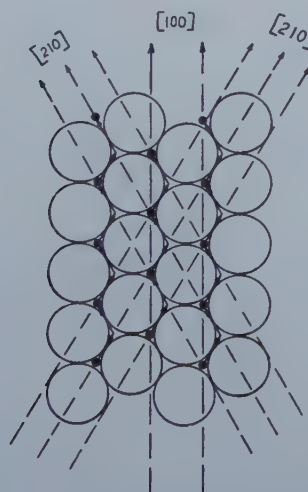


Fig. 2—Hypothetical slip in alternating [210] directions compared with simple [100] slip on basal plane of zinc crystal.

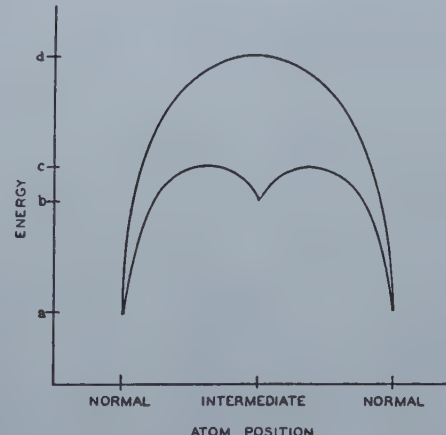


Fig. 3—Hypothetical energy changes during slip in alternating [210] directions compared with those during simple [100] slip.



Fig. 4—Parts of grip assembly for tension tests of zinc single crystals.

0.00012. No tests were made for A, Br, Cl, F, He, H, I, Kr, Ne, N, O, Se, S, or Xe. Other elements were not detected or were in insignificant amounts. Total impurities detected were 0.00088 pct and the percent zinc by difference was 99.99912. An 8 in. gauge length was marked on the specimens by applying soft red crayon to the specimens in the approximate positions and scribing light, sharp lines in the crayon marks (not in the specimen) with a sharp needle.

It was believed that axiality of loading was of great importance, and special grips were designed as shown in fig. 4. The specimen is inserted into the split, tapered collet (upper right), threaded on the inside, which is snugged gently into a tapered sleeve, shown below the collet, fastened in the clamp (next below). The taper gives a self-tightening action under load. The clamp, the ring shown below it, and the ring attached to the hook (upper left) have knife-edges at right angles. Assembling is done with the greatest of care to avoid deformation of the specimen. A similar gripping system is applied to the other end and the specimen is hung in position on the test rack. The assembly is checked for axiality and for straightness at this time (and periodically throughout the test) with the aid of surveyor's transits in positions 90° from each other about the axis of the specimen.

A bucket was suspended from a hook fastened to

Table II. Critical Stresses Resolved in [210] Directions

Specimen No.	S_{λ_a}	S_{λ_b}
XL45F	16.22	15.74
XL48G	16.36	15.45
XL44	16.55	15.05
XL47E	17.58	14.72
XL47D	17.10	14.78
XL48F	17.42	13.86
XL47G	18.22	13.65
XL47F	18.21	13.38
XL45C	18.51	13.07
XL47C	18.46	13.13
XL48B	19.44	13.24
XL45A	19.36	12.51
XL48A	18.23	12.12
XL47B	20.00	12.28
XL45B	19.93	11.96

the lower grip assembly, and water was added to the bucket at a constant rate by maintaining a constant head of water at a constant temperature behind a given orifice (fig. 5). By changing the size of the orifice and the head of water, it was possible to obtain the rate of flow desired in every case. This was determined from the orientation of the specimen to give a rate of increase of stress in the glide plane in the [100] glide direction of 0.1 g per mm² per min.

The tests were run in a constant-temperature, constant-humidity testing room at 25.0° ± 0.5°C and 60 ± 5 pct relative humidity.

A two-scope optical cathetometer was chosen for measuring elongations. The positions of the fiducial marks on the specimen were read to the nearest 0.001 cm. The error in strain with an 8 in. gauge length was estimated at ±1 x 10⁻⁴ and was minimized further by the method of plotting.

Readings were taken alternately on the upper and lower marks at about 30-sec intervals until the specimen had stretched about 1.5 pct.

The readings of the upper and lower scopes were plotted separately against time and a curve was drawn for each, trying not to average out any fluctuations that might be due to the nature of the deformation. The differences between the two curves were then determined and a stress-elongation curve was plotted. Elongations were also recalculated into

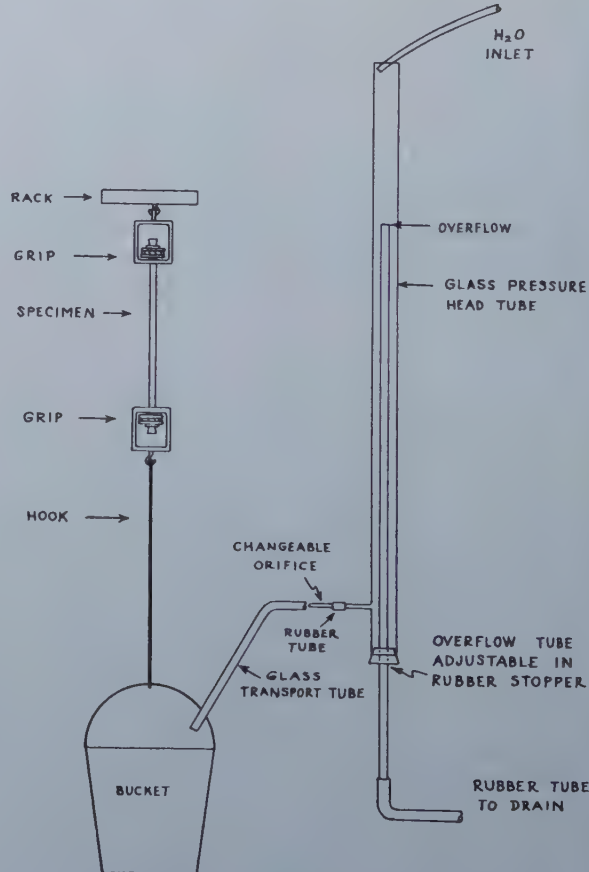


Fig. 5—Apparatus used for loading single-crystal specimens.

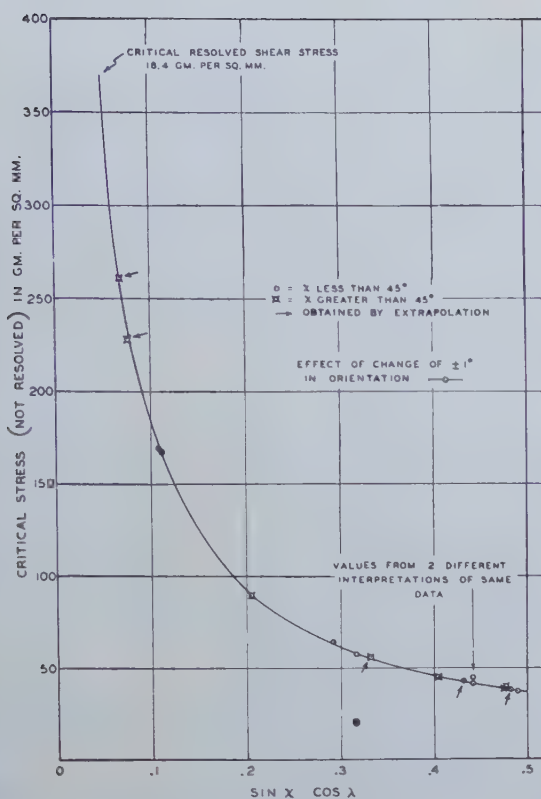


Fig. 6—Relation between critical stress and orientation of single-crystal specimens of 99.999+ pct zinc.

terms of shear, and a stress-shear curve plotted, by means of the formula (reference 6, p. 64):

$$\frac{L}{L_0} = \sqrt{1 + 2 a \sin \chi \cos \lambda + a^2 \sin^2 \chi}$$

where L_0 and L are the original and new lengths, a is the shear, and χ and λ as described previously. The critical stress was determined from an examination of these curves and was recalculated into resolved stresses in the [100] glide direction and the [210] directions on each side of this by means of the formula (reference 6, p. 111):

$$S = \frac{F}{A} \sin \chi \cos \lambda$$

where $\frac{F}{A}$ is the critical stress (force divided by cross-

sectional area) and S is the critical resolved shear stress. The results are tabulated in table I.

Discussion of Results

Examination of the values in table I for $S \lambda_a$, the critical stress resolved in the (001) plane in the [100] glide direction, shows a good average value of 18.4 g per mm². Of the 15 specimens tested, 12 yielded values within about ± 1 pct of this value, one was within ± 2 pct, and two were within ± 5 pct. This degree of consistency, despite wide variations in orientation, indicated no need for an alternating [210] hypothesis of the mechanism of slip. Furthermore, if the critical stresses resolved in the alternating [210] directions are arranged in the order of increasing angle between [100] and the projection of the specimen axis on (001), as in table II, the [210] hypothesis, according to the suggested

analysis, would require that the $S \lambda_a$ values down to some intermediate orientation and the $S \lambda_b$ values up to some intermediate orientation, as suggested by the broken lines, should be constant.

Such is not the case. They show a definite trend rather than a constancy and hence fail to substantiate the [210] hypothesis. Perhaps, however, they do not disprove it. It may be that the premises upon which the analysis was based were incorrect. Perhaps the stress must be resolved first in the [100] direction and then multiplied by a cosine factor to describe the sidewise movement. As far as stress calculations go, we would then be blind to the mechanism. Maddin, working with single crystals of brass, has recently obtained evidence of a different nature in support of the [210] hypothesis,⁷ and Barrett has obtained supporting X-ray evidence from certain silicon alloys.⁸

The critical stress values of table I have been plotted in fig. 6 against $\sin \chi \cos \lambda_a$ for comparison with Rosbaud and Schmid's plot shown in fig. 1. The improvement in consistency of experimental data is gratifying.

A consideration of the effect of an error of $\pm 1^\circ$ in determining the orientations of specimens, indicated in fig. 6, shows that the values obtained for the critical resolved shear stress for basal slip in ten of the specimens are constant well within the anticipated experimental error. The author felt justified, therefore, in drawing all ten stress vs. shear curves through the average critical value, 18.4 g per mm², in order to present them all clearly in a single figure (fig. 7). The other five specimens began to deform before the resolved stress attained a value of 18.4 g per mm². The value at which this started varied with the specimens; but no correlation with orientation, the only intentional variable, could be shown. The only variable which should have lowered the critical resolved shear stress significantly is non-axiality, which could have resulted

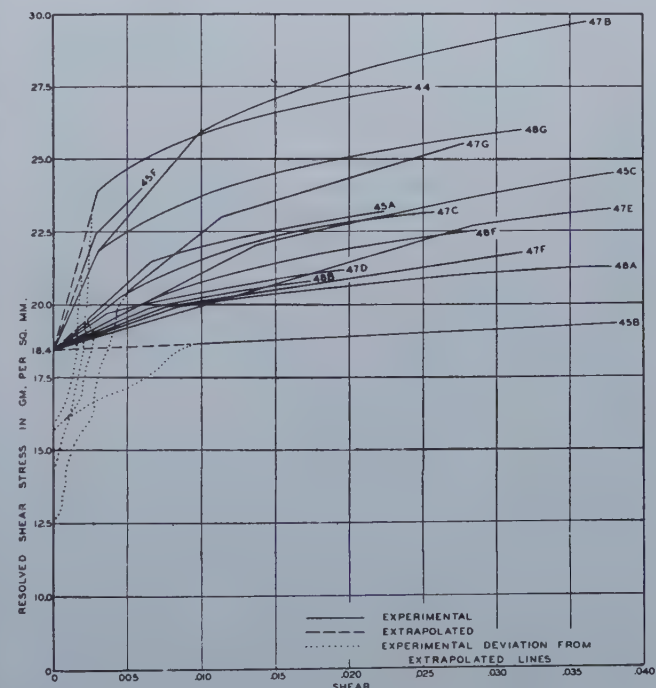


Fig. 7—Stress-strain curves for single-crystal specimens of 99.999+ pct zinc.

Adjusted (within limits of experimental error) to a critical resolved shear stress of 18.4 g per mm².

from unintentional deformation before the start of the test. These tests might be eliminated on this basis. However, it must be significant that every one of the other ten curves contained a *straight-line portion* that passed through the 18.4 critical point (well within the limits of error imposed by the inaccuracies of the determination of orientations) and that those showing initial deviations always reached and then followed a similar *straight-line portion* which could be extrapolated to a similar value, as though the initial effect of the tension was to eliminate or correct the effects of previous slight bending or non-axiality. The author believes that the *straight-line* extrapolations represent the true curves (Andrade⁹) and that the initial deviations should be ignored. For these specimens, the *extrapolated* values are shown in table I and fig. 6. The average critical resolved stress is 18.4 g per mm² whether these values are included or not.

The stress vs. shear curves of fig. 7 (or a similar plot of stress vs. elongation) showed definite differences in the strain-hardening characteristics of different specimens, both in the initial rates of hardening and in the total hardening for any given amount of shear or elongation. All attempts to establish a correlation with some function of orientation failed. This failure may have been due to the fact that once deformation had started, it tended to proceed inhomogeneously, resulting in non-axialities and resultant bendings of the specimens. It might also have resulted from differences in lead distribution in the different specimens, but these, in turn, might be expected to be a function of orientation. Speculation might be made as to the exact differences in the nature of the deformation in the different parts of the stress-strain curve, but it seems that such discussion might well be deferred until the effects of various variables in the testing procedure, as surface condition, size and shape of specimen, rate and temperature of test, etc., have been investigated and a firmer foundation for speculation has been obtained.

It was also observed that extension frequently occurred in tiny jumps, as has been mentioned by many investigators with zinc and with other metals.¹⁰⁻¹⁸ The nature and cause of these jumps has not been definitely established. It has been demonstrated that their occurrence, magnitude, and frequency are dependent upon temperature. The present investigator is inclined to suspect a connection with the rumpling or kinking mechanism discussed in another paper.¹⁹ Variations in temperature were shown to affect this mechanism. The explanation of these jumps is a matter of fundamental importance and it is hoped that as the various phases of the present work are expanded, information may be obtained that will serve this purpose.

Conclusions

Highly consistent data have been obtained which indicate that the critical resolved shear stress for slip is 18.4 g per mm², on the basal plane in the close-packed direction of single-crystal specimens of 99.999+ pct zinc. The specimens were cylindrical in shape with a ½-in. diam, lightly etched with 50 pct HCl, and tested in tension with a rate of increase of stress resolved along the basal plane in the close-packed direction of 0.10 g per mm² per min, at a temperature of 25.0° ± 0.5°C and a relative humidity of 60 ± 5 pct. The effects of many variables on the magnitude of this critical resolved stress remain to be investigated, but specimens and

equipment for many such tests have been made available.

An effort to obtain confirmation, by appropriate stress analysis, of the hypothesis of slip involving alternating [210] unit movements failed, probably because the method of analysis was based upon incorrect premises.

The work-hardening characteristics of specimens of different orientations were observed to vary under the particular conditions of test. Efforts to correlate differences in work-hardening with differences in orientations failed, perhaps because of experimental complications.

Acknowledgments

The author wishes to express his most sincere gratitude to C. H. Mathewson, of Yale University, and E. A. Anderson, of The New Jersey Zinc Co. (of Pa.), for their inspiration and guidance, to A. G. Lesko, III and others of the technical staff of The New Jersey Zinc Co. (of Pa.) for their invaluable assistance, and to The New Jersey Zinc Co. (of Pa.) for support and facilities without which the work could not have been attempted.

References

- ¹ P. Rosbaud and E. Schmid: Increase in Strength of Single Crystals by Alloying and Cold Rolling. *Ztsch. Physik.* (1925) **32**, 197.
- ² Richard F. Miller: Creep and Twinning in Zinc Single Crystals. *Trans. AIME* (1936) **122**, 176.
- ³ Alvin W. Hanson: Elastic Behavior and Elastic Constants of Zinc Single Crystals. *Phys. Rev.* (1934) **45**, 324.
- ⁴ C. H. Mathewson: Structural Premises of Strain-Hardening and Recrystallization. *Trans. A.S.M.* (1944) **32**, 38.
- ⁵ D. C. Jillson: Production and Examination of Zinc Single Crystals. *Trans. AIME*, **188**, 1005; *Jnl. Met.* (Aug. 1950) TP 2898E.
- ⁶ E. Schmid and W. Boas: *Kristallplastizität*. (1935) Berlin. Julius Springer.
- ⁷ Robert Maddin, C. H. Mathewson, and Walter R. Hibbard, Jr.: The Origin of Annealing Twins in Brass. *Trans. AIME*, **185**, 655; *Jnl. Met.* (Sept. 1949) TP 2676E.
- ⁸ Charles S. Barrett: Faults in the Structure of Copper-Silicon Alloys. *Trans. AIME*, **188**, 123; *Jnl. Met.* (Jan. 1950) TP 2754E.
- ⁹ E. N. daC. Andrade and R. Roscoe: Glide in Metal Single Crystals. *Proc. Phys. Soc.* (1937) **49**, 169, 177.
- ¹⁰ E. N. daC. Andrade: On the Viscous Flow in Metals, and Allied Phenomena. *Proc. Roy. Soc. (London)* (1911) **84**, 1.
- ¹¹ E. Schmid and M. A. Valouch: The Discontinuous Translation of Zinc Crystals. *Ztsch. Physik.* (1932) **75**, 531.
- ¹² R. Becker and E. Orowan: Discontinuous Extension of Zinc Crystals. *Ztsch. Physik.* (1932) **79**, 566.
- ¹³ M. N. Davidenkov and I. N. Mirolyubov: Plasticity of Zinc. *Jnl. Tech. Phys. (U.S.S.R.)* (1936) **6**, 60.
- ¹⁴ E. S. Yakovleva and M. V. Yakutovich: Jump-like Deformation of Zinc Crystals. *Jnl. Tech. Phys. (U.S.S.R.)* (1935) **5**, 1744.
- ¹⁵ T. Sutoki: Serrated Elongation in Different Metals. *Sci. Rept. Tohoku Imp. Univ. First Ser.* (1941) **29**, 673.
- ¹⁶ U. Dehlinger, A. Kochendörfer, H. Held, and E. Lörcher: The Development of Stresses on Bending Single and Multicrystalline Materials. *Ztsch. Met.* (1941) **33**, 233.
- ¹⁷ E. P. Tyndall and C. Wert: Private Communication to Andrew W. McReynolds, p. 34 of ref. 18.
- ¹⁸ Andrew W. McReynolds: Plastic Deformation Waves in Aluminum. *Trans. AIME*, **185**, 32; *Jnl. Met.* (Jan. 1949) TP 2499E.
- ¹⁹ D. C. Jillson: An Experimental Survey of Deformation and Annealing Processes in Zinc. *Trans. AIME*, **188**, 1009; *Jnl. Met.* (Aug. 1950) TP 2900E.

The Vapor Pressure of Silver

by H. M. Schadel, Jr. and C. E. Birchenall

The vapor pressure of silver has been measured by the Knudsen orifice effusion method 750° to 1050°C using radioactive Ag¹¹⁰ as a tracer. The pressures are given by the following equations:

$$\text{Solid silver: } \log p = 8.887 - 1.402 \times 10^4/T.$$

$$\text{Liquid silver: } \log p = 8.342 - 1.334 \times 10^4/T.$$

The heats of sublimation and vaporization are respectively, 64.1 ± 0.7 and 61.0 ± 0.2 kcal/mol.

THE purpose of this study was to measure the vapor pressure of silver as the first step in the determination of activities in silver alloys and to test the limitations of the method adopted. In order to work at low pressures, below 2×10^{-2} mm of mercury, the orifice effusion technique was employed. To shorten the time of collection of silver from the atomic beam, radioactive silver (Ag¹¹⁰) was used as a tracer.

The rate of effusion of a monatomic vapor from an "ideal" orifice, where the thickness of the orifice edge is negligible compared with the orifice diameter, can be readily calculated from the kinetic theory of gases,

$$G = \frac{\sqrt{M} a p}{\sqrt{2\pi RT}} \quad [1]$$

where G is the weight of material effusing from the orifice per unit time; p is the vapor pressure at oven temperature, T ; R is the gas constant; M is the molecular weight of the vapor; and a is the orifice area.

H. M. SCHADEL, JR. is Research Associate and C. E. BIRCHENALL, Junior Member AIME, is Member of Staff, Metals Research Laboratory, Carnegie Institute of Technology, Pittsburgh, Pa.

AIME Chicago Meeting, October 1950.

TP 2911 E. Discussion (2 copies) may be sent to Transactions AIME before Dec. 15, 1950. Manuscript received April 14, 1950; revision received June 14, 1950.

Consolidating constants and expressing as the weight of material effusing from the orifice in a period of time, t ,

$$G_t = \frac{(5.83)(10^{-3})(\sqrt{M})(a)(t)(p)}{\sqrt{T}} \quad [2]$$

where G_t is total weight of monatomic vapor effused (g); M is molecular weight of the effusing tracer vapor; a is orifice area (cm^2); t is time of effusion (sec); p is vapor pressure of effusing material (mm of Hg); and T is oven temperature (°K).

The vapor effuses from the orifice in a hemispherical pattern, and the intensity of the beam in any direction is given by the cosine distribution law.¹ Considering this, the weight of effused material can be calculated from the amount of material passing through a circular collimator intersecting the beam. If such a collimator is in a plane parallel to the plane of the orifice and with center on the normal to the orifice center,

$$G_\theta = \frac{G_\theta}{1 - \cos^2\theta} = \frac{G_\theta}{\sin^2\theta} \quad [3]$$

where G_θ is the weight of effused material passing through the collimator, and θ is one half the apex angle of the cone defined by the collimator circumference and the orifice center. Reducing eq 3 to the more directly measurable quantities of orifice to collimator distance, d , and collimator diameter, D , the expression becomes,

$$G_t = \frac{G_\theta (D^2 + 4d^2)}{D^2} \quad [4]$$

The vapor passing through the collimator, G_θ , was condensed on a target and the weight of the micro-quantity of Ag^{110} so collected was determined by a radiochemical assay with a Geiger-Müller tube. The activity of the condensate, C_t , was then compared with that of a standard, C_s , containing a known weight, W_s , of the oven charge. The weight of material which passed through the collimator, on the basis of $M = 110$, is then given by

$$G_{\theta 110} = \frac{C_t}{C_s} \cdot W_s \quad [5]$$

To correct for difference in weights between Ag and Ag^{110} , the factor $\sqrt{\frac{110}{107.88}}$ must be introduced if results are to be reported as the vapor pressure of the normal mixture of stable silver isotopes or

$$G_{\theta 107.88} = \frac{C_t}{C_s} \cdot W_s \cdot \sqrt{\frac{110}{107.88}} \quad [5a]$$

Substituting the equivalents for $G_{\theta 107.88}$ and G_t and solving eq 2 for $p_{107.88}$, the final equation is obtained,

$$p_{107.88} = \frac{17.153}{at} \cdot \frac{C_t}{C_s} \cdot W_s \cdot \sqrt{\frac{110}{107.88}} \cdot \frac{D^2 + 4d^2}{D^2} \sqrt{\frac{T}{M}} \quad [6]$$

If eq 6 is to apply, certain geometrical and physical conditions must be established within the system.² These may be summarized as follows.

1. The mean free path, λ , of the vapor within the oven must be several times the orifice diameter, ϕ . To better establish the ratio of λ/ϕ , permissible if the cosine distribution law is to be obeyed, a series of four determinations were made at 1280°K. The results are summarized in table I.

Table I. Variation of Apparent Pressure with λ/ϕ

Temp, °K	Approximate Mean Free Path $\lambda = 1/\sqrt{2} \pi$ $\delta^2 n$ (cm)	Orifice Diam, ϕ (cm)	λ/ϕ	Appar- ent Pressure (mm of Hg)
1280.2	2.5	0.026	104	7.01×10^{-3}
1280.0	2.5	0.045	58	7.42×10^{-3}
1280.5	2.5	0.10	25	7.28×10^{-3}
1280.5	2.5	0.20	12.5	6.86×10^{-3}

For the purpose of this experiment, λ was calculated

from $\lambda = \frac{1}{\sqrt{2} \pi \delta^2 n}$, where δ is the molecular di-

ameter (estimated as 4×10^{-8} cm for Ag), and n is the number of molecules per cm^3 at the temperature and pressure under consideration. The "true" value of the pressure at 1280°K, again for the purpose of this investigation, was chosen from the best line for 10 points, above 1233.5°K, presented in this paper. The value is approximately 7.30×10^{-3} mm of Hg. The results indicate no significant difference in the apparent pressure as λ/ϕ decreases from 104 to 12.5. For all points determined by the molecular beam technique and presented in this paper, the

ratio of λ/ϕ was always considerably in excess of this minimum value.

2. The mean free path, λ_r , of the residual gases between the orifice and target must be several times the orifice to target distance. For the data herein presented, the ratio is less than 0.03, considering a residual gas pressure of 3×10^{-5} mm Hg and an orifice to target distance of less than 6 cm. This assures collection of at least 97 pct of the portion of the beam defined by the collimator.

3. The effective sample area, O , from which evaporation takes place should be large compared to the orifice area, a , i.e., the rate of evaporation should be much greater than the rate of effusion.

4. All components between the orifice and target should be adequately cooled to condense the incident beam.

5. The orifice temperature must be as high or higher than other portions of the oven.

Apparatus

Details of the assembled apparatus are shown in fig. 1. The oven assembly (A) consisted of a tantalum body containing the $\text{Ag} + \text{Ag}^{110},^*$ covered by

* Ag^{110} implies radioactive silver, mass No. 110.

Ag implies the normal mixture of stable isotopes, at. wt = 107.88.

a nickel oven lid upon which was welded a 0.003 in. nickel orifice plate. Orifices were prepared from the nickel sheet by dimpling and then polishing the convex protrusion until a hole of the desired diameter was produced. The coolest portion of the oven, hence the effective temperature of the system, was that of the oven base where temperature measurements were made.

The oven was supported by three, pointed tungsten wire legs which rested in a conical hole, V-groove, and rectangular notch in the silica block (B). The cell was surrounded by three, concentric, clear quartz radiation shields (C), between which was placed 0.003 in. slotted tantalum sheet. An outer shield of alundum (D) surrounded the entire assembly. Heating of the oven was effected by the externally wound induction coil (E).

Oven temperatures were determined by a Pt-Pt-10 pct Rh thermocouple (F) tamped into a drilled hole in the oven bottom. The couple was calibrated against a standard couple inserted into the oven cavity through the opening in the oven lid.

The copper collimator (G), containing a sharp edged hole of known area, was screwed into the copper tubing target container (H) and held the copper guide block (I) rigidly against the bottom edge of the target container. The entire collimator-target container assembly was held against the ground shoulder of the dry ice-acetone cooling jacket (J) by means of the tension spring (K). A magnetically operated target ejector (L) was used to push target disks (M) into the target receiver (N). Alternate disks served only as shields to interrupt the beam and permit adjustment of temperatures and accurate timing of each target exposure. Disks used for targets and the standard were identically prepared. Each consisted of an aluminum disk, 0.870 in. in diam by 0.185 in. thick. One face was recessed 0.030 in. to permit reception of a 0.003x0.800 in. diam tantalum target. The target was secured by a wire ring to permit removal of the tantalum and re-use of the aluminum disks. Tantalum was chosen for the target material because of its great inertness to atmospheric at-

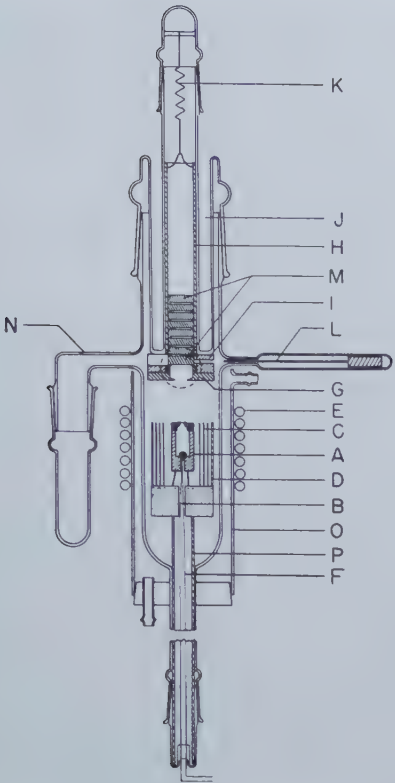


Fig. 1—Vapor pressure apparatus.

A. Oven assembly	I. Guide block
B. Silica block	J. Dry ice-acetone jacket
C. Quartz radiation shields	K. Tension spring
D. Alundum radiation shield	L. Target ejector
E. Induction coil	M. Target disks
F. Pt-Pt-10 pct Rh thermocouple	N. Target receiver
G. Collimator	O. Water jacket
H. Target container	P. Pyrex support

tack and apparently higher accommodation coefficient for the silver beam.**

** Three trial runs were made using both Ta and Ag sheet as the target material. In all cases, the vapor pressure as determined from the amount of condensate, was significantly higher (20 pct) for the Ta targets. The effect is not that expected and appeared to be due to the presence of an oxide or sulphide layer on the Ag which lowered its condensation coefficient for Ag vapor below that of Ta. The latter had a much cleaner appearance than the silver. The edge of the beam shadow was always sharp on the tantalum target, and no activity was found on other parts of equipment between collimator and target.

The collimator and targets were cooled by conduction from the dry ice-acetone mixture, while the walls of the pyrex vacuum chamber were cooled by a water jacket (O). The collimator temperature was always below 200°C to remove effectively all of the silver vapor striking it.

The orifice to collimator distance was adjusted by using thin cylindrical spacers at the bottom of the pyrex support (P), and the distance was measured indirectly from the similar triangles defined by the orifice, collimator diameter, shadow diameter, and the fixed collimator to target distance.

The system was evacuated through a liquid nitrogen trap by an air-cooled oil diffusion pump backed by a mechanical pump. The residual gas pressure was measured with an ionization gauge. This system permitted maintenance of pressures less than 3×10^{-5} mm of Hg with the oven at 1050°C.

Experimental Procedure

The oven charge was prepared by diluting 1/5 unit of radioactive Ag¹¹⁰ (\approx 7 millicurie) with 2.7

g of fine silver powder, Lot No. 4303-D of the U. S. Metals Refining Co. Since the radioisotope was received as AgNO₃, it was necessary to precipitate Ag¹¹⁰ as the hydroxide and then decompose this to metallic Ag¹¹⁰ by heating.

Following melting to effect homogenization of Ag¹¹⁰ throughout the charge, a weighed sample was taken from the oven and dissolved in dilute HNO₃. An aliquot part representing 18.8 micrograms of the oven charge was then evaporated upon one of the target disks for use as a standard. To reduce the possibility of counting errors due to unevenness of the evaporated layer, several disks were prepared. Their counting rates were similar within the limitations of the counting equipment. The apparatus was assembled as indicated in fig. 1.

Both the oven and charge were outgassed by heating in vacuo to greater than 1000° until the residual pressure, at the temperature of the run, was less than 3×10^{-5} mm of Hg. Upon attainment of the desired pressure and temperature of operation, the first target was exposed by magnetically ejecting the interrupting disk into the target receiver. During the exposure, temperature readings were taken at intervals of from 3 to 10 min depending upon the total exposure time. The average of the temperature measurements was taken as the effective cell temperature, and the average root mean square deviation for all points reported was approximately 0.8°C. The accuracy of the reported temperatures is within $\pm 1^\circ$ C.

Target exposures were made for various temperatures and orifice sizes, the time in each case being adjusted to collect approximately the same amount of silver on each target. By using the magnetically operated ejector, exposure times were controlled within ± 0.05 pct.

Under no condition of exposure reported was the ratio λ/ϕ less than 35, this minimum value being applicable to the highest point, 4-Y, at 1328.8°K. Measurement of orifice areas before and after exposures indicated a difference of less than ± 2 pct, attributable only to accuracy of the method of measurement used.

The weight of silver deposited on each target was determined by counting the rate of radioactive dis-

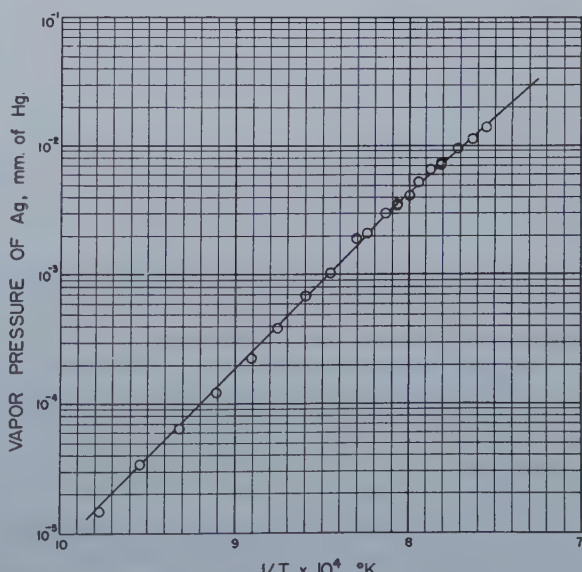


Fig. 2—Vapor pressure of silver ($T < 1233.5^\circ$ K).

integration (C_r) with a Geiger-Müller tube. This rate was compared with that of the standard (C_s), counted both before and after the unknown target. For each experimental point reported, the value of the product of their ratio (C_r/C_s) and the weight of silver on the standard (W_s) is the average of the corrected counting rates[†] for three counts totaling at

[†] The corrected counting rate is the observed rate corrected for background and coincidence.

least 10,000 counts each for both the standard and the unknown.

To ascertain whether both the standard and experimental targets contained the same material, decay curves were run on both the standard and one of the targets prepared by condensation of the vaporized material. Statistically, there is no significant difference in the half-lives of the two Ag¹⁰⁰ specimens prepared by independent methods. This would indicate that the two specimens represent the same population, i.e., radiocontaminants, if any are present, are of no consequence in the determination of vapor pressure by the method employed.

Data and Results

The geometrical conditions applicable to and the results of 21 target exposures, covering the temperature range 1023.6° to 1323.8°K, are given in table II.[‡] The methods of determining orifice area (*a*),

[‡] For tables II and III (2 pages) order Document 2856 from American Documentation Institute, 1719 N St., N.W., Washington 6, D.C., remitting \$0.50 for microfilm (images 1 in. high on standard 35 mm motion picture film) or \$0.50 for photocopies (6x8 in.) readable without optical aid.

orifice to collimator distance (*d*), exposure time (*t*), average temperature (*T*), and the weight of target

silver ($C_r/C_s \cdot W_s \sqrt{\frac{110}{107.88}}$), have been previously described. Vapor pressures were calculated by substitution of the observed values in eq 6.

A plot of the results showing $\log P$ vs. reciprocal temperature is given in fig. 2. The indicated curve was derived by first determining the best straight lines, by the least square criterion, for all data below the melting point (1233.5°K) and another for all data above the melting point. From these, the pressure at the melting point was calculated from the statistically weighed data for each curve extrapolated to the melting point. So calculated, the best value for the vapor pressure at the melting point is 3.34×10^{-3} mm of Hg as against 3.30×10^{-3} mm of Hg for the solid curve and 3.36 mm of Hg for the liquid curve. This value is well within the standard deviation for either set of data.

With the pressure at the melting point fixed, the best line for the solid phase was recalculated to give that shown in fig. 2. The applicable equation follows:

$$\text{I. } \log p = 8.887 - 1.402 \cdot 10^4/T \quad (\text{for } 1023.6^\circ\text{K} < T < 1233.5^\circ\text{K}) \quad \Delta H_s = 64.1 \pm 0.7 \text{ kcal/mol}$$

where ΔH_s is the heat of sublimation.

Since the experimental data included in this paper cover only a relatively narrow portion of the liquid silver range, the curve for temperatures greater than 1233.5°K has been recalculated to include the data of both von Wartenberg³ and Fischer⁴ for reasons to be discussed later.

Fig. 3 is a replot of 26 points for liquid silver from this determination, von Wartenberg, and Fischer. The curve for the solid phase is given as for fig. 2 and again the pressure at the melting point

is fixed at 3.34×10^{-3} mm of Hg. The vapor pressure equation for the liquid curve is calculated to be,

$$\text{II. } \log p = 8.342 - 1.334 \times 10^4/T \quad (1233.5^\circ\text{K} < T < 2443.0^\circ\text{K}) \quad \Delta H_v = 61.0 \pm 0.2 \text{ kcal/mol}$$

where ΔH_v is the heat of vaporization. From this curve, the boiling point of silver is calculated to be 2443.0°K.

Both sets of data used in calculating eqs. I and II show excellent correlation (>0.999) to a linear plot of $\log P$ vs. $1/T$. This would indicate little or no

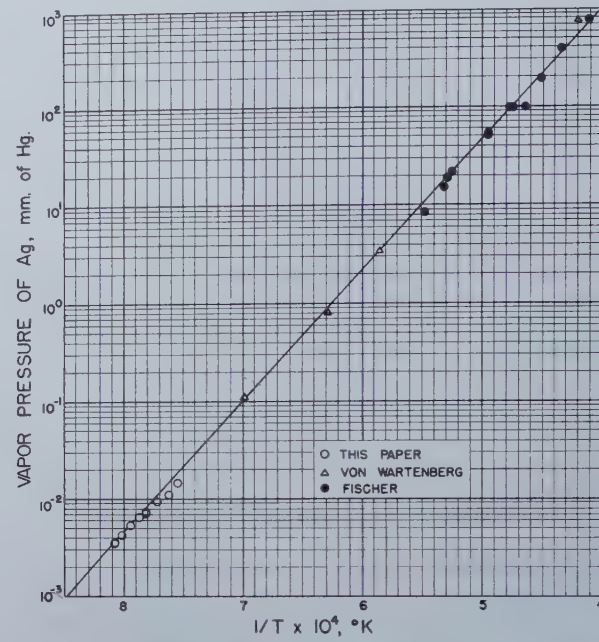


Fig. 3—Vapor pressure of silver ($T > 1233.5^\circ\text{K}$).

deviation from the empirical relationship existing between the temperature and vapor pressure over the range covered.

From the two equations, ΔH_{fusion} is found to be 3.1 ± 0.7 kcal/mol, which includes Kelley's⁵ best value of 2.855 kcal/mol.

Discussion of Results

Of the previous studies on the vapor pressure of silver, only one, that of Jones, Langmuir, and MacKay,⁶ covered the low-temperature range included in this work. Their results were obtained from free vaporization of silver from a heated filament, and it has been realized for some time that their values are much too low.

Measurements were made by Harteck⁷ over the temperature range 1196° to 1344°K by measuring the weight loss of silver contained in a quartz crucible with an orifice. The orifices used were 1 to 3 mm in diameter, and if it is assumed that Harteck used the 1 mm orifice at 1344°K, his ratio of λ/ϕ was considerably less than 10 and in the range where the probability of collision at the orifice has an appreciable value. Moreover, precise information is lacking on the residual pressure within Harteck's system. Conceivably it could have been great enough to cause back scattering at the orifice, hence a further lowering of the apparent pressure.

The boiling point given by Hansen⁸ has been disregarded for lack of information concerning his methods. The experiments of Greenwood⁹ and of Ruff and Bergdahl¹⁰ appear to be unacceptable due to the use of porous crucibles which lead to anom-

alous effects when gases are present in the system. A complete discussion of these porosity effects is given by Fischer,⁴ who repeated the methods of Greenwood and Ruff and Bergdahl with nonporous crucibles to show that reliable results could be obtained. Fischer's work covers the range from 1823°K to the boiling point (2425°K by his determination). The latter point was determined by the method of Greenwood, i.e., by visually observing the start of surface agitation as the temperature of the silver was slowly raised. For his other points, Fischer employed the technique of Ruff and Bergdahl which involved the determination of the rate of weight loss of silver through an orifice as the temperature of the crucible was raised at a uniform rate. When the vapor within the crucible reached the pressure of the residual gas in the surrounding vessel, the rate of weight loss increased markedly.

Von Wartenberg used the gas saturation method. Pure nitrogen was passed over the silver and then analyzed for the silver picked up. This procedure was repeated at the same temperature for several different gas velocities. The gas velocity vs. silver concentration curve obtained was then extrapolated to a zero gas velocity to give the saturation value and a measure of the equilibrium pressure.

From a survey of the high-temperature data on silver vapor pressures, it would appear that the results of von Wartenberg and Fischer are the most reliable. For determination of the vapor-pressure curve for the liquid phase, the results of other observers have been disregarded.

The test for consistency generally applied to vapor-pressure data is the calculation of the heat or energy of vaporization at absolute zero (ΔH°_0), combining thermodynamic properties of the condensed phases determined by thermal measurements with the thermodynamic properties of the vapor phase determined by the statistical mechanical treatment of spectral data and the experimentally determined vapor pressures. A complete discussion is given by Aston¹¹ and by Speiser and Johnston.¹²

This relation can be expressed as,

$$\frac{\Delta H^\circ_0}{T} = \left(\frac{F^\circ - H^\circ_0}{T} \right)_{\text{condensed}} - \left(\frac{F^\circ - H^\circ_0}{T} \right)_{\text{vapor}}$$

where, ΔH°_0 is heat of vaporization at absolute zero; H°_0 is heat content at absolute zero; F° is standard free energy; and T is absolute temperature. $F^\circ - H^\circ_0/T$ for the condensed phases may be obtained from Kelley.⁵ Graphical integration of heat capacity data from Kelley¹³ leads to $H^{208.1} - H^\circ_0 = 1374$ cal/mol and $S^{208.1} - S^\circ = 10.20$ entropy units. For temperatures above 1600°K, Kelley's⁵ equations for $H_T - H_{208}$ and C_p have been employed. A small error possibly results from this extrapolation.

For the vapor phase,

$$\frac{F^\circ - H^\circ_0}{T} = R \ln \left(\frac{(2\pi)^{3/2} k^{5/2}}{h^3 N^{3/2}} \right) + 5/2 R \ln T + \frac{3/2 R \ln M + R \ln Q - R \ln P}{T}$$

where, M is molecular weight; k is Boltzman's constant; h is Planck's constant; N is Avogadro's number; P is the observed vapor pressure; and Q is the multiplicity of the ground state of the atom, which is 2 for silver.¹⁴ Higher energy states may be neglected for few Ag atoms will exist at higher levels for the temperatures under consideration.

The test of the data is given in table III, and the consistency of ΔH°_0 (67.7 ± 0.6 kcal/mol) must be considered satisfactory. It compares very favorably with similar tests on vapor-pressure data reported for other metals. This test does not check the absolute values of the vapor pressures, but it does show that the $\log p$ vs. $1/T$ straight line relationship is an adequate representation of the data over the temperature range employed and that the slope is consistent with the heat-capacity measurements over that same range.

Summary

The vapor pressure of silver in the temperature range 1023.6° to 1323.8°K has been experimentally determined using radioactive Ag^{110} and the molecular beam technique. From these determinations, the vapor-pressure curve for solid silver has been recalculated to give appreciably higher pressures in the low-temperature range than heretofore reported by Harteck. For the liquid silver range (1233.5° to 2443°K), data from this paper and higher temperature data of von Wartenberg and Fischer have been considered in a recalculation of the vapor-pressure curve. All data used have been checked thermodynamically by determining the consistency of the heat of vaporization at absolute zero (ΔH°_0) as calculated from the experimentally determined vapor pressures and accepted heat capacities, entropies, and heat of fusion.

Acknowledgments

This work was done under contract with the Office of Naval Research. The Ag^{110} was supplied by the Isotopes Division, U. S. Atomic Energy Commission. The chemical processing of the radiation unit was done in our laboratory by Mrs. Elizabeth Duncan. Radioactive counting was under the supervision of L. F. Gronholz. Assistance during the vapor-pressure runs was provided by J. Miller. For this help and the discussions with G. Derge, W. O. Philbrook, and R. F. Mehl, the authors offer their thanks.

References

- R. G. J. Fraser: *Molecular Rays*. 1931. New York. McMillan Co.
- Estermann: *Rev. of Modern Physics*. (1946) **18**, 306.
- Von Wartenberg: *Ztsch. anorg. allgem. Chem.* (1908) **56**, 320.
- Fischer: *Ztsch. anorg. allgem. Chem.* (1934) **119**, 1 and 367.
- Kelley: Contributions to the Data on Theoretical Metallurgy. U. S. Bur. Mines Bull. 476, 158 (1949).
- Jones, Langmuir, and Mackay: *Phys. Rev.* (1927) **30**, (2) 201.
- Harteck: *Ztsch. physik Chem.* (1928) **134**, 1.
- Hansen: *Ber.* (1909) **42**, 210.
- Greenwood: *Proc. Roy Soc. (London)* (1909) **A82**, 396; (1910) **A83**, 483; and *Ztsch. Physik Chem.* (1911) **76**, 484.
- Ruff and Bergdahl: *Ztsch. anorg. allgem. Chem.* (1919) **106**, 76.
- Aston: The Third Law of Thermodynamics and Statistical Mechanics, in reference H. S. Taylor and S. Glasstone: *A Treatise on Physical Chemistry*. 1942. New York. Van Nostrand.
- Speiser and Johnston: A.S.M. Preprint No. 11 (1949).
- Kelley: Contributions to the Data on Theoretical Metallurgy. U. S. Bur. Mines. Bull. 434 (1941).
- Bacher and Goudsmit: *Atomic Energy States*. 1932. New York. McGraw Hill.

On the Martensitic Transformation at Temperatures Approaching Absolute Zero

by S. A. Kulin and Morris Cohen

Plastic deformation and straight-cooling experiments on 18-8 and 1 pct C, 20 pct Ni steels demonstrate that the martensitic transformation proceeds with characteristic rapidity even at temperatures approaching absolute zero. These results indicate that the atom-by-atom growth mechanism for martensite formation is invalid, at least in the alloys studied.

AT a recent symposium on thermodynamics in physical metallurgy¹ two opposing theories of the austenite-martensite transformation were presented. Both theories agreed that this type of reaction involves a nucleation process which requires activation and that the activated nuclei develop into the well-known martensite plates with tremendous speed. However, there were essential differences in the two points of view concerning the nature of the nucleus and the mechanism by which the nucleus propagates.

According to Cohen, Machlin, and Paranjpe,² the nucleus is a strain center with sufficient elastic energy to initiate a cooperative displacement among the atoms of the parent phase when a sufficiently low temperature is reached. This displacement propagates as a wave in shear-like fashion to transform the austenite into martensite without benefit of diffusion. On the other hand, Fisher, Hollomon, and Turnbull³ regard the nucleus as a solute-poor region (in the austenite) of a size which becomes supercritical relative to coherent growth into martensite when an appropriately low temperature is reached. This growth process is taken to be an atom-by-

S. A. KULIN, Student Associate AIME, and MORRIS COHEN, Member AIME, are associated with the Department of Metallurgy, Massachusetts Institute of Technology, Cambridge, Mass.

AIME Chicago Meeting, October 1950.

TP 2907 E. Discussion (2 copies) may be sent to Transactions AIME before Dec. 15, 1950. Manuscript received April 15, 1950.

The research was sponsored by the Office of Naval Research under Contract No. N5 ori-78, Task No. XIV, Designation No. NR 031-142.

atom transfer from the receding austenite lattice to the advancing martensite lattice through the coherent interface that exists between the two phases.

The present paper is not concerned with the divergent views as to the nature of the nucleus but describes some critical experiments which differentiate between the two proposed mechanisms of propagation. Fisher⁴ has summarized the latter issue in the following way: According to the cooperative displacement theory, the speed of formation of martensite plates should not be decreased by lowering the temperature, and martensite should form with extreme rapidity at very low temperatures; whereas with the alternate growth process, the speed of the martensite transformation should be retarded at very low temperatures, decreasing to zero at the absolute zero. The atom-by-atom growth mechanism predicts a marked slowing down of the reaction rate with decreasing temperature because the rate of self-diffusion in the austenite is involved in this picture. For example, Fisher, Hollomon and Turnbull⁵ estimate that the activation energy for this growth process in steel is $(0.34)^*(0.36)^*$ times the activation energy for self-diffusion in γ -iron. The two most recent determinations of the latter quantity are 67,900⁶ and 74,200⁷ cal/mol, which may be averaged as 71,000 cal/mol. This, in turn, gives a value

* 0.36 is the fraction of the activation energy required to move an atom one full lattice spacing, and 0.34 is the fraction of a lattice spacing that an atom is assumed to move in the growth of martensite out of austenite.

of 3000 cal/mol for the activation energy of the atom-by-atom process, and hence the rate of growth

should vary as $e^{-\frac{3000}{RT}}$, where R is the gas constant

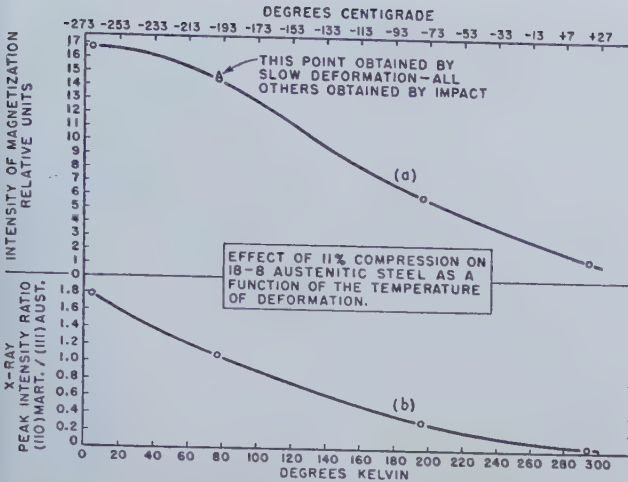


Fig. 1—Transformation in commercial 18-8 steel produced by compressive impact of 11 pct strain at various temperatures.

Relative extent of transformation is shown in terms of (a) magnetic intensity measurements and (b) ratio of X-ray diffraction intensities, using the (110) line of the martensite (ferrite) and the (111) line of the austenite.

($1.99 \text{ cal/mol}^\circ\text{K}$) and T the absolute temperature. Förster and Scheil⁸ report the time of formation of a martensite plate as about 70 microsec in a 29 pct Ni-71 pct Fe alloy which has an M_s temperature at approximately 223°K (-50°C). Let us assume that these observations would apply at a temperature as low as 196°K (-77°C) — the dry ice and acetone temperature. Then at 77°K (-196°C) — the liquid nitrogen temperature, the time of formation would

$$\text{be } 70 \times 10^{-6} \times \frac{e^{-\frac{3,000}{196R}}}{e^{-\frac{3,000}{77R}}} = 10 \text{ sec, which is long}$$

enough to permit suppression by fast cooling. Correspondingly, the time of formation at 4°K (-269°C) — the liquid helium temperature, would be $70 \times$

$$10^{-6} \times \frac{e^{-\frac{3,000}{196R}}}{e^{-\frac{3,000}{4R}}} = 25 \times 10^{15} \text{ sec or } 8 \times 10^{10} \text{ centuries.}$$

In other words, the atom-by-atom mechanism requires that the propagation of martensitic plates, although extremely rapid at ordinary temperatures, must stop at temperatures approaching absolute zero. This is a necessary consequence, even if the activation energy were an order of magnitude less than 3000 cal/mol, say, 300 cal/mol. With the latter value, a 70 microsec process at 196°K (-77°C) would take 250 centuries at 4°K (-269°C).

On the other hand, the propagation of a shear-like displacement of atoms in a cooperative movement would not be subject to such retardation at very low temperatures because the elastic constants

of a lattice are relatively insensitive to temperature variations compared to the effect on atom-by-atom diffusion rates. Accordingly, it becomes possible to distinguish between the two theories by ascertaining whether the martensitic transformation proceeds in a characteristically rapid fashion at temperatures approaching absolute zero or whether it becomes prohibitively slow. Of course, in designing such a critical experiment, one must choose alloys which have sufficiently low M_s temperatures so that reasonable quantities of austenite are available for the transformation near absolute zero. Furthermore, the conditions of the experiments must be selected to avoid stabilizing effects⁹ which might stop or inhibit the transformation even at moderately high temperatures.

The Approach

There are two general ways of conducting these experiments. First, an alloy might be selected which has such a low M_s temperature that the martensitic transformation curve (percent martensite vs. temperature) shows the normal increase with decreasing temperature below about 100°K (-173°C). Then the question would be "does the transformation continue in the usual manner if the cooling is extended to 4°K or does it stop below a certain temperature because of time limitations?" Secondly, one might select an alloy which remains austenitic even down to 4°K and then apply plastic deformation to see if any appreciable amount of martensite results. This should be quite possible according to the shear mechanism, but not according to the atom-by-atom process. In the latter instance, nuclei might be generated by the deformation, but no substantial growth to form martensitic plates could occur when the diffusion rate is virtually nil. Both types of experiments were performed in this work, using 18-8 stainless steel for the plastic deformation tests, and 20 pct nickel steels for the straight cooling tests. In both cases, the results clearly demonstrated that the atom-by-atom growth theory is invalid, at least for these materials.

In addition, attempts were made to detect some evidence that the martensitic transformation could be inhibited by rapid cooling at low temperatures. Kurdjumov and Maksimova¹⁰ have reported that the reaction can be suppressed at temperatures in the range of 208° to 77°K (-65° to -196°C) in a 0.6 pct carbon, 6 pct manganese steel, and this has been cited as support for the nucleation and atom-by-atom growth theory. In the present experiments, no suppression was observed even down to 4°K .

Plastic Deformation Experiments

Commercial 18-8 steel of the composition given in table I was found to undergo no martensitic transformation on cooling to 1°K (-272°C). However, it is known that the transformation can be induced by plastic deformation¹¹ at temperatures below

Table I. Analysis of Materials

Designation	C	Cr	Ni	Mn	Si	S	P	O	N	Al
18-8	0.057	20.00	8.95	0.39	1.05	0.002				
1C, 12 Ni	0.95	0.08	11.97	0.17	0.61	0.027	0.009		0.008	
0.5C, 20 Ni	0.52	0.04	19.99	0.37	0.47	0.015	0.010			
1C, 20 Ni	1.00*	0.05	19.58	0.39	0.80	0.022	0.010			
0.6C, 8 Mn	0.62			8.1	0.47	0.034	0.023			0.030

* Of this amount, 0.14 pct is graphitic carbon.

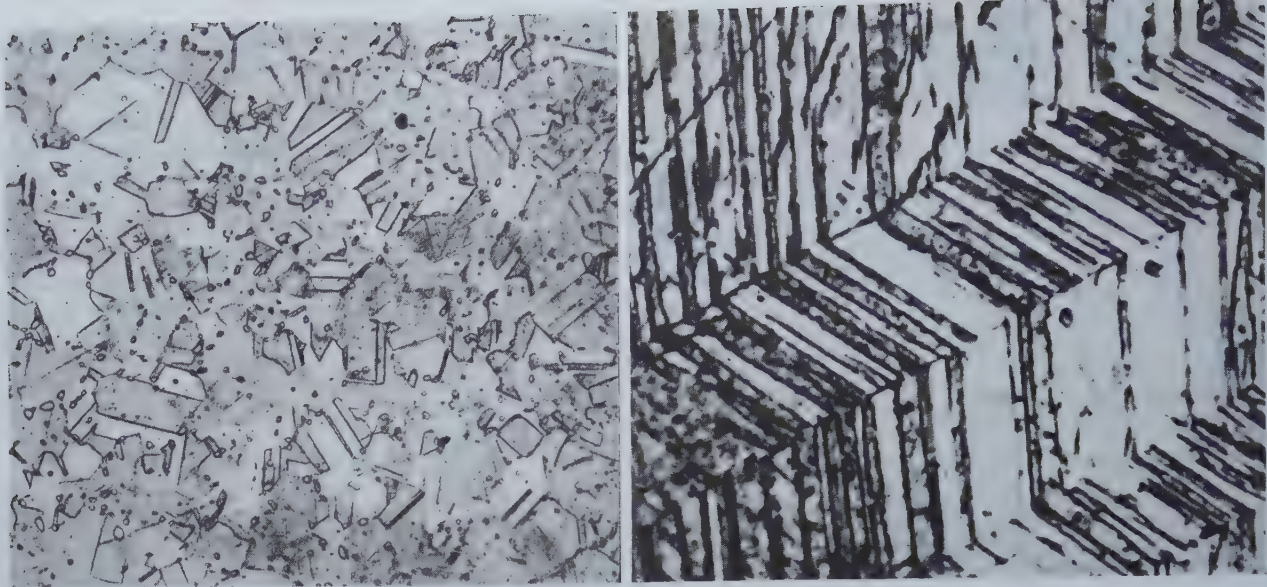


Fig. 2—Microstructure of 18-8 austenitic steel.

(a, left) before and (b, right) after 11 pct compressive deformation at 77°K (-196°C). Originally austenitized at 1150°C (2100°F) and water quenched to room temperature. Etched with HCl and HNO₃ in methyl alcohol. (a) X150 and (b) X2500.

373°K (100°C), and hence 18-8 stainless is an appropriate material for this type of experiment. Specimens 0.500 in. long x 0.250 in. diam were austenitized for 30 min at 1150°C (2100°F) in prepurified nitrogen and were water quenched to room temperature. Each specimen was then placed in a fixture, cooled to a predetermined temperature, and deformed by compressive impact to a strain of approximately 11 pct. The temperatures used were 293°K (20°C), 196°K (-77°C), 77°K (-196°C) and 4°K (-269°C), the latter three temperatures being attained by immersion in dry ice + acetone, liquid nitrogen and liquid helium respectively.

The magnetic and X-ray measurements plotted in fig. 1 show that the amount of transformation resulting from the deformation increases progressively with decreasing temperature. Typical microstructures are shown in fig. 2. There is no question but that the reaction responded promptly to the deformation, even at 4°K, during the split-second taken by the straining operation. Some magnetic determinations were made at the low temperatures immediately after the deformation, and it was assured that the transformation occurred during the straining, and not on warming back to room temperature.

In order to demonstrate that these phenomena were not a peculiarity of impact deformation, a comparatively slow compression was carried out at 77°K (-196°C), with the 11 pct strain being accomplished in 2 to 3 min. As indicated in fig. 1, the extent of transformation was virtually identical with that produced by the impact.

It was also suggested** that the heat generated

over a period of 90 min at 4°K, without any bubble evolution in the liquid helium, thus insuring no detectable rise in temperature. Magnetic tests on the strained specimens while still in the liquid helium showed that the transformation had taken place.

Straight Cooling Experiments

High-carbon, high-nickel steels have a suitable martensitic temperature range for critical transformation studies on straight cooling. The three nickel steels listed in table I were available for this work, but only the 1 pct C, 20 pct Ni steel had a sufficiently low M_s temperature to throw any light on the issue at hand. However, the results on the three steels are included here for comparison.

Samples ½ in. long x ¼ in. diam were austenitized at 1095°C (2000°F) for 30 min in prepurified nitrogen, and were oil quenched to room temperature.

† Furnished by S. G. Fletcher, of the Latrobe Electric Steel Co., Latrobe, Pa.

They were then cooled to various subzero temperatures for 3 min and returned to room temperature. The extent of transformation was determined in two ways, (1) magnetically without further treatment, and (2) by lineal analysis¹² after "darkening" the martensite at 315°C (600°F) for 10 sec. Both types of measurements clearly revealed the course of the martensitic reaction, but only the lineal-analysis results are reported here because they provide absolute values without requiring any calibration.

The martensite transformation characteristics for the three steels, as shown in fig. 3, are quite typical. The 1 pct C, 12 pct Ni and 0.5 pct C, 20 pct Ni curves flatten out at about 80 pct martensite below 77°K (-196°C), but this is not due to lack of diffusion. Self-stopping of the martensitic reaction on cooling, even at much higher temperatures, is well known. In the later stages of the transformation, stabilization effects and obstruction by the existing martensite¹³ inhibit the reaction. For example, the cooling transformation stops at 173°K (-100°C) in both high-speed steel¹³ and high-carbon, high-chromium

** Private communication, J. H. Hollomon.

during the deformation might raise the specimen temperature enough to provide much higher diffusion rates than would be expected at the nominal temperatures of the liquid baths. This possibility was eliminated by means of a special device which permitted very slow straining in tension of 0.125-in. diam specimens while completely immersed in liquid helium. Specimens were pulled slowly in this way

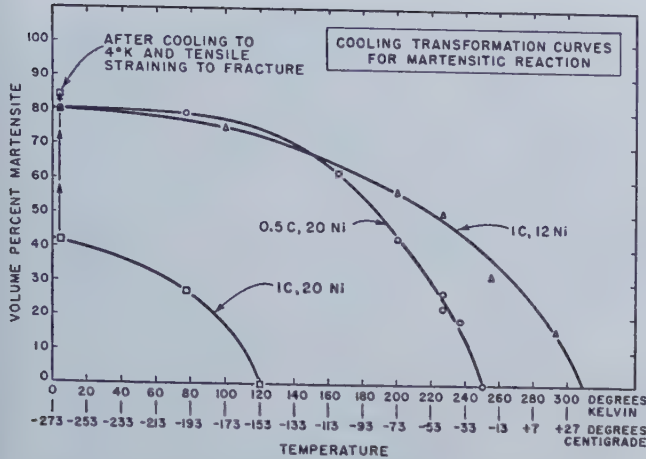


Fig. 3—Martensitic transformation curves for three nickel steels, austenitized at 1095°C (2000°F) and oil quenched to room temperature.

Specimens were then cooled to the indicated temperatures for 3 min, returned to room temperature, and tempered at 315°C (600°F) for 10 sec to "darken" the martensite for lineal analysis.

steel,⁹ and at 113°K (−160°C) in plain carbon tool steel.¹⁴

The curve for the 1 pct C, 20 pct Ni steel in fig. 3 is displaced to lower temperatures relative to the other two curves, and so the transformation is well underway as 77°K (−196°C) is approached. It is evident that the transformation does not stop on cooling below this temperature; the amount of martensite increases from 27 pct at 77°K (−196°C) to 42 pct at 4°K (−269°C). Despite the low temperatures involved, there is no indication that the transformation is being retarded. In fact, the 1 pct C, 20 pct Ni curve has the same general shape as the other two curves in the family and the pattern is quite similar to that observed for plain carbon¹⁵ and low alloy¹⁶ steels at higher temperatures.

Micrographs of the low-temperature martensite are presented in fig. 4. Many of the plates are extremely thin, compared to those formed at higher temperatures, presumably due to the prevailing constraints. Fig. 4c illustrates a new phenomena: some of the intersecting plates pass right through each other. Apparently, at these low temperatures, an advancing plate is not necessarily stopped by a plate lying in its path, but may propagate through to the other side. This suggests that the advancing plate strikes the first one with considerable momentum and the impulse may nucleate the process on the opposite side of the obstruction. Such a phenomenon is entirely consistent with a cooperative shear displacement but would be most unlikely on the basis of an atom-by-atom growth mechanism.

The formation of martensite in the 1 pct C, 20 pct Ni steel was observed "in action" by cooling polished specimens under a microscope. Surface upheavals due to the martensitic displacements were clearly visible. In all cases, each plate popped into view with such rapidity that the time of formation could only be estimated as a small fraction of a second. Moreover, there was no noticeable retardation in the propagation rate as the temperature dropped.

In all these experiments, no evidence of suppressibility of the martensitic reaction was detected. Small specimens of the 1 pct C, 20 pct Ni steel underwent the expected amount of transformation when the cooling time from room temperature to 4°K (−269°C) was reduced to 5 sec. Admittedly, this is

not an extremely fast quench, but it adequately demonstrates that the suppression predicted by the atom-by-atom theory does not occur. An attempt was also made to find suppression in manganese steels, as reported by Kurdjumov and Maksimova¹⁰ for a 0.6 pct C, 6 pct Mn alloy having an M_s at −65°C. The composition available[†] for this test (see

[†] Furnished by Howard Avery, of the American Brake Shoe and Foundry Co., Mahwah, N. J.

table I) had a slightly higher manganese content, and therefore should have a somewhat lower M_s temperature, than that of the 0.6 pct C, 6 pct Mn alloy. Instead the M_s temperature, after austenitizing at 980°C (1800°F) to dissolve all the carbide was found to lie slightly above room temperature, and no suppression was observed despite drastic quenching.

One final experiment was tried with the 1 pct C, 20 pct Ni steel. An austenitized specimen was cooled to 4°K in the tensile device previously mentioned, and pulled slowly (to avoid possible temperature rise) to fracture in liquid helium. The amount of martensite increased from the 42 pct produced by straight cooling to 84 pct as a result of the plastic deformation. The latter structure is shown in fig. 4d.

Conclusions

1. The martensitic transformation has been studied at temperatures approaching absolute zero in plastic deformation and straight cooling experiments, using commercial 18-8 and 1 pct C, 20 pct Ni steels. In both cases, the transformation proceeds with characteristic rapidity, even at 4°K (−269°C).

2. The extent of the transformation produced by a given amount of deformation increases with decreasing temperature of deformation, and is insensitive to the rate of straining within the limits investigated.

3. The straight cooling transformation in the 1 pct C, 20 pct Ni steel continues in typical fashion down to 4°K (−269°C), the lowest temperature employed. The martensitic plates propagate with great speed, even at low temperatures. No suppression of the reaction due to fast cooling was detected.

4. These findings invalidate the atom-by-atom growth mechanism of martensite formation, at least in the alloys studied, because such a process would become infinitesimally slow at temperatures approaching absolute zero.

5. On the other hand, a mechanism of martensite formation involving a shear-like displacement of atoms in a cooperative movement is strongly supported by these findings.

Acknowledgments

The authors are indebted to the Office of Naval Research for its sponsorship of this program. Steels were kindly furnished by S. G. Fletcher, of the Latrobe Electric Steel Co. and Howard Avery, of the American Brake Shoe and Foundry Co. The authors also wish to express their thanks to Miriam Yoffa for the metallographic work and to R. D. Cavileer, of the Low-Temperature Laboratory at M.I.T., for assistance in connection with the liquid helium experiments. A number of stimulating discussions were held with John Fisher and J. H. Hollomon, of the General Electric Co.

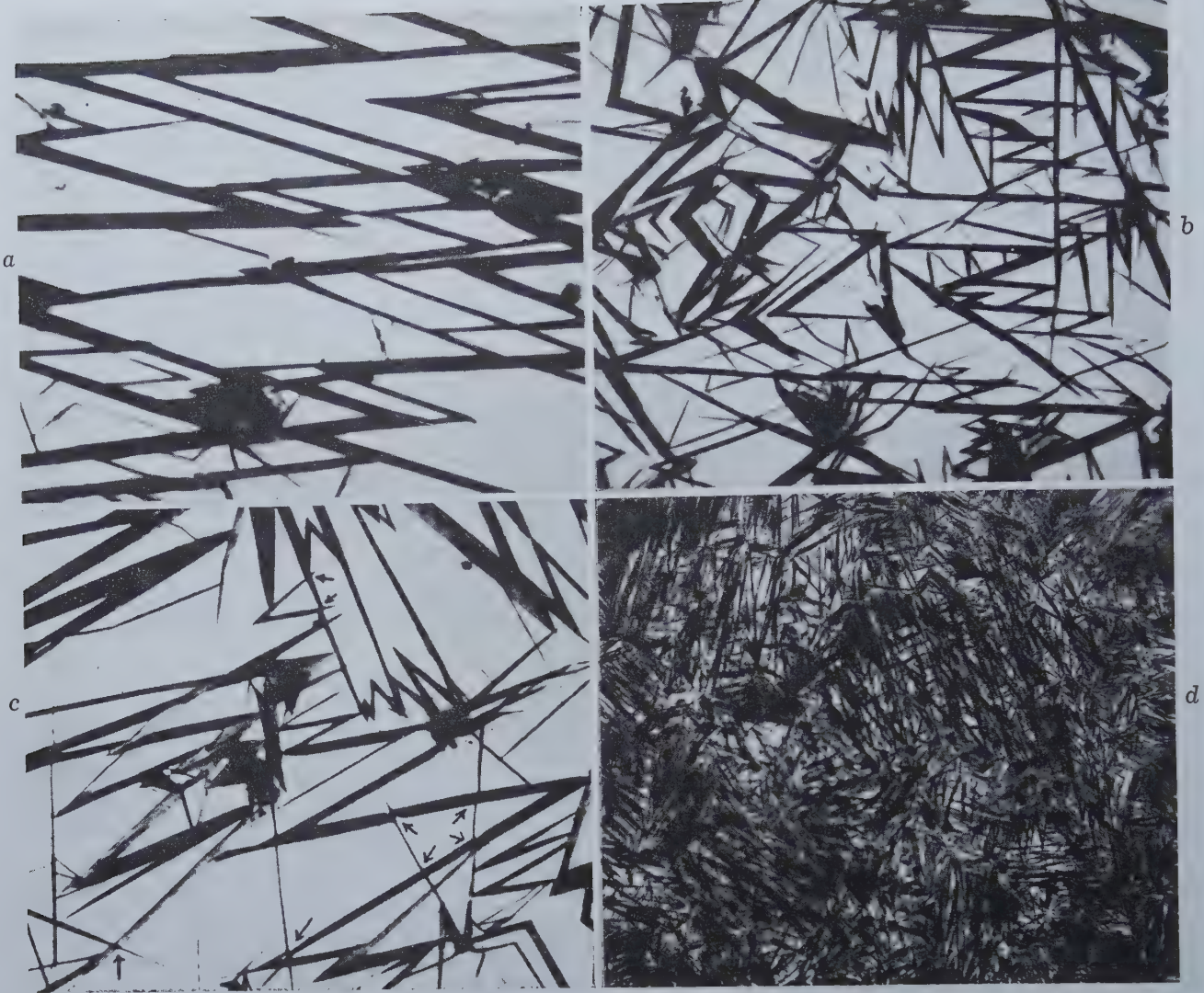


Fig. 4—Microstructures of 1 pct C, 20 pct Ni steel after heat treatment according to caption of fig. 3.

(a) Cooled to 77°K (-196°C). X1000. (b) Cooled to 4°K (-269°C). X1000. (c) Cooled to 77°K (-196°C). Arrows indicate where martensitic plates cross each other. X1500. (d) Cooled to 4°K (-269°C) and pulled to fracture. X200. All etched with 4 pct nital containing 1 pct zephiran chloride.

References

- ¹ Symposium on Thermodynamics in Physical Metallurgy. A.S.M., Cleveland, Ohio. (Oct. 1949).
- ² M. Cohen, E. S. Machlin and V. G. Paranjpe: Thermodynamics of the Martensitic Transformation. Thermodynamics in Physical Metallurgy. *Trans. A.S.M.* (1950) **42A**, 242.
- ³ J. C. Fisher: Eutectoid Decompositions. Thermodynamics in Physical Metallurgy. *Trans. A.S.M.* (1950) **42A**, 201.
- ⁴ J. C. Fisher: A.S.M. Seminar on Thermodynamics in Physical Metallurgy. *Metal Prog.* (Dec. 1949) 816.
- ⁵ J. C. Fisher, J. H. Hollomon and D. Turnbull: Kinetics of the Austenite-Martensite Transformation. *Trans. AIME*, **185**, 691; *Jnl. Met.* (Oct. 1949) TP 2674E.
- ⁶ F. S. Buffington, I. D. Bakalar and M. Cohen: Self-Diffusion in Iron. Sylvania Conf. on The Physics of Sintering, Aug. 1949. To be published by National Research Council.
- ⁷ E. Birchenall and R. F. Mehl: Self-Diffusion in Alpha and Gamma Iron. *Trans. AIME*, **188**, 144; *Jnl. Met.* (Jan. 1950) TP 2752E.
- ⁸ F. Förster and E. Scheil: Untersuchung des Zeitlichen Ablaufes von Umklappvorgängen in Metallen. *Ztsch. f. Metallkunde*. (1940) **32**, 165.
- ⁹ M. Cohen: Retained Austenite. *Trans. A.S.M.* (1949) **41**, 35.
- ¹⁰ G. V. Kurdjumov and O. P. Maksimova: Kinetics of the Transformation of Austenite to Martensite at Low Temperatures. *Doklady Adademi Nauk, SSSR*. (1948) **61** (No. 1), 83.
- ¹¹ B. L. Averbach, S. A. Kulin and M. Cohen: The Effect of Plastic Deformation on Solid Reactions, Part II—The Effect of Applied Stress and Strain on the Martensite Reaction. The Cold Working of Metals. A.S.M. (1949).
- ¹² R. T. Howard and M. Cohen: Quantitative Metallography by Point-Counting and Lineal Analysis. *Trans. AIME* (1947) **172**, 413; *Met. Tech.* (Aug. 1947) TP 2215C.
- ¹³ P. Gordon and M. Cohen: The Transformation of Retained Austenite in High Speed Steel at Subatmospheric Temperatures. *Trans. A.S.M.* (1942) **30**, 569.
- ¹⁴ S. G. Fletcher, B. L. Averbach and M. Cohen: The Dimensional Stability of Steel. Part II—Further Experiments on Subatmospheric Transformations. *Trans. A.S.M.* (1948) **40**, 703.
- ¹⁵ R. T. Howard and M. Cohen: Austenite Decomposition Above and Within the Martensite Range. *Trans. AIME* (1948) **176**, 384; *Met. Tech.* (Sept. 1947) TP 2283C.
- ¹⁶ W. J. Harris and M. Cohen: Stabilization of the Austenite-Martensite Transformation. *Trans. AIME* (1949) **180**, 447; *Met. Tech.* (Sept. 1948) TP 2446E.

The Supercooling of Aggregates of Small Metal Particles

by David Turnbull

Aggregates of small metal droplets of mercury, bismuth, gallium, and lead have been supercooled to a much greater extent than have large continuous liquid masses of the same metals. These results are interpreted on the basis that breaking a large liquid mass into small droplets isolates inclusions that usually catalyze nucleation in a small fraction of the droplets so that most must nucleate homogeneously.

RECENTLY it has been shown that aggregates of small liquid droplets of tin,¹ mercury² or gallium² kept from intercommunicating by suitable films do not solidify at an appreciable rate unless the supercooling is very much greater than that usually necessary to cause a large continuous mass of the metal to solidify. For example oxide-coated tin droplets¹ (1 to 10 micron diam) must be supercooled 100° to 110°C before their rate of solidification becomes rapid, although large continuous masses of liquid tin usually begin to solidify when supercooled 30° or less.³

These experiments have been interpreted² on the hypothesis that nucleation of crystals in large continuous metal samples is almost always catalyzed by accidental inclusions. Therefore, if the metal is dispersed into a number of isolated droplets large in comparison with the number of inclusions, most of the droplets should not crystallize until a temperature sufficiently below the thermodynamic melt-

ing point, T_m , has been reached to permit an appreciable rate of homogeneous (noncatalyzed) nucleation. In general this temperature is very much less than the temperature at which the rate of heterogeneous (catalyzed) nucleation is appreciable. If this interpretation is correct then investigation of the kinetics of crystallization of small droplet aggregates should be one of the most fruitful methods of obtaining information about the homogeneous formation of crystal nuclei in liquids.

In this paper the results obtained on gallium and mercury are reported more fully. In addition, results on the supercooling of aggregates of liquid bismuth and lead droplets are included.

Experimental Procedure

Some care must be exercised in the choice of a barrier to prevent the liquid droplets from coalescing lest the barrier itself catalyze the formation of crystal nuclei. From this standpoint, the most desirable barrier is vacuum or inert gas, but, because of the difficulty of experimental arrangement, solid compounds and adsorbed films have been selected. There are two guiding principles in the selection of compounds as barriers in addition to the requirement that they prevent coalescence of liquid droplets. First, the compound should be almost insoluble in the liquid metal and second, its lattice structure should be quite unlike that of the forming metal crystal. Even so, there is no *a priori* assurance that the solid compound film will not catalyze to some extent the formation of metal crystal nuclei. An adsorbed protective monolayer is less likely to be catalytic than a crystal compound film, but it is not often possible to find a monolayer that is stable under the experimental conditions. Also, it is desirable, though not generally essential, that the aggregate of droplets be prepared by breaking up the massive metal rather than from a powdered compound of the metal.

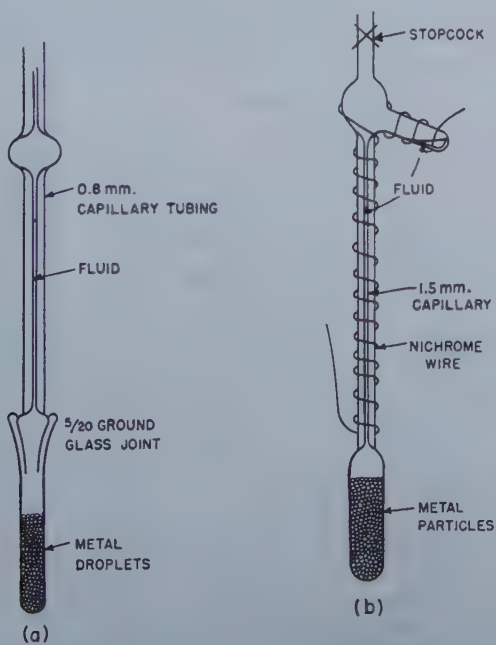


Fig. 1—Low (a) and high (b) temperature dilatometers.

DAVID TURNBULL, Associate Member AIME, is associated with the Research Laboratory, General Electric Co., Schenectady, N. Y.

AIME Chicago Meeting, October 1950.

TP 2910 E. Discussion (2 copies) may be sent to Transactions AIME before Dec. 15, 1950. Manuscript received Feb. 16, 1950; revision received June 15, 1950.

The sources and purity of the metals used in this investigation are given in table I. Aggregates of gallium or mercury droplets were prepared by manually shaking the molten metal in the appropriate solution. To form the droplet aggregates coated with sodium oleate, the solution used was 95 pct ethyl alcohol saturated with sodium oleate. A solution of $\frac{1}{2}$ g of iodine per 100 cc of 95 pct ethyl alcohol served to disperse mercury droplets and coat them with an iodide film. The resulting droplet sizes are given in table I.

A film of bismuth oxide was formed on bismuth particles by heating the powder in air for 1 hr at 125°C.

Lead "chloride" or "sulphate" coatings were formed by treating the powder with one half normal solutions of the corresponding acids. The particles were then filtered, washed with alcohol, and heated in an oven at 125°C to drive off moisture. Lead iodide coatings were formed similarly excepting that an alcoholic solution of iodine and acetic acid was used instead of the aqueous acid solution. It seems likely that the lead surface coatings were basic salts rather than the normal salts.

Dilatometry, Low Temperature

A typical dilatometer employed in the low-temperature work on gallium and mercury is shown in fig. 1a. The dilatometer fluid used was 95 pct ethyl alcohol. The liquid level in the capillary was read to ± 0.02 cm by means of a cathetometer. The dimensions of the dilatometer and size of the samples were chosen so that the liquid level changed 3 to 6 cm upon solidification and so that readings could be taken from temperatures well above the melting point to well below the solidification temperature.

Temperatures were determined from measurements with a G.E. thermocouple potentiometer of the potentials developed by a copper-constantan thermocouple. Above dry-ice temperature, a constant temperature bath containing trichlorethylene and controlled by a bimetallic thermoregulator was used. The coolant, acetone at dry-ice temperature, was pumped through a copper coil immersed in the bath. For below dry-ice temperature, the bath arrangement that proved most satisfactory consisted

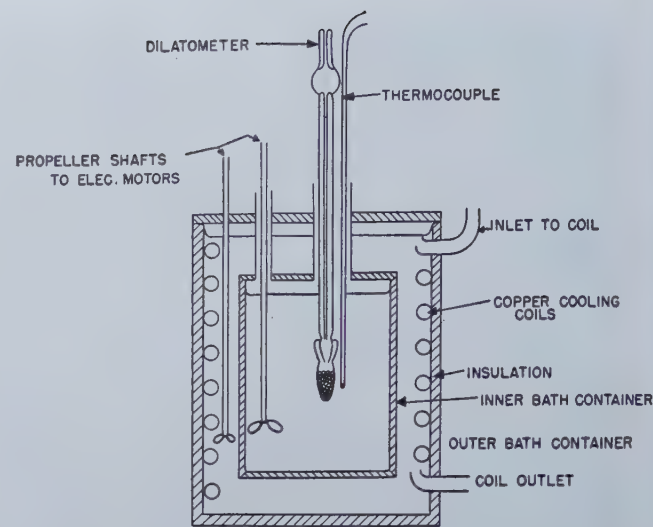


Fig. 2—Bath used in low temperature experiments.

of a well insulated can containing freon 11 entirely surrounded (except for outlets) by a controlled bath of the same fluid, as shown in fig. 2. The external bath was cooled by liquid nitrogen circulated in copper coils.

Dilatometer readings were taken as a function of temperature through a cooling-heating cycle that began and terminated above the thermodynamic melting point and that extended to the temperatures of complete solidification. In cooling, the bath was held at a given temperature until the dilatometer reading remained constant for an appreciable period before the temperature was again lowered. After solidification, the sample was warmed at a constant rate of approximately 1°C per min. With this heating rate the temperature of the sample differed from that of the bath by only a fraction of a degree excepting while melting took place.

High Temperature

Fig. 1b is a sketch of the high-temperature dilatometer. Para (mp 212°C, bp 376°C) or meta (mp 86°C, bp 363°C) diphenyl-benzene proved satisfactory as dilatometer fluids for the lead and bismuth

Table I. Source, Purity, and Droplet Size of Metals Investigated

Metal	Source	Purity, Wt Pct	Initial Form	Protective Film	Particle Size Range, (Micron)	Diam of Particle Having Mean Volume, (Micron)
Mercury	Triple distilled	99.9999+	Liquid	Adsorbed sodium oleate	50-500	200
				Mercuric iodide	2-100	50
Gallium	Eagle-Picher	99.94	As cast	Sodium oleate adsorbed on gallium oxide	50-300	200
Bismuth	Eimer & Amend	99.999	Powder	Bismuth, oxide	4-12	10
Lead	Eimer & Amend	99.95	Powder	Lead { iodide, chloride, or sulphate}	2-20	17

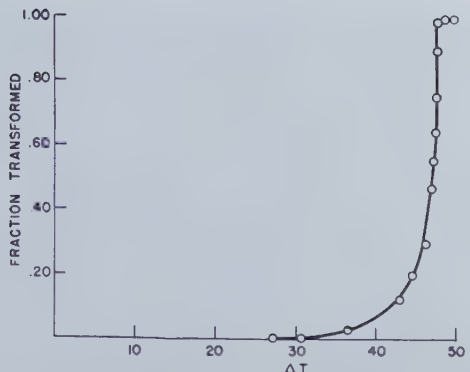


Fig. 3—Fraction of iodide-coated mercury particles solidified as a function of amount of supercooling ($\Delta T.$).

respectively. During the measurements, $1\frac{1}{2}$ atm pressure of nitrogen or helium was maintained in the dilatometer in order to prevent cavitation. An electrically heated, 32 mil nichrome wire wound around the fluid reservoir and capillary caused the diphenyl-benzene to remain liquid.

Temperatures were obtained by a Woods metal bath heated in a vertical nichrome wound furnace, and a chromel-alumel couple was used in temperature measurement. Dilatometer readings were taken as a function of temperature in a cooling-heating cycle during which the temperature was changed continuously (1° to $\frac{1}{2}^\circ$ C per min) both in cooling and heating. Close agreement between bath and sample temperatures, excepting during melting and rapid solidification, was confirmed by the fact that cooling and heating curves coincided within the experimental error when the metal was completely melted or solid.

Thermal Method

For measuring the temperature at which the major part of the transformation took place, the thermal method proved more convenient, though as applied, less accurate than the dilatometric method. One junction of a copper-constantan thermocouple was placed in a thermocouple well embedded in the sample that was contained in an evacuated pyrex tube, and the other was placed in a well in the

Woods metal bath. The ends of the copper wires were connected to a G.E. portable high sensitivity (10^{-9} amp/mm) galvanometer that thus registered deflections proportional to the temperature difference between the sample and the bath.

Galvanometer readings were taken as a function of temperature during a heating-cooling cycle that was scheduled in the same way as in the dilatometric experiments.

Results, Mercury

Fig. 3 shows the percent of iodide-coated mercury particles transformed, calculated from dilatometric data, as a function of the supercooling, $\Delta T.$. Appre-
ciable solidification begins at $\Delta T. = 43$ but most takes place at $\Delta T. = 46$ (-85° C). These results were reproducible for a given sample and for others prepared in the same way.

Quantitative measurements of the isothermal rate of solidification are being made now. However qualitative experiments have indicated that the fre-

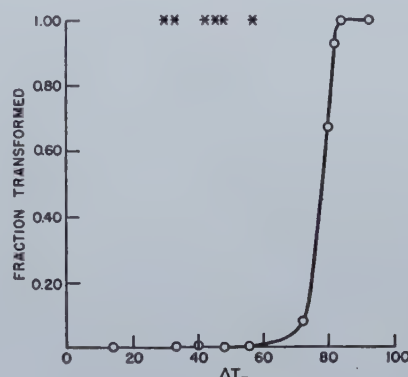


Fig. 5—Fraction of small gallium particles solidified as function of supercooling ($\Delta T.$) and (*) supercooling of 1-g continuous samples.

quency of solidification of iodide-coated droplets changes by a factor of at least 10 per 1° C in the range -82° to -85° C. For example, in one experiment no transformation was perceptible in a sample for a period of 1 hr at -82° , but it solidified completely within 1 min at -85° .

Fig. 4 shows dilatometer reading as a function of temperature during a cooling-heating cycle for an aggregate of droplets dispersed in alcoholic sodium oleate. Most of the transformation takes place at $\Delta T. = 39$, but it is interesting that the rate at $\Delta T. = 33$ is much more rapid upon quenching from $\Delta T. = 39$ than upon cooling from the melting temperature. In view of the results with iodide-coated particles, these phenomena cannot be accounted for in terms of slow growth of mercury crystals at $\Delta T. = 39$. Rather, since the droplets often agglomerated upon melting, a reaction in which the film becomes no longer protective (possibly due to precipitation or discharge of adsorbed ions) is indicated. If the film no longer prevents welding at $\Delta T. = 39$, the sample could be completely solidified by nuclei formed heterogeneously.

Gallium

Fig. 5 shows the fraction of an aggregate of gallium droplets solidified as a function of $\Delta T.$. Transformation begins at $\Delta T. = 70$ (-40° C) and is completed at $\Delta T. = 82^\circ$ (-52°).

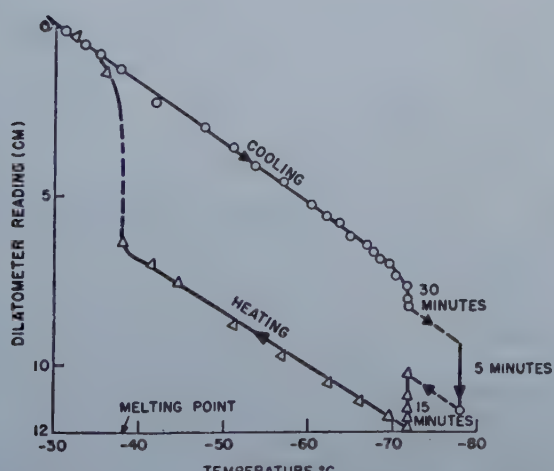


Fig. 4—Dilatometer readings vs. temperature on aggregate of mercury particles coated with sodium oleate.

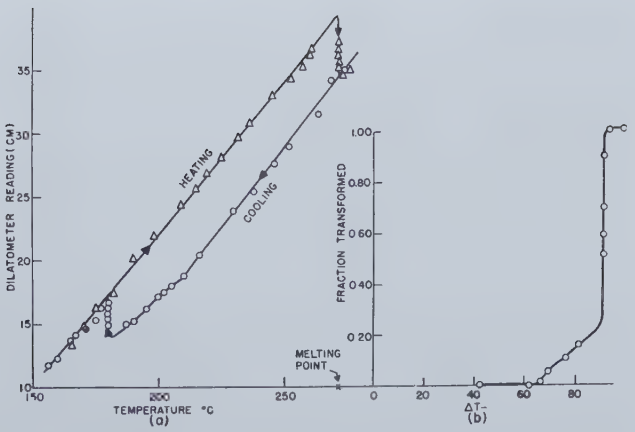


Fig. 6—(a) Dilatometer reading vs. temperature in cooling heating cycle of oxide-coated bismuth powder (b) fraction of bismuth solidified as a function of supercooling (ΔT_-).

Solidification of some continuous 1-g samples of gallium sealed in evacuated quartz tubes was followed by the thermal method. When the maximum temperature, T_m , attained in the liquid state after melting was only a few degrees above the melting point, T_o , ΔT_- was a function of thermal history (i.e., $\Delta T_- \propto T_m - T_o = \Delta T_+$). However, ΔT_- was independent of ΔT_+ for values of the latter ranging between 50° and 1000°C. Values of ΔT_- corresponding to solidification of various 1-g samples for which $\Delta T_+ = 50$ are indicated in fig. 5 by asterisks. The values were characteristic of each sample and ranged between 30° and 56°. The supercooling of these specimens was very sensitive to mechanical vibrations. Vigorous manual shaking sometimes decreased the characteristic ΔT_- by about 15°.

Bismuth

Dilatometer readings obtained in an experiment on the solidification of bismuth powder are plotted against temperature in fig. 6a. The fraction of the sample solidified, calculated from these data, is shown as a function of the supercooling in fig. 6b. Although there is perceptible solidification at ΔT_- as small as 65°, the major part of the sample (more than 70 pct) transforms at $\Delta T_- = 90$.

For the experiment just described $\Delta T_+ = 9^\circ$. In a second experiment for which $\Delta T_+ = 2.5$ the major part of the sample again solidified at $\Delta T_- = 90^\circ$ and observations⁴ confirmed this for values of ΔT_+ as large as 100°.

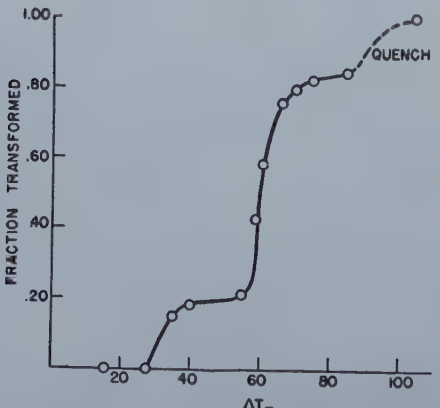


Fig. 7—Fraction of "iodide" coated lead particles solidified as function of supercooling.

These experiments show that the marked thermal history dependence of solidification temperature observed by Webster⁵ on large continuous bismuth samples is entirely absent in small particles that solidify at the maximum supercooling. From this result it may be concluded that the thermal history phenomenon in solidification generally is not inherent in the properties of the substance itself but is connected with extraneous influences.

It was established that the temperature coefficient of the solidification frequency of bismuth droplets is also very large. For example one sample of bismuth droplets was cooled slowly to $\Delta T_- = 86^\circ$ then heated slowly to $\Delta T_- = 46^\circ$ and held there for 12 hr. Upon subsequent slow cooling no perceptible solidification took place until $\Delta T_- = 90^\circ$.

Lead

Fig. 7 shows the fraction of "iodide" coated lead particles solidified as a function of ΔT_- as calculated from dilatometric data. Essentially the same curve was obtained from two experiments. The major part of the sample crystallized in the range $\Delta T_- = 55^\circ$

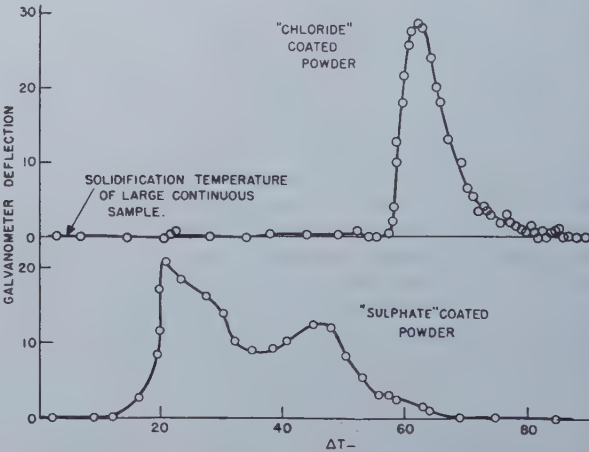


Fig. 8—Supercooling (ΔT_-) of lead particles with different surface coatings.

to 65° but a small significant fraction does not crystallize until the sample is quenched to $\Delta T_- > 80^\circ$.

The course of solidification of chloride-coated lead powder was followed by the thermal method. In fig. 8 the galvanometer deflection (proportional to amount of solidification) is plotted against ΔT_- . The major fraction of the sample solidified in the same range as the iodide-coated powder in the dilatometric experiments (i.e. $\Delta T_- = 55^\circ$ to 65°). A small fraction appears to solidify in the range $\Delta T_- = 80^\circ$ to 90° although the evidence is less definite than in the dilatometric experiments. This curve was very reproducible and independent of ΔT_+ values ranging from 15° to 55° .

Although most of the particles crystallized around $\Delta T_- = 60$ in the two sets of experiments, the temperature of appreciable homogeneous nucleation is believed to be in excess of 80° supercooling because of the dilatometric evidence. If this be so, then the crystallization that took place at $\Delta T_- = 60^\circ$ must have been catalyzed either by some heterogeneities within the particle or by surface films. In order to impart the property to the films of preventing the particles from coalescing when liquid, it was necessary to heat the aggregates at 100° C in air before

the experiments. Therefore it seems reasonable to suppose that the films consisted of basic lead halide.

Definite evidence of nucleation catalysis by surface films was found in the thermal experiments on "sulphate"-coated lead powder. Fig. 8 shows galvanometer deflections as a function of supercooling in one of these experiments. Two definite peaks were observed and their presence and location checked in several experiments. One of them centers at $\Delta T_c = 20^\circ$ and the other at $\Delta T_c = 47^\circ$ and both are well above the temperature range at which the major part of the "chloride" and "iodide" coated samples crystallized. Essentially the same results were obtained for $\Delta T_c = 15^\circ$ or 55° .

Since the particle size distribution was identical in the several sets of experiments, the most reasonable interpretation of the results seems to be that the products of a reaction between lead and the sulphate coating (possibly PbO or Pb₂O and PbS) catalyze the formation of lead crystals. Apparently nucleation was catalyzed by two major substances in the film. The most effective of these could have been in contact with the metal in only a fraction of the particles else the entire sample would have crystallized around $\Delta T_c = 20^\circ$.

These results are reminiscent of those obtained by Wang and Smith⁶ on the solidification of tin particles in an aluminum matrix and suggest that the solidification behavior of an aggregate of droplets may be described conveniently in terms of a number distribution curve with respect to solidification temperature. It is evident that the particles do not distribute themselves uniformly with respect to solidification temperature but tend to fall within certain discrete narrow bands of temperature each of which is perhaps associated with the catalytic action of a particular impurity.⁷

Discussion of Results

Table II summarizes the data on supercooling that were obtained in this investigation. In this table, the maximum supercooling observed on small particles is compared with the maximum reported on large continuous samples by various investigators. Generally, the amount of supercooling of small particles is very much greater than that of the large continuous samples. However, it is an important fact that in gallium, which has the most complex crystal structure of the metals studied, the disparity is not so great (76° to 55°).

Table II. Summary of Supercooling Data

Metal	Protective Film on Small Particles	Diam of Particles Having Mean Volume, (Micron)	Maximum Supercooling °C(ΔT_c)		$\Delta T_c/T_0$
			Small Particles	Large Continuous Samples	
Mercury	Sodium oleate	400	39	4*	0.20
	Mercuric iodide	50	46		
Gallium	Sodium oleate + gallium oxide	200	76	55	0.25
Bismuth	Bismuth oxide	10	90	30*	0.165
Lead	Lead iodide + Lead oxide	12	80	3*	0.13

* Data from reference 3.

There is good evidence that the rate determining step in the solidification of small particles is not the growth but the nucleation of crystals. For example, in continuous 1-g samples of gallium supercooled to $\Delta T_c = 35^\circ$ to 55° , the crystal growth rate after the nucleation period was too rapid to measure and was certainly greater than 1 cm per sec. It might be expected that metal crystals having more simple structures than gallium would grow into their melts with even greater rapidity at comparable supercooling.

Also, it is an important fact that mild mechanical vibrations that have such a marked effect in promoting the crystallization of the larger continuous gallium samples have no observable effect upon the course of small particle solidification.

Summary

Aggregates of small particles of liquid mercury, gallium, bismuth, and lead were supercooled to temperatures that are respectively 0.80, 0.75, 0.84, and 0.87 of the absolute melting temperature before the rate of crystal nucleation became appreciable. This amount of supercooling is much greater than usually observed on large continuous samples.

The rate determining step in the solidification of small particle aggregates is not the rate of crystal growth but the rate of crystal nucleation.

These results can be interpreted satisfactorily if it is supposed that the effective crystal nucleation catalysts usually present in large continuous specimens are isolated on a small fraction of the resulting particles when the specimen is broken up.

There is no thermal history effect upon the solidification behavior of the major fraction of liquid bismuth small particle aggregates.

It has been demonstrated that lead sulphate films are more effective in catalyzing the formation of lead crystals than are the lead halide films. Two well-defined temperature ranges of solidification were found in the sulphate-coated lead powder. It is believed that each of these ranges is associated with the catalytic action of a specific product of the reaction between liquid lead and lead sulphate.

Although the solidification of large continuous gallium samples is promoted by mild mechanical vibrations, these have no observed effect upon the solidification behavior of small particle aggregates.

Acknowledgment

The author thanks H. C. Rogers and R. E. Cech for designing, in large part, the low-temperature baths used.

References

- 1 B. Vonnegut: Variation with Temperature of the Nucleation Rate of Supercooled Tin and Water Drops. *Jnl. Colloid Science*. (1948) **3**, 563.
- 2 D. Turnbull: The Subcooling of Liquid Metals. *Jnl. Applied Phys.* (1949) **20**, 817.
- 3 V. Danilov and W. Neumark: Über das Vorhandensein von Kristallisations-Keimen Oberhalb des Schmelzpunktes und die Struktur der Flüssigkeiten. *Physik. Zeits. Sowjet Union*. (1937) **12**, 313.
- 4 D. Turnbull and R. E. Cech: Microscopic Observations of the Solidification of Small Metal Particles. To be published, *Jnl. Applied Phys.* (1950).
- 5 W. L. Webster: Phenomena Occurring in the Melting of Metals. *Proc. Roy. Soc. (London)* (1933) **140A**, 653.
- 6 C. Wang and C. S. Smith: Undercooling of Minor Liquid Phases in Binary Alloys. *Trans. AIME*, **188**, 136; *Jnl. Met.* (Jan. 1950) TP 2756E.
- 7 D. Turnbull: Principles of Solidification. A.S.M. Seminar on Thermodynamics. Cleveland (1949).

The Ductility of Cast Molybdenum

by R. B. Fischer and J. H. Jackson

The ductility of a cast ingot of carbon-deoxidized molybdenum was studied by means of a series of bend tests. The ductility of the cast molybdenum was shown to be a highly directional property. Heat treatment at 2100°F improved the ductility. The cast texture, cleavage planes, and microstructure of cast molybdenum are discussed.

VERY little is known about the properties of relatively pure refractory metals in the cast state since these metals are customarily made by powder-metallurgy methods. Recently, the development of the vacuum arc-melting furnace has made possible the study of large, sound ingots of cast molybdenum.

The ductility of molybdenum, at room temperature, may vary considerably. Often the brittle state depreciates the utility of molybdenum, even for the material prepared by powder-metallurgy techniques. At the outset of this program, it was felt that if the causes of brittleness were to be determined it might be possible to reduce the difficulties met in the working of molybdenum. Also, the problem of producing strong, fusion weldments of molybdenum might be solved.

The conditions required to produce ductile molybdenum by the powder-metallurgy technique are

R. B. FISCHER is Assistant Supervisor, and J. H. JACKSON, Member AIME, is Supervisor, Battelle Memorial Institute, Columbus, Ohio.

AIME Chicago Meeting, October 1950.

TP 2896 E. Discussion (2 copies) may be sent to Transactions AIME by Dec. 15, 1950. Manuscript received March 29, 1950; revision received June 5, 1950.

This research was supported by ONR (Contract No. N9onr 82100, Task Order No. N9onr 82101, Project NR031-339.

reasonably well known. A fibrous or elongated-grain structure has good ductility although this property is probably directional. The equiaxed structure obtained in fully recrystallized molybdenum has been considered to be brittle. The reasons for this behavior of molybdenum have not been established.

The preparation of cast molybdenum ingots by the vacuum-arc method was described by Parke and Ham.¹ By this method, ingots weighing up to 250 lb were produced.² Parke and Ham¹ found that molybdenum ingots containing more than approximately 0.0025 pct oxygen could not be hot forged. On the other hand, they found that fully deoxidized cast molybdenum, containing up to 0.06 pct carbon, could be hot forged. However, the as-cast ingots containing either carbon or oxygen were brittle at room temperature. Parke and Ham,¹ Woodside,³ and Zapffe, Landgraf, and Worden⁴ noted the intergranular precipitation of oxide or carbide in cast molybdenum.

This study—part of an extensive program on molybdenum—had the following objectives: (1) To investigate the causes for the brittleness of cast molybdenum at room temperature, (2) to investigate the means for improving the ductility of cast molybdenum at room temperature, and (3) to add to the knowledge of cast molybdenum and of cast metals in general.



Fig. 1—Grain patterns in transverse sections of cast molybdenum, ingot No. 447.

Note "arc centers" and porosity rings. Etched by Coons' method.⁵ XI. Area reduced approximately one third in reproduction.

The cast molybdenum ingot used in this research was made by the vacuum-arc melting process.* This ingot, No. 447, was about 4 in. in diam and 13 in. in length. It weighed 56 lb.

* The ingot was obtained from the Climax Molybdenum Co.

The surface defects of the ingot had been removed by machining. The cutting tool had alternately



Fig. 2—Same specimens as shown in fig. 1 after fracture by impact blow.

Note radial fracture. XI. Area reduced approximately one third in reproduction.

glazed and cut the stock at the ends of the ingot so that a rough macrostructure was revealed. This indicated the effect of grain orientation on machinability.

The ingot was reported by the supplier to contain 0.034 pct carbon. A check analysis of 0.032 pct carbon was obtained at Battelle. Qualitative estimations of impurities in the ingot were determined spectroscopically. The analyses for Si, Fe, Mn, and Sn, were within the limits of 0.001 to 0.01 pct; less than 0.001 pct of Cu, Ca, Cr, and Mg were detected.

The density of the 56-lb ingot was measured by the water displacement method and found to be 10.14 g per cm³ at about 78°F. The density of molybdenum at room temperature is usually considered to be 10.2 g per cm³.

Type of Fracture

The initial problem was to determine the type of fracture that occurred in the cast molybdenum ingot at room temperature. Parke and Ham¹ inferred



Fig. 3—Fractured surfaces of specimens shown in fig. 2.

XI. Area reduced approximately one fifth in reproduction.

that intercrystalline fractures occurred in cast molybdenum. Zapffe, Landgraf, and Worden⁴ reported that both intergranular and transgranular fractures occurred in cast molybdenum at room temperature.

Two slabs, $\frac{1}{2}$ in. in thickness, were sectioned from the top and bottom of the ingot. The faces of these slabs were electropolished and etched by Coons' method⁵ to bring out the grain structure shown in fig. 1. The pattern of the grain indicated that the arc had been off-center part of the time during the melting operation. A ring of small gas holes was concentric about the "arc center."

The section in fig. 1a was fractured by an impact blow on the edge of the polished face. The bottom section was fractured by a blow on the machined face. These fractures are shown in figs. 2 and 3. The respective photographs of fig. 2 and fig. 1 can be matched to show that the fractures were largely intercrystalline. The fractures converged on the "arc center" of the ingot sections. The observations indicated that the grain boundaries of the cast molybdenum were considerably weaker than its cleavage planes under impact loading. The porosity ring did not form a line of weakness in the top section of the ingot.

The grain pattern of the ingot was such that small, narrow splinters of grains could be obtained from the fractured surfaces. It was possible to bend the very ends of the splinters to form minute hooks. This indicated that the individual grains were ductile.

Grain and Crystal Orientation

The grains of the ingot were found to be elongated with irregular, cross-sectional areas of less than about $\frac{1}{8}$ sq in. and up to about 2 in. in length. The longer grains were shaped like boomerangs. Typical grain patterns are sketched in fig. 4. Fig. 4a indicates that the isotherm pattern was somewhat regular during the solidification period. Fig. 4b shows a condition in the same ingot in which the isotherm pattern probably changed rapidly at some time during solidification. The result was that the longitudinal axes of some adjacent grains formed large angles with one another as shown in fig. 4b. Evidently wide ranges of grain patterns are possible in ingots prepared by the vacuum-arc process.

The cleavage facets, where transgranular fractures had occurred, were examined by use of an X-ray spectrometer. These facets were found to be the cube faces or (100) planes of the crystals.

The cleavage facets were oriented so that the major axis of the grains was approximately either perpendicular or parallel to the facets. This means that molybdenum, like other cubic metals (see reference 6) has a casting texture in which the [100] direction is normal to the isotherms during solidification.

Tsien and Chow⁷ reported that slip occurs in molybdenum along the (112) planes at 20° and 300°C , and along the (100) planes at 1000°C . The slip direction was always [111].⁷

Microscopical Examination

The microscopical examination of various specimens from ingot No. 447 revealed the presence of inclusions at the grain boundaries and also within the grains. These inclusions have been identified tentatively as a molybdenum carbide. Fig. 5 shows the inclusions and gas porosity within the grain. Figs. 6 and 7 show the inclusions at the grain bound-

Table I. Bend Test Data for As-cast Molybdenum at Room Temperature.

Specimens from Climax Ingot No. 447

Specimen No.	Orientation of Major Axes of Grains	Platen Speed, In. per Min	Breaking Load, Lb	Angle of Bend, Deg
15*	Transverse, vertical†		94	0
19	Transverse, horizontal	0.005	434	0
20	Transverse, horizontal	0.005	449	0
Average			442	0
41	Longitudinal	0.0012	735	22.5
43	Longitudinal	0.0014	898	42.0
44	Longitudinal	0.0014	742	19.0
Average			792	28.5
16	Longitudinal	0.005	964	36.5
17	Longitudinal	0.005	921	27.5
18	Longitudinal	0.005	754	11.0
56	Longitudinal	0.005	858	21.5
Average			924	24.0
45	Longitudinal	0.02	830	11.5
51	Longitudinal	0.02	890	13.5
59	Longitudinal	0.02	1,124	29.0
Average			948	18.0

* Accidentally given an impact loading.

† Terminology indicates major axes of grains were transverse to specimen axis and parallel to direction of applied load.

‡ Specimen size, 0.15 in. by 0.25 in. by approximately 1 in.

daries. The shapes of the inclusions in three dimensions are probably needle-like. The inclusions were surprisingly well distributed throughout the specimens. The width of the inclusions was about 0.0006 in. maximum. The hardness of the inclusions appeared greater than that of the matrix because scratches in the matrix caused by polishing compounds were often interrupted by the inclusions which stood in relief. A Knoop hardness number of 230 (100-g load) was obtained on one inclusion, although the indentation was not confined to the inclusion alone. The Knoop hardness number of the matrix was 170 (100-g load).

Transverse Bend Tests

The transverse bend test was selected as a means of evaluating the ductility of cast molybdenum because: (1) The bend test is commonly used to evaluate the strength and ductility of brittle materials. (2) Small specimens of cast molybdenum could be tested. Thus, greater utility could be made of the available ingot. (3) Specimens could be selected to have a rather definite grain orientation. (4) Speci-



Fig. 4—Typical grain patterns of longitudinal sections of cast molybdenum ingots.



Fig. 5—Micrograph of carbide inclusions and gas porosity within a grain of cast Mo. (upper left).

Red rouge-chromic acid polish followed by electrolytic etch. X1500. Area reduced approximately one third in reproduction.

Fig. 6—Micrograph of carbide inclusion at a grain boundary of cast Mo. (upper right).

Red rouge-chromic acid polish followed by electrolytic etch. X4500. Area reduced approximately one third in reproduction.

Fig. 7—Micrograph of carbide inclusion at a grain boundary in cast Mo. (lower left).

Etched by Coons' method.⁵ X1500. Area reduced approximately one third in reproduction.

mens could be machined easily in the form of rectangular beams.

It was determined that a satisfactory size for the specimens was 0.15 in. depth by 0.25 in. width by about 1.0 in. length. The specimens were machined from slabs cut from the ingot. Some cracks were noted in these slabs. These cracks were along grain boundaries and were probably the result of shrinkage of the ingot during cooling. The slabs were etched to reveal their grain orientation, as shown in fig. 4. In this way, specimens with definite grain orientation could be prepared. A quadrant system was established so that the original position of each specimen in the ingot could be identified. The specimens were cut from the slabs and ground to the proper cross-section with a Norton 32A46K5VBE

wheel. The grind marks ran longitudinally so that notch effects were minimized.

The specimens were selected with the major grain axes either approximately parallel or approximately transverse to the longitudinal axis of the specimen. It was difficult to prepare the "transverse-grain" specimens because intergranular fractures occurred frequently during the grinding process. The "longitudinal-grain" specimens were machined without difficulty and consisted of about 5 grains. These observations showed that the grain boundaries were particularly weak when exposed to tensile stresses normal to the boundaries.

The specimens were loaded at the center by means of a load applicator of $\frac{1}{8}$ -in. diam. The distance between supports of the specimen was $\frac{5}{8}$ in.

Table II. Bend Test Data for Heat-treated Cast Molybdenum at Room Temperature.
Specimens from Climax Ingots No. 447

Specimen No.	Treatment	Orientation of Major Axes of Grains	Breaking Load, Lb*	Angle of Bend, Deg
28	Packed in titanium chips and heated in vacuum (1 micron pressure) at 2100°F for 2 hr	Transverse, horizontal	640	7.0†
29		Transverse, horizontal	433	1.5†
53		Longitudinal	1,016	37.0
54		Longitudinal	858	27.0
48	Packed in titanium hydride and heated in purified hydrogen at 2100°F for 20 hr‡	Transverse, horizontal	606	5.0†
31		Longitudinal	842	23.0
52		Longitudinal	922	29.0
57	Packed in molybdenum chips and heated in nitrogen at 2100°F for 2 hr	Longitudinal	771	21.0
58		Longitudinal	1,002	53.0

* Platen speed was 0.005 in. per min. Specimen size was 0.15 in. by 0.25 in. by approximately 1 in.

† Compare these values with those for specimens Nos. 19 and 20 in table I.

‡ Specimens were slightly warped after this treatment.

The first series of tests was conducted at room temperature. The specimens were loaded at a uniform speed until fracture occurred. The angle of bend for the specimens was measured to an accuracy of $\pm 0.5^\circ$. The results are given in table I.

Table III. Bend Test Data for Hot-rolled Cast Molybdenum at Room Temperature.

Specimens from Climax Ingot No. 447

Specimen No.	Direction of Hot Rolling	Reduction of Area, Per cent	Specimen Orientation	Breaking Load, Lb*	Angle of Bend, Deg
25A	Parallel to longitudinal axes of as-cast grains	50	Transverse to direction of rolling	930	13
25B		50		1,040	24
25C		50		1,136	33

* Platen speed was 0.005 in. per min. Specimen size was 0.15 in. by 0.25 in. by approximately 1 in.

No ductility was observed for the "transverse-grain" specimens. The "longitudinal-grain" specimens were ductile and bend angles for these specimens ranged from 11.0° to 42° . Although scatter of the data was too great to suggest a high level of significance, there appeared to be a trend for the average bend angle to decrease with increase in the rate of bending; 28° for a rate of 0.001, 24° for 0.005, and 18° for 0.02 in. per min. Specimen No. 15 was accidentally given an impact loading and the breaking load of this specimen was about one fifth that of the other "transverse-grain" specimens.

The "transverse-grain" specimens fractured intergranularly in contrast to the predominately transgranular fractures of the "longitudinal-grain" specimens.

Another series of bend tests was made on specimens machined from ingot No. 447. These specimens were heat treated to determine if the grain-boundary inclusions could be removed or altered in shape by heat treatment. The data are summarized in table II.

Specimens Nos. 28, 29, 53, and 54 were heated in a vacuum for 2 hr at 2100°F . Specimens Nos. 28 and 29, both "transverse-grain" specimens, were tested and the bend angles obtained were 7° and 1.5° , respectively. Bend angles of 0° were obtained for similar specimens in the as-cast conditions, as given in table I. Therefore, the ductility of the specimens was improved by heat treatment. No significant improvement in ductility resulting from the heat treatment was noted for the "longitudinal-grain" specimens, Nos. 53 and 54.

Similar results were obtained for specimens heat treated in purified hydrogen for 2 hr. A "transverse-grain" specimen, No. 48, had an angle of bend of 5° .

Specimens Nos. 57 and 58, both "longitudinal-grain" type, were heated in purified nitrogen for 2 hr at 2100°F . The treatment did not impair their ductility and Specimen No. 58 had a bend angle of 53° .

Examinations of the heat-treated molybdenum specimens under the microscope did not reveal why the "transverse-grain" specimens were more ductile than when in the as-cast condition. The fractures and microstructures of the specimens heat treated at 2100°F were not distinguishable from those of the as-cast material.

Additional information was obtained from bend test specimens prepared from hot-rolled sections of ingot No. 447. Four sections of the ingot were heated

to 2300°F and hot-rolled in one direction. The material was reheated to 2300°F after each pass. Attempts to roll cross-grain were not successful. The disastrous effect of tensile stresses normal to the grain boundaries was evident at high temperature. However, it was found possible to roll in a direction parallel to the long axes of the grains. From one of the rolled sections, three bend test specimens were obtained.

The bend test data for these specimens are given in table III. It seems significant that these hot-rolled specimens, when tested in what was the cross-grained direction of the original structure of the ingot, showed substantial ductilities with bend angles up to 33° and an average for the tests, about 23° . This is in quite marked contrast with about zero bends for the original material.

Summary of Results

The present study was confined to one cast molybdenum ingot which had been deoxidized by addition of carbon. The following tentative conclusions have been made: (1) During solidification, the grains of the molybdenum ingot apparently grew with a major crystallographic axis parallel to the long axis of the grain and normal to the critical isotherm. (2) The grain boundaries of the ingot were particularly weak when subjected to tensile stress normal to the boundaries. (3) The ductility of the cast molybdenum ingot was highly directional as shown by bend tests on small polycrystalline specimens. (4) Individual grains appeared ductile. (5) Heat treatment of the cast molybdenum at 2100°F in vacuum, or in purified hydrogen, improved the ductility. (6) Heat treatment of the cast molybdenum at 2100°F did not result in detectable changes in the microstructure. (7) Hot working of the cast molybdenum at 2300°F materially improved the ductility in what had been the cross-grain direction in the original ingot. (8) The cleavage plane of the cast molybdenum was the cube face.

Acknowledgment

Special acknowledgment is due the Office of Naval Research for their support of this investigation of molybdenum.

The guidance of R. M. Parke, H. W. Russell, and L. R. Jackson is appreciated. E. F. Ferrell and C. J. Williams, in particular, and other staff members of Battelle Memorial Institute were generous in their assistance in carrying out the experimental work.

References

- Robert M. Parke and John L. Ham: The Melting of Molybdenum in the Vacuum Arc. *Trans. AIME* (1947) **171**, 416-427. *Met. Tech.*, (Sept. 1946) TP 2052.
- N. L. Dueble: Private communication.
- G. C. Woodside: Deoxidation Control by Fractography. *Iron Age* (1947) **160**, No. 23, 78-79.
- C. A. Zapffe, F. K. Landgraf, and C. O. Worden: Fractographic Study of Cast Molybdenum. *Trans. AIME* (1949) **180**, 616-636; *Met. Tech.* (Aug. 1948) TP 2421.
- William C. Coons: Simple Electrolytic Polishing Procedures for Molybdenum Metallographic Specimens. *Trans. A.S.M.* (1949) **41**, 1415-1424.
- Charles S. Barrett: Structure of Metals. p. 436. 1943. McGraw-Hill Book Co.
- L. C. Tsien and Y. S. Chow: Glide of Single Crystals of Molybdenum. *Proc. Royal Society (London)* (1937) **163A**, 19-28.

The Textures of Cold-Rolled and Annealed Titanium

by Howard T. Clark, Jr.

Pole figures showing both cold-rolled and annealed (sub-transformation temperature) textures of high-purity titanium are presented. These textures are significantly different from those of other hexagonal close-packed metals in two respects: (1) for heavily cold-rolled material the basal-plane pole figures show two high intensity regions lying in the transverse direction, and (2) the annealed texture is different from the rolled texture.

No previous determinations of the deformation or recrystallization textures of titanium or of titanium-base alloys have been reported in the literature. The room-temperature structure of titanium is hexagonal close-packed with a c/a ratio less than 1.633. It would be expected, therefore, to have a rolling texture similar to that of other hexagonal close-packed metals, namely (0001) [1010]. Burgers and Jacobs¹ have shown that zirconium, a metal isomorphous with titanium in its structure and similar in many of its properties, has such a texture with a scatter of the basal plane toward the transverse direction. This scatter is in the opposite direction from that found in magnesium by Bakarian² but similar to that reported by Smigelskas and Barrett³ for beryllium. The rolling and annealing textures reported here for high-purity iodide titanium are significantly different from the textures of any other hexagonal close-packed metal.

All titanium used during this investigation was prepared by the iodide process.⁴ The annealed hardness of this material varied from 73 (material used for sample No. 2) to 97 Vickers hardness number. An estimate of the chemical composition of this grade of titanium has been reported by Finlay and Snyder.⁵ With one exception, shown in table I,

the as-deposited titanium was cast into 10 to 20 g ingots in an electric arc furnace in purified argon before being rolled to sheet.

The cast ingots were forged and ground until their cross-section was approximately rectangular, annealed 1 hr at 700°C in vacuum and cold rolled. Rolling was carried out in a two-high, 4 in. diam mill, using reductions no greater than 10 pct per pass. The direction of rolling was reversed after each pass, and, in order to avoid temperature effects, the sheet was allowed to cool after each pass. Unless the rolled sheet was sufficiently thin for X-ray penetration (about 0.004 in.), it was reduced to this thickness by pickling. Because of the possibility of introducing twinning or other deformation during grinding, no attempt was made to maintain uniform thickness of the sample during pickling by intermediate grinding or sanding operations. Those samples to be used for determining the annealed texture were recrystallized by vacuum annealing the cold-rolled sheet for 1 hr at 500°C. These thin samples were held between thick titanium sheets during annealing to prevent distortion.

Table I outlines the rolling and annealing schedule of those samples for which photographs or texture patterns are shown.

X-ray Techniques

The usual techniques for determining textures were employed during this work. Molybdenum radiation was used for the transmission exposures and copper radiation for the glancing angle ones. Since titanium fluoresces under these conditions, it is necessary to employ a filter between the sample and the film. The $K\beta$ radiation filters are very satisfactory for this purpose.

Sufficient grains having favorable orientation were present in both the cold-worked and in the cold-worked—500°C annealed samples to provide satisfactory patterns with the samples stationary.

Because of the difficulties of comparing intensities of transmission photographs with those obtained

HOWARD T. CLARK, JR., Member AIME, is Research Metallurgist, Metals Research Unit, Remington Arms Co., Inc., Bridgeport, Conn.

AIME Chicago Meeting, October 1950.

TP 2916 E. Discussion (2 copies) may be sent to Transactions AIME before Dec. 15, 1950. Manuscript received April 14, 1950; revision received June 26, 1950.

Table I. The Rolling and Annealing Schedule of Samples Investigated

Sample	Preparation	Reduction in Area, Pct
1	Annealed ingot cold rolled from 0.385 to 0.006 in. Pickled to 0.004 in.	98.4
2*	As-deposited rod ground to 0.268 in. thick, annealed, cold rolled to 0.0026 in.	99
3	Ingot ground to 0.165 in., annealed, cold rolled to 0.041 in. Part of sample pickled to 0.004 in.	75
4	Ingot ground to 0.120 in., annealed, cold rolled to 0.012 in., pickled to 0.004 in.	90
5	Sample 1 + 500°C anneal.	
6	Sample 2 + 500°C anneal.	

* Material of especially high purity prepared by the iodide process using iodide titanium as the raw material, i.e., by redistillation. Its as-deposited and vacuum-annealed hardness was 73 Vickers hardness number.

when using glancing angles, and because of differences due to beam absorption as a function of sample orientation, only three degrees of intensity—heavy, light, and absent—were determined. This was done visually.

Discussion of Results

A few, typical, glancing angle photographs taken with CuK α radiation are shown in fig. 1. Fig. 2 shows the pole figures of material cold rolled 98.4 pct reduction in area while the basal-plane pole figure for this same sample after a 500°C vacuum anneal is shown in fig. 3.

While the rolling and annealing textures reported here for high-purity iodide titanium tend toward the (0001) [1010] texture common to other hexagonal close-packed metals, particularly those having a c/a ratio less than 1.633, the basal-plane pole figure shows the development of two high-intensity regions spread about the transverse direction. Examination of fig. 1 shows that this double texture for the basal plane has started to develop at about 75 pct reduction in area and becomes more pronounced as reduction is continued. It is also shown that the sub-transformation recrystallized texture of heavily cold-rolled titanium, fig. 3, is different from its deformation texture, at least in degree if not in type, and further emphasizes this basal-plane double texture. This difference is also very apparent from a comparison of fig. 1c with 1d. This marked difference between the deformation and the recrystallization textures is not as pronounced for material having reductions in area less than about 96 pct. It was also observed during this investigation that the material at the center of the sample reduced 75 pct (sample 3, 0.041 in. thick) had a somewhat more pronounced basal-plane double texture than did the surface material. This difference was not observed on the thin samples resulting from greater reductions.

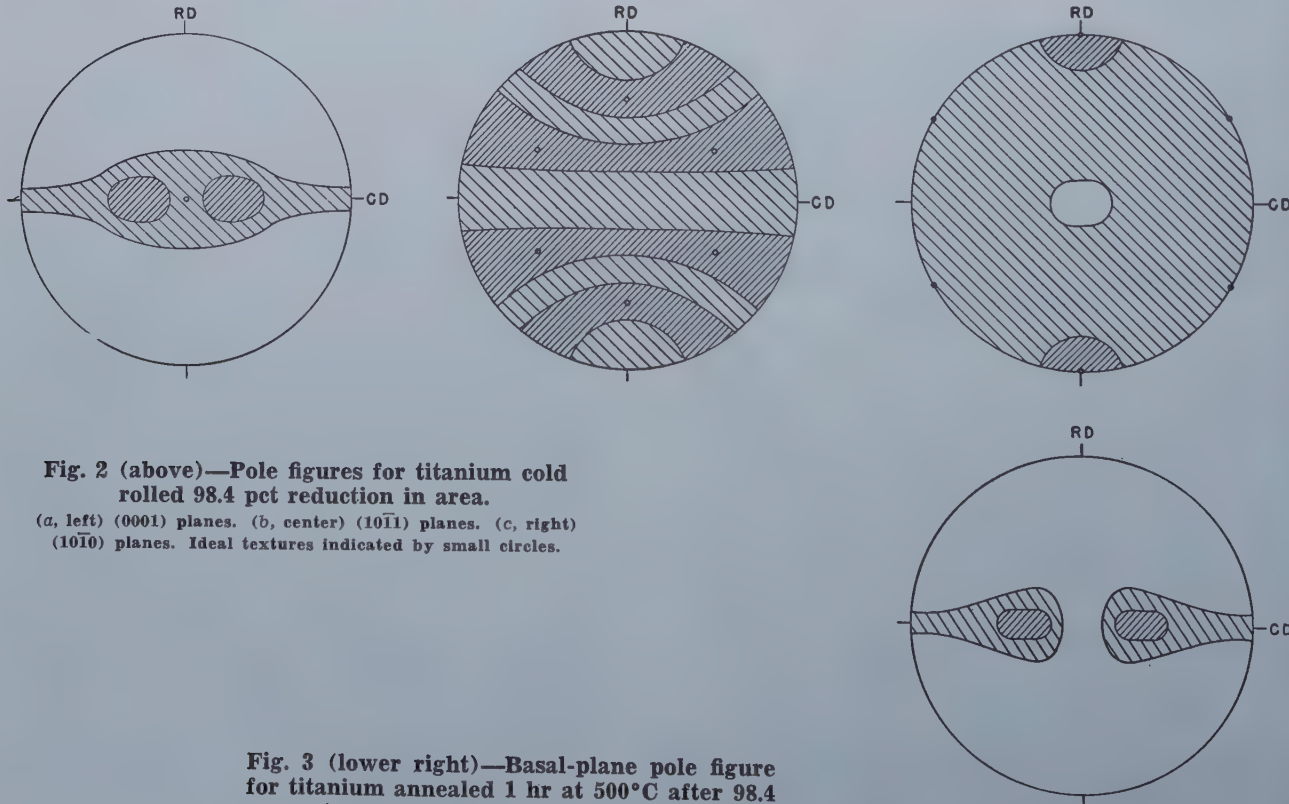


Fig. 1—Glancing angle X-ray photograms for alpha titanium.

(a) cold rolled 75 pct (b) cold rolled 90 pct (c) cold rolled 99 pct (d) cold rolled 99 pct and recrystallized at 500°C. Beam 90° to cross direction and 20° to rolling direction. Rolling direction vertical. Inner ring, faint in most photograms, (1010) planes; middle ring (0001) planes; outer ring (1011).

Critical examination of the three pole figures shown in fig. 2 leads to the conclusion that the (1011) plot (fig. 2b) is not a realistic representation of the texture that would be expected for these planes if the basal-plane texture is as represented in fig. 2a and if the (1010) poles are in the rolling direction. This is explicable on the basis that an insufficient number of intensity gradations were

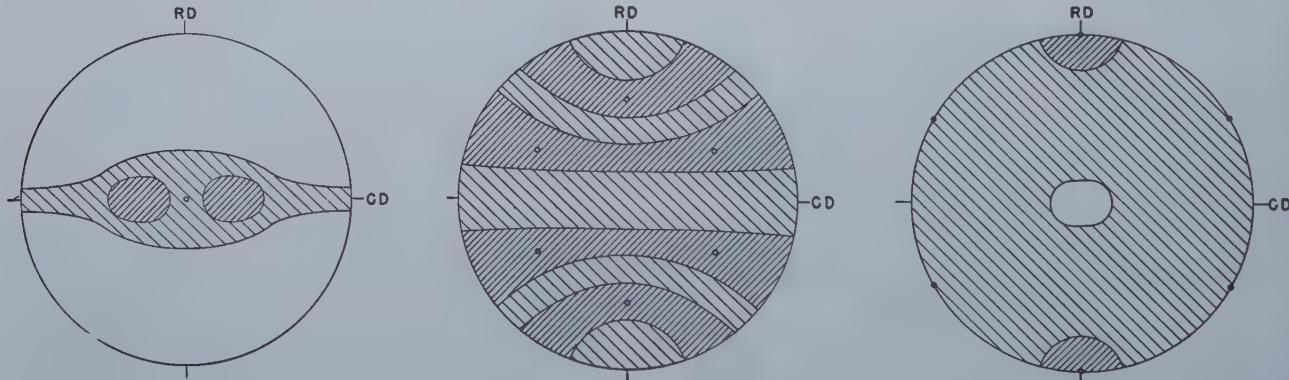


Fig. 2 (above)—Pole figures for titanium cold rolled 98.4 pct reduction in area.

(a, left) (0001) planes. (b, center) (1011) planes. (c, right) (1010) planes. Ideal textures indicated by small circles.

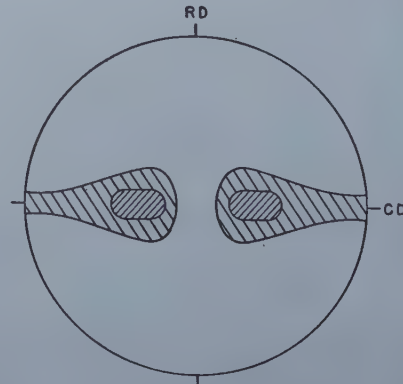


Fig. 3 (lower right)—Basal-plane pole figure for titanium annealed 1 hr at 500°C after 98.4 pct reduction in area by cold rolling.

employed to represent accurately small but important differences.

The c/a ratio of the titanium lattice is 1.5873⁶ and, therefore, the angle between the basal plane and the (1012) planes (the common twinning planes for all hexagonal close-packed metals,⁷ is 42°30'. Because of this condition, reorientation of the basal planes out of the plane of the sheet during the later stages of rolling cannot be accounted for by twinning on this plane since such twinning would result in an increase in thickness of the metal. Unfortunately, as pointed out by Smigelskas and Barrett, the mechanisms of deformation cannot be determined from the deformation textures.

Acknowledgments

Permission from the Remington Arms Co., Inc. to publish these data is acknowledged. The writer is

greatly indebted to W. R. Hibbard, Jr. for his continued advice and criticism during this investigation and for his help in interpreting the results.

References

- ¹ W. G. Burgers and F. M. Jacobs: *Metallwirtschaft*. (1935). **14**, 285.
- ² P. W. Bakarian: *Trans. AIME* (1942) **147**, 266.
- ³ A. Smigelskas and C. S. Barrett: *Trans. AIME*, **185**, 145; *Jnl. Met.* (Feb. 1949) TP 2522 E.
- ⁴ U. S. Pat. No. 1,671,213 Van Arkel et al. (1928).
- ⁵ W. L. Finlay and J. A. Snyder: *Trans. AIME*, **188**, 277; *Jnl. Met.* (Feb. 1950) TP 2759 E.
- ⁶ H. T. Clark, Jr.: *Trans. AIME*, **185**, 588; *Jnl. Met.* (Sept. 1949) TP 2656 E.
- ⁷ C. S. Barrett: *The Structure of Metals*. p. 312. (1943) New York. McGraw-Hill Book Co.

Technical Note

Migration of Carbon in Steel Under the Influence of Direct Current

by P. Dayal and L. S. Darken

THE migration of carbon in austenite under the influence of an electric current has been observed qualitatively several times.¹⁻⁴ Lebedev and Guterman⁵ recently have reported quantitative measurements; their method consisted of welding a low-carbon to a high-carbon wire, passing current, and later estimating the carbon distribution metallurgically. We believe the method reported in this paper is superior in principle since electrolytic migration and ordinary diffusion are not necessarily coupled as in the weld method; also for the first time the extent of migration is determined by combustion analysis for carbon.

A uniform tubular specimen (S.A.E. 1045 or 1095) was mounted as illustrated in the figures, the whole

P. DAYAL is with the Office of the Director of Supplies, Ballard Estate, Bombay, India, and L. S. DARKEN, Member AIME, is Adjunct Professor, Polytechnic Institute of Brooklyn: Research Laboratory, U. S. Steel Corp., Kearny, N. J.

TN 42 E. Manuscript received May 24, 1950.

Based on a thesis submitted by P. Dayal in partial fulfillment of the requirements for the degree of Master of Metallurgical Engineering from Polytechnic Institute of Brooklyn.

assembly being in an atmosphere of purified nitrogen. Direct current (129 to 226 amp at 0.65 to 1.0 v) served as source both of heat and of potential gradient for carbon migration. The duration of experiment was 7.5 to 12 hr, during which time the temperature was controlled ($\pm 10^\circ\text{C}$) manually. The experimental conditions are indicated in the first five columns of table I.

With this experimental arrangement, the temperature initially has a maximum value at the central plane. Also, in this vicinity (by virtue of the symmetry), the carbon entering any volume element is equal in quantity to that leaving; the loss or accumulation of carbon occurs near the electrodes since the carbon moves uniformly near

the center and is "frozen" at the cold ends. Hence, providing the time of experiment is not sufficiently long to seriously influence the conditions at the central plane, carbon crosses this plane only under the influence of the electrical potential gradient and not under the influence of temperature or concentration gradient. The amount of carbon which has crossed this plane was determined by combustion analysis of the two halves of the specimen. The results of these analyses are shown in the sixth and seventh columns of table I. It will be noted that substantial amounts of carbon migrated from the anode portion to the cathode portion (except at 920°C , which temperature was too low to exhibit the effect in the allotted time). In spite of precautions taken, considerable decarburization occurred as may be seen by comparing cols. 8 and 5.

In three cases (indicated by asterisks in table I) the specimen was ground on one side, polished, and examined metallographically before analysis. One specimen was normalized and re-examined. Micrographs of selected areas in specimens 4 and 6 are shown in figs. 1 and 2, respectively. Evidence of carbon migration from the anode toward the cathode is quite apparent. Fig. 2 shows abundant graphite as well as cementite in a region near the cathode. The temperature of this zone is estimated at about 800°C . In fig. 1, particularly in the micrograph on the extreme right (the right side of which is of unaltered carbon content), there is evidence of slight depletion of carbon in the immediate vicinity of the cathode as contrasted to the general increase in carbon of the cathode half of the specimen. Although this may be attributed in part to decarburization, it is believed that it is occasioned also by thermal diffusion—migration (of carbon) from a cool to a hot zone⁴—a phenomenon superimposed upon the electrical migration.

Evidence of carbon migration was visible particularly during the course of the high-temperature,

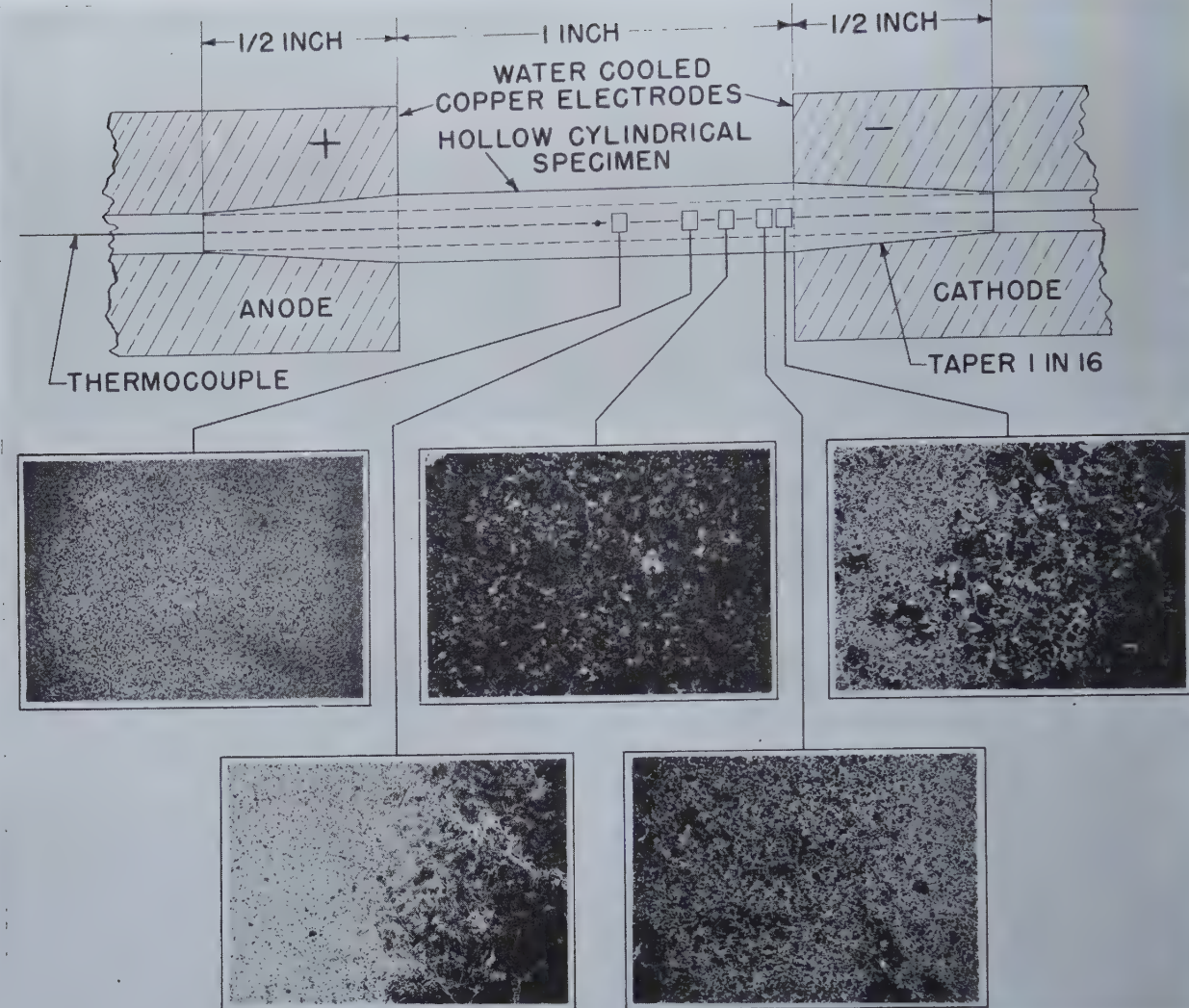


Fig. 1—Micrographs of indicated portions of specimen 4, after normalizing. Picral etch. X100.

high-carbon experiment. Initially the glowing specimen appeared as expected—bright red in the center tapering off gradually through dull red to “black” about 4 mm from the copper electrode. After several hours’ passage of current, a bright red ring developed at or near the zone where graphitization occurred, as shown in fig. 2. This phenomenon occurred only in high-carbon specimens and is believed to be occasioned by the increased resistivity in the high-carbon region.

The mobility, B , (mean velocity of carbon ion under unit potential gradient) is given in col. 9 of table I. This was computed as the ratio of one hundred times the mass of carbon transported across

the central plane to the product of the duration of the experiment times the percent carbon at the central plane times the density times the cross-sectional area times the potential gradient; the potential gradient was calculated from the current, dimensions, and resistivity.

The mobility of carbon also may be represented^a by the relation

$$B = \frac{D\epsilon\nu}{kT}$$

where D is the diffusivity, ϵ is the electronic charge, k is Boltzmann’s constant, T is the absolute temperature, and ν is the number of fundamental

Table I. Mobility, Charge, and Transport Number of Carbon in Austenite

Steel Specimen No.	Central Temp., °C	Duration of Experiment, Hr	Mean Current, Amp	Carbon, Pct			Mobility of Carbon, B , $\text{cm}^2 \text{sec}^{-1} \text{volt}^{-1}$		Charge on Carbon Ion in Austenite (Valence)	Transport No. of C		
				Initial (Uniform)	Final		Observed	Calculated $B = \frac{4D\epsilon}{kT}$				
					Anode Half	Cathode Half						
1*	920	8.5	129	0.46	0.43	0.43	0.43	2.0×10^{-5}	8.6×10^{-5}	+0.9	2.5×10^{-6}	
2	1,277	7.5	168	0.46	0.36	0.43	0.39 ₅	5.8	6.0	3.9	5.7	
3	1,226	9.5	160	0.46	0.24	0.45	0.34 ₅	2.7	4.1	2.6	2.4	
4*†	1,175	10.0	204	0.46	0.22	0.35	0.28	4.1	8.2	2.7	14.2	
5	1,226	9.0	185	1.11	0.54	1.16	0.86	5.6	5.7	3.5	12.7	
6*	1,175	9.0	226	1.11	0.55	1.19	0.86	4.9	4.1	4.9	13.0	
7	1,124	12.0	171	1.11	0.51	1.24	0.89	5.0				

* Examined metallographically before analysis.

† Normalized (1600°F) for metallographic examination.

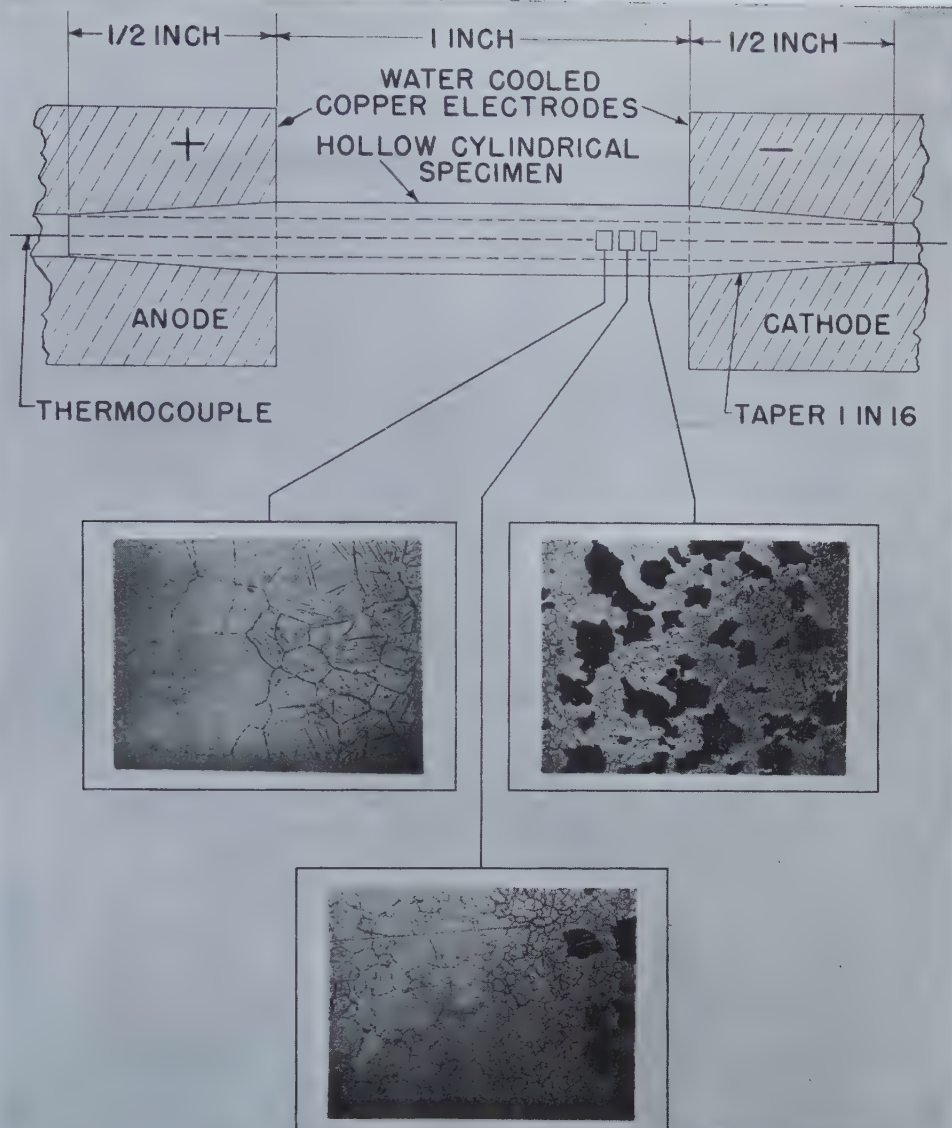


Fig. 2—Micrographs of indicated portions of specimen 6.

Abundant graphite (large black regions) and cementite near cathode. Alkaline sodium picrate etch. X100.

charges carried by the carbon ion ("valence"). Taking D from the data of Mehl and Wells⁷ and using the observed value of B , it is seen that ν may be calculated from this expression. Values of ν , so determined, are listed in the next to the last column of table I. Discarding the anomalous value found for specimen No. 2, the average of the charge is found as +3.5 (standard deviation is 0.4); the average of the values for the steel of higher carbon content, where the spread is less and hence the reliability is presumably greater, is +3.7.

The approximation involved in estimating the mean carbon content at the central plane probably tends toward a high value since the curve representing carbon content vs. time is probably concave upward. Further, the assumption that decarburization was equal in the two halves is not exact; decarburization was probably more severe in the higher carbon half. These further corrections would raise the calculated value of ν slightly. Hence, if one wished to postulate *a priori* that the charge on the carbon ion had the classical value of four, nothing in the present experiments would contradict this. Pauling⁸ also assigns carbon a metallic valence of four. In col. 10, values of B

calculated from the above equation and the value of 4 for ν are tabulated.

The transport number is defined as the fraction of the total current carried by carbon. This is tabulated in the last column of table I. At a given temperature the transport number is expected to be proportional to the carbon content;⁹ it is seen that this expectation is realized, at least roughly, the transport number and the carbon content each increasing about threefold.

References

- ¹ W. Seith and O. Kubaschewski: *Ztsch. Elektrochem.* (1935) **41**, 551.
- ² V. I. Prosvirin: *Vestnik Metallopromishlennosti*. (1937) No. 12.
- ³ O. Kubaschewski: *Ber. d. naturforschenden Ges. zu Freiburg i. Br.* (1936) **35**, 2, 209.
- ⁴ T. A. Lebedev: *Metallurg.* (1940) **15**, 61.
- ⁵ T. A. Lebedev and V. M. Guterman: *Doklady Akad. Nauk. (SSSR)* (1948) **60**, 1201.
- ⁶ Karl E. Schwarz: *Elektrolytische Wanderung in flüssigen und festen Metallen*. Leipzig 1940; Lithoprinted by Edwards Bros. Michigan. 1945.
- ⁷ C. Wells and R. F. Mehl: *Trans. AIME* (1940) **140**, 279.
- ⁸ L. Pauling: *Jnl. Amer. Chem. Soc.* (1947) **69**, 542.

A Study of the Plastic Behavior of High-Purity Aluminum Single Crystals at Various Temperatures

by F. D. Rosi and C. H. Mathewson

The plastic properties of extended aluminum (99.996) single crystals were investigated in the temperature range 77° to 353°K. Both the critical resolved shear stress and coefficient of shear hardening were found to increase with a decrease in temperature, and were consistent with the Schmid law of critical shear stress governing the initiation of the slip process. Measurements were also made on the density of slip bands, which was found to increase with decreasing temperature in a manner similar to the shear hardening coefficient. Some observations were made on the appearance of slip bands on etched and unetched electrolytically polished surfaces, and on the general complexity of the slip process.

THE plastic properties of face-centered cubic metals below room temperature present a field of investigation which has not been extensively explored. The work by Schmid and Boas¹ has demonstrated the importance of temperature upon such properties as strain hardening and critical resolved shear stress. The work by Yamaguchi² upon the shear stress as related to the number of slip bands accentuates the necessity for further experiments of a similar nature. The approach to a mechanical equation of state from the standpoint

F. D. ROSI, Junior Member AIME, is with Sylvania Research Laboratories, Bayside, L. I., N. Y.; formerly, Graduate Laboratory Assistant, Yale University, and C. H. MATHEWSON, Member AIME is Professor of Metallurgy, Yale University, New Haven, Conn.

AIME Chicago Meeting, October 1950.

TP 2877E. Discussion (2 copies) may be sent to Transactions AIME by Dec. 15, 1950. Manuscript received Dec. 16, 1949; revision received June 5, 1950.

This paper is part of a dissertation presented by F. D. Rosi to the Faculty of the Graduate School of Yale University in partial fulfillment of the requirements for the degree of Doctor of Philosophy.

of thermal fluctuations and activation energies by Becker³ and more recently by Kauzmann⁴ further emphasizes the need for a quantitative and more comprehensive analysis of the dependence of fundamental plastic properties on temperature.

The purpose of the present work was to investigate specifically: (1) The gross shape of the stress-strain curves at several temperatures, (2) the change in the critical shear stress as a function of temperature, and (3) the number and appearance of slip bands as a function of strain and temperature.

Preparation of Specimens

Single-crystal specimens of 99.996+ pct aluminum, $\frac{1}{2}$ in. in diam and 5 to 6 in. in length, were made by the Bridgman method of gradual solidification from the liquid state.⁵ The crystallographic orientation of the single crystals was determined from back-reflection, Laue X-ray photographs according to the method described by Greninger.⁶ In most specimens the Laue photographs showed double diffraction spots indicative of the lineage structure type of imperfection, discussed in great detail by Buerger.⁷ The angular spread of these

spots was never observed to exceed 2°. Most of the crystals were radiographed to insure against microporosity.

In preparing the metal surface for optical microscopy, the following sequence of operations gave good results: The as-cast crystals were turned down in a lathe, 0.001 in. per cut, to obtain a 2.5 in. gauge length. The cold-worked layer resulting from this operation was removed chemically by etching with Tucker's reagent. Then the specimen was polished mechanically through 2/0 metallographic emery paper, after which it was etched again to remove the cold-worked layer resulting from the mechanical treatment. A 48-hr anneal at 580°C \pm 10°C followed so as to insure an essentially stress-free single crystal. After the annealing treatment, the specimen was electrolytically polished in a 2:1 solution of methyl alcohol and concentrated nitric acid. With a current density of 10 amp per sq dm (decimeter) the time required to obtain a satisfactory surface varied from 10 to 12 min. The polishing was carried out for short periods of 2 min to avoid rapid deterioration of the solution as well as to enable the rotation of the specimen 180° for uniformity of polish. It was necessary to place the solution in a bath of dry ice in view of its explosive nature at room temperature. Etching of the electrolytically polished surface was accomplished by using the fuming etch-pit method recommended by Lacombe and Beaujard⁸ for high-purity aluminum.

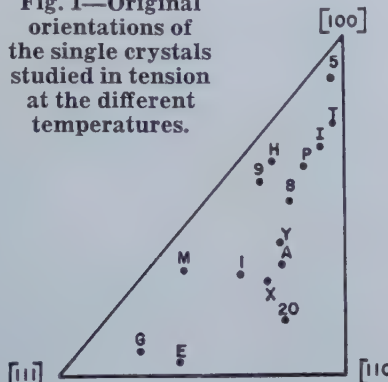
Method for Tensile Testing

A modification of the loading equipment devised by Miller⁹ was used. In this apparatus, the specimen was suspended from a chain and gimbal arrangement (for axial loading) in a heavy steel framework connected at the bottom to a balanced 6:1 lever and bucket system. Loading of the specimen was accomplished by allowing sand to flow from a reservoir into the bucket suspended from the longer end of the lever-arm at a rate of approximately 3 lb per min.

Strain measurements were made using the Baldwin SR-4, bonded, resistance-wire, strain gauge and an SR-4 portable strain indicator (type K), which permits a reading accuracy of 2 microinches per inch. For low-temperature study, the gauge was calibrated by measuring the elastic modulus of an annealed stainless steel rod, which is known to be independent of temperature.¹⁰

The apparatus used for the low-temperature experiments consisted of a stove pipe, 4 in. in diameter, surrounded by another pipe which was 8 in. in diam. The inner pipe was supported by means of four legs which were soldered to a 3-in. steel ring at its bottom and to a stainless steel plate which was, in turn, soldered to the outside pipe. A highly flexible brass bellows, at each end of which was soldered a brass slug containing a $\frac{3}{8}$ in. concentric bore, was used to permit extension of the specimen. Surrounding the bellows arrangement was a stainless steel tube which extended from the bottom of the inner pipe to the plate. The bottom brass plug of the bellows was soldered to the stainless steel plate, thereby eliminating any source of leakage. The space between the two pipes was filled with Santocel powder which is a reasonably good thermal insulator. A wooden ring was inserted between the pipes for purposes of rigidity and insulation.

Fig. 1—Original orientations of the single crystals studied in tension at the different temperatures.



The furnace used for the elevated temperature experiments (80°C) is that described by Miller.⁹ Temperature control was obtained by using a powerstat which was connected directly across a 110 ac source. Temperature readings were obtained with a mercury thermometer inserted through a diagonal port that permitted contact with the specimen. In order to prevent burning of the strain gauge paper, a mixture of hydrogen and nitrogen gas was introduced in the heating chamber through a second diagonal port, which was well below the level of the specimen.

Presentation of Data

The loading characteristics of the single-crystal specimens are presented as curves of stress (g per mm^2) vs. strain (mm per mm). The formulas used in the evaluation of shear stress and shear strain, as in deriving the coefficient of shear hardening, are conventionally given by Schmid and Boas¹ in terms of the original orientation and the change in length of the crystal. For calculating the critical resolved shear stress the standard equation was used.

The data on slip bands are presented as the num-

Table II. Critical Shear Stress Data for Dry Ice Tests

Specimen No.	Diam, In.	χ Deg.	λ Deg.	$\sin \chi / \cos \lambda$	Critical Shearing Stress, g per mm^2
I	0.4143	43.5	45	0.4860	124.1
M	0.4413	32	34.5	0.4367	122.1
X	0.4227	48	43.5	0.4853	126.2

ber of bands per unit length along the normal to the slip plane (No. per mm). The formula used for this calculation is given by Yamaguchi.²

The original orientations of the single crystals studied in tension at the different temperatures are stereographically presented in fig. 1.

Experimental Results, Shear Stress Determinations

The values of the critical shear stress were obtained from stress-strain curves by noting the value at which plastic flow set in at a constant rate. The yield stress was taken as the extrapolated point which represents the intersection of the elastic range with the straight portion of the stress-strain curve, which occurs almost immediately after plastic flow begins, as shown in fig. 2.

Table I contains the data pertinent to the evaluation of the critical resolved shear stress for four crystals tested at room temperature. The average value of the critical shear stress is 104.5 g per mm^2 , with a variation between the two extreme values of approximately 2 pct. This is a verification of the independence of critical shear stress from orientation (law of resolved shear stress), since the distribution of orientation of the crystals (see fig. 1) covers the triangle satisfactorily.

Comparison of the present critical shear stress

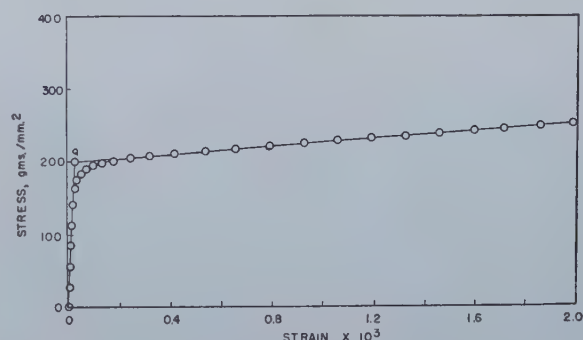


Fig. 2—Stress-strain diagram of crystal A at room temperature.

The value of stress at Q is used for obtaining the critical shear stress.

value with those of Dehlinger¹¹ and Miller and Milligan¹² show good agreement, considering the high-purity aluminum (99.99+) used in the present investigation. The Dehlinger values for aluminum of 99.5 and 99.8 pct purity are 319 g per mm^2 and 210 g per mm^2 , respectively. His extrapolated value for 99.99 pct purity is approximately 95 g per mm^2 . Miller's determination shows a value of critical shear stress of 138 g per mm^2 for a gradually solidified aluminum single crystal of 99.90 pct purity under conditions of very slow loading.

The critical shear stress results of the dry ice ($205^{\circ}\text{K} \pm 3^{\circ}\text{K}$) and liquid nitrogen tests (77.35°K) are recorded in tables II and III. Crystal 1 was tested at a temperature of $93^{\circ}\text{K} + 10^{\circ}\text{K}$, at a time when the supply of liquid nitrogen had run out. Temperatures were read directly with a pentane thermometer.

Table I. Critical Shear Stress Data for Room Temperature Tests

Specimen No.	Diam, In.	χ Deg.	λ Deg.	$\sin \chi / \cos \lambda$	Critical Shearing Stress, g per mm^2
A	0.4388	43	44.5	0.4388	104.4
E	0.4313	33	43.5	0.3920	104.2
H	0.4458	37	38	0.4760	103.0
T	0.4080	44	46.5	0.4782	103.6

Quantitative data on the critical resolved shear stress of aluminum single crystals below room temperature are very incomplete. Boas and Schmid¹³ experimented with aluminum crystals at 88°K but did not state definite values of critical shear stress. They did observe however, that extensive slip was produced by a resolved shear stress of 800 g per mm², which is almost double the average value (421.3 g per mm²) obtained in the present investigation.

The critical shear stress data for tests at 353°K ± 3°K are presented in table IV. The average value is 91.8 g per mm², which compares favorably with that obtained by Miller and Milligan,¹² who reported values of 55 and 115 g per mm² for 99.5 and 99.90 pct purity aluminum at 373°K.

A summary of the critical shear stress data compiled in the present investigation at the four temperatures is given in fig. 3. As in most investigations of the properties of single crystals, these data

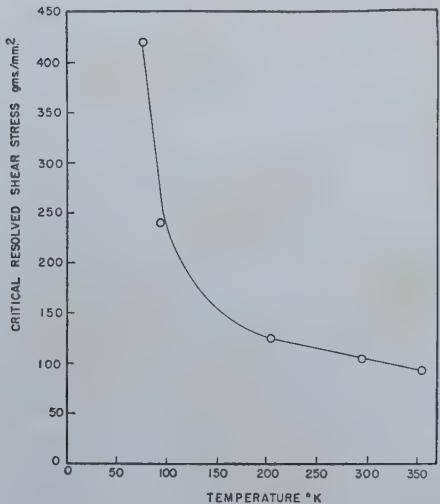


Fig. 3—Effect of temperature on the critical shear stress.

demonstrate that the critical shear stress necessary to initiate slip increased with decreasing temperature. They indicate a rather small, but linear increase in the critical shear stress in the temperature range 353° → 205°K with an extremely sharp upturn in the curve from 205° → 77.35°K. This is in direct contrast with the curves for the hexagonal metals, cadmium and zinc,¹⁴ which show no marked increase in critical shear stress with decreasing temperature. On the other hand, a somewhat similar behavior was obtained for bismuth¹⁵ and magnesium¹⁶ crystals.

Stress-Strain Diagrams

The room temperature curve of single crystals H, fig. 4, demonstrates a rather sharp advent of plastic flow and a measurable increase in the resistance to glide, even for the small amounts of strain involved. In all cases the linear rate of strain hardening sets in almost immediately after the small anelastic portion of the curve. Generally speaking, after removal of the load, a small amount of hysteresis was

Table III. Critical Shear Stress for Data for Liquid Nitrogen Tests

Specimen No.	Diam., In.	χ Deg.	λ Deg.	Sin χ / Cos λ	Critical Shearing Stress, g per mm²
9	0.4636	37	37	0.4894	415.1
20	0.4595	44	48	0.4826	427.5
1 (95°K)	0.4243	40	40	0.4924	240.5

Table IV. Critical Shear Stress for Tests at 353°K (80°C)

Specimen No.	Diam., In.	χ Deg.	λ Deg.	Sin χ / Cos λ	Critical Shearing Stress, g per mm²
5	0.4562	38.5	44	0.4478	95.0
8	0.4588	42	42	0.4972	87.0
Y	0.4381	43.5	43	0.5035	93.3

observed, which may be attributed to an anelastic effect. A slight increase in the rate of strain hardening was observed after about 0.4 pct elongation in the stress-strain curves of the crystals extended at room temperature. This is probably the end of the so-called "yield-point elongation" zone observed and defined by Miller and Milligan.¹²

From the data pertinent to the dynamic behavior of the single crystals tested at the four temperatures, the elastic modulus did not appear to vary with a change in orientation, which may be attributed to the isotropic character of aluminum. The coefficient of shear hardening, which is defined as the slope of the shear stress-shear curves, also did not appear to vary with the orientation of the crystal. The constancy of this coefficient with orientation is simply a confirmation of an extension of the critical shear stress law to include plastic flow. At room temperature the average value for the coefficient of shear hardening is 11,750 g per mm² after approximately 0.3 pct extension, while that for the so-called "yield-point elongation zone" is 7750 g per mm². At the other temperatures this unique zone was not observed.

Typical stress-strain diagrams for specimens tested at the various temperatures are shown in fig. 5. As at room temperature, the strain hardening at the three temperatures is linear after the advent of plastic flow. In the case of specimen 5 tested at 353°K (80°C), in the anelastic portion of the stress-strain curve, plastic deformation proceeded in several periodic steps of the order 2×10^{-6} in. per in. Between these steps the flow apparently ceased, and the steady application of load produced an elastic deformation of 5×10^{-6} in. per in. This step-wise character was observed very recently in polycrystalline aluminum at room temperature and at a

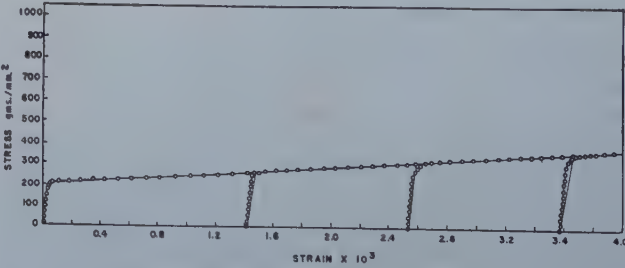


Fig. 4—Stress-strain diagram of crystal H tested at 295°K (22°C). Extensions 1, 2, 3, and 4.

slow, constant loading rate by McReynolds,¹⁷ who gave 5×10^{-4} in. per in. as the order of magnitude for the steps. This stepped character was found by McReynolds and earlier by Sutoki¹⁸ to increase with an increase in the temperature of testing.

Specimen A, which previously had been prestrained approximately 0.22 pct at 273°K, was then reloaded at 205°K. It was found that the stress necessary for plastic flow at 205°K after the 0.22 pct extension was less than that which would be expected had the crystal been extended this amount

of strain at 205°K, as shown by the dotted line in fig. 6. Furthermore, the increase of stress with strain at 205°K after the prestrain at 295°K was the same as that obtained by a specimen initially extended at 205°K. These observations substantiate the contention of Dorn et al.¹⁹ that the strain alone is not a measure of the strain-hardened state. However, they do suggest that for small amounts of extension the stress necessary for plastic flow is a measure of the strain-hardened state.

The dependence of the coefficient of shear hardening on temperature is illustrated in fig. 7, with each point representing the mean value of 2 to 4 crystals. The amount of shear hardening decreases markedly as the temperature is raised. This same general dependence has been observed by Boas and Schmid in aluminum¹⁸ and cadmium crystals,²⁰ and by other investigators in magnesium¹⁹ and zinc.²¹ Fig. 8 shows that the modulus of elasticity also decreases with an increase in temperature. The resolved shear stress-shear curves of fig. 9 summarize the effect of temperature on the gross shape of these curves.

Measurement of Slip Bands

Since the slip bands in aluminum single crystals show a reasonable regularity of spacing, measurement of these bands with some degree of accuracy

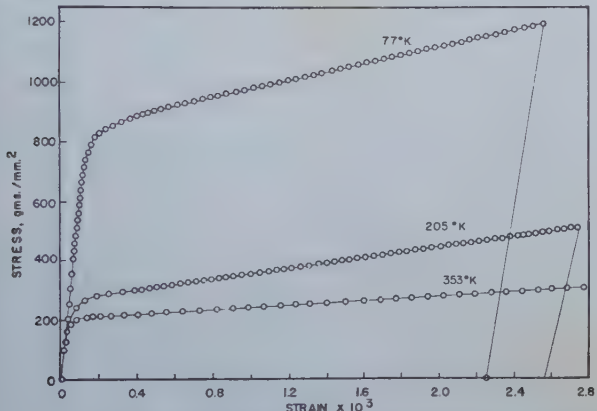
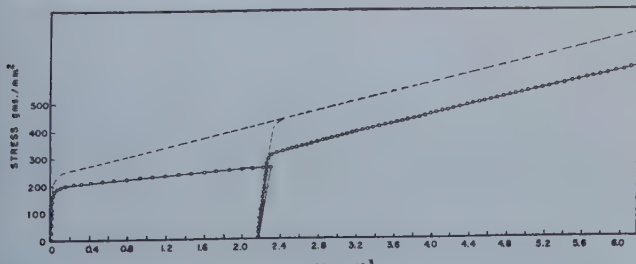


Fig. 5—Stress-strain diagram of crystal 20 at 70°K (−196°C).

Fig. 6—Effect of prestraining at 295°K (22°C) on the stress-strain diagram of crystal A at 205°K (−68°C).



was considered possible for small amounts of extension, using a microscope with the vertical type of illumination at a magnification of 600.

The density of slip markings was obtained by counting the number of bands appearing per unit length along a line on the surface joining the major axes of the glide ellipses. In this manner the number of slip bands per unit length along the normal to the slip plane may be obtained directly. The measurement was carried out over a length of 32 mm, 16 mm to the left and right of a reference mark at approximately the center of the gauge length. A mean value per unit length was taken,

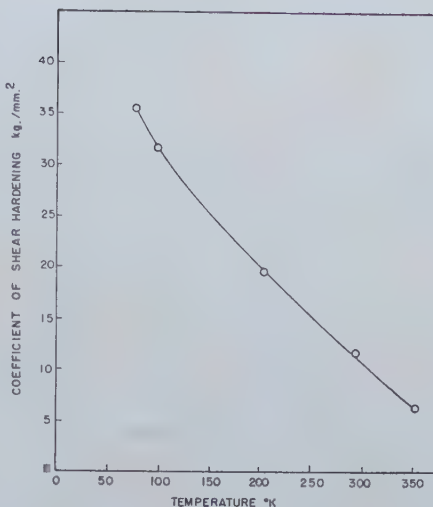


Fig. 7—Effect of temperature on coefficient of shear hardening.

which represented an average of the two 16-mm readings. Measurements were made after extensions of approximately 0.2 pct up to about 2 pct, as shown in the reloading curves of fig. 4.

The relation between the number of slip bands per unit length normal to the slip plane and the strain is shown in fig. 10 for four crystals of different orientation extended at room temperature. It may be seen that the points do not lie on a straight line, which is contrary to the results of Yamaguchi.⁸ Instead, a group of curves is obtained, which show a series of plateaus. These results are in general agreement with the recent work of Crussard²² on aluminum single crystals of the same purity. He obtained curves which were parabolic during the early stages of deformation, and then became linear with increasing extension. It is also apparent from the curves that the orientation of the crystals has a marked effect on the density of visible slip bands for a given amount of strain.

To see if the resolved shear stress relationship could be extended to apply to the increase in the number of slip bands with stress, the density of slip bands was plotted against the resolved shear stress, fig. 11, in an attempt to bring the curves of crystals E, H and T of fig. 10 together. Furthermore, this relation would also indicate whether the plateaus were due to a recovery effect. It may be seen from fig. 11 that the curves have been drawn together somewhat, and that the straight line portions of each curve have approximately the same slope. Moreover, the parabolic character of the curves has been minimized particularly in the region of higher stress, indicating that some recovery occurs even at such small amounts of plastic flow.

It appears significant that the first plateau appears

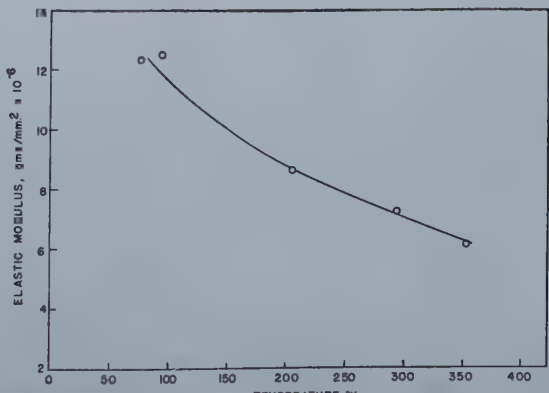


Fig. 8—Effect of temperature on the elastic modulus.

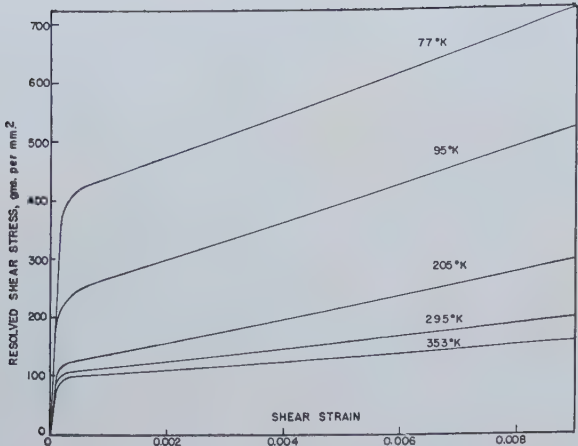


Fig. 9—Shear hardening at different temperatures.

in all crystals at approximately the same values of shear stress and strain (strain shown in previous diagram) regardless of the number of slip bands. This region of stress and strain corresponds approximately to the end of the Miller "yieldpoint elongation zone," and to an increase in the amount of strain hardening. At the higher extension where the strain hardening begins to decrease, it can be seen from the curves of crystals H and T in fig. 11, that the density of slip bands increases markedly. This is reasonable since in these regions slip is continuing for the most part on those bands already formed, with the result that the width of the bands grows so as to make previous submicroscopic* slip

* By submicroscopic slip is meant any slip which is beyond resolving power of microscope at X600.

visible, and on this basis strain hardening is primarily associated with submicroscopic slip. The mean value of the spacing between resolvable slip bands for an extension of 0.25 pct varies from 2.31×10^{-2} to 2.81×10^{-2} mm, which is of the order of magnitude of a lineage structure. This suggests that slip bands, corresponding to the first plateau, are nucleated in regions of crystalline imperfections arising from irregularities in the growth process. Similarly the other plateaus may correspond to favorable conditions arising from other imperfections of structure. The three curves of fig. 11 intersect the abscissa at approximately the same point,

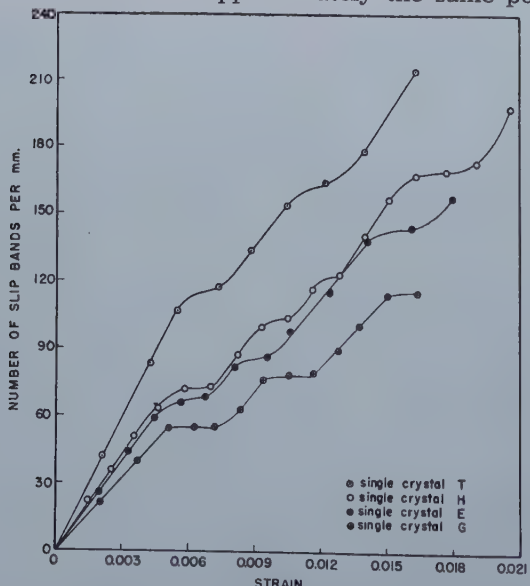


Fig. 10—Effect of increasing strain on density of slip bands in early stages of plastic flow.

which is the value of the critical shear stress for these crystals.

Measurements of the density of slip bands were made on several of the crystals extended at dry ice and at 353°K (80°C), and these were compared with those previously made on single crystals of similar orientation studied at room temperature. The number of slip bands per millimeter for approximately 0.25 pct extension increases almost linearly with a decrease in the temperature from 353°K (80°C) to 205°K (-68°C), as shown in fig. 12. No value was obtained at the liquid nitrogen tests, since the slip bands were scarcely visible and were difficult to resolve at such small extensions. The extrapolated value for this temperature, assuming a linear relation, is 172 bands per mm, which gives a spacing between bands of approximately 6×10^{-8} mm. This is within the resolving power of the microscope, which was calculated to be 5.5×10^{-4}

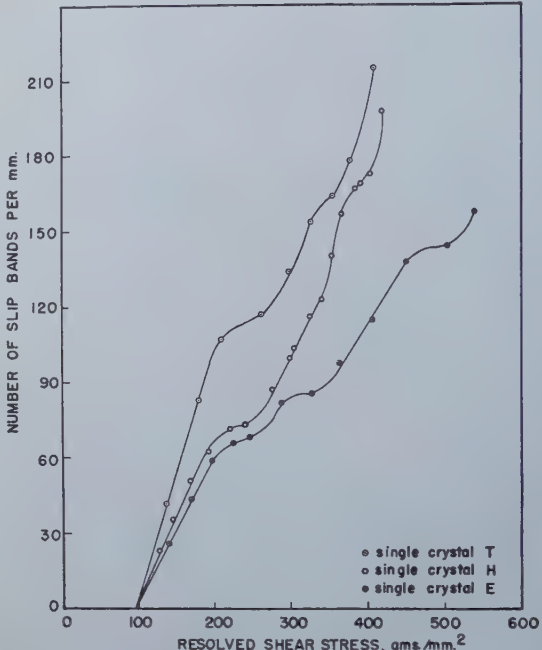


Fig. 11—Effect of increasing shear stress on density of slip bands in early stages of plastic flow.

mm from wavelength of illumination and the numerical aperture of the objective used for these measurements. However, slip bands may be recognized only after the differences in level between the bands have reached a value approximately one tenth of the resolving power of the microscope. Therefore, for a 0.25 pct extension the mean value of strain within each band in liquid nitrogen would be of the order of 1.3×10^{-5} mm, which is below the limit of the microscope.

Nature and Appearance of Slip Bands

It is known that the oxide film which forms very rapidly on electrolytically polished aluminum in contact with air has a disturbing effect on the appearance of slip bands, making them wavy rather than straight. Since it is believed that the magnitude of this effect depends to a great extent upon the electrolytic polish used, and perhaps unintentional variations in the technique of polishing, the character of slip bands was examined on both etched and unetched electrolytically polished surfaces. There was little, if any, difference in their general appearance. Furthermore, the values of critical shear stress on both etched and unetched specimens did not vary appreciably.

Figs. 13 and 14, taken from an unetched specimen, show the increase in the number of slip bands with increasing strain. This increase in the number of glide bands as deformation is continued is characteristic of aluminum, having been observed by Yamaguchi² and more recently by Crussard.²² It appears that the spacing of these markings is much more regular than would correspond to statistical disorder.

It was the general rule that at the early stage of deformation the slip bands often appeared not as lines traversing the whole of the crystal, but as segments whose ends seemed to vanish in their path through the crystal. The appearance of this

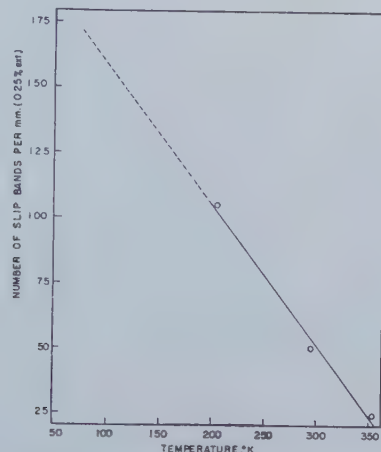


Fig. 12—Effect of temperature on density of slip bands for 0.25 pct extension.

microscopic slip in its early stages is shown in fig. 15. At the temperature of dry ice, this early stage character of slip bands is even more pronounced, while at the elevated temperature the bands are thicker and run completely through the specimen.

In all specimens certain adjacent slip bands were observed to terminate opposite one another. This phenomenon is shown in the micrographs of figs. 13 and 14. Andrade and Roscoe²³ observed this same behavior in single crystals of lead, and in no case were the bands found to overlap by more than the distance of separation between them, which led those investigators to conclude that the bands are really paths of dislocations propagated somewhat in the Taylor manner. In the present investigation the extent of this overlapping was found in some cases to agree with the observations of Andrade and Roscoe; but in other cases, fig. 13, the bands pass one another by an amount much greater than the distance between them. It is believed that the degree of overlapping depends to a great extent upon the magnitude of slip which has occurred in the individual bands.

The appearance of "cross-slip," which is step-like in its character, was found in all specimens tested at room temperature but not at the temperature of dry ice or at 353°K (80°C). At the low temperature, it is possible that with further extension cross-slip might have been observed, in view of the undeveloped character of the bands at the earlier stages of deformation. Fig. 16 shows cross-slip at X1000. It can be seen that this phenomenon occurs in a step-like fashion in such a manner that slip occurs alternately on the cross-slip plane and the primary octahedral plane. From the symmetry of the etch-pit it can be further seen that the cross-slip plane

must be one of two possible octahedral planes whose trace makes a 90° angle with that of the primary plane.

Changes in the Mechanism of Deformation

At the commencement of the plastic deformation in aluminum single crystals, slip occurs first in that octahedral {111} plane and dodecahedral <110> direction where the shear stress is at a maximum, at the same time producing a rotation of the crystal with respect to the fixed direction of the tensile force. With the necessity for lattice accommodation during slip, which may produce rotations of various types, it is possible to have stress conditions modified so that momentarily, in certain regions, the shear stress may be a maximum on a different set of planes. The probability of this becomes even greater when the orientation of the crystal is critical; that is, when the specimen axis is, at most, 2° from a leg of the spherical triangle. In this case slip may be expected to occur sparingly on other sets of slip planes in addition to the primary slip plane.

As may be seen in fig. 2, specimen T has a critical orientation, being only 1° from a boundary line. In this crystal three slip systems were observed, as shown in fig. 17, which was taken along the line joining the major axis of the primary glide ellipses. Fig. 18 shows the presence of a second slip system in crystal G, which was found to be slip on the conjugate plane. Stereographic analysis of back-reflection Laue photographs describing the region where slip was observed shows that four operative slip planes are indicated in the plastic deformation of these crystals. These are: (1) the primary plane, (2) the cross-slip plane, (3) the conjugate plane, and (4) a "critical" plane, since this type of slip seems possible only in crystals which have a particular critical orientation, such as T. The analogous critical orientation of specimen G would indicate extra slip on plane I, the primary plane, but in another direction not distinguishable in these experiments. Figs. 19a and b are standard projections indicating the different slip planes observed in the micrographs of figs. 17 and 18, respectively. Of these systems, the first three have been observed by Maddin, Mathewson and Hibbard²⁵ in α-brass crystals well within the range of orientation conventionally requiring slip on a single (primary) plane.

Discussion of Results, Critical Shear Stress

The law associating a critical resolved shear stress with slip was confirmed at the four temperatures of testing. This uniformity of behavior seems to indicate that the method used in producing and preparing specimens for tensile testing resulted in single crystals which were, within the sensitivity of the tests, uniform in structure. Further, it has been shown that the critical shear stress necessary to cause glide to set in at a given rate in the active slip system increases with decreasing temperature in the manner shown in fig. 3. The extremely sharp upturn in this curve from 205°K to 77°K indicates a form of function

$$\sigma = Ae^{Q/RT} \quad [1]$$

where σ = critical shear stress
 A = stress constant
 Q = activation energy
 R = gas constant, and
 T = absolute temperature.



Fig. 13 (top left)—Showing slip bands on unetched surface after 0.25 pct extension. Crystal G. X800.

Fig. 14 (bottom left)—Showing slip bands on unetched surface after 0.75 pct extension. Crystal G. X800.

Fig. 15 (top center)—Showing slip bands at early stages of deformation (0.21 pct). Crystal T. X800.

Fig. 16 (bottom center)—Showing segmented slip occurring alternately on cross-slip plane and pri-

All illustrations reduced in area approximately two thirds for reproduction.

In this formula, the expression $e^{Q/RT}$ provides a measure of the proportion of atoms in the lattice (probably associated with imperfections) involved in the physical change of plastic flow. To apply this formula to the curve of fig. 3, it is convenient to express it in a logarithmic form, that is

$$\log \sigma = \log A + Q/RT$$

Fig. 20 shows a plot of the logarithm of the critical shear stress against the reciprocal of the absolute temperature from which it may be seen that the points fall on a straight line, with the exception of the one which represents the test at 95°K. It will be remembered that in this test insufficient liquid nitrogen was available, with the result that marked temperature fluctuations may have oc-

curred. The values of the activation energy Q and the constant A are calculated to be 300 cal per g-atom and 61 g per mm², respectively. In this connection the work of Zener and Hollomon²⁸ on the yield point of steel is significant. They found that the shear stress varies at only about the one-hundredth power of the strain rate and the heat of activation, which describes the dependence upon temperature, is of the order of magnitude of only 100 cal per g-atom. It is interesting to mention here that if a $\log \sigma$ vs. $1/T$ plot were made from the data on magnesium,²⁷ an activation energy of 200 cal per g-atom and a stress constant of 60 g per mm² are obtained.

Strain Hardening

With increasing strain hardening during plastic flow, new active glide planes continually appear between the old, which suggests that slip has ceased in the lamellae on which it began. This was also observed by Yamaguchi² with aluminum crystals, who further found that the spacing between slip bands varied inversely with the stress. In the present experiments a linear relation between density of slip bands and shear stress was not obtained in the early stages of plastic deformation. Instead, small plateaus are found which tend to disappear at higher extensions. In all cases the first plateau (or parabola) was related rather closely to the end of the Miller "yield-point elongation zone" (approximately 0.4 pct ex-

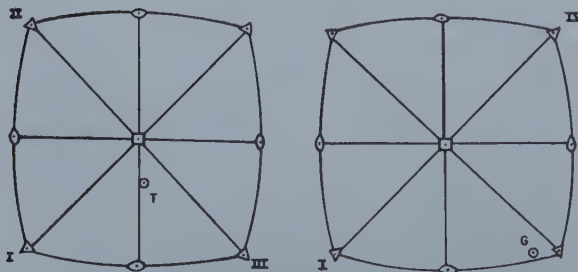


Fig. 19a and b—Standard projections indicating slip planes observed in figs. 17 and 18.

I—Primary slip plane. II—Cross-slip plane. III—"Critical" plane. IV—Conjugate plane.

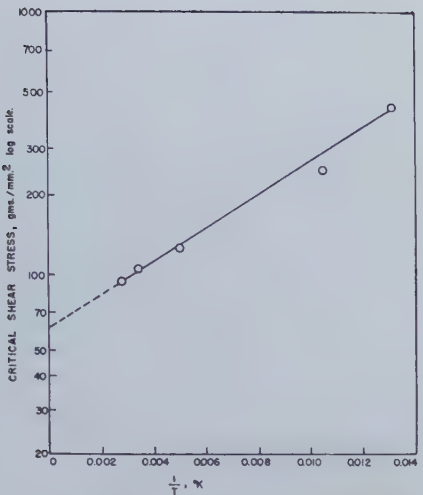


Fig. 20— $\log \sigma = \log A + \frac{Q}{RT}$

tension). It is possible that both the plateaus and the increase in number of slip bands with stress are due to different orders of energy associated with the lineage imperfection.

Temperature is found to affect the rate of strain hardening to a considerable extent, and it may be seen from fig. 7 that the amount of hardening decreases as the temperature is raised. This observation is made by all investigators of the properties of single crystals at low temperatures, and evidently is a fundamental behavior of metals.

The straight line in fig. 21 indicates that a parabolic relation exists between the coefficient of shear hardening and the temperature according to the formula,

$$\left(\frac{\tau}{a}\right) = \left(\frac{\tau}{a}\right)_{T=0} \left[1 - C_1 \sqrt{T} \right] \quad [2]$$

where τ = change in resolved shear stress (σ) for given change in shear strain (a),

$\left(\frac{\tau}{a}\right)$ = coefficient of shear hardening at temperature T ,

$\left(\frac{\tau}{a}\right)_{T=0}$ = coefficient of shear hardening at 0° absolute

C = constant

T = absolute temperature.

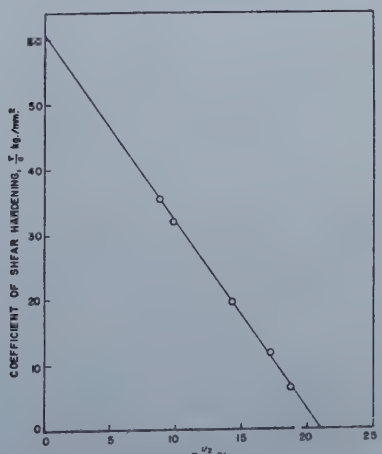


Fig. 21—Effect of temperature on the coefficient of shear hardening, $\frac{\tau}{a}$ vs. $T^{1/2}$.

From fig. 21, the value of $\left(\frac{\tau}{a}\right)_{T=0}$ and the constant

C are found to be 61 kg per mm² and 0.0476 deg^{-1/2}, respectively; and the temperature for zero shear hardening is 440°K. Thus, from the above formula it appears that the apparent shear hardening at some finite temperature T may be regarded as equal to the difference between the "athermal" shear hardening, which may be observed directly at 0° absolute, and a shear softening, which is a result of a thermal recovery process occurring during the deformation process at finite temperatures. Interestingly enough, the temperature for zero shear hardening falls within the equi-cohesive temperature range reported by Crussard²⁷ for Al (99.995 pct).

In connection with the dependence of shear hardening on temperature, fig. 22 shows that the density of slip bands at 0.25 pct extension is also found to decrease in a parabolic manner with an increase in temperature according to the formula,

$$N = (N)_{T=0} \left[1 - C_1 \sqrt{T} \right] \quad [3]$$

where N = number of slip bands per millimeter at temperature T

$(N)_{T=0}$ = number of slip bands per millimeter at 0° absolute

C_1 = constant

T = absolute temperature.

From fig. 22, the values of $(N)_{T=0}$ and C_1 are found to be 362 bands per mm and 0.0491 deg^{-1/2}, respectively. Significantly this constant has the same dimension and is very nearly equal to that appearing in eq 2. Thus the temperature (405°K) at which theoretically slip would occur in a very small number of bands corresponds closely to that for zero shear hardening.

The marked similarity in the dependence of shear hardening and density of slip bands on temperature indicates that a high shear hardening coefficient at low temperatures is associated with a more widespread distribution of the deformation by slip. Thus, for a given amount of extension the total amount of shear in each slip band at the low temperature must be less than in those at the higher temperatures. This suggests that there is a maximum amount of shear possible within each slip band which is dependent on temperature and which controls the distribution of slip. Furthermore, it is possible that above 420°K a large portion of the deformation may occur by a mechanism different from what might be conventionally referred to as slip.

Summary and Conclusions

Determinations of critical resolved shear stress and coefficient of shear hardening were made at four temperatures in the range 77° to 353°K. Both properties were found to increase with a decrease in temperature and were consistent with the Schmid law of critical shear stress governing the initiation of the slip process. The density of slip bands also was found to increase with decreasing temperature in a manner similar to the shear hardening coefficient. This indicates that the high rate of shear hardening at low temperatures is associated with a more widespread distribution of deformation by slip. With an increase in the extent of distribution, the total amount of shear in each slip band must be less

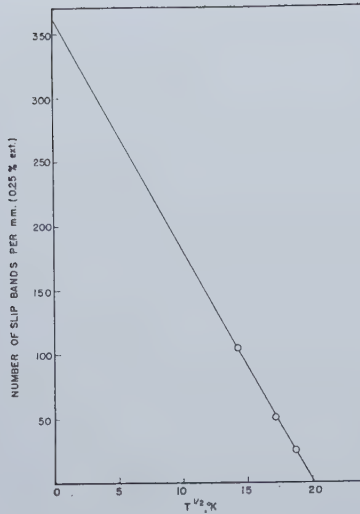


Fig. 22—Effect of temperature on the density of slip bands, N vs. $T^{1/2}$.

than in those formed at the higher temperatures for a given amount of extension. This suggests a maximum amount of shear within the slip band which is dependent on temperature.

Measurements of slip bands after small extensions (0.2 pct) at room temperature showed that an increase in strain hardening was accompanied by the appearance of new glide planes between the ones first observed. Plots of the density of slip bands against strain or shear stress gave curves showing small plateaus or parabolas, which are attributed to different orders of imperfection structures of the lineage type. In all cases, the first plateau was associated with the end of the Miller "yield-point elongation zone."

Microscopic observations on the appearance of slip bands disclosed that, at the early stages of plastic flow, slip manifests itself as segmented lines, the ends of which disappear in their paths through the crystal. This characteristic of slip was more pronounced at the lower temperatures.

Experiments on etched and unetched specimens, electrolytically polished with a solution of nitric acid and methyl alcohol, showed that the resulting oxide film did not have a disturbing effect on the critical shear stress, nor on the character and distribution of slip bands. Several slip systems were observed in the plastic deformation of these crystals, and their very existence suggests that the slip process is microscopically complex.

An analysis was given of the influence of temperature upon the critical resolved shear stress, the coefficient of shear hardening and the density of slip bands. The critical shear stress was found to decrease exponentially with an increase in temperature, which indicated a value of activation energy for plastic flow equal to 300 cal per g-atom, while the coefficient of shear hardening and the density of slip bands were found to decrease parabolically with increasing temperature.

Acknowledgments

The authors wish to extend their gratitude to W. R. Hibbard, Jr., of the Metallurgical Faculty, for his helpful criticism throughout the course of this investigation, and to C. T. Lane, of the Physics Department, for his encouragement and assistance with the low-temperature phase of the experiments. Thanks are also due to the Aluminum Company of America for cooperation in supplying the high-

purity aluminum used, and to Yale University for financial assistance.

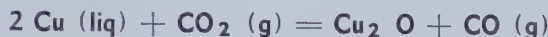
References

- ¹ E. Schmid and W. Boas: *Kristallplastizität*. 1935. Berlin. J. Springer.
- ² K. Yamaguchi: The Slip-Bands Produced when Crystals of Aluminum are Stretched, I—Extension at Room Temperature. *Sci. Papers. Inst. Phys. Chem. Res. Tokyo* (1928) **8**, 289; II—Extension at High (and Low) Temperatures. (1929) **9**, 277.
- ³ R. Becker: The Plasticity of Amorphous and Crystalline Solids. *Physik. Zeitz.* (1926) **26**, 919.
- ⁴ W. Kauzmann: Flow of Solid Metals from the Standpoint of the Chemical-rate Theory. *Trans. AIME* (1941) **143**, 57.
- ⁵ P. W. Bridgman: Certain Physical Properties of Single Crystals of Tungsten, Antimony, Bismuth, Cadmium, Zinc and Tin. *Proc. Amer. Acad. Arts and Sci.* (1925) **60**, 305; (1923) **58**, 165.
- ⁶ A. B. Greninger: Determination of Orientation of Metallic Crystals by Means of Back-Reflection Laue Photographs. *Trans. AIME* (1935) **117**, 61.
- ⁷ M. J. Buerger: The Lineage Structure of Crystals. *Ztsch. Krist.* (1934) **89**, 193.
- ⁸ P. Lacombe and L. Beaujard: The Application of Etch-Figures on Pure Aluminum (99.99%) to the Study of Some Micrographic Problems. *Jnl. Inst. Metals* (1947) **74**, 1.
- ⁹ R. F. Miller: Creep and Twinning in Zinc Single Crystals. *Trans. AIME* (1937) **122**, 176.
- ¹⁰ S. J. Rosenberg: *Jnl. Res. Bur. Stds.* (Dec. 1940) **25**, 673.
- ¹¹ U. Dehlinger: Submicroscopic Study of Metals. *Physik. Zeitz.* (1933) **34**, 836.
- ¹² R. F. Miller and W. E. Milligan: Influence of Temperature on Elastic Limit of Single Crystals of Aluminum, Silver and Zinc. *Trans. AIME* (1937) **124**, 229.
- ¹³ W. Boas and E. Schmid: Dependence of Crystal Plasticity on Temperature, III—Aluminum. *Ztsch. Physik.* (1931) **71**, 703.
- ¹⁴ W. Boas and E. Schmid: Dependence of Crystal Plasticity of Crystals of Cadmium and Zinc upon Temperature. *Ztsch. Physik.* (1930) **61**, 767; Dependence of the Critical Thrust in Cadmium Crystals upon the Temperature. *Ztsch. Physik.* (1929) **57**, 575.
- ¹⁵ M. Georgieff and E. Schmid: The Tenacity and Plasticity of Bismuth. *Ztsch. Physik.* (1926) **36**, 759.
- ¹⁶ E. Schmid: Plastic Deformation of Magnesium Crystals. *Ztsch. Elektrochem.* (1931) **37**, 447.
- ¹⁷ A. W. McReynolds: Plastic Deformation Waves in Aluminum. *Trans. AIME*, **185**, 32; *Jnl. Met.* (Jan. 1949) TP 2499E.
- ¹⁸ T. Sutoki: On the Serrated Elongation in Different Metals. *Sci. Rept. Tokoku Imp. Univ.* (1941) **29**, 673.
- ¹⁹ J. E. Dorn, A. Goldberg and T. E. Tietz: Effect of Thermal-Mechanical History on the Strain Hardening of Metals. *Trans. AIME* (1949) **180**, 205; *Met. Tech.* (Sept. 1948) TP 2445 E.
- ²⁰ W. Boas and E. Schmid: Dependence of Crystal Plasticity of Crystals of Cadmium and Zinc upon Temperature. *Ztsch. Physik.* (1930) **61**, 767.
- ²¹ W. Fahrenhorst and E. Schmid: The Temperature Coefficient of Crystal Plasticity. *Ztsch. Physik.* (1930) **64**, 845.
- ²² M. C. Crussard: Slip in High Purity Aluminum Crystals. *Rev. Met.* (1945) **42**, 286.
- ²³ E. N. da C. Andrade and R. Roscoe: Glide in Metal Single Crystals. *Proc. Phys. Soc.* (1939) **49**, 152.
- ²⁴ K. Greenland: Slip-Bands on Mercury Single Crystals. *Proc. Roy. Soc. (London)* (1937) **163A**, 28.
- ²⁵ R. Maddin, C. H. Mathewson, and W. R. Hibbard, Jr.: The Active Slip Systems in the Simple Axial Extension of Single Crystalline Alpha Brass. *Trans. AIME*, **185**, 529; *Jnl. Met.* (Aug. 1949) TP 2658E.
- ²⁶ C. Zener and J. H. Hollomon: Effect of Strain Rate upon Plastic Flow of Steel. *Jnl. Appl. Phys.* (1944) **15**, 22.
- ²⁷ C. Crussard: Creep and Fatigue as Affected by Grain Boundaries. *Metal Treatment* (1947) **149**.

Equilibrium in the Reaction of Carbon Dioxide with Liquid Copper from 1090° to 1300°C

by D. J. Girardi and C. A. Siebert

A study has been made of the equilibrium in the reaction of carbon dioxide with liquid copper. The equation for the reaction may be written as follows:



The equilibrium constant for this reaction was determined from 1090° to 1300° C.

PRACTICALLY every metallurgical process involves, at some stage or another, the contact of a metal with a gas. Because of this, gas-metal reactions are of great practical importance and have been subjected to numerous investigations.

It has long been recognized that the presence of cuprous oxide in liquid copper has an important effect on its casting characteristics and physical properties. This has led to the desirability of determining the quantitative relationships between cuprous oxide in the liquid copper and the usual gases present during processing. Such data are not only of practical importance but also of a theoretical interest in that they provide a means of applying the principles of physical chemistry to problems in applied metallurgy.

The object of this investigation was to determine the quantitative relationship at equilibrium between the gases carbon monoxide and carbon dioxide and the cuprous oxide content of liquid copper. The reaction and its equilibrium constant may be expressed as follows:



$$K_1 = \frac{a_{\text{Cu}_2\text{O}} \times a_{\text{CO}}}{a_{\text{Cu}}^2 \times a_{\text{CO}_2}}$$

Here the underlined symbol Cu_2O designates cuprous oxide dissolved in liquid copper and (a) , the activity of the various constituents. The activities of carbon monoxide and carbon dioxide are assumed to be directly proportional to their re-

D. J. GIRARDI, Member AIME, is Metallurgist, Timken Roller Bearing Co., Canton, Ohio, and C. A. SIEBERT, Member AIME, is Professor of Metallurgical Engineering, University of Michigan, Ann Arbor, Mich. AIME Chicago Meeting, October 1950.

TP 2917 DE. Discussion (2 copies) may be sent to Transactions AIME before Dec. 15, 1950. Manuscript received April 14, 1950.

spective partial pressures and the activities of cuprous oxide and copper are taken to be proportional to their respective mol fractions. The equilibrium constant may then be expressed as follows:

$$K_2 = \frac{N_{\text{Cu}_2\text{O}} \times P_{\text{CO}}}{[N_{\text{Cu}}]^2 \times P_{\text{CO}_2}} \quad [2]$$

where N = mol fraction

The solubility of carbon monoxide and carbon dioxide in liquid copper is a rather controversial subject.¹⁻⁴ A review of the literature is given by O. W. Ellis.¹ It appears that carbon monoxide and carbon dioxide are both only very slightly, if at all, soluble in liquid copper.

Volskii and Slobodskoi⁵ determined the equilibrium between carbon monoxide, carbon dioxide, and liquid copper at 1100°C. Their results show a higher cuprous oxide content for a given CO/CO₂ ratio than found in the present work. The system hydrogen, water vapor, and liquid copper was investigated by Allen and Hewitt⁶ over the temperature range of 1090° to 1350°C. Equilibrium values for the system carbon monoxide, carbon dioxide, and liquid copper calculated from these data agree reasonably well with the present work.

Materials and Procedure

The copper used was oxygen free, designated as OF and analyzed as 99.98 pct copper with no appreciable amount of any one impurity based upon spectrographic determinations. The carbon dioxide was cylinder gas averaging about 99.95 pct CO₂ with air as the major impurity. The carbon monoxide was produced by passing carbon dioxide over heated charcoal. Alundum combustion boats were used as containers for the liquid copper. No appreciable reaction took place between the copper and the alumina. This was evident from the fact that the copper sample after a run did not ordinarily adhere to the bottom of the boat and that the

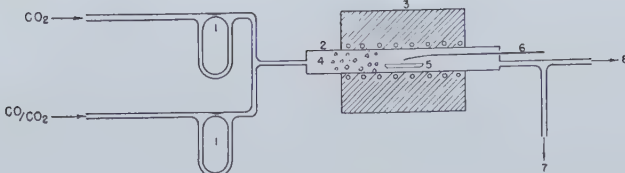


Fig. 1—Diagram of apparatus.

1. Flowmeter.
2. Refractory tube.
3. Furnace.
4. Refractory packing.
5. Alundum boat.
6. Thermocouple.
7. Gas analysis.
8. Exhaust.

alumina showed no indication of appreciable attack, only slight discoloration.

The general experimental procedure involved passing, at a given temperature, a constant mixture of carbon monoxide and carbon dioxide over the liquid copper until equilibrium was established. A schematic diagram of the apparatus is shown in fig. 1. Carbon dioxide gas from two tanks was passed as separate streams through suitable drying trains. One of the carbon dioxide streams then was taken through a flow meter and to the reaction furnace. The other stream of carbon dioxide was passed through a charcoal furnace, a mechanical separator to remove entrained dust, a drying train, a flow meter and then, forming a common stream with the gas from the other tank, to the reaction furnace. The rate of gas flow through the charcoal furnace and its temperature could be readily adjusted to give the desired carbon monoxide content in the final gas mixture. The entrance end of the reac-

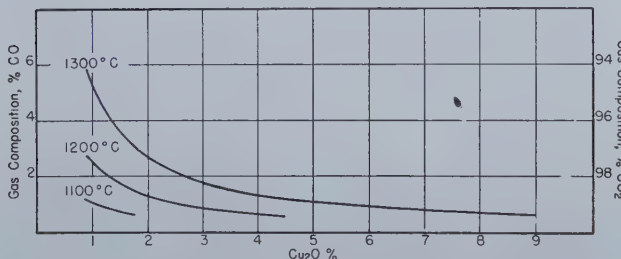


Fig. 2—Effect of gas composition on cuprous oxide content of copper at various temperatures.

tion furnace tube was packed with refractory material to preheat the gases. Temperature was measured with a platinum-platinum-rhodium thermocouple positioned over the center of the alundum boat and was controlled in general within $\pm 2^\circ\text{C}$ during a run. A special bulbous gas burette⁷ was

Table I—Data Obtained during a Typical Run

Run No.	Time	Temp, °C	CO, Pct	CO ₂ , Pct	Cu ₂ O, Pct
In	8:15	1,181			
	9:15	1,180	1.07	98.93	
Out	10:00	1,180	1.02	98.98	
	10:45	1,179	1.06	98.94	
		Avg. 1.05	Avg. 98.95	0.210	

Table II—Time Necessary to Attain Equilibrium from Low Oxygen Side at 1120°C

Run No.	Time at Temp	CO, Pct	CO ₂ , Pct	Cu ₂ O, Pct	K ₂
1	20 min	1.20	98.80	0.056	3.0×10^{-6}
2	40 min	1.35	98.65	0.071	4.3×10^{-6}
3	1 hr	1.20	98.80	0.103	5.6×10^{-6}
4	2 hr	1.16	98.84	0.101	5.3×10^{-6}

connected to the exit gas stream permitting gas analysis to be run at will. The system was maintained under slight positive pressure.

In making a run, 30 g of copper suitably cleaned was placed in an alundum boat which was inserted into the cool end of the furnace tube. Gas flow of the desired analysis was started and allowed to flush out the system while the reaction furnace was being brought to the desired temperature. The sample was then pushed into the furnace. Temperature and gas analysis were checked continually throughout the run but were recorded only at definite intervals. After the desired time at temperature had elapsed, the sample was moved to the air-cooled section of the furnace tube, where it rapidly solidified. The sample was allowed to remain in contact with the furnace gases until it reached a

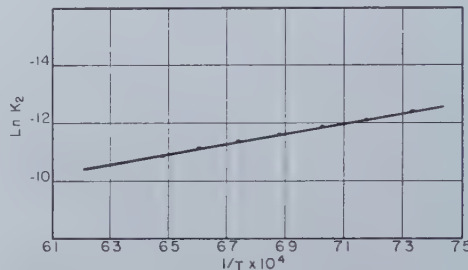


Fig. 3—Effect of temperature on equilibrium constant

$$K_2 = \frac{N_{\text{Cu}_2\text{O}} \times P_{\text{CO}}}{[N_{\text{Cu}}]^2 \times P_{\text{CO}_2}}$$

convenient handling temperature and then was quenched into water. A typical run is shown in table I.

The oxygen contents of the copper samples were determined by absorbing and weighing the H₂O formed in the standard hydrogen reduction method.^{8,9} The analytical results were further checked by determining the decrease in weight of the copper samples. The results obtained by the above two methods checked within a ± 0.001 pct oxygen (± 0.009 pct Cu₂O).

Experimental Results

Series of runs were made at 1120° and 1240°C to establish the time necessary to attain equilibrium. At 1120°C the equilibrium was approached from both the low and the high oxygen sides, while at 1240°C equilibrium was attained from the low oxygen side alone. These data are given in tables II,

Table III—Time Necessary to Attain Equilibrium from High Oxygen Side at 1120°C

Run No.	Time at Temp	CO, Pct	CO ₂ , Pct	Cu ₂ O, Pct	K ₂
6	0	1.10	98.90	0.340	
7	30 min	1.10	98.90	0.147	7.3×10^{-6}
8	1 hr	1.23	98.77	0.115	6.4×10^{-6}
9	2 hr	1.07	98.93	0.104	5.0×10^{-6}
	4 hr	1.30	98.70	0.109	6.4×10^{-6}

Table IV—Time Necessary to Attain Equilibrium from Low Oxygen Side at 1240°C

Run No.	Time at Temp	CO, Pct	CO ₂ , Pct	Cu ₂ O, Pct	K ₂
26	1 hr	0.86	99.14	0.357	13.8×10^{-6}
27	1 1/2 hr	0.65	99.35	0.472	13.8×10^{-6}
28	2 1/2 hr	0.72	99.28	0.424	13.7×10^{-6}
29	4 hr	0.71	99.29	0.513	16.4×10^{-6}

Table V—Summarized Equilibrium Data from 1090° to 1300°C

Run No.	Temp., °C	CO, Pct	CO ₂ , Pct	Cu ₂ O, Pct	K ₂	ln K ₂
10	1,090	1.53	98.47	0.040	2.8 × 10 ⁻⁶	— 12.79
11	1,090	1.57	98.43	0.097	6.9 × 10 ⁻⁶	— 11.88
12	1,090	1.58	98.42	0.058	4.0 × 10 ⁻⁶	— 12.43
13	1,090	1.59	98.41	0.067	4.8 × 10 ⁻⁶	— 12.25
					Avg. — 12.34	
3	1,120	1.20	98.80	0.103	5.6 × 10 ⁻⁶	— 12.09
4	1,120	1.16	98.84	0.101	5.3 × 10 ⁻⁶	— 12.15
5	1,120	19.4	80.60	0.009	9.7 × 10 ⁻⁶	
7	1,120	1.23	98.77	0.115	6.4 × 10 ⁻⁶	— 11.96
8	1,120	1.07	98.93	0.104	5.0 × 10 ⁻⁶	— 12.21
9	1,120	1.30	98.70	0.109	6.4 × 10 ⁻⁶	— 11.96
					Avg. — 12.07	
14	1,150	0.83	99.17	0.184	6.9 × 10 ⁻⁶	— 11.88
15	1,150	1.05	98.95	0.150	7.1 × 10 ⁻⁶	— 11.86
16	1,150	0.95	99.05	0.178	7.6 × 10 ⁻⁶	— 11.79
17	1,150	1.01	98.99	0.190	8.6 × 10 ⁻⁶	— 11.66
					Avg. — 11.80	
18	1,180	1.32	98.68	0.158	9.4 × 10 ⁻⁶	— 11.58
19	1,180	1.16	98.84	0.174	9.1 × 10 ⁻⁶	— 11.61
20	1,180	1.14	98.86	0.204	10.5 × 10 ⁻⁶	— 11.46
21	1,180	1.05	98.95	0.210	9.9 × 10 ⁻⁶	— 11.52
					Avg. — 11.54	
22	1,210	1.44	98.56	0.190	12.4 × 10 ⁻⁶	— 11.30
23	1,210	1.25	98.75	0.197	11.1 × 10 ⁻⁶	— 11.41
24	1,210	1.12	98.88	0.222	11.2 × 10 ⁻⁶	— 11.40
25	1,210	1.08	98.92	0.247	12.0 × 10 ⁻⁶	— 11.33
					Avg. — 11.36	
26	1,240	0.86	99.14	0.357	13.8 × 10 ⁻⁶	— 11.19
27	1,240	0.65	99.35	0.472	13.8 × 10 ⁻⁶	— 11.19
28	1,240	0.72	99.28	0.424	13.7 × 10 ⁻⁶	— 11.20
29	1,240	0.71	99.29	0.513	16.4 × 10 ⁻⁶	— 11.02
					Avg. — 11.15	
30	1,270	4.22	95.78	0.105	20.6 × 10 ⁻⁶	— 10.79
31	1,270	2.32	97.68	0.211	22.3 × 10 ⁻⁶	— 10.71
32	1,270	1.72	98.28	0.250	19.5 × 10 ⁻⁶	— 10.85
33	1,270	1.34	98.66	0.322	19.5 × 10 ⁻⁶	— 10.85
					Avg. — 10.80	
34	1,300	1.22	98.78	0.403	22.2 × 10 ⁻⁶	— 10.72
35	1,300	2.50	97.50	0.276	31.6 × 10 ⁻⁶	— 10.36
36	1,300	3.16	96.84	0.223	32.4 × 10 ⁻⁶	— 10.34
37	1,300	4.78	95.22	0.139	31.1 × 10 ⁻⁶	— 10.38
					Avg. — 10.45	

III, and IV. The values of the equilibrium constant at 1120°C indicate that equilibrium was reached with equal ease from either the low or high oxygen sides in approximately 1 hr. At 1240°C, with final Cu₂O contents over four times greater than those at 1120°C, equilibrium was attained in less than 1 hr. Based on the above results, the time at temperature for the remainder of the runs was set at 2½ hr for temperatures below 1240°C and at 1¾ hr at 1240°C and above.

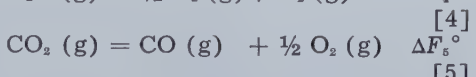
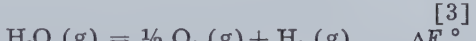
The equilibrium constant was determined in the temperature range from 1090° to 1300°C at 30°C intervals. A summary of these data is shown in table V. The nature of the reaction in most of this temperature range is such as to impose experimental limitations on the opportunity of varying the gas compositions of the runs. The carbon monoxide content of the gas phase and the resulting oxygen content of the copper had to be held in such a range as to minimize the effect of experimental error in their determinations. Relatively low carbon monoxide contents in the gas phase, although yielding

desirably high oxygen values in the copper, would appreciably effect the degree of error in determining the gas composition. Similarly relatively high carbon monoxide contents in the gas phase would result in oxygen values too low for reasonable accuracy as indicated in run 5. At the higher temperatures the gas composition was varied over the approximate range of 1 to 5 pct carbon monoxide. The cuprous oxide content of liquid copper for various gas compositions and at several temperatures was calculated from the equilibrium constants and is shown in fig. 2.

The average values for ln K₂ at each temperature are plotted against the reciprocal of the absolute temperature in fig. 3. The data give a reasonably straight line from which the value of ΔH for reaction 1 is found to be 34,800 cal per g mol of cuprous oxide.

Comparison of Results

The value of ΔF₁° for reaction 1 may be computed from the data of Allen and Hewitt⁶ as follows:



$$\text{Then } \Delta F_1^{\circ} = \Delta F_s^{\circ} - \Delta F_4^{\circ} + \Delta F_5^{\circ}$$

The values of ΔF₄° and ΔF₅° were computed from the free energy equations for these reactions.¹⁰ The values of ln K₂ obtained in this investigation are compared with those calculated from Allen and Hewitt's data in table VI. The value of ln K₂ at 1100°C computed from the data of Volskii and Slobodskoi is also shown. There is no apparent explanation for the discrepancy between the value at 1100°C obtained in this investigation and that obtained by Volskii and Slobodskoi. On the other hand, the values obtained in this investigation agree reasonably well with those calculated from the data of Allen and Hewitt.

Summary

1. The equilibrium for the reaction 2 Cu (liq) + CO₂ (g) = Cu₂O + CO (g) has been determined over the temperature range of 1090° to 1300°C.

2. The heat of reaction over this temperature range was found to be 34,800 cal per g mol of cuprous oxide.

References

- O. W. Ellis: *Trans. AIME* (1933) **106**, 487.
- H. Sieverts and W. Krumbhaar: *Ztsch. für physik. Chemie*. (1910) **74**, 277.
- A. Sieverts: *Ztsch. f. Metallkunde*. (1929) **21**, 37.
- K. Iwase: *Sci. Repts. Tohoku Imp. Univ.* (1926) **15**, (1) 531.
- A. N. Volskii and Ya. Ya. Slobodskoi: *Tsvetnye Metal.* (1936) **1**, 102.
- N. P. Allen and T. Hewitt: *Jnl. Inst. of Metals* (1933) **51**, (1) 257.
- A. H. White: *Gas and Fuel Analysis*. McGraw-Hill Book Co.
- W. H. Bassett and H. A. Bedworth: *Trans. AIME* (1926) **73**, 784.
- R. Keffer: *Methods in Non-Ferrous Metallurgical Analysis*. McGraw-Hill Book Co.
- K. K. Kelley and C. T. Anderson: *Contributions to the Data on Theoretical Metallurgy*. U. S. Bur. Mines Bull. 384 (1935).
- C. E. Ransley: *Jnl. Inst. Metals* (1939) **65**, (2) 147.

Table VI—Comparison of Results for ln K₂

Temp., °C	ln K ₂		
	This Investigation	Allen and Hewitt*	Volskii and Slobodskoi
1,100	— 12.25	— 10.68	— 6.22
1,150	— 11.80	— 10.25	
1,250	— 11.00	— 9.50	

* Calculated values.

The Effect of Sodium Contamination on Magnesium-Lithium Base Alloys

by P. D. Frost, J. H. Jackson, A. C. Loonam, and C. H. Lorig

THIS paper describes (1) the effect of sodium on the tensile ductility of magnesium-lithium base alloys, and (2) the precautions necessary to avoid sodium contamination.

Effect of Sodium on Properties

The harmful effect of sodium in magnesium-lithium base alloys has been recognized by other investigators.^{1,2} However, quantitative data on its

¹J. H. Jackson, P. D. Frost, A. C. Loonam, L. W. Eastwood, and C. H. Lorig; Magnesium-Lithium Base Alloys—Preparation, Fabrication, and General Characteristics. *Trans. AIME* 185, 149-168. *Jnl. Met.* (Feb. 1949) TP 2534E.

²W. Hume-Rothery, G. V. Raynor, and E. Butchers: Equilibrium Relations and Some Properties of Magnesium-Lithium and Magnesium-Lithium-Silver Alloys. *Jnl. Inst. Metals.* (1945) 71, 589-601.

effect have not hitherto been published.

The effect of sodium on the ductility of an 87 pct Mg-9 pct Li-4 pct Zn alloy is shown in fig. 1. The sodium was introduced by adding sodium chloride to the flux, which consisted of 50 pct LiCl-50 pct KCl. Moderately high ductility was obtained at an indicated sodium content of about 0.05 pct. Actually, the value probably was less than 0.05 pct, because analyses of the lithium, which were more accurate than those of the alloy, indicated that the highest ductility was obtained when its sodium content was 0.02 pct or less. In fact, in alloys having somewhat greater strength than this particular composition, the sodium content of the lithium must be under 0.01 pct to avoid embrittlement.

The effect of sodium on the ductility of several alloys having fairly low strength levels is shown in fig. 2. These alloys were melted with a flux containing 75 pct LiCl-25 pct LiF, to which various quantities of sodium chloride had been added. Sodium had no significant effect in pure magnesium but markedly decreased the ductility of the magnesium-lithium-zinc alloy, even though the alloy contained only 3 pct Li. As the lithium content of the binary

P. D. FROST and J. H. JACKSON, Members AIME, are Research Engineer and Supervisor, respectively, Battelle Memorial Institute, Columbus, Ohio; A. C. LOONAM, Member AIME, is Consultant, Deutsch and Loonam, New York, N. Y.; and C. H. LORIG, Member AIME, is Assistant Director, Battelle Memorial Institute.

AIME Chicago Meeting, October 1950.

TP 2923 E. Discussion (2 copies) may be sent to Transactions AIME before Dec. 15, 1950. Manuscript received Feb. 15, 1950; revision received July 12, 1950.

The work described in this paper was done in connection with an alloy development project now in progress at Battelle Memorial Institute. It was carried out during the period 1942 to 1947, and the paper was prepared originally in October 1948.

alloys was increased, the ductility of the sodium-free alloys also increased. However, the effect of sodium on ductility became progressively more pronounced.

Sodium raised the minimum hot-rolling temperatures, particularly those of the high-strength alloys, but its effect, in this respect, was less critical than its effect on tensile ductility. For optimum cold rollability, a low-sodium content was required. No deleterious effect of sodium on the stability of properties at slightly elevated temperatures was found.

Control of Sodium in the Alloys

Optimum ductility is obtained in the magnesium-lithium base alloys when sodium-free materials are used. Commercial lithium was formerly the chief source of contamination. Now purified lithium is usually available. When lithium of ordinary purity is used, the effects of sodium can be minimized by using a flux consisting of 75 pct LiCl-25 pct LiF. Bubbling nitrogen through the melt also helps remove sodium.

The damaging influence of sodium on the ductility of the magnesium-lithium base alloys was observed very early in the alloy development program. The discovery came about as a result of chemical analyses made on the lithium used in the alloys. Ductile alloys had been made from lithium containing about 0.2 pct Na, whereas the lithium used in the brittle alloys contained about 0.9 pct Na.

The first magnesium-lithium alloys were melted under commercial fluxes ordinarily used in melting magnesium alloys. These fluxes were unsuited for scavenging the contaminating sodium, and the resulting alloys were not ductile. Next, a flux containing 50 pct KCl-50 pct LiCl was tried. This was somewhat more effective but still was not satisfactory. After a number of different experimental fluxes had been investigated, one containing 75 pct LiCl-25 pct LiF was adopted. This flux made it possible to obtain good ductility in the alloys. The

Table I. Effect of Melting Flux on Mechanical Properties of an 87 pct Mg-9 pct Li-4 pct Zn Alloy*

Flux	Elongation, Pct	Reduction of Area, Pct	Yield Strength, psi	Tensile Strength, psi
Commercial	3.5	8.0	25,100	29,300
50 pct KCl and 50 pct LiCl	8.5	15.0	25,800	30,200
75 pct LiCl and 25 pct LiF	33.5	62.3	26,900	31,500

* Commercial-purity melting materials were used. The sodium content of the lithium was 0.9 pct. Test data were averaged from 5 heats for each flux.

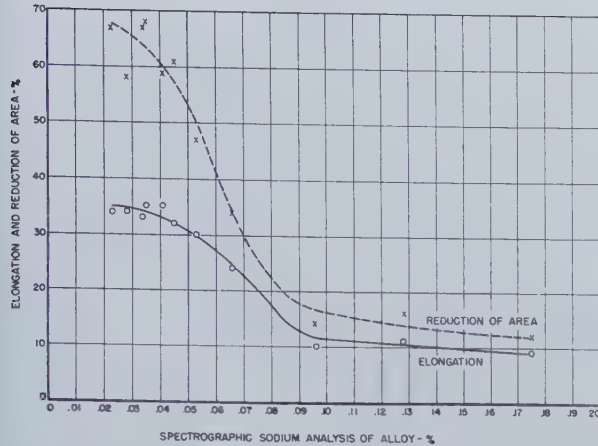


Fig. 1—Effect of sodium content on ductility of an 87 pct Mg-9 pct Li-4 pct Zn alloy.

effects of the three types of fluxes on the tensile properties of an alloy containing 87 pct Mg-9 pct Li-4 pct Zn are shown in table I. To obtain maximum ductility it was necessary to use the LiCl-LiF flux in quantities weighing at least 35 pct of the metallic charge.

Other methods of reducing the sodium content of the 87 pct Mg-9 pct Li-4 pct Zn alloy were also found. The effect of one of these methods, bubbling nitrogen gas through the melt, is shown in fig. 3. In this experiment, three heats of this alloy were prepared from lithium which showed, respectively, low, intermediate, and high sodium analyses. The heats were melted with the 50 pct LiCl-50 pct KCl flux. Nitrogen was bubbled through the melt for a predetermined length of time and part of the heat poured off. Then the bubbling was resumed and the process repeated. The ductility of the extruded alloy depended upon the lithium used and the duration of the nitrogen treatment. Thus, nitrogen, bubbled through the melts for 5 min, had a beneficial effect on the ductility of the two least ductile alloys but no significant effect on the low-sodium alloy. When nitrogen was bubbled through the melts for 20 min, the less ductile alloys were improved sufficiently to compare favorably with the most ductile alloy. Detailed tests showed that a minimum bubbling period of about 20 min was required for optimum ductility, but that a 30-min period afforded no significant advantage. Other gases, such as argon or chlorine, were of some benefit but were not so effective as nitrogen.

Also of interest in fig. 3 is the effect of holding a graphite rod in a heat of the 87 pct Mg-9 pct Li-4 pct Zn alloy. The mechanism by which the graphite rod improved the ductility of the alloy was not investigated. It would appear that sodium was absorbed by the graphite.

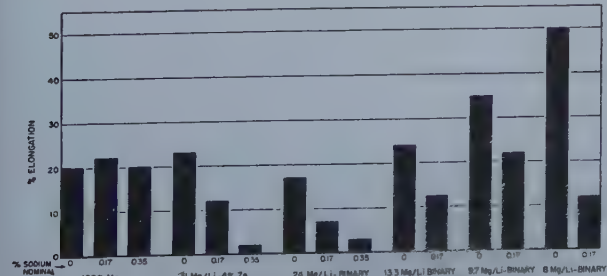


Fig. 2—Effect of sodium content on ductility of various alloys.

Of the devices described above for controlling the sodium content in the magnesium-lithium base alloys, the most convenient and most effective was the use of the 75 pct LiCl-25 pct LiF flux. However, as higher strength alloys, which were more sensitive to sodium contamination, were developed, this flux was no longer adequate for reducing the sodium content to the value where the ductility of the alloys was no longer impaired. It became necessary to purify further the commercial lithium before using it in alloys. This was accomplished by distilling the sodium from the lithium at temperatures around 1200°F and pressures of 0.03 mm of mercury. By this method, the sodium content of the lithium was reduced to 0.01 pct or under.

When alloys were prepared from lithium of this low-sodium content, the purity of the lithium chloride-lithium fluoride flux was an important factor. In some instances, it was better to eliminate the flux and to substitute an argon atmosphere instead to secure maximum ductility. Melting by this method is, of course, less convenient than melting in an open crucible with flux. Furthermore, it is more difficult

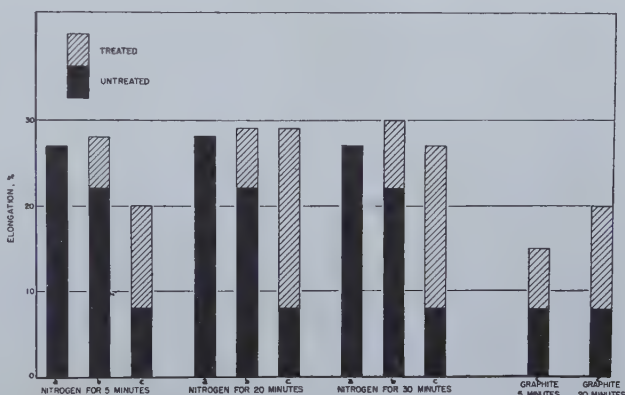


Fig. 3—Effect on ductility of bubbling nitrogen gas through or holding graphite rod in 87 pct Mg-9 pct Li-4 pct Zn alloy.

- a. Low-sodium alloy.
- b. Intermediate sodium alloy.
- c. High-sodium alloy.

to produce ingots free from dross inclusions when flux is not used. For these reasons, the majority of the alloys were melted with flux and considerable care was taken that only low-sodium materials were used.

Summary

Magnesium-lithium base alloys are embrittled by very small amounts of sodium. Purification of lithium and selection of fluxes to minimize sodium contamination are required for high-quality alloys.

When purified lithium is not available, reduction of the sodium content of the alloys can be accomplished by the use of a suitable flux or by bubbling nitrogen through the melt. Holding a graphite rod in the melt is also effective.

The best quality alloys are produced by using purified lithium and low-sodium flux ingredients.

Acknowledgments

The authors express their appreciation to the Mathieson Chemical Corp. and the Navy Department, Bureau of Aeronautics, who jointly sponsored the alloy development and permitted this phase of the work to be published. They also wish to thank the many individuals who helped plan and carry out the work.

The Structure of Intermediate Phases in Alloys of Titanium with Iron, Cobalt, and Nickel

by Pol Duwez and Jack L. Taylor

The crystal structure of the intermediate phases in the binary systems of titanium with iron, cobalt, and nickel has been studied and the results compared with those previously published. The phases of the Ti_2X type are face-centered cubic with 96 atoms per cell, and the TiX phases are body-centered cubic. $TiFe_2$ and $TiCo_2$ are hexagonal but not isomorphous. The nickel-rich phase has the composition $TiNi_3$ and is hexagonal.

PARTIAL phase diagrams of titanium with iron, cobalt, and nickel have been established by previous investigators.¹⁻⁸ These diagrams seem to be reliable, at least for concentrations of titanium ranging from 0 to about 50 at. pct. More recently, Long and his collaborators have presented a tentative titanium-nickel diagram covering the titanium-rich side.⁴ These various studies indicate that in each system three intermediate phases exist and correspond to the compositions Ti_2X , TiX , and TiX_2 (or TiX_3). The purpose of this paper is to review the available information on the crystal structure of these phases and to give the results of additional X-ray diffraction studies.

Previous Work

A summary of the work of Wallbaum and his collaborators⁵⁻⁷ is presented in table I. The first intermediate phase on the titanium-rich side of the three systems, with iron, cobalt, and nickel, is of the Ti_2X type and has a face-centered cubic structure. Although it is stated that the unit cell contains 96 atoms,⁵ no lattice parameters are given. The second phase is centered around the compositions TiX for the three systems. The crystal structure of this phase is mentioned in a short note⁸ as being body-centered cubic ($CsCl$ type), but no parameters are given.

The analogy between the three systems, which is perfect as far as the two phases of the type Ti_2X and TiX are concerned, disappears at the titanium-poor end of the diagrams. In the system titanium-

iron, $TiFe_2$ has an hexagonal ($MgZn_2$ type) structure with the parameters given in table I. The existence of $TiFe_3$ has also been reported⁹ (table I) but was questioned by other investigators² and is also refuted by the present study.

In the system titanium-cobalt, a phase corresponding to the composition $TiCo_2$ has been investigated by Wallbaum and Witte⁶ who claim that the structure is cubic ($MgCu_2$ type) for alloys slightly deficient in cobalt and hexagonal ($MgNi_2$ type) for alloys slightly deficient in titanium. The parameters of the two phases are given in table I. In the system titanium-nickel, the nickel-rich phase corresponds to the composition $TiNi_3$ and has been described as hexagonal⁷ with the parameters given in table I.

The present investigation was initiated for the purpose of filling in the gaps in the knowledge concerning the structure of the various phases summarized in table I. Since the titanium used by Wallbaum and his collaborators was only 95 pct pure,¹ it was found desirable to redetermine the lattice parameters of the alloys prepared with a

POL DUWEZ and JACK L. TAYLOR, Members AIME, are Associate Professor of Mechanical Engineering and Chief of the Materials Section, and Research Engineer, respectively, Jet Propulsion Laboratory, California Institute of Technology, Pasadena, Calif.

AIME Chicago Meeting, October 1950.

TP 2922 E. Discussion (2 copies) may be sent to Transactions AIME by Dec. 15, 1950. Manuscript received April 14, 1950; revision received July 10, 1950.

Table I. Crystal Structure Data for Ti (Fe, Co, Ni) Compounds

Compound	Previous Publications	This Investigation
Ti ₂ Fe Ti ₂ Co Ti ₂ Ni	FCC. 96 atoms per cell, no parameters (ref. 5)	FCC. $a = 11.305$. 96 atoms per cell FCC. $a = 11.283$. 96 atoms per cell FCC. $a = 11.310$. 96 atoms per cell
TiFe TiCo TiNi	BCC. A ₂ type (CsCl), no parameters (ref. 5)	BCC. (A ₂ type). $a = 2.969$. 2 atoms per cell BCC. (A ₂ type). $a = 2.988$. 2 atoms per cell BCC. (A ₂ type). $a = 2.980$. 2 atoms per cell
TiFe ₂	Hexag. C ₁₄ type (MgZn ₂). 12 atoms per cell. $a = 4.77$. $c = 7.79$. $c/a = 1.633$. (ref. 2)	Structure confirmed $a = 4.769$. $c = 7.745$. $c/a = 1.624$
TiFe ₃	Tetrag. D ₀₂₂ type (TiAl ₃). 16 atoms per cell. $a = 5.19$. $c = 8.15$. $c/a = 1.57$. (ref. 8)	No evidence of the existence of this phase
TiCo ₂ (Co rich)	Hexag. C ₆₈ type (MgNi ₂). 24 atoms per cell. $a = 4.715$. $c = 15.37$. $c/a = 1.57$. (ref. 6)	This structure confirmed for both Co rich and Co poor phases. $a = 4.720$. $c = 15.392$. $c/a = 3.261$
TiCo ₃ (Co poor)	Cubic C ₁₄ type (MgCu ₃). 24 atoms per cell. $a = 6.691$. (ref. 6)	No evidence for the existence of this structure
TiNi ₃	Hexag. D ₀₂₄ type (TiNi ₃). 16 atoms per cell. $a = 5.096$. $c = 8.304$. $c/a = 1.630$. (ref. 7)	Structure confirmed $a = 5.093$. $c = 8.276$. $c/a = 1.625$

metal of higher purity. Hence, all the alloys, including those for which previous work was apparently very complete, were reinvestigated.

X-ray Diffraction Technique

The metals used in preparing the alloys were received from various sources (table II). Spectrographic analyses were obtained for the iron, cobalt, and nickel powders. The approximate analysis given for titanium in table II is typical for the Bureau of Mines titanium powder.⁴

Most of the alloys were prepared by powder metallurgy methods. The metal powders were mixed in suitable proportions and then compacted in a cylindrical steel die $\frac{1}{2}$ in. in diam, under a pressure of 80,000 psi. The compacts, about $\frac{1}{4}$ in.

containing equal atomic proportions of titanium with iron, cobalt, or nickel (type TiX) were not homogeneous after sintering under the conditions indicated in table III. When the sintering temperature was increased, local melting of the specimens took place. This melting probably occurred in regions of the specimen where the composition corresponded to that of a low melting point eutectic in the phase diagram.

In order to avoid these difficulties, the alloys of the TiX type were first sintered at rather low temperature and then melted in a small thoria crucible in an atmosphere of pure helium. The crucible, about $\frac{1}{4}$ in. ID and 1 in. high, was placed inside another crucible of tungsten, about $\frac{3}{4}$ in. ID and $1\frac{1}{4}$ in. high. The tungsten crucible was heated by induction. Melting of the specimens TiFe, TiCo, and TiNi occurred in a range of temperature from 1400° to 1550°C . As soon as melting was observed, the power was shut off in order to minimize the reaction between the molten alloy and the crucible. Only a slight reaction was noticed for TiFe and TiNi, but TiCo proved to be very corrosive and several melts had to be made before a satisfactory specimen was obtained.

The X-ray diffraction measurements were carried out with a 14.32 cm powder camera, using $K\alpha$ cobalt radiation and also $K\alpha$ copper radiation for additional measurements on the titanium-nickel alloys. The film mount in the camera was the asymmetrical type; hence the exact diameter of the camera and the actual shrinkage of the film were not required for computing the interplanar spacings. Since an accuracy in lattice parameter measurements greater than 1 part in 2000 was not sought, no corrections were applied for absorption and eccentricity of the specimen.

Results: Ti₂Fe, Ti₂Co, and Ti₂Ni Phases

The X-ray diffraction patterns of these three phases were readily interpreted on the basis of a face-centered cubic lattice. A list of interplanar spacings for Ti₂Ni is given in table IV. The interplanar spacings for Ti₂Fe and Ti₂Co were practically the same as those given in table IV for Ti₂Ni and the difference could be noticed for only high values of (hkl) . The lattice parameters of the three phases

Table II. Source of Supply and Analysis of Raw Materials

Metal	Source of Supply	Analysis
Titanium	U.S. Bur. Mines	0.15 pct Fe 0.005 pct Si 0.30 pct Mg 0.1 - 0.2 pct O ₂ 0.036 pct Ca 0.7 pct H ₂ (taken from ref. 4)
Iron	Carbonyl iron, type L Charles Hardy, Inc.	0.05 pct Si Traces of 0.05 pct Mn Cu, Mo, Ti, 0.05 pct Ca and Cr 0.01 pct Ni
Cobalt	Charles Hardy, Inc.	0.5 pct Ni Traces of 0.1 pct Ca Mg, Mn, Cu, 0.05 pct Si and Al 0.05 pct Fe
Nickel	International Nickel Co.	0.05 pct Ca Traces of 0.05 pct Si Mn, Co, and 0.05 pct Fe Cu

thick, were then sintered at various temperatures for various lengths of time (table III). The sintering was done in a molybdenum-wound furnace placed inside the vacuum bell jar of a glass-coating vacuum unit. The pressure maintained during sintering was 10^{-4} mm of Hg or less.

The alloys rich in titanium (type Ti₂X) and those poor in titanium (type Ti₂X₃ or TiX₃) were homogeneous after sintering, the criterion for homogeneity being that all the reflections in the X-ray diffraction pattern were sharp and checked the spacings of the expected single phase. The alloys

were computed from these high (*hkl*) back-reflection lines, using the least-square method, and are given in table I. The density of the three phases Ti_2Fe , Ti_2Co , and Ti_2Ni were 5.49, 5.64, and 5.77 respectively, from which the number of molecules per cell was computed to be approximately 32 (96 atoms).

Because of the almost equal size of the iron, cobalt, and nickel atoms, it is not surprising that the lattice parameters of the three isomorphous phases of the Ti_2X types are very nearly the same. These lattice parameters, however, do not decrease in the sequence iron, cobalt, nickel, which would be expected on the basis of the atomic diameter of these three elements. This case is not unusual. A similar

three compounds, Ti_2Fe , Ti_2Co , or Ti_2Ni . It is probable that these three pseudo ternary systems will exhibit a great degree of similarity.

TiFe, TiCo, and TiNi Phases

The results of X-ray diffraction measurements confirmed the fact that these three phases have the body-centered CsCl type cubic structure with the parameters given in table I. As explained before, it was necessary to melt these alloys in order to obtain a homogeneous phase. In spite of this precaution, a few extra lines were still present in the powder patterns. These lines were very weak, however, and were identified as being the strongest lines of the Ti_2X phase. As a result of the presence of a small amount of Ti_2X , the TiX phase may have been slightly deficient in titanium. Since no attempt was made to determine accurately the width of the TiX phase, the lattice parameters given in table I may vary with composition.

The possibility of having an ordered structure in the three phases of the TiX type was investigated by maintaining specimens sealed in evacuated quartz tubes for 10 days at 650° and at 800°C. Although no noticeable reaction was found due to contact with silica, the powder used for diffraction studies was taken from the center portion of the specimens. After each of these treatments, the $TiCo$ phase still had the disordered body-centered cubic structure. Additional heat treatment of 20 days at 540°C also failed to induce ordering. The $TiFe$ phase behaved quite differently. After the 800°C treatment the structure was still disordered body-centered cubic, but after the 650°C treatment the phase had decomposed into a mixture of $TiFe_2$ and Ti_2Fe . A similar phenomenon was observed for the $TiNi$ phase, except that the decomposition into Ti_2Ni and $TiNi_3$ took place in the specimens heated at both 800° and 650°C.

From these somewhat cursory experiments it appears that the $TiCo$ phase is stable down to at least 540°C, but both $TiFe$ and $TiNi$ are stable only at high temperature. $TiFe$ decomposes during cooling into Ti_2Fe and $TiFe_2$. This reaction takes place between 800° and 650°C. $TiNi$ decomposes into Ti_2Ni

Table III. Data on Preparation of Alloys

Alloy	Treatment
Ti_2Fe	Sintered 4 hr in vacuum at 1000°C
Ti_2Co	Sintered 4 hr in vacuum at 1000°C
Ti_2Ni	Sintered 4 hr in vacuum at 925°C
$TiFe$	Sintered 4 hr in vacuum at 1000°C; melted in thorium crucible in helium atmosphere; then homogenized for 24 hr at 1000°C in evacuated fused silicon tube
$TiCo$	Sintered 4 hr in vacuum at 875°C; then same as $TiFe$
$TiNi$	Sintered 4 hr in vacuum at 800°C; then same as $TiFe$
$TiFe_2$	Sintered 4 hr in vacuum at 1000°C
$TiCo_2$	Sintered 4 hr in vacuum at 1000°C
$TiNi_3$	Sintered 4 hr in vacuum at 925°C

example is found in the three compounds $AlFe$, $AlCo$, and $AlNi$, for which the lattice parameters decrease in the order iron, nickel, and cobalt.

The similitude in the unit cells of the three phases Ti_2Fe , Ti_2Co , and Ti_2Ni leads to the conclusion that these three phases will most probably form an uninterrupted series of solid solutions. Consequently, iron, cobalt, and nickel probably will replace each other in all proportions in a phase of the form $Ti_2(Fe, Co, Ni)$. It follows that in the ternary diagrams involving titanium with any two of the three elements, iron, cobalt, and nickel, the titanium-rich corner may be considered as a pseudo ternary system between titanium and two of the

Table IV. Interplanar Spacings of Ti_2Ni , $TiFe_2$, $TiCo_2$, $TiNi_3$

Ti_2Ni				$TiFe_2$		$TiCo_2$		$TiNi_3$	
(<i>hkl</i>)	Spacing (kx)*	(<i>hkl</i>)	Spacing (kx)*	(<i>hkl</i>)	Spacing (kx)*	(<i>hkl</i>)	Spacing (kx)*	(<i>hkl</i>)	Spacing (kx)*
111	6.53 w	951-773	1.095 vw	100	4.14 vw	100	4.08 vw	100	4.38 vw
220	3.97 vw	666	1.087 vw	002	3.86 vw	101	3.93 vw	101	3.89 vw
222	3.26 w	775	1.019 vw	101	3.65 vw	004	3.85 vw	110	2.55 vw
400	2.83 vw	955-971	0.9886 w	110	2.38 m	102	3.63 vw	200	2.21 w
331	2.59 w	882	0.9847 w	103	2.19 s	105	2.41 vw	201	2.13 m
422	2.31 m	866	0.9697 w	112	2.03 s	110	2.36 w	004	2.07 m
333-511	2.17 s	10,62	0.9563 vw	201	1.99 s	106	2.17 m	202	1.95 s
440	2.00 m	12,00-884	0.9423 m	004	1.94 w	201-114	2.02 s	203	1.72 w
531	1.91 vw	11,51-777	0.9330 m	202	1.82 m	202	1.98 m	122	1.54 vw
442-600	1.88 w	12,22-10,64	0.9172 m	104	1.75 m	107-008	1.93 m	204	1.51 w
622	1.72 w	11,53-975	0.9090 vw	203	1.61 w	203	1.90 w	205	1.327 w
444	1.63 w	12,40	0.8935 vw	300	1.375 vw	204	1.80 w	220	1.273 m
551-711	1.59 w	10,82	0.8726 vw	123	1.336 m	108		206	1.171 w
642	1.51 w	13,11-11,55-11,71-993	0.8648 w	302	1.296 m	205	1.71 vw	401	1.093 vw
553-731	1.472 w	11,73-13,31-977	0.8456 w	205	1.240 m	206		224	1.085 m
800	1.413 vw	13,33-955	0.8277 vw	124	1.216 w	211	1.53 vw	402	1.066 m
733	1.382 w	888	0.8162 vw	220	1.191 m	213	1.48 w	207	1.044 w
660-822	1.334 m	13,51-11,75	0.8095 vw	312	1.098 w	214	1.42 vw	008	1.036 w
555-751	1.305 w	14,20-10,86	0.7997 w	313	1.048 w	300	1.362 vw	403	1.025 w
911-753	1.242 vw	14,22-10,10,2	0.7920 w	401	1.024 w	10,11-216	1.325 w	404	0.9723 vw
842	1.234 w	12,80	0.7842 w	224	1.016 w	209	1.308 w	226-412	0.9375 vw
931	1.185 vw			402	0.9983 vw	304-00,12	1.280 w	405	0.9182 vw
933-771-755	1.136 m			314	0.9872 vw	217	1.263 vw	421	0.8288 vw
862	1.109 vw			306-320	0.9466 w	20,10	1.229 vw	422	0.8174 w
				410	0.9023 vw	220	1.181 m	423	0.7975 vw
								505-424	0.7767 vw

* The kx unit is defined on the basis of the Siegbahn scale of X-ray wave lengths. s = strong, m = medium, w = weak, vw = very weak.

and TiNi₃ during cooling at a temperature which is probably above 800°C.

TiFe₂, TiCo₂, and TiNi₃ Phases

The results obtained on TiFe₂ confirm the hexagonal (MgZn₂ type) structure proposed by Witte and Wallbaum.² The list of interplanar spacings with their indexes is given in table IV. The lattice parameters (table I) are only slightly lower than the previously published values. This decrease in lattice parameter may be explained by the difference in the purity of the titanium used in each investigation (about 95 pct in ref. 1 and 99 pct in the present work).

A study was made of an alloy of the composition corresponding to the formula TiFe₃, for which a tetragonal structure was reported by Jellinghaus.⁸ Powder patterns were taken of the specimens after sintering and also after annealing for 10 days at 800° and 650°C. In all cases, the patterns contained the lines of TiFe₃ and those of iron; hence, there is no intermediate phase between TiFe₂ and the iron terminal solid solution. These findings confirm those of Witte and Wallbaum.²

The investigation of the structure of TiCo₂ was of particular interest because of the findings of Wallbaum and Witte⁶ who assigned the hexagonal (MgNi₂ type) structure to an alloy containing 32 1/3 at. pct titanium and the cubic MgCu₂ type structure to an alloy containing 35 at. pct titanium. They also show schematically how the phase boundaries could be located in the titanium-cobalt diagram in order to explain this rather unusual behavior. The alloys prepared in the present investigation contained 37, 35, 33 1/3, and 32 at. pct titanium. The X-ray diffraction patterns of these four alloys were identical, and a typical set of measured interplanar spacings is given in table IV. All the spacings observed in this investigation agree quite closely with those given by Wallbaum for the hexagonal (MgNi₂ type) structure. In fact, quite a number of extra lines were observed and were identified as reflections from planes of an MgNi₂ structure. Hence, the results of this investigation failed to confirm the existence of a cubic (MgCu₂ type) structure for alloys around the TiCo₂ composition.

No obvious reason could be found for this lack of agreement with the work of Wallbaum. The possibility of mistaking a powder pattern of the MgNi₂ type for a MgCu₂ type, and vice versa, can hardly be suggested. It is true that the interplanar spacings of cubic TiCo₂ are very close to some of the spacings of hexagonal TiCo₂.^{*} However, the relative intensities of the lines are quite different, and the two patterns are distinguished easily.

The influence of impurities also may be suggested as an explanation for the existence of a cubic form of TiCo₂. The titanium powder used by Wallbaum and Witte contained approximately 5 pct impurities. If a metal like silicon, aluminum, or magnesium were the predominant impurity, a new phase between titanium, cobalt, and this unknown impurity might have been produced. Unless the impurities are known, it is of course impossible to clarify the question.

The results of X-ray diffraction studies of TiNi₃ are presented in table IV. All the interplanar spacings and the relative intensities agree with the study of Laves and Wallbaum;⁷ the structure is hexagonal, and the parameters are as given in table I. The existence of a phase of TiNi₃, instead of TiNi₂, breaks the otherwise perfect similitude among the three systems of titanium with iron, cobalt, and nickel. It seems quite certain, however, that TiNi₂ does not exist. Several alloys containing about 66.6 at. pct nickel were prepared, and, after various heat treatments, always yielded a diffraction pattern containing the lines of TiNi and TiNi₃.

Conclusions

The results of this investigation may be summarized as follows:

The intermediate phases Ti₂Fe, Ti₂Co, and Ti₂Ni are face-centered cubic with 96 atoms per unit cell. The lattice parameters of these phases are very nearly the same.

The intermediate phases TiFe, TiCo, and TiNi are body-centered cubic (CsCl type) and have approximately the same lattice parameters.

In the titanium-iron system the intermediate phase rich in iron is TiFe₂. It is an hexagonal structure of the MgZn₂ type. The existence of a phase of TiFe₃ composition has not been confirmed.

In the titanium-cobalt system, the intermediate phase rich in cobalt is TiCo₂. It has an hexagonal structure of the MgNi₂ type. The existence of a cubic (MgCu₂ type) modification of the same phase previously reported in the literature has not been confirmed.

In the titanium-nickel system, the intermediate phase rich in nickel is TiNi₃. It has an hexagonal structure specific to this alloy.

Acknowledgment

This work was done at the Jet Propulsion Laboratory, California Institute of Technology, under contract number W-04-200-ORD-455 with the Army Ordnance Department, Washington, D. C. The authors wish to thank this agency for the permission to publish the results of this investigation.

References

- ¹ H. J. Wallbaum: The Systems of the Iron Group Metals with Titanium, Zirconium, Columbium, and Tantalum. *Archiv f. das Eisenhuttenwesen*. (1941) **14**, 521-526.
- ² H. Witte and H. J. Wallbaum: Thermal and X-Ray Diffraction Studies in the Iron-Titanium System. *Ztsch. f. Metallkunde*. (1938) **30**, 100-102.
- ³ R. Vogel and H. J. Wallbaum: The System Iron-Nickel-Titanium. *Archiv f. das Eisenhuttenwesen*. (1938) **12**, 299-305.
- ⁴ J. R. Long, E. T. Hayes, D. C. Root, and C. E. Armantrout: A Tentative Titanium-Nickel Diagram. U. S. Bur. Mines. *R.I. 4463* (Feb. 1949).
- ⁵ F. Laves and H. J. Wallbaum: The Crystal Chemistry of Titanium Alloys. *Naturwissenschaften*. (1939) **27**, 674-675.
- ⁶ H. J. Wallbaum and H. Witte: The Crystal Structure of TiCo₂. *Ztsch. f. Metallkunde*. (1939) **31**, 185-187.
- ⁷ F. Laves and H. J. Wallbaum: The Crystal Structure of Ni₃Ti and Si₂Ti. *Ztsch. f. Kristallographie*. (1939) **101**, 78-93.
- ⁸ W. Jellinghaus: The Crystal Structure of Fe₃Ti. *Ztsch. f. Anorg. und allgem. Chem.* (1936) **227**, 62-64.
- ⁹ F. Laves and H. Witte: The Crystal Structure of MgNi₂ and Its Relation to the MgCu₂ and MgZn₂ Types. *Metallwirtschaft*. (1935) **14**, 645-649.



aime NEWS

AIME Features "Research in Progress" Theme at Metal Congress

THE Technical program of the American Institute of Mining & Metallurgical Engineers at the National Metal Congress and Exposition, Oct. 23 to 27, at Chicago, will feature reports of "Research in Progress." These reports will be part of several of the regular technical sessions, and a special session will be inaugurated as well. Designed to bring to light research that is not yet far enough along to give any indication of final results or complete descriptions of methods, processes, or achievements, these "Research in Progress" presentations may set a new pattern in technical meeting discussions. They should prove of benefit to many who have research projects underway similar in nature to those discussed at the meetings.

Headquarters of the Institute of Metals Div., AIME, will be the Hotel Sheraton during the Metal Show week. The technical meetings will be held at that hotel. Registration for the AIME technical sessions will be conducted prior to the meetings and during the entire week. Member registration fee is \$2 and nonmember fee is \$4.

The annual fall dinner and cocktail party will be held Tuesday evening Oct. 24, at the Hotel Sheraton. Individual tickets will be on sale prior to the affair, and complete tables of 10 may be reserved at a cost of \$50 a table. J. H. Reese, Revere Copper and Brass, Inc., 2200 No. Natchez Ave., Chicago 35, will be in charge of reservations for complete tables. Obtain individual tickets at \$5 each at the registration desk.

Institute of Metals Div. AIME Fall Meeting Hotel Sheraton, Chicago

Tentative Program

Monday A.M.—Oct. 23

Plastic Deformation

B. Averbach, Chairman

P. Kosting, Secretary

An Experimental Survey of Deformational and Annealing Processes in Zinc. D. C. Jillson.

Quantitative Stress-Strain Studies on Zinc Single Crystals in Tension. D. C. Jillson.

A Study of the Plastic Behavior of High-Purity Aluminum Single Crystals at Various Temperatures. F. D. Rosi and C. H. Mathewson.

A Study of Strain Markings in Aluminum. B. R. Banerjee.

Research in Progress

Rolling Textures of Aluminum. H. Hu and Paul Beck.

Monday P.M.—Oct. 23

Recrystallization and Annealing Textures

R. Maddin, Chairman

C. Dunn, Secretary

Activation Energy for Recrystallization in Rolled Copper. B. F. Decker and D. Harker.

Recrystallization Reaction Kinetics and Texture Studies of a 50 Iron 50 Nickel Alloy. W. E. Seymour and D. Harker.

The Textures of Cold-Rolled and Annealed Titanium. H. T. Clark, Jr.

Relative Energies of Grain Boundaries in Silicon Iron. C. G. Dunn, F. W. Daniels and M. J. Bolton. Production and Examination of Zinc Single Crystals. D. C. Jillson.

Research in Progress

Recrystallization Texture in Aluminum. Paul Beck and H. Hu

Structure of Alloys

B. D. Cullity, Chairman

Earl Parker, Secretary

Solid Solubility of Cementite in Alpha Iron. C. A. Wert.

The Structure of Intermediate Phases in Alloys of Titanium with Iron, Cobalt and Nickel. P. Duwez and J. L. Taylor.

The Alloys of Titanium with Carbon, Oxygen and Nitrogen. R. I. Jaffee, H. R. Ogden and D. J. Maykuth.

Informal Evening Session—Panel Discussion on Precipitation Hardening Arranged by M. Cohen

Tuesday A.M.—Oct. 24

Transformations

A. R. Troiano, Chairman

J. B. Hess, Secretary

On the Martensitic Transformation at Temperatures Approaching Absolute Zero. S. A. Kulin and M. Cohen.

Austenite Formation During Tempering and Its Effects on Mechanical Properties. E. F. Bailey and W. J. Harris, Jr.

The Isothermal Transformation of a Eutectoid Beryllium Bronze. R. H. Fillnow and D. J. Mack.

The Ordering Reaction in Cobalt-Platinum Alloys. J. B. Newkirk, A. H. Geisler, D. L. Martin and R. Smoluchowski.

Properties of Alloys
R. M. Parke, Chairman
V. Pulsifer, Secretary

The Effect of Alloying Elements on the Plastic Properties of Aluminum Alloys. J. E. Dorn, P. Pietrokowsky and T. E. Tietz.

The Properties of Some Mg-Li Alloys Containing Al and Zn. R. S. Busk, D. L. Leman and J. J. Casey.

The Effect of Sodium Contamination on Magnesium-Lithium Base Alloys. P. D. Frost, J. H. Jackson, A. C. Loonam and C. H. Lorig.

Young's Modulus and Its Temperature Dependence in 36 to 52% Nickel-Iron Alloys. M. E. Fine and W. C. Ellis.

Tuesday P.M.—Oct. 24

Metal—Gas Reactions
M. Bever, Chairman
T. Leontis, Secretary

Equilibrium in the Reaction of Carbon Dioxide with Liquid Copper from 1090° C to 1300° C. D. J. Girardi and C. A. Siebert.

Hydrogen Solubility in Aluminum and Some Aluminum Alloys. W. R. Opie and N. J. Grant.

The Vapor Pressure of Silver. H. M. Schadel, Jr. and C. E. Birchenall.

Composition of Atmospheres Inert to Heated Carbon Steel. R. W. Gurry.

The Intermittant Oxidation of Some Nickel-Chromium Base Alloys. B. Lustman.

Solidification, Thermal Expansion & Ductility
R. S. Busk, Chairman
A. J. Smith, Secretary

Dendritic Crystallization of Alloys. B. H. Alexander and F. N. Rhines.

The Supercooling of Aggregates of Small Metal Particles. D. Turnbull.

The Thermal Expansion Characteristics of Beryllium. R. M. Treco.

Thermal Expansion Characteristics of Stainless Steels between 300° and 1000° F. D. E. Furman.

The Ductility of Cast Molybdenum. R. B. Fischer and J. H. Jackson.

Correlation Between Electrical and Thermal Conductivity in Ni and Ni Alloys. M. E. Fine.

Wednesday P.M.—Oct. 25

Technical Session on Research in Progress
Arranged by M. Cohen

On the Temperature Dependence of Self-Diffusion in Alpha-Iron. I. D. Bakalar.

Effect of Uniaxial Compressive Stresses on Self-Diffusion in Alpha-Iron. F. S. Buffington.

Secondary Recrystallization of Silver. F. D. Rosi.

Plastic Properties and the Extension of Silver Single Crystals. F. D. Rosi.

On the Gamma (259) Planes Habit of Martensite. E. S. Machlin.

The Transition Carbide in Tempered Martensite. E. C. Roberts.

Powder Metallurgy

F. V. Lenel, Chairman

J. C. Redmond, Secretary

A Process for Hot Pressing Beryllium Powder. A. U. Seybolt, R. M. Linsmayer and J. P. Frandsen.

The Densification of Pre-reduced Copper Powder Compacts in Vacuum and in Hydrogen. C. B. Jordan and P. Duwez.

Research in Progress

Experiments on the Mechanism of Sintering. B. H. Alexander and R. Bullifff.

Notes on the Powder Metallurgy of Zirconium. H. H. Hausner, R. P. Angier and H. Kalish.

Studies on Control of Growth or Shrinkage of Iron-Copper Compacts During Sintering. J. S. Kuzmick and E. N. Mazza.

Annual Meeting Paper Deadline

Oct. 15, 1950 is the deadline for all Institute of Metals, Extractive Metallurgy, and Iron and Steel Division papers to be preprinted for the Annual Meeting to be held in St. Louis, Feb. 19 to 22, 1951.

Metals Branch activities at the Annual Meeting will be at the Hotel Statler, despite the fact that the headquarters hotel for the entire meeting will be the Hotel Jefferson.

tember reports may reflect this effort.

It remains, however, up to the individual members of AIME to give the membership drive any real impetus. Prospective members' names, sent in by present members, will be welcomed, and immediate efforts will be made to get them to join. "Aims and Activities of AIME," outlining functions, activities, benefits, and advantages of AIME membership, has just been revised and will be used in the membership solicitation effort. This publication will be sent every prospective member so that he can see exactly what AIME is and stands for—an outstanding professional society of the minerals industries engineers.

Get behind the membership drive! Every member get a member.

AIME Directory for 1950

One of the most valuable of the AIME's publications—often called the *Who's Who of the Mineral Industries*—the Directory of members, will be published this fall. Several changes will be made, including the addition of a company listing. To that end, inquiries were sent to every member. A large proportion of these have been returned with the desired information.

Another feature will be the listing of members not only alphabetically, but by companies in the various states. Those not employed by a company, the Government, or an educational institution will be listed according to the city in which they live, as formerly.

The personnel of committees, and the officers of Branches, Divisions, and Local Sections will be included. Names and addresses of Student Associates will be omitted because much of this information will be obsolete by the date of publication.

Membership Drive Opened by Every Member Canvas for Prospects

July reports indicate a total of 102 new members added to AIME rolls, somewhat below what is desired, but encouraging nevertheless. The letter to members, from D. H. McLaughlin, AIME president, which was the opening shot in the membership drive, yielded a good list of excellent prospects, and Ruth Garrett, who is heading up the headquarters efforts in the membership drive, is now processing these prospects in an effort to get them to join. One factor that is difficult to understand, however, with respect to the prospects received from the President's letter is that there were very few prospects from the Metals Branch. The Mining and Petroleum Branches accounted for the bulk of such prospects.

The Metals Branch is lagging behind on new members, but this situation should improve somewhat in the next two months. Both the Iron and Steel Div., and the Extractive Metallurgy Div., are getting underway on a concentrated effort to build up the membership of the respective divisions. August and Sep-

Plans Underway for 1951 Annual Meeting



Fred J. Meek



Howard I. Young



S. J. Swainson

The AIME Annual Meeting will be held in St. Louis, Mo., Feb. 19 to 22, 1951, under the General Chairmanship of Howard I. Young. Mr. Young is a director of AIME, and president of the American Zinc, Lead & Smelting Co. Secretary for the meeting is Fred J. Meek, Plant Engineer of the American Zinc Co. of Ill. The committees have been chosen, and work is underway to complete all necessary details.

The major part of the planning will be done by members of the St. Louis Section. Papers for presentation will be selected by the Technical Publications Committee. The program schedule will be arranged by the Coordinating Committee on Technical Program for the Annual Meeting, under the Chairman-

Time: February 19 to 22, 1951

Place: St. Louis, Mo.

Headquarters: Hotel Jefferson

Meetings: Hotel Jefferson and Hotel Statler

ship of S. J. Swainson. Present plans call for a student forum under the guidance of faculty sponsors of student chapters. Because of the large program, some technical meetings will be held at the Hotel Jefferson, and some, including those of the Metals Branch, will be held at the Hotel Statler.

ANNUAL MEETING COMMITTEES

General Committee

G. C. Bartholomées	W. T. Isbell
O. W. Bilharz	J. W. MacDonald
Gilbert H. Cady	John L. McManamy
W. R. Chedsey	Ernest L. Ohle
James D. Forrester	R. J. Piersol
O. R. Grawe	Verne Pulsifer
A. P. Green	N. A. Stockett

John M. Thompson

Finance Committee

Carl G. Stifel, Chairman
Jules C. George, Vice-chairman
Fred W. Green

Smoker Committee

Herbert A. Franke, Chairman
Neal Ham, Vice-chairman

Bernard F. Desloge	G. S. Jenkins
A. F. Frederickson	Gill Montgomery
Paul R. Hamilton	H. LeRoy Scharon

Clyde S. Smith

Reception Committee

Carl Tolman, Chairman
Curtis L. Wilson, Vice-chairman

Elmer Isern	B. F. Murphy
Harold E. Krueger	Victor Rakowsky
M. M. Leighton	J. H. Steinmesch
James B. Macelwane	H. L. Walker

Banquet Committee

John D. Kerr, Chairman
H. A. Bell
Arthur Bevan
James B. Macelwane

Bernard F. Desloge
H. R. Hanley

James B. Macelwane

Welcoming Luncheon Committee

L. P. Davidson, Chairman

Hotel Committee

Nat. L. Shepard, Chairman
Albert J. Frank, Vice-chairman

F. S. Elfred

Mrs. Herbert A. Franke

Informal Dance Committee

Kenneth A. Phillips, Chairman
DeWitt Smith, Vice-chairman

H. E. Butters

H. A. Neustaedter

Mrs. G. L. Spencer, Jr.

Field Trips Committee

Edward L. Clark, Chairman
Norman S. Hinchee, Vice-chairman

John S. Brown
S. S. Clarke
F. S. Elfred
H. E. Gross
H. R. Hanley
Jack James

W. D. Keller
R. G. Knickerbocker
J. E. Lamar
Arthur Mallans
Harold A. Neustaedter
Frank H. Reed

Publicity Committee

Arthur B. Cleaves, Chairman
H. E. Butters, Vice-chairman

O. M. Bishop
John S. Brown

A. B. Campbell
Harold N. Underhill

Student Activities Committee

Curtis L. Wilson, Chairman

W. R. Chedsey
Albert J. Frank
A. F. Frederickson

Charles O. Frush
D. R. Schooler
D. F. Walsh

Proposed for Membership — Metals Branch AIME

Total AIME membership on June 30, 1950, was 16,339; in addition 4256 Student Associates were enrolled.

ADMISSIONS COMMITTEE

E. C. Meagher, Chairman; Albert J. Phillips, Vice-Chairman; George B. Corless, H. P. Croft, Lloyd C. Gibson, Ivan A. Given, F. W. Hanson, T. D. Jones, P. Malozemoff, Richard D. Mollison, and John Sherman.

Institute members are urged to review this list as soon as the issue is received and immediately to wire the Secretary's office, night message collect, if objection is offered to the admission of any applicant. Details of the objection should follow by mail. The Institute desires to extend its privileges to every person to whom it can be of service but does not desire to admit persons unless they are qualified.

In the following list C/S means change of status; R, reinstatement; M, Member; J, Junior Member; AM, Associate Member; S, Student Associate.

Alabama

Homewood—Johnson, Leland, Harold (M) (R, C/S—S-J).

California

El Cajon—Tyrrell, John Francis (J) (R, C/S—S-M).

Pasadena—Golda, Edward Walter (M).

Dist. of Columbia

Washington—McNutt, James E. (C/S—S-J).

Florida

Gulfport—Brown, John A. (J) (C/S—S-J).

Illinois

Chicago—Crossley, Frank A. (C/S—S-J). Murway, Edward (J) (C/S—S-J). Whiteson, Bennett V. (J) (C/S—S-J).

Freeport—Tucker, Kenneth K. (C/S—S-J).

La Salle—Miller, Pierce J. (J) (C/S—S-J).

Riverside—Orr, Harry E. (R,M).

Michigan

Ann Arbor—Gilkerson, Murray M., Jr. (J). Keith, Robert Eugene (J) (C/S—S-J).

Detroit—Bartlett, Edwin S. (R,C/S—S-J). Sharp, Marcus (J).

Minnesota

Minneapolis—Pennington, James W. (R,C/S—S-M).

Missouri

Bonne Terre—Reilly, John G., Jr. (C/S—S-J).

Louisiana—Gardner, G. Douglas. (C/S—A-M).

New Jersey

Garwood—Blackmun, Edward V. (M).

Maplewood—Bailey, Carroll C. (A).

New Mexico

Hurley—Smith, Paul R., Jr. (J).

New York

Bayside—Frankel, Herbert A. (J) (C/S—S-J).

Tuckahoe—Lloyd, Thomas E. (M).

Tuxedo Park—Packer, Kenneth F. (J).

New York—Nichols, Charles W., Jr. (A).

Ohio

Steubenville—Copp, Warren F. (M).

Pennsylvania

Pittsburgh—Wright, Haydn V. (C/S—S-J).

Sewickley—McLain, Charles D. (M).

State College—Clendenin, John D. (C/S—J—M).

Meadville—Sundback, Paul Philip (J) (C/S—S-J).

Argentina

Buenos Aires—Acevedo, Arturo. (M).

Canada

Ontario—Disano, Russell Patsy (J) (C/S—S-J).

Toronto—Pidgeon, Lloyd M. (M).

England

Northwood—Richardson, Frederick D. (M).

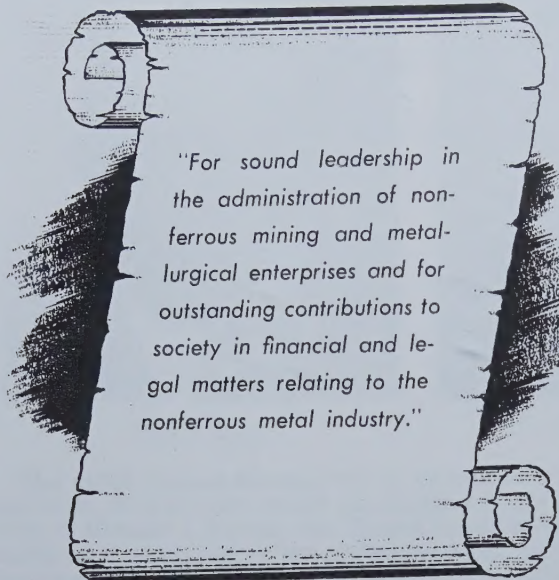
Germany

Stuttgart—Köster, Werner O. (M).

Japan

Tokyo—Mishima, Yoshitsugu. (J).

An Optimist at 83



"For sound leadership in the administration of non-ferrous mining and metallurgical enterprises and for outstanding contributions to society in financial and legal matters relating to the nonferrous metal industry."

Thus read the citation, presented with the Charles F. Rand Memorial Gold Medal for 1950 to Francis Herbert Brownell, conferred by the American Institute of Mining and Metallurgical Engineers. The presentation was made at a meeting of the AIME Board of Directors at the Engineers' Club on June 22, 1950, a ceremony that was deferred from the time of the AIME Annual Meeting in February. Mr. Brownell is retired, but until recently was chairman of the board of American Smelting and Refining Co.

The Rand Medal itself is quite a newsworthy achievement, but Mr. Brownell's attitude toward current events, and the future of social systems bespeaks a man who has faced issues as they arose, kept faith in himself and his fellow men, and overcame reverses. His remarks upon receiving the Medal are heart warming, and a lesson in faith and fortitude to everyone. Because of optimistic view of the future and the faith expressed in mankind, Mr. Brownell's remarks are printed here in full to serve not only as encouragement to the faint of heart but to preserve for the record the words of an "optimist at 83".—The Editor

IT is difficult for me adequately to express my deep appreciation and gratitude for the honor you are bestowing upon me, both in the Rand Medal and the complimentary citation accompanying it. It is all the more appreciated because this honor has come after I retired from an active business career.

"I deeply regretted not being able to come to the Annual Dinner, when normally the presentation would have been made, but I had been down in Florida and at my age—over eighty years—my doctor thought it would be unwise for me to subject myself to the extreme change of climate. It is an added honor to be asked to come before you tonight to receive the Medal.

"Recently I read the autobiography of Dr. Millikan, one of America's greatest physicists, who led the California School of Technology to its present important position. He was born in 1868 and I was born the previous year. Dr. Millikan expressed the opinion that during the past 80 years there has occurred a greater advancement of man's knowledge of nature, more new industries and more new inventions, than in all preceding history. The anthropologists, having studied the Java, Peking, and South African skulls and artifacts and having correlated them with the age of geological formations, now estimate that *homo sapiens* existed at least 200,000 years ago, and probably somewhat longer. Stated in statistical terms, man's scientific knowledge and inventions have increased in the last 80 years more than in the preceding 200,000 years of his existence.

"Eighty years ago, the scientific world knew of the existence of electricity, but knew little about it and could not utilize it. The epoch-making theory of electromagnetism of Dr. Clark Maxwell, the great English physicist, was not published until 1873. It outlined the scientific theory that made possible the development of to-

day's electrical industry, the light and power which make this the so-called *electrical age*. Think for a moment in what condition the United States would be were we back in our knowledge and use of electricity to the days of 1873.

"Eighty years ago, the telephone was not yet discovered, nor the X-rays, nor radioactivity, nor the radio, radar, or cosmic rays. The internal combustion engine yet was to be invented, making possible our modern motor and airplane development. The discovery of anesthesia and asepsis in the last 80 years has entirely changed surgical practice, and in medicine the discovery by Pasteur of the bacterial or virus origin of many diseases has now placed them under control.

"One result has been to prolong the average human life by many years and has confronted industry today with the entirely unexpected and unforeseen problem of old-age pensions for those who now live over the age of 65 years and who 80 years ago would have disappeared from this life before that age.

"In agriculture, increased knowledge of soil, chemistry, fertilizers, insecticides and improved seeds enables us now to raise approximately twice the amount per acre that was formerly the case. When I was a boy, hens laid about 50 eggs per year; now they lay 200, and the average production per cow has been doubled in quality and quantity.

"When I was in college, we were taught that the atom was the ultimate form of matter. No one dreamed anything could be smaller. But today the atom is a whole universe in itself, with its electrons, neutrons, protons, mesons, and above all, a force binding its particles together, which is probably the strongest force in the universe and the cause of our greatest anxiety should a third World War break out.

"Older men are apt to be pessimistic in out-

look. Their physical powers are failing and they look back to the happier days of real sport, when all the world was young, lad, and all the grass was green, and every goose a swan, lad, and every lass a queen. It is easy to apply this purely personal feeling to the outside happenings and conditions, and so to conclude that men and governments have deteriorated and will continue to do so. An older man must be careful not to fall into such conclusions.

"There are two schools of pessimism in the world today, one of which is based on the fear that the atom bomb, in the event of a third World War, may possibly destroy civilization; or at best bring on a new dark age for centuries. This fear seems unjustified. Such a war might, it is true, destroy the plants, even the cities, of the United States or of Russia and other countries, but it would not destroy the knowledge which mankind has already achieved. That would remain. Even the Russians are not opposed to science, however much they may be opposed to religion. Their efforts are all directed to finding out what other nations have done, as well as to carry on their own research. They may ridiculously claim that all scientific discoveries are made, in the first instance, by Russians, but they do not disparage the value of scientific discoveries, or wish to destroy present knowledge.

"The destruction of the ancient civilizations of Greece and Rome by the inroads of the barbarians is no precedent. Scientific knowledge was at that time limited to a very small area around the Mediterranean. A deliberate effort was made to destroy all books and other scientific knowledge. But even so, much of the former knowledge remained in the Arab world and ultimately, following the Crusades, came back into Europe in the Renaissance to be the foundation and beginning of the rebirth of European civilization. Today, we have our scientific knowledge scattered widely, not only throughout the United States and Europe, but also in Australia, Japan, Latin America—and over such a large area outside of Europe and the United States that it is impossible to believe that any war would completely eradicate the knowledge which mankind has so slowly achieved.

"Another school of pessimism is based on the fear that if the world continues to use its coal, oil and metals, both ferrous and nonferrous, at the present rate, it will, in less than a century, have exhausted the earth's supply of some of them, and probably of all in from five hundred to a thousand years.

"Five hundred years ago takes us back practically to the discovery of America. One thousand years ago was the period between the reign of Charlemagne and the invasion of England by the Normans under William the Conqueror. A thousand years is a short period in history and such geological knowledge as we now have rather indicates the possibility that a thousand years from now the earth's supply of oil, coal and metals, now the basis of our operations, will be largely exhausted.

"But we need entertain, it seems to me, little fear of the consequence to mankind. Chemistry has but just begun its marvelous advance in the production of plastics and other synthetic substances. Aluminum and magnesium have great



F. H. Brownell

possibilities. We know that the atom, by loss of electrons, can change from one element to another; for example, from radium into uranium, and from uranium into lead. It is quite possible that further knowledge of the atom will enable us to realize the transmutation of metals dreamed of centuries ago. Atomic power may take the place of coal and oil. If not, with the aid of chemistry and agriculture the world can produce various forms of combustibles for fuel purposes. Science will also learn to use more advantageously the direct power of the sun, wind, wave and water. There is little doubt that mankind will continue to have adequate heat and power.

"To my mind, the greatest promise of the future lies in the modern prevalence of research. Eighty years and more ago new inventions and discoveries were made by individuals, using their own funds and time. Little or no effort was made by either our institutions of learning or by our business enterprises to develop research for new processes and new inventions. Today, philanthropy frequently finances research by our higher institutions of learning. Witness the cyclotrons in many of our universities, the 200 in. telescope on Mt. Palomar, and many similar enterprises. Nearly every large industrial company today has its own research department, with skilled scientists employed and devoting their lives to new methods of production and new discoveries to take the place of old. No one can tell what eighty years of activity like this will produce in the future, but it is not overly optimistic to express the belief that with research adequately financed and carried on to the extent that it is being carried on today, the next eighty years will see discoveries, inventions and improvements made, not incomparable with those made in the last 80 years. A third World War might postpone such a result. We cannot expect to advance continuously and steadily, without interruption. Ups and downs in rate of progress are to be expected, but the trend will be upward and man will continue his evolution and advance in both science and government. We may confidently look forward to higher and better standards of living and greater happiness of the average man.

"Again, let me thank you most sincerely for the honor you have conferred upon me."

